

Precision tools and models to narrow in on the 750 GeV diphoton resonance

Florian Staub,^a Peter Athron,^b Lorenzo Basso,^c Mark D. Goodsell,^d Dylan Harries,^e Manuel E. Krauss,^f Kilian Nickel,^f Toby Opferkuch,^f Lorenzo Ubaldi,^g Avelino Vicente,^h Alexander Voigtⁱ

^a*Theoretical Physics Department, CERN, Geneva, Switzerland*

^b*ARC Centre of Excellence for Particle Physics at the Terascale, School of Physics, Monash University, Melbourne, Victoria 3800, Australia*

^c*CPPM, Aix-Marseille Université, CNRS-IN2P3, UMR 7346, 163 avenue de Luminy, 13288 Marseille Cedex 9, France*

^d*LPTHE, UMR 7589, CNRS and Université Pierre et Marie Curie, Sorbonne Universités, 75252 Paris Cedex 05, France*

^e*ARC Centre of Excellence for Particle Physics at the Terascale, Department of Physics, The University of Adelaide, Adelaide, South Australia 5005, Australia*

^f*Bethe Center for Theoretical Physics & Physikalisches Institut der Universität Bonn, Nussallee 12, 53115 Bonn, Germany*

^g*Raymond and Beverly Sackler School of Physics and Astronomy, Tel-Aviv University, Tel-Aviv 69978, Israel*

^h*Instituto de Física Corpuscular (CSIC-Universitat de València), Apdo. 22085, E-46071 Valencia, Spain.*

ⁱ*Deutsches Elektronen-Synchrotron DESY, 22607 Hamburg, Germany*
E-mail: florian.staub@cern.ch, peter.athron@coepp.org.au, basso@cppm.in2p3.fr, goodsell@lpthe.jussieu.fr, dylan.harries@adelaide.edu.au, mkrauss@th.physik.uni-bonn.de, nickel@th.physik.uni-bonn.de, toby@th.physik.uni-bonn.de, ubaldi.physics@gmail.com, avelino.vicente@ific.uv.es, alexander.voigt@desy.de

ABSTRACT: The hints for a new resonance at 750 GeV from ATLAS and CMS have triggered a significant amount of attention. Since the simplest extensions of the standard model cannot accommodate the observation, many alternatives have been considered to explain the excess. Here we focus on several proposed renormalisable weakly-coupled models and revisit results given in the literature. We point out that physically important subtleties are often missed or neglected. To facilitate the study of the excess we have created a collection of 40 model files, selected from recent literature, for the `Mathematica` package `SARAH`. With `SARAH` one can generate files to perform numerical studies using the tailor-made spectrum generators `FlexibleSUSY` and `SPheno`. These have been extended to automatically include crucial higher order corrections to the diphoton and digluon decay rates for both CP-even and CP-odd scalars. Additionally, we have extended the `UFO` and `CalcHep` interfaces of `SARAH`, to pass the precise information about the effective vertices from the spectrum generator to a Monte-Carlo tool. Finally, as an example to demonstrate the power of the entire setup, we present a new supersymmetric model that accommodates the diphoton excess, explicitly demonstrating how a large width can be obtained. We explicitly show several steps in detail to elucidate the use of these public tools in the precision study of this model.

Contents

1	Introduction	1
2	Motivation	4
2.1	Calculation of the diphoton and digluon widths	5
2.1.1	The diphoton and digluon rates beyond leading order	5
2.1.2	Constraints on a large diphoton width	6
2.1.3	How do the tools help?	9
2.2	Properties of the 750 GeV scalar	11
2.2.1	Mixing with the SM Higgs	11
2.2.2	To VEV or not to VEV?	13
2.2.3	Additional decay channels	14
2.2.4	How do the tools help?	15
2.3	Considering a full model	15
2.3.1	Additional constraints in a full model	15
2.3.2	Theoretical uncertainties of other predictions	16
2.3.3	How do the tools help?	16
3	Using SARAH to understand a model	17
3.1	General	17
3.2	Models supported by SARAH	18
3.3	Supported models and features	19
3.3.1	Global symmetries	19
3.3.2	Gauge sector	19
3.3.3	Matter sector	20
3.4	Checks of implemented models	21
3.5	Analytical calculations performed by SARAH	21
3.5.1	Tree-level properties	21
3.5.2	Renormalization group equations	22
3.5.3	One- and two-loop corrections to tadpoles and self-energies	22
4	Spectrum calculation, Monte-Carlo studies, and more	23
4.1	SPheno	23
4.1.1	Mass calculation with SPheno	23
4.1.2	Decay widths and branching ratios	25
4.1.3	Flavour observables	25

4.1.4	Fine-Tuning	25
4.2	FlexibleSUSY	26
4.2.1	Mass calculation with FlexibleSUSY	26
4.2.2	Decay widths and branching ratios	27
4.3	Mass spectrum calculation: SUSY vs. Non-SUSY	27
4.4	Calculation of the effective diphoton and digluon vertices in SPheno and FlexibleSUSY	28
4.5	Monte-Carlo studies	31
4.5.1	Output of models files	32
4.5.2	Interplay SARAH – Spectrum-Generator – MC-Tool	33
4.5.3	Effective diphoton and digluon vertices for neutral scalars	33
4.6	Checking Higgs constraints	33
4.7	Checking the Vacuum stability	34
4.8	Accuracy of the diphoton calculation	34
4.8.1	Loop corrections to $ZZ, WW, Z\gamma$ production	34
4.8.2	BSM NLO corrections	35
4.8.3	Tree vs pole masses in loops	36
5	Models	37
5.1	Toy models	38
5.2	Models based on the SM gauge-group	42
5.2.1	Singlet extensions with vector-like fermions	43
5.2.2	Two-Higgs doublet models	54
5.3	$U(1)$ extensions of the SM	60
5.3.1	Models with SM states uncharged under the new $U(1)$	60
5.3.2	Models with SM states charged under the new $U(1)$	65
5.4	Non-abelian gauge-group extensions of the SM	74
5.4.1	Left-right symmetric models	74
5.4.2	331 models	81
5.4.3	Other models	87
5.5	Supersymmetric models	89
5.5.1	NMSSM extensions with vector-like multiplets	89
5.5.2	Broken MRSSM	93
5.5.3	$U(1)'$ -extended MSSM	95
5.5.4	E_6 -inspired SUSY models with extra $U(1)$ model	96

6	Study of a natural SUSY explanation for the diphoton excess	99
6.1	The model	99
6.2	Analytical results with <code>Mathematica</code>	102
6.2.1	Consistency Checks	102
6.2.2	Gauge sector	103
6.2.3	Scalar Sector	104
6.2.4	Vector-like sector	108
6.2.5	RGEs and gauge kinetic mixing	109
6.2.6	Boundary conditions and free parameters	112
6.3	Analysis of the important loop corrections to the Higgs mass	113
6.3.1	New loop corrections to the SM-like Higgs	114
6.3.2	Loop corrections to the 750 GeV scalar	116
6.4	Diphoton and digluon rate	117
6.5	Constraints on choice of parameters	118
6.5.1	Singlet-doublet mixing	118
6.5.2	Constraints from Higgs coupling measurements	120
6.5.3	Large decay width and constraints from vacuum stability	123
6.5.4	Dark matter relic density	125
6.5.5	Flavour constraints	126
6.6	Z' mass limits	127
7	Summary	129
A	How to use SARAH and related tools	130
B	What is necessary to implement a model in SARAH?	141
C	How can I define the features of a SPheno or FlexibleSUSY version?	146

1 Introduction

The first data from the 13 TeV run of the Large Hadron Collider (LHC) contained a surprise: ATLAS and CMS reported a resonance at about 750 GeV in the diphoton channel with local significances of 3.9σ and 2.6σ , respectively [1, 2]. When including the look-elsewhere-effect, the deviations from standard model (SM) expectations drop to 2.3σ and 1.2σ .

This possible signal caused a lot of excitement, as it is the largest deviation from the SM which has been seen by both experiments. Such an excitement, in turn, led to an avalanche of papers in a very short time which analysed the excess from various perspectives [3–212].

It is hard to explain the excess within the most commonly considered frameworks for physics beyond the standard model (BSM), like two-Higgs-doublet models (THDM) or the minimal supersymmetric standard model (MSSM) [213], to mention a couple of well-known examples. Thus, many alternative ideas for BSM models have been considered, some of which lack a deep theoretical motivation and are rather aimed at just providing a decent fit to the diphoton bump. Most of the papers in the avalanche were written quickly, some in a few hours, many in a few days, so the analyses of the new models are likely to have shortcomings. Some effects could be missed in the first attempt and some statements might not hold at a second glance. Indeed we have found a wide range of mistakes or unjustified assumptions, which represented the main motivation that prompted this work.

Now that the dust has settled following the stampede caused by the presentation of the ATLAS and CMS data, the time has come for a more detailed and careful study of the proposed ideas. In the past few years several tools have been developed which can be very helpful in this respect. In the context of renormalisable models, the Mathematica package `SARAH` [214–219] offers all features for the precise study of a new model: it calculates all tree-level properties of the model (mass, tadpoles, vertices), the one-loop corrections to all masses as well as the two-loop renormalisation group equations, and it can be interfaced with the spectrum generators `SPheno` [220, 221] and `FlexibleSUSY` [222]. These codes, in turn, can be used for a numerical analysis of any model, which can compete with the precision of state-of-the-art spectrum generators dedicated just to the MSSM and NMSSM [223]. The RGEs are solved numerically at the two-loop level and the mass spectrum is calculated at one loop. Both codes have the option to include the known two-loop corrections [224–229] to the Higgs masses in the MSSM and NMSSM, which may, depending on the model, provide a good approximation of the dominant corrections. `SPheno` can also calculate the full two-loop corrections to the Higgs masses in the gaugeless limit at zero external momentum [230, 231]. `FlexibleSUSY` has an extension to calculate the two-loop Higgs mass corrections using the complementary effective field theory approach, which is to be released very soon. `SPheno` makes predictions for important flavour observables, which have been not yet implemented in `FlexibleSUSY`. Of particular importance for the current study is that `SPheno` and `FlexibleSUSY` calculate the effective vertices for the diphoton and digluon couplings of the scalars, which can then be used by Monte-Carlo (MC) tools like `CalcHep` [232, 233] or `MadGraph` [234, 235]. Other numerical tools like `MicrOmegas`

[236], HiggsBounds [237, 238], HiggsSignals [239] or Vevacious [240] can easily be included in the framework.

These powerful packages provide a way to get a thorough understanding of the new models. The main goal of this work is to support the model builders and encourage them to use these tools. We provide several details about the features of the packages in the spirit of making this paper self-contained and bringing the reader unfamiliar with the tools to the level of knowledge necessary to use them. More information can be found in the manuals of each package. We have created a database of diphoton models in SARAH, by implementing 40 among those proposed in recent literature, which is now available to all interested researchers. For each model we have written model files to interface SARAH with SPheno and FlexibleSUSY.

Although in each case we have tried to check very carefully that we implement the model which has been proposed in the literature, it is of course possible that some details have been missed. The original authors of these models are encouraged to check the implementation themselves to satisfy that what we have implemented really does correspond to the model they proposed. In the description of some of the models we state cases where the model has problems or where we find difficulties for the proposed solution. This helps inform potential users about what they may see when running these models through the tools we are discussing here. *However especially in these cases we encourage the original authors to check what we have written and let us know if they disagree with any claim we make.*

This paper is long but modular, and each section is to a large extent self contained, so the reader can easily jump to the section of greater interest. We have structured it as follows:

- In Section 2, we give a list of common mistakes we have found in the literature and emphasise how they are easily avoided by using the tools. This provides the main motivation of this paper and we hope that other model builders will also see the necessity of using these packages.
- In Section 3, we discuss the basic features of SARAH, describing how one can use it to extract all analytical properties of the model and how to generate model files or source code for the numerical tools.
- In Section 4, we give an introduction to SPheno and FlexibleSUSY and explain how these codes can be easily interfaced with MC tools. We also discuss at some length the implementation of the diphoton and digluon effective vertices.

- In Section 5, we give an overview of the models which we have implemented in SARAH and briefly discuss their main features.
- In Section 6, we provide an explicit example of how to quickly work out the details of a model, analytically with SARAH and numerically with the other tools. For this purpose we extended a natural supersymmetric (SUSY) model to accommodate the 750 GeV resonance.
- We conclude in Section 7.
- We provide three appendices containing frequently asked questions (FAQs) aimed at further clarifying the use of the packages.

2 Motivation

Precision studies in high energy physics have reached a high level of automation. There are publicly available tools to perform Monte-Carlo studies at LO or NLO [241–246], many spectrum generators [220, 221, 247–258] for the calculation of pole masses including important higher order corrections, codes dedicated only to Higgs [259–262] or sparticle decays [263–265], and codes to check flavour [266–270] or other precision observables [271]. This machinery has been used in the past mainly for detailed studies of some promising BSM candidates, like the MSSM, NMSSM or variants of THDMs. There are two main reasons why these tools are usually the preferred method to study these models: (i) it has been shown that there can be large differences between the exact numerical results and the analytic approximations; (ii) writing private routines for specific calculations is not only time consuming but also error prone. On the other hand, the number of tools available to study the new ideas proposed to explain the diphoton excess is still limited. Of these tools, many are not yet widely used largely due to the community’s reluctance in adopting new codes. However, we think it is beneficial to adopt this new generation of generic tools like SARAH.

We noticed that several studies done in the context of the 750 GeV excess have overlooked important subtleties in some models, neglected important higher order corrections, or made many simplifying assumptions which are difficult to justify. Using generic software tools in this context can help address these issues: many simplifications will no longer be necessary and important higher order corrections can be taken into account in a consistent manner. In order to illustrate this we comment, in the following subsections, on several issues we became aware of when revisiting some of the results in the literature.

2.1 Calculation of the diphoton and digluon widths

2.1.1 The diphoton and digluon rates beyond leading order

A precise calculation of the diphoton rate is of crucial importance. In the validation process of this work, we identified several results in the literature that deviate, often by an order of magnitude or more, in comparison to our results [65, 178, 201]. Additionally we observed that in many cases there are important subtleties which we think are highly relevant.

First of all, the choice of the renormalisation scale of the running couplings appearing in the calculation. The majority of recent studies use the electromagnetic coupling at the scale of the decaying particle. However, one should rather use $\alpha_{em}(0)$, i.e. the Thompson limit (see for instance Refs. [272, 273]), in order to keep the NLO corrections under control. Taking this into account already amounts to an $\mathcal{O}(10\%)$ change of the diphoton rate compared to many studies in the literature. In addition, as we will discuss in Section 2.2.3, an important prediction of a model is the ratio $\text{Br}(S \rightarrow gg)/\text{Br}(S \rightarrow \gamma\gamma)$, where S is the 750 GeV scalar resonance. It is well known that the digluon channel receives large QCD corrections. If one neglects these corrections the ratio will be severely underestimated.

To demonstrate these effects we show in Fig. 1 the total decay width¹ of the singlet S as a function of the mass M_{F_1} and coupling Y_{F_1} for a simple toy model containing only the vector-like fermions Ψ_{F_1} , presented in Section 5.1. Table 1 contains benchmark points for the partial widths of the digluon and diphoton channels as well as the ratio of these two channels for both CP-even and CP-odd scalar resonances. This table contains the LO calculations performed using `SPheno` as a comparison to results previously shown in the literature [165]. We also show the partial widths including NLO corrections for the diphoton channel² and N³LO QCD corrections to the gluon fusion production as implemented in Section 4.4. The discrepancies between the LO calculations arise purely through the choice of the renormalisation scale for the gauge couplings. However, the NLO results clearly emphasise that loop corrections at the considered mass scales are the dominant source of errors. To our knowledge, these uncertainties have thus far not received a sufficiently careful treatment in the literature; we give further discussion of this (and the remaining uncertainty in the `SARAH` calculation) in Section 4.8.

¹Here, the total width is simply the sum of the diphoton and digluon channels ignoring small contributions from other sub-dominant channels.

²NLO corrections in the case of a CP-odd vanish in the limit $m_f \gg m_S$, see Section 4.4 for more detail.

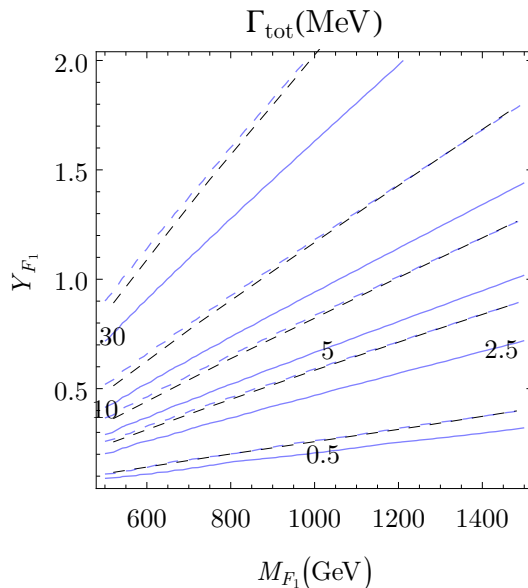


Figure 1. The approximate total width (sum of the diphoton and digluon channels) of S as a function of the coupling Y_{F_1} and the mass m_{F_1} of the vector-like particle F_1 , calculated using SPheno (blue) at LO (dashed) and NLO (solid). The black-dashed contours are the results of the LO calculation from Ref. [165]. Here we assume a single generation of vector-like quarks.

2.1.2 Constraints on a large diphoton width

In order to explain the measured signal, one needs a large diphoton rate of $\Gamma(S \rightarrow \gamma\gamma)/M_S \simeq 10^{-6}$ assuming a narrow width for S , while for a large width one requires $\Gamma(S \rightarrow \gamma\gamma)/M_S \simeq 10^{-4}$ [114]. In weakly-coupled models there are three different possibilities to obtain such a large width:

1. Assuming a large Yukawa-like coupling between the resonance and charged fermions
2. Assuming a large cubic coupling between the resonance and charged scalars
3. Using a large multiplicity and/or a large electric charge for the scalars and/or fermions in the loop

However, all three possibilities are also constrained by very fundamental considerations, which we briefly summarise in the following.

2.1.2.1 Large couplings to fermions A common idea to explain the diphoton excess is the presence of vector-like states which enhance the loop-induced coupling of a neutral scalar to two photons or two gluons. This led some authors to consider

Model		Br($gg/\gamma\gamma$)	$\Gamma_{S \rightarrow gg}$ [MeV]	$\Gamma_{S \rightarrow \gamma\gamma}$ [MeV]
Ψ_{F_1}	Ref. [165] LO	11.62/-	6.74/-	0.58/-
	SPheno LO	13.47/12.22	6.78/14.27	0.50/1.17
	SPheno NLO	23.27/20.27	11.04/23.71	0.47/1.17
Ψ_{F_2}	Ref. [165] LO	24.42/-	15.14/-	0.62/-
	SPheno LO	28.32/25.70	15.26/32.12	0.54/1.25
	SPheno NLO	48.93/42.67	24.85/52.34	0.51/1.25
Ψ_{F_3}	Ref. [165] LO	33.80/-	6.76/-	0.20/-
	SPheno LO	39.20/35.56	6.78/14.27	0.17/0.40
	SPheno NLO	67.72/59.06	11.04/23.71	0.16/0.40
Ψ_{F_4}	Ref. [165] LO	49.84/-	14.95/-	0.30/-
	SPheno LO	57.80/52.44	15.26/32.12	0.26/0.61
	SPheno NLO	99.85/87.09	24.85/53.34	0.25/0.61
Ψ_{F_5}	Ref. [165] LO	150.0/-	1.50/-	$10.0 \times 10^{-3}/-$
	SPheno LO	177.0/160.6	1.70/3.57	$9.58 \times 10^{-3}/22.22 \times 10^{-3}$
	SPheno NLO	305.8/266.7	2.76/5.93	$9.03 \times 10^{-3}/22.22 \times 10^{-3}$
Ψ_{F_6}	Ref. [165] LO	390.0/-	7.80/-	$2.00 \times 10^{-2}/-$
	SPheno LO	453.2/411.1	6.78/14.27	$1.50 \times 10^{-2}/3.47 \times 10^{-2}$
	SPheno NLO	782.8/682.8	11.04/23.71	$1.41 \times 10^{-2}/3.47 \times 10^{-2}$

Table 1. Branching fraction ratio, as well as the partial decay widths for the digluon and diphoton channels for the toy model (Section 5.1) containing only the relevant vector-like fermion pair Ψ_{F_i} . The above values are for the benchmark points $Y_{F_i} = 1$ and $m_{F_i} = 1$ TeV, where the values are for a CP-even/CP-odd scalar resonances, respectively. The SPheno NLO calculation includes N³LO corrections for the digluon channel, while the diphoton decay width is calculated at NLO and LO for a CP-even and odd scalar respectively.

Yukawa-like couplings of the scalar to the vector-like fermions larger than $\sqrt{4\pi}$, which is clearly beyond the perturbative regime³. Nevertheless, a one-loop calculation is used in these analyses to obtain predictions for the partial widths [208], despite being in a non-perturbative region of parameter space.

Moreover, even if the couplings are chosen to be within the perturbative regime at the scale $Q = 750$ GeV, they can quickly grow at higher energies. This issue of a Landau

³This diphoton excess could be triggered by strong interactions. Of course, in this case one cannot use perturbative methods to understand it.

pole has been already discussed to some extent in the literature [22, 36, 114, 124, 204, 205], and one should ensure that the model does not break down at unrealistic small scales.

2.1.2.2 Large couplings to scalars One possibility to circumvent large Yukawa couplings is to introduce charged scalars, which give large loop contributions to the diphoton/digluon decay. A large cubic coupling between the charged scalar and the 750 GeV one does not lead to a Landau pole for the dimensionless couplings because of dimensional reasons. However, it is known that large cubic couplings can destabilize the scalar potential: if they are too large, the electroweak vacuum could tunnel into a deeper vacuum where $U(1)_{\text{em}}$ gauge invariance is spontaneously broken, depending on the considered scenario. The simplest example with such a scenario is the SM, extended by a real scalar S and a complex scalar X with hypercharge Y . The scalar potential of this example is

$$V \supset \kappa S|X|^2 + \frac{1}{2}M_2 S^2 + M_X|X|^2 + \dots \quad (2.1)$$

In Fig. 2 the dependence of the diphoton partial width as a function of κ and M_X is shown, and the stability of the electroweak potential as well as the life-time of its ground state is checked with `Vevacious` and `CosmoTransitions`. For more details

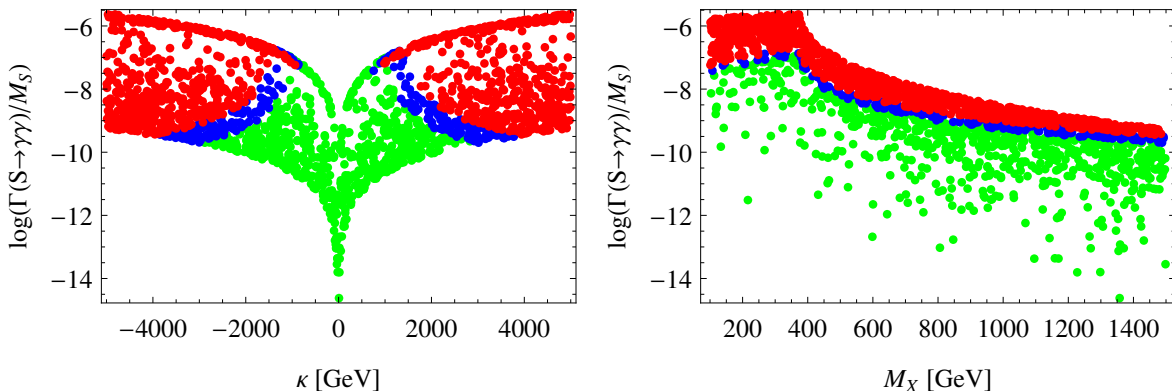


Figure 2. $\Gamma(S \rightarrow \gamma\gamma)/M_S$ as a function of κ (left) and M_X (right). Green points have a stable vacuum, blue points have a meta-stable but long-lived vacuum, while for the red ones it decays in a short time, in comparison to cosmological time scales, with a survival probability below 10%. The hypercharge of X was set to $Y = 1$.

about vacuum stability in the presence of large scalar cubic terms, we refer to Ref. [204]. The overall conclusion of [204] is that the maximal possible diphoton width, even when allowing for a meta-stable but sufficiently long-lived electroweak vacuum, is not much larger than in the case of vector-like fermions when requiring that the model is

perturbative up to the Planck scale. It is therefore essential to perform these checks when studying a model that predicts large cubic scalar couplings.

2.1.2.3 Large multiplicities To circumvent large Yukawa or cubic couplings, other models require a large number of generations of new BSM fields and/or large electric charges. As a consequence the running of the $U(1)_Y$ gauge coupling, g_1 , gets strongly enhanced well below the Planck scale. Moreover, even before reaching the Landau pole, the model develops large (eventually non-perturbative) gauge couplings. This implies an enhancement of Drell-Yan processes at the LHC, with current data already setting stringent constraints and potentially excluding some of the models proposed to explain the diphoton excess [125, 274]. For general studies on running effects in the context of the diphoton excess see [22, 36, 114, 124, 205]. We briefly discuss dramatic examples of this class of models proposed in Refs. [157] and [193], which feature approximately ~ 100 and 6000–9000 generations of doubly-charged scalar fields respectively. In the model of Ref. [193] the SM particle content is enlarged by a vector-like doubly-charged fermion E , a Majorana fermion N_R , a singlet scalar S , a singly-charged scalar h^+ and N_k generations of the doubly-charged scalar field k^{++} . At the one-loop level the running of g_1 is governed by the renormalisation group equation (RGE)

$$\frac{dg_1}{dt} = \beta_{g_1} = \frac{1}{16\pi^2} \beta_{g_1}^{(1)}, \quad (2.2)$$

where $t = \log \mu$, μ being the renormalisation scale, and

$$\beta_{g_1}^{(1)} = \frac{g_1^3}{10} (75 + 8 N_k) \quad (2.3)$$

is the one-loop β function. It is clear from Eq. (2.3) that a large value of N_k necessarily leads to a very steep increase of g_1 with the renormalisation scale, soon reaching a Landau pole. This is shown in Fig. 3, obtained by setting the masses of all the charged BSM states to $\mu_{\text{NP}} = 2.5$ TeV, which is already the largest mass considered in this analysis. The running up to μ_{NP} is governed by the SM RGEs, and the result for g_1 is displayed with a black dashed line. For scales above $\mu_{\text{NP}} = 2.5$ TeV, the contributions from BSM fields become effective. Fig. 3 shows that a Landau pole can be reached at relatively low energies once we allow for such large values of N_k . In fact, for $N_k = 9000$, we find that a Landau pole appears already at $\mu \simeq 2.6$ TeV. In this specific example the appearance of a Landau pole below 10^{16} GeV is unavoidable as soon as $N_k > 10$, as shown in Table 2.

2.1.3 How do the tools help?

The tools which we describe in more detail in the following sections can help to address all the above issues:

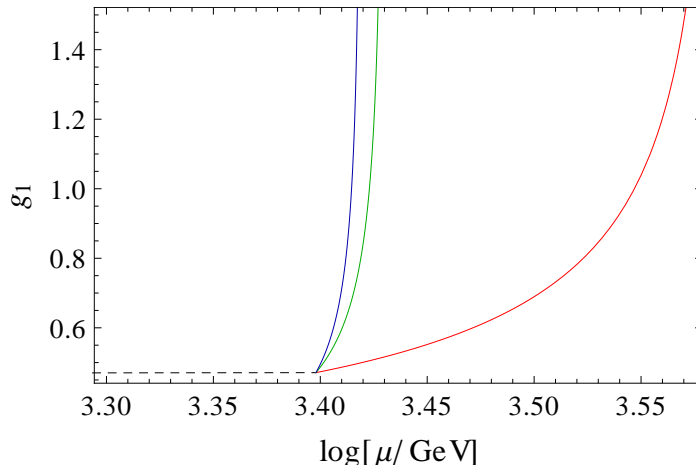


Figure 3. Running of the $U(1)_Y$ gauge coupling, g_1 , in the model presented in [193] for $N_k = 1000$ (red), $N_k = 6000$ (green) and $N_k = 9000$ (blue). The black dashed line corresponds to the SM running below $\mu_{NP} = 2.5$ TeV.

N_k	μ_{Landau}
10	$2 \cdot 10^{13}$ GeV
100	$1.2 \cdot 10^5$ GeV
1000	3.8 TeV
6000	2.7 TeV
9000	2.6 TeV

Table 2. Energy scale at which a Landau pole in g_1 appears as a function of N_k in the model of Ref. [193].

1. **FlexibleSUSY** and **SPheno** can calculate the diphoton and digluon rate including important higher order corrections.
2. Using the effective vertices calculated by **FlexibleSUSY/SPheno** and the interface to **CalcHep** or **MadGraph**, the gluon-fusion production cross-section of the 750 GeV mediator can be calculated numerically and one does not have to rely on analytical (and sometimes erroneous⁴) approximations.
3. **SARAH** calculates the RGEs for a model which can be used to check for the presence

⁴It is straightforward to see that the analytical estimate of the production cross section in Eq. (10) of Ref. [201] (which has also been used by Ref. [178]) is wrong by orders of magnitude: consider the production of a SM-like scalar H with $m_H = 750$ GeV via top-loops. Then, the factor $h_F^2 m_t^2 / m_F^2$ drops out and one obtains $\sigma = 1440$ pb which is too large by roughly three orders of magnitude [275].

of Landau pole.

4. `Vevacious` can be used to check the stability of the scalar potential.

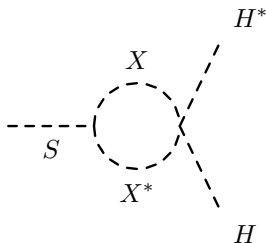
2.2 Properties of the 750 GeV scalar

2.2.1 Mixing with the SM Higgs

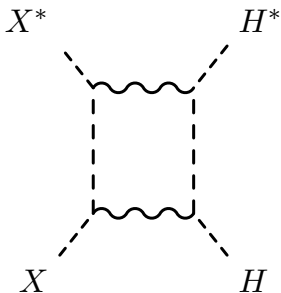
It is often assumed that S , although it is a CP-even scalar, does not mix with the SM-like Higgs h . However, if this is done in a very ad hoc way and not motivated by any symmetry, this assumption will not hold when radiative corrections are taken into account. To see this, one can consider, for example, the scalar potential

$$\begin{aligned}
 V = & \frac{1}{2}M_S S^2 + M_X |X|^2 + \mu^2 |H|^2 + \kappa S |X|^2 \\
 & + \lambda_S S^4 + \lambda_{SX} S^2 X^2 + \lambda_{HX} |H|^2 |X|^2 + \lambda |H|^4,
 \end{aligned}
 \tag{2.4}$$

where H is the SM Higgs $SU(2)_L$ doublet, which contains the SM Higgs h . This potential in principle has all ingredients to get a large diphoton decay of S via a loop involving the charged scalar X . Note, however, that the potentially dangerous term $\kappa_H S |H|^2$ has been omitted. One can see immediately that this term would be generated radiatively by the diagram below.



Note that it is also not possible to circumvent this decay by forbidding the λ_{HX} term: since H and X are charged under $SU(2)_L \times U(1)_Y$, also the $\lambda_{HX} |H|^2 |X|^2$ term would be generated radiatively via diagrams like



Such a mixing has important consequences since it opens the decay channels $S \rightarrow hh$ and $S \rightarrow ZZ$, $S \rightarrow W^+W^-$ at tree-level, which are tightly constrained.

Another possibility is that all terms allowed by symmetries are taken into account, but very special relations among them are imposed like in Ref. [185]. When these relations hold, the above-mentioned tree-level decays in SM particles would cancel. However, as long as there is no symmetry behind these relations, they will not be invariant under RGE running. Therefore, immediately the question arises how large the tuning among the parameters must be to have a point that fulfils all constraints. To illustrate this issue, we make small variations in the couplings λ_{H3} and λ_{36} , which cause non-vanishing tree-level couplings between S and the massive vector bosons, and check for which size of the deviations the condition $\text{Br}(S \rightarrow W^+W^-)/\text{Br}(S \rightarrow \gamma\gamma) < 20$ holds. The result is shown in Fig. 4. Here, the diphoton rate was maximized by setting the masses of the vector-like fields to 375 GeV and using a Yukawa coupling of $O(1)$. In principle, one could try to check what this means for the scale dependence of these

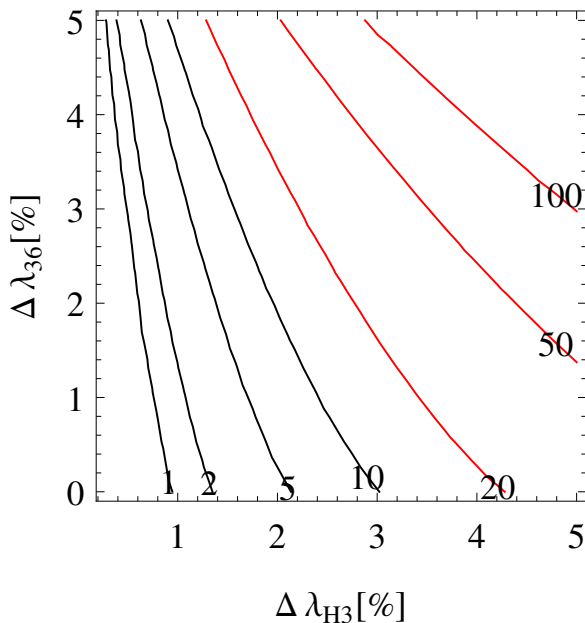


Figure 4. The impact on small deviations from the parameter relations assumed in Ref. [185]. Specifically, the y-axis axis represents the deviation in the coupling λ_{36} , while the x-axis represents deviations in the coupling λ_{H3} . The contour lines show the ratio $\text{Br}(S \rightarrow W^+W^-)/\text{Br}(S \rightarrow \gamma\gamma)$. The red line indicates where the model would already be in conflict with current collider limits.

ratios by calculating the RGEs. However, this cannot really be done for this setup since one obtains the following condition from the relations which have been imposed:

$\lambda_{03} = f_Y^2 \frac{M_S^2}{M_F^2}$, i.e. $\lambda_{03} = 4f_Y^2$ is needed to maximize the diphoton branching ratio. Thus, f_Y of $\mathcal{O}(1)$ immediately leads to a huge quartic coupling.

Thus, in general, it is very difficult to justify the assumption that the 750 GeV particles do not mix with the SM-like Higgs if there is no fundamental symmetry to forbid this mixing. However, this can already be forbidden using the CP symmetry: the mentioned problems can be circumvented in models where the diphoton excess stems from a CP-odd particle. While, in the case of a CP-even particle, it is crucial to include the mixing effects and to check at least how large the tuning in parameters must be.

2.2.2 To VEV or not to VEV?

The possibility that the new scalar receives a vacuum expectation value (VEV) is also often neglected. However, as we have just discussed, it often occurs that a H – S mixing will be induced, at least radiatively, in many models. Such radiative effects would immediately lead to a non-zero VEV for the new scalar. Even in cases where there is a symmetry which prevents a mixing with the SM Higgs, the 750 GeV particle will still receive a VEV if it is a CP-even scalar. This arises due to the introduced couplings to charged particles which are necessary to allow diphoton and digluon decays. More specifically, these introduced couplings will generate one-loop tadpole diagrams for S as shown in Fig. 5. Thus, the tadpole equation reads at the one-loop level

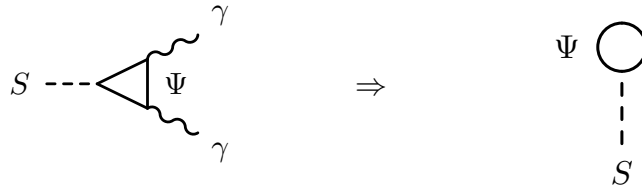


Figure 5. Tadpole terms for S generated at one-loop level.

$$\frac{\partial V^{(1L)}}{\partial v_S} = T^{(1L)} = T^{(T)} + \delta T = 0, \quad (2.5)$$

where $T^{(T)}$ is the tree-level tadpole, given by

$$\frac{\partial V^{(T)}}{\partial v_S} = T^{(T)} = c_1 v_S + c_2 v_S^2 + c_3 v_S^3 = 0. \quad (2.6)$$

Here, we have parametrised the tree-level expression so that the general form has the solution $v_S = 0$. One finds in general that the one-loop corrections are

$$\delta T = \begin{cases} \kappa A(M_X^2) & \text{for a scalar loop,} \\ 2Y M_\Psi A(M_\Psi^2) & \text{for a fermion loop,} \end{cases} \quad (2.7)$$

with $A(x^2) = \frac{1}{16\pi^2}x^2 [1 + \log(Q^2/x^2)]$. Taking M_Ψ, κ, M_X of the order 1 TeV, results in a VEV which is naturally of order $1 \text{ TeV}^3/(16\pi^2 c_1)$. As a result, the simplifying assumption that v_S vanishes is in general hard to justify. Therefore, it is important to check how the conclusions made about the model depend on this assumption. Here, the tools discussed in the following sections can really help, as including the non-vanishing v_S is no more difficult than assuming the VEV vanishes.

2.2.3 Additional decay channels

Many analyses concentrate only on the decay $S \rightarrow \gamma\gamma$ and completely neglect other potential decay channels. However, there are stringent constraints on the branching ratios of S into other SM final states, which are summarised in Table 3. Thus, any

$e^+e^- + \mu^+\mu^-$	$\tau^+\tau^-$	$Z\gamma$	ZZ	Zh	hh	W^+W^-	$t\bar{t}$	$b\bar{b}$	jj	inv.
0.6	6	2	6	10	20	20	300	500	1300	400

Table 3. Limits on $\Gamma(S \rightarrow X)/\Gamma(S \rightarrow \gamma\gamma)$ assuming a production of S via gluon fusion or heavy quarks. Values are taken from Ref. [114].

model which tries to explain the excess via additional coloured states in the loop must necessarily worry about limits from dijet searches [276]. Therefore, an accurate calculation of the digluon decay rate is a necessity. As an example that illustrates why both additional channels and the diphoton/digluon width calculation are important we consider the model presented in Refs. [48, 99] and considered in more detail here in Sec. 5.2.1.2.

This model extends the SM with a singlet and a scalar $SU(2)$ -doublet colour octet. As an approximation the ratio of the singlet decays to gluons and to photons is

$$\frac{\Gamma(S \rightarrow gg)}{\Gamma(S \rightarrow \gamma\gamma)} \simeq \frac{9 \alpha_s^2}{2 \alpha^2}. \quad (2.8)$$

In [48] this is quoted as $\simeq 750$; before any NLO corrections are applied, we find 700. However, once we include all of the N³LO corrections this is enhanced to 1150, near the bound for constraints on dijet production at 8 TeV and significantly squeezing the parameter space of the model.

Additionally in many works we observed that potential decay channels of the resonance were missed. For instance in Ref. [108], the authors, who considered the Georgi-Machacek model [277], missed the decay of the scalar into $W^\pm H^\mp$, which can be the dominant mode when kinematically allowed.

2.2.4 How do the tools help?

Many of the assumptions which we criticised were made to keep the study simple. However, when using the public tools presented in the next two sections, there is no need for these simplifying assumptions:

1. `SARAH` automatically calculates all expressions for the masses and vertices, no matter how complicated they are.
2. `FlexibleSUSY` and `SPheno` give numerical predictions for the mass spectrum and the mixing among all states including higher order corrections.

Thus, for the user the study becomes no more difficult when he/she drops all simplifying assumptions but considers the model in full generality. Moreover, there is no chance to miss important effects in the decays of the new scalar:

1. As outlined above and described in detail in Section 4.2.2, `FlexibleSUSY` and `SPheno` calculate the diphoton and digluon rate very accurately
2. `SPheno` does calculate all other two body decays⁵ of the scalar. This makes it impossible to miss any channel.

2.3 Considering a full model

2.3.1 Additional constraints in a full model

There are several studies which extend an already existing model by vector-like states and then assume that this part of the model is decoupled from the rest. When this assumption is made it is clear that the results from toy models, with the minimal particle content will be reproduced. However, it is often not clear if this decoupling can be done without invoking specific structures in the choice of parameters, and if these assumptions hold at the loop level.

On the other hand, if model-specific features are used to explain the diphoton excess, it is likely that there will be important constraints on the model coming from other sectors. For instance, there might be bounds from flavour observables, dark matter, Higgs searches, neutrino mixing, electroweak precision observables, searches for BSM particles at colliders, and so on. All of that has to be checked to be sure that any benchmark point presented is indeed a valid explanation for all observations. Such a wide range of constraints is much easier to address by making exhaustive use of tools which provide a high level of automation.

⁵Even three-body decays into another scalar and two fermions can be calculated with `SPheno`.

2.3.2 Theoretical uncertainties of other predictions

Even if the attempts are made to include the effects of the new states on other sectors of the model, it is important to be aware that there are large uncertainties involved in certain calculations. If the level of uncertainty is underestimated, this can have an impact on what is inferred from the calculation. The large uncertainty in a LO calculation of the diphoton and digluon rate has already been addressed in Section 2.1.1. However, there are also other important loop corrections especially in SUSY models: the accurate calculation of the Higgs mass is a long lasting endeavour where for the simplest SUSY models even the dominant three-loop corrections are partially tackled [278]. The current ball-park of the remaining uncertainty is estimated to be 3 GeV.

However, it is clear that the MSSM cannot explain the excess, hence it must be extended. A common choice is to add additional pairs of vector-like superfields together with a gauge singlet, see Section 6. These new fields can also be used to increase the SM-like Higgs mass. However, this will in general also increase the theoretical uncertainty in the Higgs mass prediction, because these new corrections are not calculated with the same precision as the MSSM corrections. For instance, Ref. [105] has taken into account the effect of the new states on the SM-like Higgs. There, they use a one-loop effective potential approach considering the new Yukawa couplings to be $\mathcal{O}(1)$ or below, while also including the dominant two-loop corrections from the stop quark. They assumed that including these corrections is sufficient in order to achieve an uncertainty of 2 GeV in the Higgs mass prediction. One can compare their results encoded in Fig. 7 of Ref. [105] with a calculation including, in addition to the corrections taken into account in the paper, momentum dependence and electroweak corrections at the one-loop level, as well as the additional two-loop corrections arising from all the newly introduced states. These corrections can be important, as was shown for instance in Ref. [279]. The result of the comparison is shown in Fig. 6. We find a similar behaviour, but still there are several GeV difference between both calculations. For $\kappa_{10} = 0.8$ and $X_t = 4$, the point would be within the interesting range for $m_h = [123, 127]$ GeV, while the more sophisticated calculation predicts a mass below 120 GeV. Thus, the assumed uncertainty of 2 GeV in Ref. [105], which would even be optimistic in the MSSM, is completely unrealistic without including all the aforementioned higher order corrections.

2.3.3 How do the tools help?

The tools help to ensure that one really considers all aspects of a full model:

1. All masses of the model are calculated with high accuracy: `FlexibleSUSY` and `SPheno` include the full, one-loop correction to all fields in a model, while `SPheno`

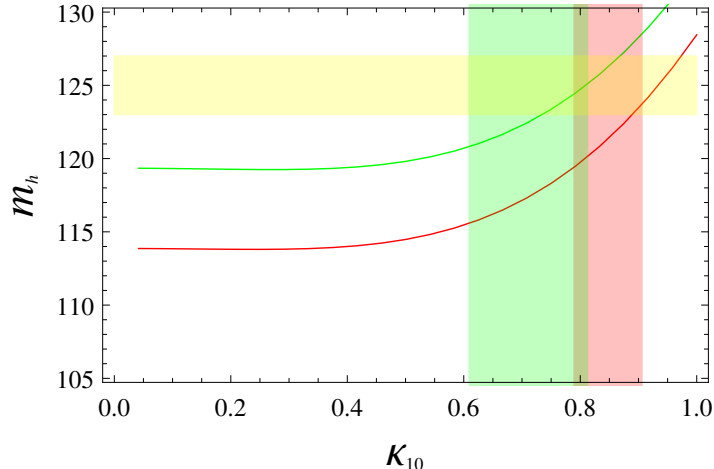


Figure 6. Comparison of the two-loop Higgs mass calculation of Ref. [105] with the results obtained by `SPheno`. The parameters are those of Fig. 7 in Ref. [105] and we fixed $X_{\kappa_{10}} = 0$. The lines are the results from `SPheno`, while the green and red shades areas are the ranges of κ_{10} which predict $m_h = [123, 127]$ GeV according to Ref. [105]. Red takes $X_t = 4$ and green $X_t = 2$, where X_t is defined in Eq. (9) of the reference.

covers even the dominant two-loop corrections introduced by adding new states.

2. `SPheno` makes predictions for all important flavour observables in the model.
3. A link to `MicrOmegas` provides the possibility to calculate the dark matter relic density.
4. The interface to `HiggsBounds` and `HiggsSignals` offers the possibility to check all constraints from Higgs searches and to check if the results for the SM-like Higgs can be reproduced.

3 Using SARAH to understand a model

3.1 General

One of the reasons that makes high energy particle physics an exciting field is the vast amount of experimental data available. When proposing a model one first has to check its self consistency, checking for instance the particle mass spectrum and vacuum stability requirements. Then it has to be tested against data related to collider searches, flavour observables, dark matter observations and Higgs measurements. A lot of effort has been devoted to developing an arsenal of specific tools to explore these quantities

with high precision for specific classes of models, such as the MSSM, the THDM and the NMSSM to some extent. However, none of them, in their simplest versions, can explain the diphoton excess. For the time being there is no specific model which is clearly preferred over others as an explanation of the excess, as reflected by the large variety of models that different authors have proposed, and it would be impractical to repeat the process of developing a code for each one of them. In the absence of a dedicated tool, the alternative is often to resort to approximations or just to leading order expressions, as described in the previous section, in which case the analysis (in particular for more complicated models) is of limited value.

Luckily, a dedicated powerful tool already exists. It is the `Mathematica` package `SARAH` [214–219], which can perform the most advanced quantum field theory computations and apply them generically to any given model. `SARAH` has been optimised for an easy, fast, and exhaustive study of renormalisable BSM models: not only can it calculate all the relevant quantities within a given model analytically – it also provides routines to export the derived information in order to use it for numerical calculations with dedicated tools. `SARAH` can be used for SUSY and non-SUSY models to write model files for `CalcHep/CompHep` [232, 233], `FeynArts/FormCalc` [280, 281], `WHIZARD/O’Mega` [282, 283], as well as in the `UFO` format [284] which can be handled for instance by `MadGraph 5` [234], `GoSam` [285], `Herwig++` [286–288], and `Sherpa` [245, 289, 290]. The modules created by `SARAH` for `SPheno` calculate the full one-loop and partially two-loop corrected mass spectrum, branching ratios and decay widths of all states, and many flavour and precision observables thanks to the `FlavorKit` [291] functionality. Moreover, an easy link to `HiggsBounds` [237, 238] and `HiggsSignals` [239] exists. One can as well use another tailor-made spectrum generator, `FlexibleSUSY` [222], which can handle both SUSY and non-SUSY models generated with `SARAH`. Finally, `SARAH` can also produce model files for `Vevacious` [240], which is a tool dedicated to studying vacuum stability.

3.2 Models supported by SARAH

`SARAH` is optimised for handling a wide range of SUSY and non-SUSY models. The basic idea of `SARAH` is to give the user the possibility to implement models in an easy, compact and straightforward way. The user simply has to declare symmetries, particle content, and the (super)potential. All steps to derive the full Lagrangian for the gauge eigenstates from this information are then fully automatised. But this is not the final aim: usually one is interested in the mass eigenstates after spontaneous gauge symmetry breaking. To perform the necessary rotations to the new eigenstates, the user has to provide additional information: (i) definition of the fields which develop VEVs, and (ii) definitions of the fields which mix. Using this information, all necessary re-definitions

and field rotations are performed by SARAH. In addition, gauge fixing terms for the new eigenstates are derived and ghost interactions are added. Plenty of information can be derived by SARAH for all states in the model, as explained in Section 3.5. Before moving into it, we elaborate on the kind of models and features supported by SARAH.

3.3 Supported models and features

3.3.1 Global symmetries

SARAH can handle an arbitrary number of global symmetries which are either Z_N or $U(1)$ symmetries. In a SUSY model one can also impose a continuous R -symmetry, $U(1)_R$, at the level of the superpotential. However, SARAH will then generate automatically the scalar potential including soft trilinear terms that do not respect the $U(1)_R$. The user has two options: either add “AddTterms = False” to the SARAH model file to forbid the automatic generation of the soft trilinear terms, or set such terms to zero manually within the input files for the spectrum generators. SARAH can also handle approximate symmetries: if the user specifies terms in the Lagrangian/superpotential which violate a global symmetry, the terms will not be forbidden but a warning will be printed.

3.3.2 Gauge sector

Gauge groups SARAH is not restricted to the SM gauge sector, but many more gauge groups can be defined. To improve the power in dealing with gauge groups, SARAH has linked routines from the Mathematica package `Susyno` [292]. SARAH, together with `Susyno`, takes care of all group-theoretical calculations: it calculates the Dynkin and Casimir invariants, derives the needed representation matrices as well as the generalised Clebsch-Gordan coefficients. For all Abelian groups one can also give a GUT normalisation; these factors usually arise from considerations about embedding a model in a larger symmetry group such as $SU(5)$ or $SO(10)$.

Gauge kinetic mixing With more than one Abelian gauge group, terms of the form

$$\mathcal{L} = -\frac{1}{4}\kappa F_{\mu\nu}^A F^{B,\mu\nu}, \quad A \neq B, \quad (3.1)$$

are allowed, where $F^{\mu\nu}$ are the field strength tensors of two different Abelian groups A , B [293]. κ is in general an $n \times n$ matrix if n Abelian groups are present. SARAH fully includes the effects of kinetic mixing for any number of Abelian groups by performing a rotation to bring the field strength to a diagonal form. The kinetic mixing is then absorbed into the covariant derivatives, which take the form

$$D_\mu \phi = \left(\partial_\mu - i \sum_{x,y} Q_\phi^x g_{xy} V_y^\mu \right) \phi. \quad (3.2)$$

The indices x, y run over all $U(1)$ groups, and g_{xy} are the entries of the gauge coupling matrix G which now also contains mixed gauge couplings. Gauge kinetic mixing is not only included in the interactions with vector bosons, but also in the derivation of the D -terms and in the gaugino interactions for SUSY models.

3.3.3 Matter sector

One can define up to 99 matter fields in a single model in **SARAH**. Each one of them can come with an arbitrary number of generations and can transform as any irreducible representation with respect to the defined gauge groups.

Supersymmetric models The matter interactions in SUSY models are usually fixed by the superpotential and the soft SUSY-breaking terms. **SARAH** takes as input the renormalisable terms in the superpotential

$$W = c_L L_i \hat{\phi}_i + c_M M^{ij} \hat{\phi}_i \hat{\phi}_j + c_T Y^{ijk} \hat{\phi}_i \hat{\phi}_j \hat{\phi}_k \quad (3.3)$$

which the user has to write in the model file, and automatically generates the corresponding soft-breaking terms

$$L_{SB,W} = c_L t_i \phi_i + c_M B^{ij} \phi_i \phi_j + c_T T^{ijk} \phi_i \phi_j \phi_k + \text{h.c.} \quad (3.4)$$

c_L, c_M, c_T are real coefficients, while the linear, bilinear, and trilinear parameters are treated by default in the most general way by taking them as complex tensors of appropriate order and dimension. If identical fields are involved in the same coupling, **SARAH** also derives the symmetry properties for the parameter.

In recent years models with Dirac gauginos have been largely explored. They feature mass terms of the form $m_D^{\hat{\phi}_i A} \lambda_A \psi_i$, where λ_A is a gaugino and ψ_i the fermionic component of a chiral superfield $\hat{\phi}_i$ in the adjoint representation of the gauge group A . In addition, there are new D -term couplings (see e.g. [294]). To generate Dirac mass terms for all the gauginos, these models always come with an extended matter sector, including at least one singlet, one triplet under $SU(2)$, and one octet under $SU(3)$. Furthermore, these models generate new structures in the RGEs [295]. All these are fully supported in **SARAH**.

Non-Supersymmetric models For non-supersymmetric models, **SARAH** supports all general, renormalisable Lagrangians of the form

$$L = m_{ij}^2 \phi_i \phi_j + \frac{1}{3} \kappa_{ijk} \phi_i \phi_j \phi_k + \frac{1}{4} \lambda \phi_i \phi_j \phi_k \phi_l + M_{ij}^F \psi_i \psi_j + Y_{ijk} \phi_i \psi_i \psi_j \quad (3.5)$$

for scalars ϕ_i , and Weyl fermions ψ_j . The Lagrangian needs to be defined by the user in the model file. Note, that we have omitted a tadpole term, $t\phi$, for a gauge singlet, as it can always be absorbed in a shift of ϕ .

3.4 Checks of implemented models

After the initialisation of a model, `SARAH` provides functions to check its (self-)consistency:

- Check for gauge anomalies, and mixed gauge/gravity anomalies;
- Check for Witten anomalies [296];
- Check if all terms in the (super)potential are in agreement with all global and gauge symmetries;
- Check if terms allowed by all symmetries are missing in the (super)potential;
- Check if additional mass eigenstates can mix in principle;
- Check if all mass matrices are irreducible.

In addition, `SARAH` performs other formal checks. For instance, it checks if the number of Particle Data Group numbers for a given family of particles fits to the number of generations for each particle class, if `LATEX` names are defined for all particles and parameters, and if the position in a Les Houches spectrum file is defined for all parameters.

3.5 Analytical calculations performed by `SARAH`

The full power of `SARAH` can be unleashed on exhaustive numerical analyses via the dedicated interfaces to other tools, discussed in the next sections. However, since `SARAH` itself is a `Mathematica` package, it is capable of many analytical computations beyond the derivation of the Lagrangian. Here we list some of them.

3.5.1 Tree-level properties

Tadpole equations During the evaluation of a model, `SARAH` calculates ‘on the fly’ all the minimisation conditions of the tree-level potential, the so-called tadpole equations.

Masses `SARAH` calculates the mass matrices for the states which are rotated to mass eigenstates. In addition, it calculates the masses of states for which no field rotation has taken place.

Vertices `SARAH` has functions to extract in an efficient way all tree-level vertices from the Lagrangian. These vertices are saved in different `Mathematica` arrays according to their generic type.

3.5.2 Renormalization group equations

SARAH calculates the full two-loop RGEs in SUSY and non-SUSY models including the full CP and flavour structure. For this purpose, it makes use of the most sophisticated generic calculations available in the literature.

SUSY RGEs The calculation of the SUSY RGEs is mainly based on Ref. [297], which however did not cover all possible subtleties which can appear in SUSY models. **SARAH** has implemented also results from more recent literature:

- In the case of multiple $U(1)$ gauge groups, gauge-kinetic mixing can arise if the groups are not orthogonal. Substitution rules to translate the results of Ref. [297] to those including gauge kinetic mixing were presented in Ref. [298] and are used by **SARAH**;
- The calculation of the RGEs in the presence of Dirac gauginos is based on Ref. [295];
- The results of Refs. [299, 300] are used to obtain the gauge dependence in the running of the VEVs.

Non-SUSY RGEs **SARAH** uses the expressions of Refs. [301–304] for the calculation of the RGEs in a general quantum field theory. These results are completed by Ref. [305] to cover gauge kinetic mixing and again by Refs. [299, 300] to include the gauge-dependence of the running VEVs also in the non-SUSY case.

3.5.3 One- and two-loop corrections to tadpoles and self-energies

One-loop corrections **SARAH** calculates the analytical expressions for the one-loop corrections to the tadpoles and the one-loop self-energies for all the particles. For states which are a mixture of several gauge eigenstates, the self-energy matrices are calculated. The calculations are performed in the $\overline{\text{DR}}$ scheme using 't Hooft gauge for SUSY models. In the case of non-SUSY models **SARAH** switches to the $\overline{\text{MS}}$ scheme.

Two-loop corrections It is even possible to go beyond one loop with **SARAH** and to calculate two-loop contributions to the self-energies of real scalars. There are two equivalent approaches implemented in the **SPheno** interface of **SARAH** to perform these calculations: an effective potential approach and a diagrammatic approach with vanishing external momenta. More details about these calculations are given in Section 4.1.1.

4 Spectrum calculation, Monte-Carlo studies, and more

As mentioned in the last section, **SARAH** can use the analytical information derived about a model and pass it to other tools. We give in the following an overview about the different possibilities.

4.1 SPheno

SARAH writes Fortran source code for **SPheno** [220, 221] using the derived information about the mass matrices, tadpole equations, vertices, loop corrections and RGEs for the given model. With this code the user gets a fully functional spectrum generator for the model of their choice. The features of a spectrum generator created in this way are

- Full two-loop running of all parameters
- One-loop corrections to all masses
- Two-loop corrections to Higgs masses
- Complete one-loop thresholds at M_Z
- Calculation of flavour and precision observables at full one-loop level
- Calculation of decay widths and branching ratios for two- and three body decays
- Interface to **HiggsBounds** and **HiggsSignals**
- Estimate of electroweak Fine-Tuning
- Prediction for LHC cross sections for all neutral scalars

4.1.1 Mass calculation with SPheno

Threshold corrections For a precise calculation of the masses it is necessary to have an accurate input for all parameters which enter the calculation. In general, the running SM parameters depend on the masses of the BSM states. This is due to the influence of the threshold scales, required to match the running parameters to the measured ones. The routines generated by **SARAH** perform a full one-loop matching in the given model to calculate the SM gauge and Yukawa couplings. This matching takes the constraints from the CKM matrix into account even if there are additional states which mix with the SM quarks.

One-loop shifts to pole masses The one-loop mass spectrum is calculated from the information about the one-loop self-energies and tadpole equations. The procedure is a generalisation of the one explained in detail for the MSSM in Ref. [306]. The main features are

- Any one-loop contribution in a given model to all fermions, scalars and vector bosons is included
- The full p^2 dependence in the loop integrals is included
- An iterative procedure is applied to find the on-shell masses $m(p^2 = m^2)$.

Two-loop shifts to Higgs pole masses SARAH can also generate Fortran code to calculate the two-loop corrections to the masses of the CP-even scalar states with SPheno⁶. The same approximations usually taken for the MSSM are also applied here: (i) all calculations are performed in the gaugeless limit, i.e. the electroweak contributions are dropped, and (ii) the momentum dependence is neglected. Using these routines, the theoretical uncertainty in the Higgs mass prediction for many models has been shrunk to the level of the MSSM. In general, there are two different techniques to calculate the two-loop corrections with SARAH–SPheno:

- **Effective potential calculation** [230]: SARAH makes use of the generic two-loop results for the effective potential given in Ref. [307]. To get the values for the two-loop self-energies and two-loop tadpoles, the derivatives of the potential with respect to the VEVs are taken numerically, as proposed in Ref. [308].
- **Diagrammatic calculation** [231]: A fully diagrammatic calculation for two-loop contributions to scalar self-energies with SARAH–SPheno became available with Ref. [231]. The advantage of the diagrammatic approach is that no numerical derivation is needed. This is now the default calculation.

The implementation of the two independent approaches provides a good possibility to double check results. It has been shown that these generic calculations can provide important two-loop corrections for the NMSSM which are not included in dedicated spectrum generators for the NMSSM [223, 309].

⁶At the moment, these calculations are just done in the $\overline{\text{DR}}$ scheme, but can be also provided for $\overline{\text{MS}}$ if necessary.

4.1.2 Decay widths and branching ratios

`SPheno` modules created by `SARAH` calculate all two-body decays for fermion and scalar states as well as for the additional gauge bosons. In addition, the three-body decays of a fermion into three other fermions, and of a scalar into another scalar plus two fermions are included.

In the scalar sector, possible decays into two particles are calculated at tree level. In case of two quarks in the final state, the dominant QCD corrections due to gluons are included [272]. In addition scalar decays into final states with off-shell gauge bosons (ZZ^* , WW^*) are included.

The loop-induced decays into two photons and gluons are calculated up to N³LO. More details about this are given in Section 4.4.

4.1.3 Flavour observables

The `SPheno` modules written by `SARAH` contain out-of-the-box routines to calculate many quark and lepton flavour violating observables:

- Lepton flavour violation:
 - $\text{Br}(\ell_i \rightarrow \ell_j \gamma)$, $\text{Br}(\ell_i \rightarrow \ell_j \ell_k \ell_k)$, $\text{Br}(Z \rightarrow \ell_i \ell_j)$
 - $\text{CR}(\mu - e, N)$ ($N=\text{Al, Ti, Sr, Sb, Au, Pb}$), $\text{Br}(\tau \rightarrow \ell P)$ (with $P=\pi, \eta, \eta'$)
- Quark flavour violation:
 - $\text{Br}(B \rightarrow X_s \gamma)$, $\text{Br}(B_{s,d}^0 \rightarrow \ell \bar{\ell})$, $\text{Br}(B \rightarrow s \ell \bar{\ell})$, $\text{Br}(K \rightarrow \mu \nu)$
 - $\text{Br}(B \rightarrow q \nu \nu)$, $\text{Br}(K^+ \rightarrow \pi^+ \nu \nu)$, $\text{Br}(K_L \rightarrow \pi^0 \nu \nu)$
 - $\Delta M_{B_s, B_d}$, ΔM_K , ϵ_K , $\text{Br}(B \rightarrow K \mu \bar{\mu})$
 - $\text{Br}(B \rightarrow \ell \nu)$, $\text{Br}(D_s \rightarrow \ell \nu)$

The calculation is based on the `FlavorKit` functionality [291], which makes use of the chain `FeynArts–SARAH–SPheno`. This provides a full one-loop calculation in a given model. In addition, this interface can be used to derive Wilson coefficients for new operators, and to calculate new observables with `SPheno` using the implemented coefficients.

4.1.4 Fine-Tuning

A widely used measure for the electroweak fine-tuning was proposed in Refs. [310, 311]

$$\Delta_{FT} \equiv \max \text{Abs}[\Delta_\alpha], \quad \Delta_\alpha \equiv \frac{\partial \ln M_Z^2}{\partial \ln \alpha} = \frac{\alpha}{M_Z^2} \frac{\partial M_Z^2}{\partial \alpha}. \quad (4.1)$$

Here, α is a set of independent parameters, and Δ_α^{-1} is a measure of the accuracy to which the parameters α must be tuned to obtain the correct VEV. The user can choose the set of parameters α in `SARAH`, and `SPheno` numerically calculates Δ_{FT} for that choice using the full two-loop RGEs from the GUT or SUSY breaking scale down to the electroweak scale.

4.2 FlexibleSUSY

`FlexibleSUSY` is a Mathematica package which uses the `SARAH`-generated expressions for the mass matrices, self-energies, tadpole equations, vertices and RGEs to create a C++ spectrum generator for both SUSY and non-SUSY models. The spectrum generators created with `FlexibleSUSY` have the following features:

- full two-loop running of all parameters
- three-loop running of all parameters in the SM and MSSM, except for the VEVs
- calculation of the pole mass spectrum at the full one-loop level
- partial two-loop corrections to the Higgs masses in the SM, SplitMSSM, MSSM, NMSSM, UMSSM and E₆SSM and partial three-loop corrections to the Higgs mass in the SplitMSSM
- complete one-loop and partial two-loop threshold corrections at the scale $Q = M_Z$ or $Q = M_t$
- calculation of the $h\gamma\gamma$ and hgg effective couplings at N³LO
- an interface to `GM2Calc` [271] in MSSM models without sfermion flavour violation

`FlexibleSUSY` aims to generate spectrum generators which are modular such that components can be easily reused or replaced. This means that it is quite easy to re-use the precision calculations in `FlexibleSUSY` spectrum generators for other purposes or add additional routines.

4.2.1 Mass calculation with FlexibleSUSY

Determination of the gauge couplings, Yukawa couplings and the Standard Model VEV `FlexibleSUSY` generates routines allowing for a one-loop calculation of the $SU(3)_c \times SU(2)_L \times U(1)_Y$ gauge couplings, if they exist in the model under consideration. Furthermore, the Yukawa couplings corresponding to the Standard Model fermions can be calculated in the considered model at the full one-loop level from the

known fermion masses. To determine the top quark Yukawa coupling, two-loop Standard Model QCD corrections are also added. `FlexibleSUSY` also performs a complete one-loop calculation of the running Z and W masses at the low-energy scale in the considered model, which can be used to determine the running Standard Model-like vacuum expectation value, v .

One-loop shifts to pole masses `FlexibleSUSY` by default performs a full one-loop $\overline{\text{MS}}/\overline{\text{DR}}'$ calculation to determine the pole masses of all particles in the model, similar to the procedure presented in Ref. [306] for the MSSM. Thereby, it makes use of the one-loop self-energies and tadpole diagrams generated by `SARAH`, taking the full momentum-dependence into account. To tune the spectrum generator, the user can choose from three different precision levels, which differ in the way two-loop momentum dependent terms are treated. By default, the Higgs masses are calculated with highest precision, where an iteration over the momentum is performed to determine the pole mass M_h at $p^2 = M_h^2$.

Two-loop and three-loop shifts to Higgs pole masses `FlexibleSUSY` allows the user to add certain predefined two-loop corrections to the Higgs masses in some specific models: In MSSM-like models the two-loop corrections of the order $O((\alpha_t + \alpha_b)^2 + \alpha_t\alpha_s + \alpha_b\alpha_s + \alpha_\tau^2)$ from [224–228] can be added to the two CP-even and one CP-odd Higgs boson. In NMSSM-like models with three CP-even and two CP-odd Higgs bosons the two-loop corrections $O(\alpha_t\alpha_s + \alpha_b\alpha_s)$ from [229] plus the MSSM-like contributions $O((\alpha_t + \alpha_b)^2 + \alpha_\tau^2)$ [225, 228] can be added. In SM-like models with one physical Higgs singlet the two-loop corrections $O(\alpha_t\alpha_s + \alpha_t^2)$ from Refs. [312] can be added to the self-energy. In the split-MSSM the three-loop gluino contribution $O(\alpha_t\alpha_s^2)$ from Ref. [313] can be added.

4.2.2 Decay widths and branching ratios

Like `SPheno`, `FlexibleSUSY` can calculate the loop-induced Higgs decays into two photons and two gluons up to NNNLO, see Section 4.4.

4.3 Mass spectrum calculation: SUSY vs. Non-SUSY

We have outlined that `FlexibleSUSY` and `SPheno` can include the radiative corrections to all particles up to the two-loop level in the $\overline{\text{DR}}'$ scheme. These corrections are included by default for supersymmetric models. It is known that loop corrections, in particular to the Higgs mass, are crucial. Typically the $\overline{\text{DR}}'$ and on-shell calculations are in good agreement. Consequently, the remaining difference between both calculations is often a good estimate for the theoretical uncertainty.

The treatment of non-supersymmetric models in `FlexibleSUSY` and `SPheno` is very similar to the treatment of supersymmetric models. The main difference is, that in non-supersymmetric models the parameters are defined in the $\overline{\text{MS}}$ scheme, while in supersymmetric ones the parameters are defined in the $\overline{\text{DR}}'$ scheme. In this paper we perform only tree-level mass calculations (if not stated otherwise), in which the definition of the renormalisation scheme is irrelevant. Thus, in the mass spectrum calculations performed in the following, one is allowed to use input parameters which are defined in the on-shell scheme. This is for instance the standard approach in the large majority of studies of the THDM: there are in general enough free parameters to perform a full on-shell renormalisation keeping all masses and mixing angles fixed. We find that the one-loop corrections in the $\overline{\text{MS}}$ scheme can give huge corrections to the tree-level masses in nearly all models presented in the following. Therefore large fine-tuning of the parameters is necessary once the loop corrections are taken into account. A detailed analysis using a full on-shell renormalisation scheme is possible for each model, but is beyond the scope of this work. Of course, for models where it turns out to be unavoidable that shifts in the masses and mixings appear at the loop-level, the user can simply turn on the loop corrections in `FlexibleSUSY` and `SPheno` via a flag in the Les Houches input file.

4.4 Calculation of the effective diphoton and digluon vertices in `SPheno` and `FlexibleSUSY`

For the calculation of the partial width of a neutral scalar Φ decaying into two gluons or two photons we follow closely [272] for the LO and NLO contributions. The partial widths at LO are given by

$$\Gamma(\Phi \rightarrow \gamma\gamma)_{\text{LO}} = \frac{G_F \alpha^2(0) m_\Phi^3}{128 \sqrt{2} \pi^3} \left| \sum_f N_c^f Q_f^2 r_f^\Phi A_f(\tau_f) + \sum_s N_c^s r_s^\Phi Q_s^2 A_s(\tau_s) + \sum_v N_c^v r_v^\Phi Q_v^2 A_v(\tau_v) \right|^2, \quad (4.2)$$

$$\Gamma(\Phi \rightarrow gg)_{\text{LO}} = \frac{G_F \alpha_s^2(\mu) m_\Phi^3}{36 \sqrt{2} \pi^3} \left| \sum_f \frac{3}{2} D_2^f r_f^\Phi A_f(\tau_f) + \sum_s \frac{3}{2} D_2^s r_s^\Phi A_s(\tau_s) + \sum_v \frac{3}{2} D_2^v r_v^\Phi A_v(\tau_v) \right|^2. \quad (4.3)$$

Here, the sums are over all fermions f , scalars s and vector bosons v which are charged or coloured and which couple to the scalar Φ . Q is the electromagnetic charges of the

fields, N_c are the colour factors and D_2 is the quadratic Dynkin index of the colour representation which is normalised to $\frac{1}{2}$ for the fundamental representation. We note that the electromagnetic fine structure constant α must be taken at the scale $\mu = 0$, since the final state photons are real [314]. In contrast, α_s is evaluated at $\mu = m_\Phi$ which, for the case of interest here, is $\mu = 750$ GeV. r_i^Φ are the so-called reduced couplings, the ratios of the couplings of the scalar Φ to the particle i normalised to SM values. These are calculated as

$$r_f^\Phi = \frac{v}{2M_f}(C_{ff\Phi}^L + C_{ff\Phi}^R), \quad (4.4)$$

$$r_s^\Phi = \frac{v}{2M_s^2}C_{ss^*\Phi}, \quad (4.5)$$

$$r_v^\Phi = -\frac{v}{2M_v^2}C_{vv^*\Phi}. \quad (4.6)$$

Here, v is the electroweak VEV and C are the couplings between the scalar and the different fields with mass M_i ($i = f, s, v$). Furthermore,

$$\tau_x = \frac{m_\Phi^2}{4m_x^2} \quad (4.7)$$

holds and the loop functions are given by

$$A_f = 2(\tau + (\tau - 1)f(\tau))/\tau^2, \quad (4.8)$$

$$A_s = -(\tau - f(\tau))/\tau^2, \quad (4.9)$$

$$A_v = -(2\tau^2 + 3\tau + 3(2\tau - 1)f(\tau))\tau^2, \quad (4.10)$$

with

$$f(\tau) = \begin{cases} \arcsin^2\sqrt{\tau} & \text{for } \tau \leq 1, \\ -\frac{1}{4} \left(\log \frac{1+\sqrt{1-\tau^{-1}}}{1-\sqrt{1-\tau^{-1}}} - i\pi \right)^2 & \text{for } \tau > 1. \end{cases} \quad (4.11)$$

For a pure pseudo-scalar state only fermions contribute, i.e. the LO widths read

$$\Gamma(A \rightarrow \gamma\gamma)_{\text{LO}} = \frac{G_F\alpha^2 m_A^3}{32\sqrt{2}\pi^3} \left| \sum_f N_c^f Q_f^2 r_f^A A_f^A(\tau_f) \right|^2, \quad (4.12)$$

$$\Gamma(A \rightarrow gg)_{\text{LO}} = \frac{G_F\alpha_s^2 m_A^3}{36\sqrt{2}\pi^3} \left| \sum_f 3D_2^f r_f^A A_f^A(\tau_f) \right|^2, \quad (4.13)$$

where

$$A_f^A = f(\tau)/\tau, \quad (4.14)$$

and r_f^A takes the same form as r_f^Φ in Eq. (4.4), simply replacing $C_{ff\Phi}^{L,R}$ by $C_{ffA}^{L,R}$.

These formulae are used by `SPheno` and `FlexibleSUSY` to calculate the full LO contributions of any CP-even or odd scalar present in a model including all possible loop contributions at the scale $\mu = m_\Phi$. However, it is well known, that higher order corrections are important. Therefore, NLO, NNLO and even N³LO corrections from the SM are adapted and used for any model under study. In case of heavy colour fermionic triplets, the included corrections for the diphoton decay are

$$r_f^\Phi \rightarrow r_f \left(1 - \frac{\alpha_s}{\pi}\right), \quad (4.15)$$

$$r_s^\Phi \rightarrow r_s \left(1 + \frac{8\alpha_s}{3\pi}\right). \quad (4.16)$$

These expressions are obtained in the limit $\tau_f \rightarrow 0$ and thus applied only when $m_\Phi < m_f$. r_f^A does not receive any corrections in this limit. For the case $m_\Phi > 2m_f$, we have included the NLO corrections in the light quark limit given by⁷

$$r_f^X \rightarrow r_f^X \left(1 + \frac{\alpha_s}{\pi} \left[\frac{2}{3} \log 4\tau + \frac{1}{18} (\pi^2 - \log^2 4\tau) + 2 \log \left(\frac{\mu_{\text{NLO}}^2}{m_f^2} \right) + i \frac{\pi}{3} \left(\frac{1}{3} \log 4\tau + 1 \right) \right] \right) \quad (4.17)$$

for $X = \Phi, A$. μ_{NLO} is the renormalisation scale used for these NLO corrections, chosen to be $\mu_{\text{NLO}} = m_\Phi/2$. For the digluon decay rate, the corrections up to N³LO are included and parametrised by

$$\Gamma(X \rightarrow gg) = \Gamma(X \rightarrow gg) \left(1 + C_X^{\text{NLO}} + C_X^{\text{NNLO}} + C_X^{\text{N}^3\text{LO}}\right), \quad (4.18)$$

with [257, 272, 315–319]

$$C_\Phi^{\text{NLO}} = \left(\frac{95}{4} - \frac{7}{6} N_F \right) \frac{\alpha_s}{\pi}, \quad (4.19)$$

$$C_\Phi^{\text{NNLO}} = \left(370.196 + (-47.1864 + 0.90177 N_F) N_F + (2.375 + 0.666667 N_F) \log \frac{m_\Phi^2}{m_t^2} \right) \frac{\alpha_s^2}{\pi^2}, \quad (4.20)$$

$$C_\Phi^{\text{N}^3\text{LO}} = \left(467.684 + 122.441 \log \frac{m_\Phi^2}{m_t^2} + 10.941 \left(\log \frac{m_\Phi^2}{m_t^2} \right)^2 \right) \frac{\alpha_s^3}{\pi^3}, \quad (4.21)$$

⁷In comparison to Ref. [272], we are using another constant in the imaginary part of the correction. The reason is that this reproduces the shape of the curves in Fig. 5 of Ref. [272] better for the mass range ($m_\Phi/m_f < 100$) we are interested in.

and

$$C_A^{\text{NLO}} = \left(\frac{97}{4} - \frac{7}{6} N_F \right) \frac{\alpha_s}{\pi}, \quad (4.22)$$

$$C_A^{\text{NNLO}} = \left(171.544 + 5 \log \frac{m_\Phi^2}{m_t^2} \right) \frac{\alpha_s^2}{\pi^2}, \quad (4.23)$$

$$C_A^{\text{N}^3\text{LO}} = 0. \quad (4.24)$$

In order to check the accuracy of our implementation, we compared the results obtained with SARAH–SPHeno for the SM Higgs boson decays with the ones given in the CERN yellow pages [320]. In Fig. 7 we show the results for the Higgs branching ratios into two photons and two gluons with and without the inclusion of higher order corrections. One

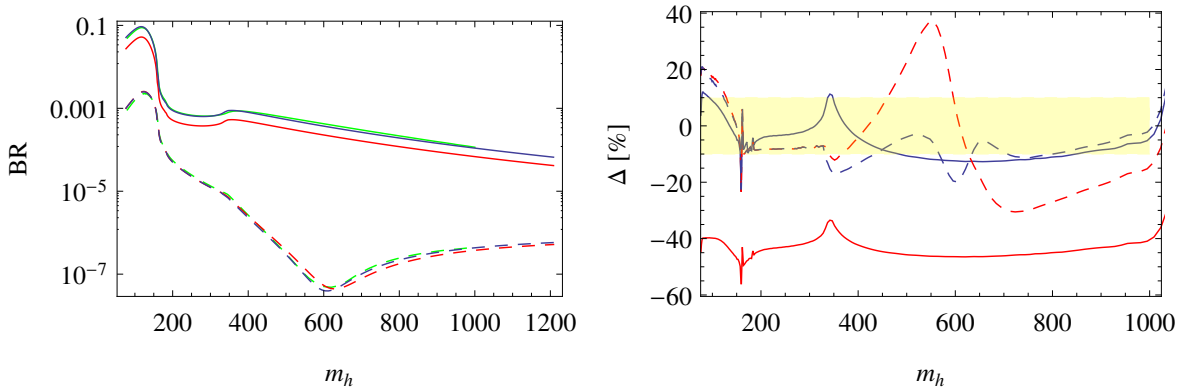


Figure 7. On the left: comparison of $\text{Br}(h \rightarrow gg)$ (full lines) and $\text{Br}(h \rightarrow \gamma\gamma)$ (dashed lines) as calculated by SPHeno at LO (red) and including higher order corrections as described in the text (blue). The green line shows the values of the Higgs cross section working group. On the right: relative difference for diphoton (dashed lines) and digluon (full lines) at LO (red) and including higher order corrections (blue).

sees that good agreement is generally found when including higher order corrections. In Fig. 8 we show the ratio $\text{Br}(h \rightarrow gg)/\text{Br}(h \rightarrow \gamma\gamma)$ and compare it again with the recommended numbers by the Higgs cross section working group [320]. Allowing for a 10% uncertainty in the mass range of 700–800 GeV, we find that our calculation including higher order corrections agrees with the expectations, while the LO calculation predicts a ratio which is 15–20% too small. We note also that if we had used $\alpha(m_h)$ instead of $\alpha(0)$ in the LO calculation, the difference would have been approximately 35–40%, with a diphoton rate overestimated by a factor $(\alpha(m_h)/\alpha(0))^2 \simeq (137/124)^2 \simeq 1.22$.

4.5 Monte-Carlo studies

SARAH writes all necessary files to implement a new model in different MC tools. First,

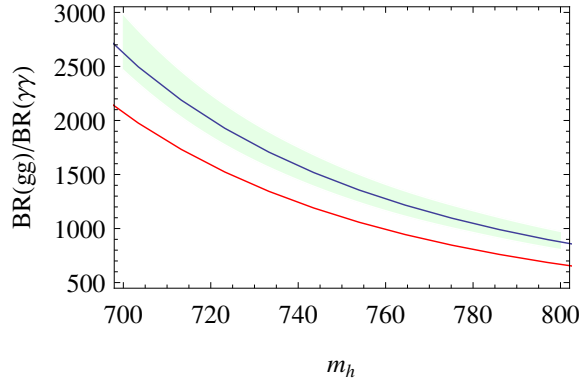


Figure 8. $\text{Br}(h \rightarrow gg)/\text{Br}(h \rightarrow \gamma\gamma)$ as calculated by `SPheno` at LO (red) and including higher order corrections as described in the text. The green band shows the values of the Higgs cross section working group including a 10% uncertainty.

a short summary of the output formats is given . Then, it is described how parameter values between `SPheno`/`FlexibleSUSY` and the MC codes can be exchanged.

4.5.1 Output of models files

CalcHep The model files for `CalcHep` [232, 233] can also be used with `MicrOmegas` [236] to perform both collider and dark matter studies. `CalcHep` is able to read the numerical values of the masses and mixing matrices from a SLHA spectrum file based on the SLHA+ functionality [321]. `SARAH` makes use of this functionality to generate model files by default in a way that they automatically *expect* to find the input values in spectrum files written by a `SARAH`-generated `SPheno` version or by `FlexibleSUSY`. However, other choices are possible: the parameters can be given via the `vars` file or tree-level expressions can be calculated internally by `CalcHep`.

UFO format `SARAH` can also write model files in UFO format [284]. This is particularly useful to implement new models in `MG5_aMC@NLO` and perform collider studies. The UFO format is also supported by other tools like `GoSam` [285], `Aloha` [322], `Herwig++` [286, 287] and `MadAnalysis 5` [323]. Moreover, the spectrum file written by `SPheno` or by `FlexibleSUSY` can be directly used as parameter card in `MadGraph`.

WHIZARD/O’Mega `SARAH` writes all necessary files to implement a model in `WHIZARD` and `O’Mega` [282, 283]. Since the SLHA reader of `WHIZARD` is at the moment restricted to the MSSM and the NMSSM, `SPheno` versions generated by `SARAH` can write all information about the spectrum and parameters in an additional file in the `WHIZARD` specific format. This file can then be read by `WHIZARD`. Currently, the handling of general Lorentz structures in `WHIZARD` and the support of the UFO format are under

development. This will provide the possibility to use WHIZARD with the calculated diphoton and digluon vertices as explained in the following.

4.5.2 Interplay SARAH–Spectrum-Generator–MC-Tool

The tool chains SARAH–SPheno/FlexibleSUSY–MC-Tools have one very appealing feature: the implementation of a model in the spectrum generator (SPheno or FlexibleSUSY) as well as in a MC tool is based on just one single implementation of the model in SARAH. Thus, the user does not need to worry that the codes might use different conventions to define the model. In addition, SPheno also provides all widths for the particles so that this information can be used by the MC-Tool to save time.

4.5.3 Effective diphoton and digluon vertices for neutral scalars

The effective diphoton and digluon vertices calculated by SPheno or FlexibleSUSY are directly available in the UFO model files and the CalcHep model files: SARAH includes the effective vertices for all neutral scalars to two photons and two gluons, and the numerical values for these vertices are read from the spectrum file generated with SPheno or FlexibleSUSY. For this purpose, a new block EFFHIGGSCOUPPLINGS is included in these files, which contain the values for the effective couplings including all corrections outlined in Section 4.4.

4.6 Checking Higgs constraints

HiggsBounds [237, 238, 324] and HiggsSignals [239] are dedicated tools to study the Higgs properties of a given parameter point in a particular model. While HiggsBounds checks the parameter point against exclusion limits from Higgs searches, HiggsSignals gives a χ^2 value to express how well the point reproduces the Higgs measurements. In general, HiggsBounds and HiggsSignals can handle different inputs: either the cross sections for all necessary processes can be given at the parton or hadron level, or the effective couplings of the Higgs states to all SM particles are taken as input. In addition, the masses and widths of all neutral as well as charged Higgs states are always needed. SPheno provides all input for the effective coupling approach. The information is distributed in the SLHA spectrum file and in separated files (called MH_GammaTot.dat, MHplus_GammaTot.dat, BR_H_NP.dat, BR_Hplus.dat, BR_t.dat, effC.dat). While SLHA files can be used with HiggsBounds for models with up to five neutral scalars, the separated files can even be used with up to 99 neutral and 99 charged scalars.

4.7 Checking the Vacuum stability

`Vevacious` is a tool to check for the global minimum of the one-loop effective potential allowing for a particular set of non-zero VEVs. For this purpose, `Vevacious` first finds all tree-level minima using `HOM4PS2` [325]. Afterwards, it minimizes the one-loop effective potential starting from these minima using `minuit` [326]. If the input minimum turns out not to be the global one, life-time of meta-stable vacua can be calculated using `CosmoTransitions` [327].

`Vevacious` takes the tadpole equations, the polynomial part of the scalar potential and all mass matrices as input. All of this information has to be expressed including all VEVs which should be tested. That means that, in case of supersymmetric models, in order to check for charge and colour-breaking minima, both the stop and the stau VEVs must be taken into account everywhere in the scalar potential, the tadpole equations and the mass matrices. Moreover, the possible mixing of all states triggered by the new VEVs must be included. To take care of all that, the corresponding input files can be generated by `SARAH`.

4.8 Accuracy of the diphoton calculation

Before concluding this section, we should draw the reader's attention to the question of how accurate the results are from `SARAH` in combination with `SPheno` and `FlexibleSUSY`. While every possible correction has been included, there are still some irreducible sources of uncertainty, as we shall discuss below.

4.8.1 Loop corrections to $ZZ, WW, Z\gamma$ production

So far in `SARAH`, loop-level decays are only computed for processes where the tree-level process is absent. This is to avoid the technical issues of infra-red divergences. If the particle that explains the 750 GeV excess is a scalar, then it must mix with the Higgs and acquire tree-level couplings to the Z and W bosons, and these are fully taken into account. However, due to the existence of such terms, the loop corrections to the decays into Z s and W s are more complicated and are therefore not yet available in `SARAH`.

To estimate the uncertainty incurred by their absence, let us assume that our 750 GeV resonance S couples to the $U(1)_Y$ and $SU(2)_L$ gauge bosons via the effective operators $SB_{\mu\nu}B^{\mu\nu}$ and $SW_{\mu\nu}W^{\mu\nu}$. If we can neglect the tree-level contributions to the decays and assume that the dominant contribution originates from a set of particles in the loops, which have the hypercharge Y and the dynkin index $D_2(W)$, then the decay

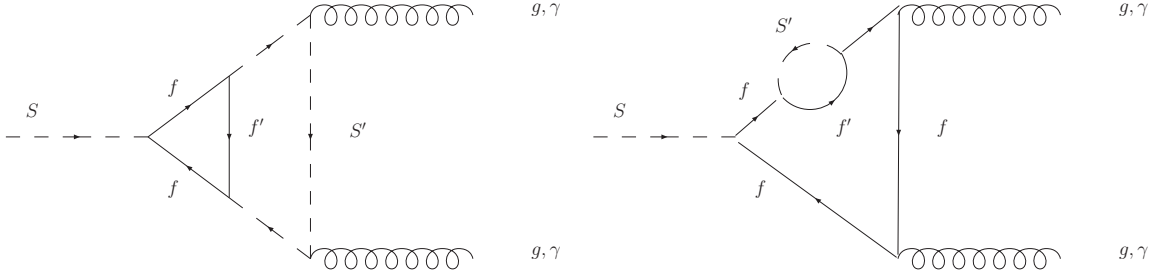


Figure 9. Examples of potentially important NLO corrections.

widths are approximately given by

$$\frac{\Gamma(S \rightarrow ZZ)}{\Gamma(S \rightarrow \gamma\gamma)} \simeq \frac{(D_2 + \tan^2 \theta_W Y^2)^2}{(Y^2 + \tan^2 \theta_W D_2)^2}, \quad \frac{\Gamma(S \rightarrow Z\gamma)}{\Gamma(S \rightarrow \gamma\gamma)} \simeq \frac{\sin^2 2\theta_W (D_2 - Y^2)^2}{(Y^2 + \tan^2 \theta_W D_2)^2},$$

$$\frac{\Gamma(S \rightarrow WW)}{\Gamma(S \rightarrow \gamma\gamma)} \simeq \frac{2D_2^2 \sec^4 \theta_W}{(Y^2 + \tan^2 \theta_W D_2)^2}. \quad (4.25)$$

Put together, the uncertainty that we find for the decay $S \rightarrow \gamma\gamma$ reads

$$\frac{\delta\Gamma(S \rightarrow \text{anything})}{\Gamma(S \rightarrow \text{anything})} \simeq \left[\frac{5.1D_2^2 - 0.8Y^2D_2 + 0.8Y^4}{Y^4 + 0.6Y^2D_2 + 0.09D_2^2} \right] \times \text{Br}(S \rightarrow \gamma\gamma). \quad (4.26)$$

The factor in square brackets is therefore largest for fields that only couple to $SU(2)_L$ gauge bosons, giving a factor of ~ 60 . Thus, provided that $\text{Br}(S \rightarrow \gamma\gamma) \lesssim 10^{-3}$, the relative uncertainty is less than 10%. In such cases, the proportional uncertainty in the total width transfers directly into the proportional uncertainty in the total cross-section:

$$\frac{\delta\sigma(pp \rightarrow S \rightarrow \gamma\gamma)}{\sigma(pp \rightarrow S \rightarrow \gamma\gamma)} \simeq - \frac{\delta\Gamma(S \rightarrow \text{anything})}{\Gamma(S \rightarrow \text{anything})}. \quad (4.27)$$

On the other hand, for models where the dominant decay channel of the singlet is into gluons, it is not possible to have $\text{Br}(S \rightarrow \gamma\gamma) \lesssim 10^{-3}$ without violating constraints from dijet production. In such models the reader should be aware of the possible uncertainties incurred. Fortunately, provided that the particles in the loop have a hypercharge, the uncertainty is much smaller, for example in the case that $D_2 = 0$ the coefficient above is less than one thus giving an uncertainty of less than 10^{-3} for $\text{Br}(S \rightarrow \gamma\gamma) = 10^{-3}$.

4.8.2 BSM NLO corrections

As discussed above, SARAH includes the leading-order computation of the diphoton and digluon decay amplitudes including the effects of all Standard-Model and Beyond-the-Standard-Model particles in the loops. Furthermore, it also includes the leading-log

corrections to the digluon rate at NLO, NNLO and N³LO order in α_s in the *Standard Model*, and some NLO corrections due to diagrams with an extra gluon to both the digluon and diphoton rates. However, the NLO corrections are absent for all other particles, which in the case of large Yukawa couplings or hierarchies could be sizeable. Two examples of such a diagrams are given in Fig. 9; in the context of supersymmetric theories, particularly important are diagrams involving the gluino, which (if it is a Majorana particle) would not couple to a singlet at leading order – naively their contribution is

$$\frac{\delta\Gamma(S \rightarrow gg/\gamma\gamma)}{\Gamma(S \rightarrow gg/\gamma\gamma)} \sim \frac{\alpha_s}{\pi} \log \frac{m_g^2}{\mu_{NLO}^2} \xrightarrow{m_{\tilde{g}}=2 \text{ TeV}} \sim 10 \%, \quad (4.28)$$

although as we shall discuss below this can be (potentially significantly) an underestimate.

4.8.3 Tree vs pole masses in loops

For consistency of the perturbative series and technical expediency, the masses inside loops (to calculate pole masses and loop decay amplitudes) are $\overline{\text{MS}}$ or $\overline{\text{DR}}'$ parameters, not the pole masses of observed particles. The difference between calculations performed in this scheme and the on-shell scheme are at two-loop order, and so is generally small. However, in particular when there are large hierarchies or Yukawa couplings in a model, there can be a large difference between the Lagrangian parameters and the pole masses, and therefore a large discrepancy between the loop amplitudes calculated from these. In principle, this should be accounted for by including higher-order corrections such as the right-hand diagram in Fig. 9 – but applying such a correction to each propagator in the loop would actually correspond to a four-loop diagram. The effect of using the pole mass instead is to essentially resum part of these diagrams, which as is well known is relevant in the case of large hierarchies of masses – and so should give a more accurate result in that case.

If we define

$$\delta m^2 \equiv (m^2)^{\overline{\text{MS}}/\overline{\text{DR}}'} - (m^2)^{\text{on-shell}} \quad (4.29)$$

then for one dominant particle p in the loop, we can estimate the uncertainty as

$$\frac{\delta\Gamma(S \rightarrow gg/\gamma\gamma)}{\Gamma(S \rightarrow gg/\gamma\gamma)} \sim \begin{cases} -\frac{2\delta m^2}{m^2} \left(\frac{A'_p}{A_p} + 1 \right), & p = s, v, \\ -\frac{4\delta m}{m} \left(\frac{A'_p}{A_p} + \frac{1}{2} \right), & p = f, \end{cases} \quad (4.30)$$

where the factor of 1 or 1/2 assumes that the couplings $C_{\bar{p}p\Phi}$ do not depend upon the mass m_p (but the prefactor in r_p^Φ therefore does). For most values of m_p the loop functions are slowly changing (only peaking around $\tau_p = 1$) so we will have a proportional uncertainty in the result of $\frac{2\delta m_{s,v}^2}{m_{s,v}^2}$ or $\frac{2\delta m_f}{m_f}$. As an example, in supersymmetric theories the soft masses of coloured scalars \tilde{S}' acquire a significant decrease from gluino loops:

$$\delta m_{\tilde{S}'}^2 \simeq \frac{C_2(\tilde{S}')\alpha_s}{\pi} m_{\tilde{g}}^2 \log \frac{m_{\tilde{g}}^2}{\mu_{NLO}^2}. \quad (4.31)$$

If the scalar is a colour triplet with a pole mass of 800 GeV, then for 2 TeV gluinos and the $\overline{\text{DR}}'$ mass is ~ 1100 GeV; but $\frac{\delta m_{\tilde{S}'}^2}{m_{\tilde{S}'}^2} \sim 1!$ This corresponds to a shift of a factor of two in the amplitude, and, if the scalar dominates the total amplitude, a factor of four in $\Gamma(S \rightarrow gg/\gamma\gamma)$; in fact in this case **SARAH** would be potentially *underestimating* the diphoton rate. This is a relatively mild example regarding this excess: given that the vast majority of models proposed to explain the diphoton signature contain large Yukawa couplings and many new particles, there is a significant potential for large values of $\frac{\delta m^2}{m^2}$, about which the user should be careful. It is worth noting that this is an effect that would not be significant in the (N)MSSM, where the Higgs couplings to photons/gluons are dominated by the top quark (and, for photons, the W bosons) whose masses are protected by chiral symmetry from large shifts: this issue is a novelty for the 750 GeV excess.

For non-supersymmetric models, due to the fact that (almost) every parameter point is essentially fine-tuned, we have not calculated loop corrections to the masses by default, and this issue does not arise in the same way. The user is then free to regard the result as involving the pole masses of particles instead, if they so desire – the issue then becomes one of tuning the potentially large corrections to the other input parameters.

5 Models

A large variety of models has been proposed to explain the diphoton excess at 750 GeV. We have selected and implemented several possible models in **SARAH**. Our selection is not exhaustive, but we have tried to implement a sufficient cross-section which are representative of many of the ideas put forward in the context of renormalisable models. These are the ones that **SARAH** can handle. Their description is organised in the subsections that follow. Before we turn to this discussion we first want to mention other proposals which we do not deal with in this paper.

Many authors [10, 16, 20, 25, 29, 35, 39, 57, 80, 89, 112, 114, 120, 149, 151, 156, 174, 188, 197, 203] have studied the excess with effective (non-renormalisable)

models, which is sensible given that there are thus far no other striking hints of new physics at the LHC. As more data becomes available and the evidence for new physics becomes more substantial, one might want to UV complete these models, at which point the tools we are advertising become relevant and necessary. Other authors [23, 26, 30, 40, 69, 73, 78, 86, 138, 139, 172, 175, 181, 186, 189, 190, 205] considered strongly coupled models, in which the resonance is a composite state. This possibility would be favoured by a large width of the resonance, as first indications seem to suggest. Another possibility is to interpret the signal in the context of extra-dimensional models [3, 5, 17, 18, 24, 47, 74, 85, 119, 131, 184], with the resonance being a scalar, a graviton, a dilaton, or a radion, depending on the scenario. However, some of these interpretations are in tension with the non-observation of this resonance in other channels. In Supersymmetry, the scalar partner of the goldstino could provide an explanation to the diphoton signal [56, 91, 98, 200]. Other ideas, slightly more exotic, include: a model with a space-time varying electromagnetic coupling constant [81], Gluionia [202], Squarkonium/Diquarkonium [176], flavons [147], axions in various incarnations [4, 14, 31, 148, 163, 201], a natural Coleman-Weinberg theory [13, 180], radiative neutrino mass models [157, 192, 193], and string-inspired models [12, 79, 110, 143, 152].

We turn now to the weakly coupled models, and discuss the ones which we implemented in SARAH. All model files are available for download at

http://sarah.hepforge.org/Diphoton_Models.tar.gz

and an overview of all implemented models is given in Tabs. 4 and 5. In case of questions, comments or bug reports concerning these models, please, send an e-mail to diphoton-tools@cern.ch which includes all authors.

5.1 Toy models

The simplest ideas proposed to explain the diphoton excess extend the SM by a scalar singlet and vector-like fermions, which serve the purpose of enhancing the diphoton rate, and – in the case of coloured states – also the production via gluon fusion. An enhancement of gluon fusion seems to be necessary because a production of the resonance purely by photon fusion is in some tension with 8 TeV data: the increase in the cross section from 8 to 13 TeV is just a factor 2, while a factor of 5 would be needed to make the results from LHC run-I and II compatible. To explore the multitude of possibilities we first consider toy models: they do not contain all possible couplings of the vector-like fermions to SM matter, but are rather engineered to allow one to easily explore the effects of different representations of vector-like matter on the diphoton rate

Model	Name	Section	Ref.
Toy models with vector-like fermions			
CP-even singlet	SM+VL/CPevenS	5.1	
CP-odd singlet	SM+VL/CPoddS	5.1	
Complex singlet	SM+VL/complexS	5.1	
Models based on the SM gauge-group			
Portal dark matter	SM+VL/PortalDM	5.2.1.1	[67, 132]
Scalar octet	SM-S-Octet	5.2.1.2	[48, 99] $\triangle!$ ⁽¹⁾
$SU(2)$ triplet quark model	SM+VL/TripletQuarks	5.2.1.3	[32]
Single scalar leptoquark	LQ/ScalarLeptoquarks	5.2.1.4	[27]
Two scalar leptoquarks	LQ/TwoScalarLeptoquarks	5.2.1.5	[65] $\triangle!$ ⁽³⁾
Georgi-Machacek model	Georgi-Machacek	5.2.1.6	[70, 108]
THDM w. colour triplet	THDM+VL/min-3	5.2.2.1	[41]
THDM w. colour octet	THDM+VL/min-8	5.2.2.1	[41]
THDM-I w. exotic fermions	THDM+VL/Type-I-VL	5.2.2.2	[155, 213]
THDM-II w. exotic fermions	THDM+VL/Type-II-VL	5.2.2.2	[155, 213]
THDM-I w. SM-like fermions	THDM+VL/Type-I-SM-like-VL	5.2.2.3	[21]
THDM-II w. SM-like fermions	THDM+VL/Type-II-SM-like-VL	5.2.2.3	[21]
THDM w. scalar septuplet	THDM/ScalarSeptuplet	5.2.2.4	[134, 187]

Table 4. Part I of the overview of proposed models to explain the diphoton excess which are now available in SARAH. The warning ($\triangle!$) shows that we found serious problems with the model during the implementation. The reasons are as follows. (1): the model is in conflict with limits from $S \rightarrow jj$; (2): we changed the quantum numbers and/or the potential because the original model had charge violating interactions; (3): we find disagreement with the diphoton rate as calculated in the original reference. For simplicity, we used the abbreviations LQ for LeptoQuarks and U1Ex for U1Extensions .

and on the relevant partial widths. Then, from section 5.2 on, we consider complete models, containing all the operators consistent with both field content and symmetries.

Toy models with vector-like fermions

- **Reference:** [109, 132, 133, 165]
- **Model names:**
 - SM+VL/CPevenS
 - SM+VL/CPoddS
 - SM+VL/complexS

Model	Name	Section	Ref.	
$U(1)$ Extensions				
Dark $U(1)'$	U1Ex/darkU1	5.3.1.1	[166]	
Hidden $U(1)$	U1Ex/hiddenU1	5.3.1.2	[83]	
Simple $U(1)$	U1Ex/simpleU1	5.3.1.3	[62]	
Scotogenic $U(1)$	U1Ex/scotoU1	5.3.1.4	[210]	$\triangle^{\text{(2)}}$
Unconventional $U(1)_{B-L}$	U1Ex/BL-VL	5.3.2.1	[185]	
Sample of $U(1)'$	U1Ex/VLsample	5.3.2.2	[66]	
flavour-nonuniversal charges	U1Ex/nonUniversalU1	5.3.2.3	[178]	$\triangle^{\text{(3)}}$
Leptophobic $U(1)$	U1Ex/U1Leptophobic	5.3.2.4	[167]	$\triangle^{\text{(1)}}$
Z' mimicking a scalar resonance	U1Ex/trickingLY	5.3.2.5	[60]	
Non-abelian gauge-group extensions of the SM				
LR without bidoublets	LRmodels/LR-VL	5.4.1.1	[42, 92, 93]	$\triangle^{\text{(2)}}$
LR with $U(1)_L \times U(1)_R$	LRmodels/LRLR	5.4.1.2	[51]	$\triangle^{\text{(2)}}$
LR with triplets	LRmodels/tripletLR	5.4.1.3	[33]	
Dark LR	LRmodels/darkLR	5.4.1.4	[95]	
331 model without exotic charges	331/v1	5.4.2.1	[44]	
331 model with exotic charges	331/v2	5.4.2.2	[53]	
Gauged THDM	GTHDM	5.4.3	[150]	
Supersymmetric models				
NMSSM with vectorlike top	NMSSM+VL/VLtop	5.5.1.1	[208]	$\triangle^{\text{(1)}}$
NMSSM with $\mathbf{5}$'s	NMSSM+VL/5plets	5.5.1.2	[105, 128, 207]	
NMSSM with $\mathbf{10}$'s	NMSSM+VL/10plets	5.5.1.3	[105, 128, 207]	
NMSSM with $\mathbf{5}$'s & $\mathbf{10}$'s	NMSSM+VL/10plets	5.5.1.4	[128]	
NMSSM with $\mathbf{5}$'s and R_pV	NMSSM+VL/5plets+RpV	5.5.1.5	[105]	
Broken MRSSM	brokenMRSSM	5.5.2	[58]	
$U(1)'$ -extended MSSM	MSSM+U1prime-VL	5.5.3	[154, 328]	
E_6 with extra $U(1)$	E6MSSMalt	5.5.4	[64]	

Table 5. Part II of the overview of proposed models to explain the diphoton excess which are now available in SARAH. The warning (\triangle) shows that we found serious problems with the model during the implementation. The reasons are as follows. (1): non-perturbative couplings needed to explain diphoton excess; (2): we changed the quantum numbers and/or the potential because the original model had charge violating interactions; (3): we find disagreement with the diphoton rate as calculated in the original reference.

To begin with we categorise the toy models according to the type of the involved scalar singlet. There are three possibilities: (i) the singlet is a real CP-even scalar, (ii) real CP-odd, or (iii) a complex scalar. Each case is considered in separate **SARAH** model files, where we introduce all possible representations of vector-like fermions. These possibilities, following Tables 3 and 4 of Ref. [165], are shown below in Table 6. This allows one to study combinations of fermion representations or individual choices by giving unwanted fermion representations a mass high enough to effectively decouple them from the model ⁸. All mixings between the extra fermions and SM fermions are neglected through the assumption of a discrete \mathbb{Z}_2 symmetry. Of course in a realistic model the mixings have to be taken into account, as they allow the necessary decays of the coloured vector-like fermions into SM particles.

Field	Gen.	$SU(3)_C$	$SU(2)_L$	$U(1)_Y$	\mathbb{Z}_2	Ref.
S	1	1	1	0	+	
Ψ_{F_1}	1	3	2	$\frac{7}{6}$	–	
Ψ_{F_2}	1	3	3	$\frac{2}{3}$	–	
Ψ_{F_3}	1	3	2	$-\frac{5}{6}$	–	
Ψ_{F_4}	1	3	3	$-\frac{1}{3}$	–	
Ψ_{F_5}	1	3	1	$\frac{2}{3}$	–	[109, 133]
Ψ_{F_6}	1	3	2	$\frac{1}{6}$	–	
Ψ_{F_7}	1	3	1	$-\frac{1}{3}$	–	[133]
Ψ_{F_8}	1	1	1	1	–	
Ψ_{F_9}	1	1	2	$-\frac{3}{2}$	–	
$\Psi_{F_{10}}$	1	1	3	1	–	
$\Psi_{F_{11}}$	1	1	2	$-\frac{1}{2}$	–	
$\Psi_{F_{12}}$	1	1	3	0	–	
$\Psi_{F_{13}}$	1	3	1	$\frac{5}{3}$	–	[132]

Table 6. Extra particle content of the toy models. S is either the CP-even, CP-odd or complex scalar. The various fermions $\Psi_{F_i} \equiv \Psi_{F_{iL}}$ each come with a right-handed partner $\Psi_{F_{iR}}$ with opposite quantum numbers. These models are based on the collection given in Ref. [165], while the last column contains other works where fermions in these specific representations are used. All SM particles have charge ‘+’ under the additional \mathbb{Z}_2 symmetry.

⁸This option has to be used carefully when including loop corrections to the mass spectrum.

We write the scalar potentials for the three different types of scalars as

$$V_{\text{even}} = \frac{1}{2}m_S^2 S^2 + \frac{1}{4}\lambda_S S^4 - \mu^2 |H|^2 + \frac{1}{2}\lambda_H |H|^4 + \frac{1}{2}\lambda_{HS} S^2 |H|^2 + \kappa_{HS} S |H|^2 + \frac{1}{3}\kappa_S S^3, \quad (5.1a)$$

$$V_{\text{odd}} = \frac{1}{2}m_S^2 |S|^2 + \frac{1}{4}\lambda_S |S|^4 - \mu^2 |H|^2 + \frac{1}{2}\lambda_H |H|^4 + \frac{1}{2}\lambda_{HS} |S|^2 |H|^2 + \left(i\kappa_{HS} S |H|^2 + i\frac{1}{3}\kappa_S S |S|^2 + \text{h.c.} \right), \quad (5.1b)$$

$$V_{\text{complex}} = m_S^2 |S|^2 + \frac{1}{2}\lambda_S |S|^4 - \mu^2 |H|^2 + \frac{1}{2}\lambda_H |H|^4 + \lambda_{HS} |S|^2 |H|^2 + \left(\kappa_{HS} S |H|^2 + \frac{1}{3}\kappa_S S |S|^2 + \text{h.c.} \right). \quad (5.1c)$$

The Yukawa interactions are given by

$$-\mathcal{L}_Y = \mathcal{L}_Y^{\text{SM}} + \sum_j \left(m_{F_j} \overline{\Psi}_{F_j L} \Psi_{F_j R} + \sum_j Y_{F_j} S \overline{\Psi}_{F_j L} \Psi_{F_j R} \right) + \text{h.c.} \quad (5.2)$$

In the Lagrangian above one should substitute the expression for the relevant scalar field

$$S_{\text{even}} = v_S + \phi_S, \quad \text{where } \langle S \rangle = v_S, \quad (5.3a)$$

$$S_{\text{odd}} = i\sigma_S, \quad (5.3b)$$

$$S_{\text{complex}} = \frac{1}{\sqrt{2}} (v_S + \phi_S + i\sigma_S). \quad (5.3c)$$

Note that imposing CP conservation forces κ_{HS} and κ_S to vanish in the CP-odd potential. For both the CP-even and complex singlet models the CP-even component ϕ_S mixes with the neutral Higgs field ϕ_h at tree-level if $\kappa_{HS} \neq 0$. As discussed in Section 2.2.1, even if one sets $\kappa_{HS} = 0$ mixing between the CP-even states is induced at the loop level.

5.2 Models based on the SM gauge-group

We now turn our attention to complete models that have been proposed to explain the 750 GeV diphoton excess. To begin with we consider models that are based on the SM gauge group, with or without additional global symmetries. We divide the possible models into two main categories: (i) models with a SM-like Higgs sector and (ii) Two-Higgs-doublet type models.

5.2.1 Singlet extensions with vector-like fermions

5.2.1.1 Portal dark matter model

- **Reference:** [67, 132]
- **Model name:** SM+VL/PortalDM

This model proposes that the resonance is produced by a 750 GeV real scalar singlet S , with the diphoton rate boosted through the introduction of vector-like quarks coupling to the new scalar singlet. In this model we have three possible options for the representation of the new vector-like matter. These choices are: (i) the addition of a vector-like up-type quark pair $t'_{L/R}$ [67], (ii) in addition to the vector-like up-type quark pair, a vector-like quark doublet pair $Q'_{L/R}$ is introduced [67] and finally, (iii) the addition of only the vector-like pair $X_{L/R}$, also triplet under $SU(3)_C$ but with exotic hypercharge [132].

The model also introduces a new real scalar singlet S_{DM} and an additional fermionic singlet Ψ_{DM} as DM candidates, with a \mathbb{Z}_2 symmetry to stabilise them. The particle content beyond the SM fields is given in Table 7. In order to avoid mixing with the SM quarks, the fields $t'_{L/R}$ and $Q'_{L/R}$ are also odd under the \mathbb{Z}_2 .

The user can choose between the three model types by setting the couplings of the unwanted fields to zero and choosing their masses to be very large (for example, 10^{12} GeV) to decouple them. Originally, the fermionic dark matter is absent from the models described in [67]. The exact settings are given below.

Field	Gen.	$SU(3)_C$	$SU(2)_L$	$U(1)_Y$	\mathbb{Z}_2
S	1	1	1	0	+
S_{DM}	1	1	1	0	−
Ψ_{DM}	1	1	1	0	−
X	1	3	1	$\frac{5}{3}$	−
t'	1	3	1	$\frac{2}{3}$	−
Q'	1	3	2	$\frac{1}{6}$	−

Table 7. Extra particle content of the portal DM model. The top/bottom part of the table corresponds to the new scalar/fermionic degrees of freedom. All additional fermionic degrees of freedom are vector-like fermions.

The scalar potential for these models reads

$$V = -\mu^2 |H|^2 + \frac{1}{2} \lambda_H |H|^4 + \frac{1}{2} M_S^2 S^2 + \frac{1}{3} \kappa_S S^3 + \frac{1}{4} \lambda_S S^4 + \frac{1}{2} M_{S_{\text{DM}}}^2 S_{\text{DM}}^2 + \frac{1}{4} \lambda_{S_{\text{DM}}} S_{\text{DM}}^4 + \kappa_{HS} |H|^2 S + \lambda_{HS} |H|^2 S^2 + \lambda_{HS_{\text{DM}}} |H|^2 S_{\text{DM}}^2 + \kappa_{SS_{\text{DM}}} S S_{\text{DM}}^2 + \lambda_{SS_{\text{DM}}} S^2 S_{\text{DM}}^2, \quad (5.4)$$

whereas the three model variants lead to three distinct forms for the Yukawa interactions, given by:

$$-\mathcal{L}_Y^{\text{I}} = \mathcal{L}_Y^{\text{SM}} + (m_{t'} + Y_{S t'} S) \bar{t}'_L t'_R + Y_{S_{\text{DM}} t'} S_{\text{DM}} \bar{t}'_L u_R + \text{h.c.}, \quad (5.5a)$$

$$-\mathcal{L}_Y^{\text{II}} = \mathcal{L}_Y^{\text{I}} + (m_{Q'} + Y_{S Q'} S) \bar{Q}'_L Q'_R + Y_{Q'_1} \bar{Q}'_L H t'_R + Y_{Q'_2} \bar{Q}'_R \tilde{H} t'_L + Y_{S_{\text{DM}} Q'} S_{\text{DM}} \bar{Q}'_L Q'_R + \text{h.c.}, \quad (5.5b)$$

$$-\mathcal{L}_Y^{\text{III}} = \mathcal{L}_Y^{\text{SM}} + (m_{\text{DM}} + \kappa_S S) \bar{\Psi}_{\text{DML}} \Psi_{\text{DMR}} + (m_X + Y_X S) \bar{X}_L X_R + \text{h.c.}, \quad (5.5c)$$

where $\tilde{H} = i\sigma_2 H^*$. In the model variants I and II, the vectorlike quarks decay into SM quarks and the scalar dark matter candidate S_{DM} via the couplings $Y_{S_{\text{DM}} Q'}$ and $Y_{S_{\text{DM}} t'}$. In model III, in turn, X is stable at the level of the Lagrangian and could only decay through higher-dimensional operators which are not included here.

The symmetry breaking pattern of the models is that of the SM, where the neutral component of the Higgs field acquires a VEV, plus the VEV of the scalar singlet S

$$S = v_S + \phi_S, \quad \text{where} \quad \langle S \rangle = v_S. \quad (5.6)$$

In general, ϕ_S mixes with the SM Higgs.

As mentioned previously, the user can choose between the three different models through the following parameter choices:

- **Model I:** $Y_{S Q'} = Y_{Q'_i} = Y_{S_{\text{DM}} Q'} = Y_X = 0$ and $m_{Q'} = m_X = 10^{12}$ GeV
- **Model II:** $Y_X = 0$ and $m_X = 10^{12}$ GeV
- **Model III:** $Y_{S Q'} = Y_{Q'_i} = Y_{S_{\text{DM}} Q'} = Y_{S t'} = Y_{S_{\text{DM}}} = 0$ and $m_{Q'} = m_{t'} = 10^{12}$ GeV

5.2.1.2 Scalar octet extension

- **Reference:** [48, 99]
- **Model name:** SM-S-Octet

A charged scalar colour octet O coupled to a scalar singlet S was proposed in Refs. [48, 99]. Here the singlet is the 750 GeV candidate, while the octet enters the loops that contribute to the generation of the couplings of the singlet to the gauge bosons. While Ref. [99] considers a toy model involving only the term $S|O|^2$, Ref. [48] takes the singlet extended Manohar-Wise model [329]. For the SARAH implementation we have used the full model. However, since the cubic and quartic terms in O do not play a significant role, they are turned off by default in the SARAH model file.

Field	Gen.	$SU(3)_C$	$SU(2)_L$	$U(1)_Y$
S	1	1	1	0
O	1	8	2	$\frac{1}{2}$

Table 8. Extra scalar field content of the octet extended SM.

The extra particle content with respect to the SM is a real singlet S and a scalar color octet O which is also charged under $SU(2)_L \times U(1)_Y$, see Table 8. The isospin components of O are

$$O^A = \begin{pmatrix} O^{+A} \\ O^{0A} \end{pmatrix}, \quad (5.7)$$

where $A = 1, \dots, 8$ is the adjoint colour index. The full scalar potential reads

$$\begin{aligned} V = & \frac{1}{2}m_S^2 S^2 + \lambda_S S^4 - \mu^2 |H|^2 + \lambda_H |H|^4 + \kappa_1 S^2 |H|^2 + 2m_O^2 \text{Tr}(O^\dagger O) + \kappa_2 S^2 \text{Tr}(O^\dagger O) \\ & + \lambda_1 |H|^2 \text{Tr}(O^\dagger O) + \lambda_2 H_i^\dagger H_j \text{Tr}(O_j^\dagger O_i) + \lambda_6 \text{Tr}(O^\dagger O O^\dagger O) + \lambda_7 \text{Tr}(O_i^\dagger O_j O_j^\dagger O_i) \\ & + \lambda_8 \text{Tr}(O^\dagger O)^2 + \lambda_9 \text{Tr}(O_i^\dagger O_j) \text{Tr}(O_j^\dagger O_i) + \lambda_{10} \text{Tr}(O_i O_j) \text{Tr}(O_i^\dagger O_j^\dagger) + \lambda_{11} (O_i O_j O_j^\dagger O_i^\dagger) \\ & + \left(\lambda_3 H_i^\dagger H_j^\dagger \text{Tr}(O_i O_j) + \lambda_4 H_i^\dagger \text{Tr}(O_j^\dagger O_j O_i) + \lambda_5 H_i^\dagger \text{Tr}(O_j^\dagger O_i O_j) + \text{h.c.} \right). \end{aligned} \quad (5.8)$$

Electroweak symmetry-breaking (EWSB) is driven by the VEV of the neutral component of the SM Higgs doublet, which can be decomposed as

$$H^0 = \frac{1}{\sqrt{2}} (v + \phi_H + i \sigma_H). \quad (5.9)$$

Here $\phi_H \equiv h$ is the Higgs boson, to be identified with the 125 GeV state discovered at the LHC. Similarly, the singlet S receives a VEV, and the neutral component of the octet is split into its CP-even and CP-odd eigenstates:

$$S = v_S + \phi_S, \quad O^0 \rightarrow \frac{1}{\sqrt{2}} (O^R + i O^I). \quad (5.10)$$

We will now briefly discuss the parameter space of the model in order to justify our choice of input parameters. First, we consider the tadpole equations, which can be automatically derived by SARAH. Their solution for μ^2 and κ_1 is

$$\begin{aligned}\mu^2 &= -\frac{1}{v^2}(\lambda_H v^4 - m_S^2 v_S^2 - 4\lambda_S v_S^4), \\ \kappa_1 &= -\frac{1}{v^2}(m_S^2 + 4\lambda_S v_S^2).\end{aligned}\tag{5.11}$$

The tree-level mass matrix for the CP-even neutral scalars in the (ϕ_H, ϕ_S) basis is given by

$$\begin{aligned}\mathcal{M}^2 &= \begin{pmatrix} \mu^2 + 3\lambda_H v^2 + \kappa_1 v_S^2 & 2\kappa_1 v v_S \\ 2\kappa_1 v v_S & m_S^2 + \kappa_1 v^2 + 12\lambda_S v_S^2 \end{pmatrix} \\ &= \begin{pmatrix} 2\lambda_H v^2 & -\frac{2v_S}{v}(m_S^2 + 4\lambda_S v_S^2) \\ -\frac{2v_S}{v}(m_S^2 + 4\lambda_S v_S^2) & 8\lambda_S v_S^2 \end{pmatrix}.\end{aligned}\tag{5.12}$$

We note that, in general, there is singlet-doublet mixing. There are two reasons to consider a small singlet-doublet mixing angle, θ . First, the stringent constraints derived from Higgs physics measurements, and second, the required suppressed decay widths into Higgses, W's and Z's in order to fit the diphoton signal – indeed in [48] values of $\sim 10^{-2}$ were found to be required. If we have a small mixing angle, then we can write

$$\mathcal{M}^2 \sim \begin{pmatrix} m_h^2 & s_\theta c_\theta (m_h^2 - m_{750}^2) \\ s_\theta c_\theta (m_h^2 - m_{750}^2) & m_{750}^2 \end{pmatrix}.\tag{5.13}$$

This implies $\lambda_S > 0$, but also

$$\mu^2 \simeq -\frac{1}{2}m_h^2 + \frac{v_S^2}{v^2}(m_S^2 + \frac{1}{2}m_{750}^2).\tag{5.14}$$

However, we also have $v_S^2 \sim m_{750}^2/8\lambda_S$, and so

$$\mu^2 \simeq -\frac{1}{2}m_h^2 + \frac{1.2}{\lambda_S}(m_S^2 + \frac{1}{2}m_{750}^2).\tag{5.15}$$

We thus require a tachyonic m_S^2 for the SM Higgs mass condition:

$$m_S^2 \simeq -\frac{1}{2}m_{750}^2 + \frac{\lambda_S}{1.2}(\mu^2 + \frac{1}{2}m_h^2) \lesssim -(500 \text{ GeV})^2\tag{5.16}$$

where in the last step we have taken $\lambda_S = 1.2$, a rather large value. If we want $\kappa_1 \sim -1$ then we require $m_S^2 \sim -(600 \text{ GeV})^2$. On the other hand, from the second tadpole equation we have

$$m_S^2 = -\kappa_1 v^2 - \frac{1}{2}m_{750}^2,\tag{5.17}$$

which, if we require $|\kappa_1| < 2$, gives

$$-(630 \text{ GeV})^2 \leq m_S^2 \leq -(400 \text{ GeV})^2, \quad (5.18)$$

so putting these together we find the narrow window

$$-(630 \text{ GeV})^2 \leq m_S^2 \leq -(500 \text{ GeV})^2. \quad (5.19)$$

Alternative implementation in SARAH

The above discussion suggests to use a different choice for the input parameters of the model in our SARAH implementation: ideally we would like the particle masses, the mixing and only dimensionless couplings to be the inputs. We shall take the input parameters to be

$$m_h, m_{750}, s_\theta, \lambda_S. \quad (5.20)$$

In terms of these the other parameters are determined to be

$$\begin{aligned} \lambda_H &= \frac{c_\theta^2 m_h^2 + s_\theta^2 m_{750}^2}{2v^2}, & v_S^2 &= \frac{c_\theta^2 m_{750}^2 + s_\theta^2 m_h^2}{8\lambda_S} \\ m_S^2 &= -\kappa_1 v^2 - \frac{1}{2} m_{750}^2, & \kappa_1 v v_S &= s_\theta c_\theta (m_h^2 - m_{750}^2) \\ \rightarrow \kappa_1 &= \frac{\sqrt{2\lambda_S} s_\theta c_\theta (m_h^2 - m_{750}^2)}{v \sqrt{(c_\theta^2 m_{750}^2 + s_\theta^2 m_h^2)}} \simeq -4.3 \times s_\theta \sqrt{\lambda_S} \end{aligned} \quad (5.21)$$

The exact version of these equations is implemented in SARAH and can be selected using the `InputFile→"SPheno_diphoton.m"` option in `MakeAll` or `MakeSPheno`.

Octet masses

One further input is taken in [48]: the physical mass of the octet scalars. These are given in terms of the Lagrangian parameters as:

$$\begin{aligned} m_{O^0}^2 &= m_O^2 + \kappa_2 v_S^2 + \frac{v^2}{2} (\lambda_1 + \lambda_2 + 2 \text{Re}(\lambda_3)) \\ m_{O_i^0}^2 &= m_O^2 + \kappa_2 v_S^2 + \frac{v^2}{2} (\lambda_1 + \lambda_2 - 2 \text{Re}(\lambda_3)) \\ m_{O^+}^2 &= m_O^2 + \kappa_2 v_S^2 + \frac{1}{2} \lambda_1 v^2 \end{aligned} \quad (5.22)$$

The values of λ_i are taken to be small and equal in order for the octets to have similar masses, but since this is not the general case, we do not impose this choice in SARAH.

The choice in that paper does however hide the possibility of tachyonic m_O^2 (and hence possible charge/colour breaking minima) – indeed, if we insist that $m_O^2 > 0$ we have a lower bound on the masses of

$$m_{O^{0,+}}^2 > \frac{\kappa_2}{8\lambda_S} m_{750}^2. \quad (5.23)$$

Clearly this is violated for $m_{O^{0,+}} = 600$ GeV when $\kappa_2 \sim 1$, $\lambda_S \ll 1$. On the other hand, this does not guarantee a problem.

The desired vacuum has energy

$$\begin{aligned} V_0 &= \frac{m_S^2 v_S^2}{2} - \frac{\lambda_H}{4} v^4 + \lambda_S v_S^4 \\ &\simeq -\frac{1}{8} v^2 m_h^2 - v_S^2 \left(\frac{1}{2} \kappa_1 v^2 + \frac{1}{4} m_{750}^2 - \frac{m_{750}^2}{8} \right) \\ &\simeq -\frac{1}{8} v^2 m_h^2 - \frac{m_{750}^2}{8\lambda_S} (-2s_\theta \sqrt{\lambda_S} + \frac{m_{750}^2}{8}) \end{aligned} \quad (5.24)$$

If we instead concentrate on the potential terms containing the octets, where only one component develops a VEV, we find

$$\begin{aligned} V(O^R) &= \frac{1}{2} (O^R)^2 \left[m_O^2 + \frac{1}{8} (\lambda_9 + \lambda_{10} + \frac{1}{9} \lambda_6 + \frac{1}{9} \lambda_7 + \frac{1}{9} \lambda_{11}) (O^R)^2 \right] \\ V(O^I) &= \frac{1}{2} (O^I)^2 \left[m_O^2 + \frac{1}{8} (\lambda_9 + \lambda_{10} + \frac{1}{9} \lambda_6 + \frac{1}{9} \lambda_7 + \frac{1}{9} \lambda_{11}) (O^I)^2 \right] \\ V(O^+) &= |O^+|^2 \left[m_O^2 + \frac{1}{4} (\lambda_9 + \lambda_{10} + \frac{1}{9} \lambda_6 + \frac{1}{9} \lambda_7 + \frac{1}{9} \lambda_{11}) |O^+|^2 \right] \end{aligned} \quad (5.25)$$

Arranging for the additional minimum of the potential to be higher than the colour-breaking one then places a *lower* bound on the octet self-couplings, but for the phenomenology of the diphoton excess – when we neglect loop corrections to the mass of the octet – they play no other role.

Comments on fitting the excess

In [48] the authors find that the diphoton excess can be easily fit with octets at 600 or 1000 GeV and $\kappa_2 \sim 1.5$ or 4.5, respectively. The scenario involves merely the simplifying assumption $\lambda_1 = \lambda_2 = \lambda_3$ so that the octets are of approximately equal mass. The ratio between the digluon and diphoton decay rates is then

$$\frac{\Gamma(S \rightarrow gg)}{\Gamma(S \rightarrow \gamma\gamma)} \simeq \frac{9 \alpha_s^2}{2 \alpha^2}. \quad (5.26)$$

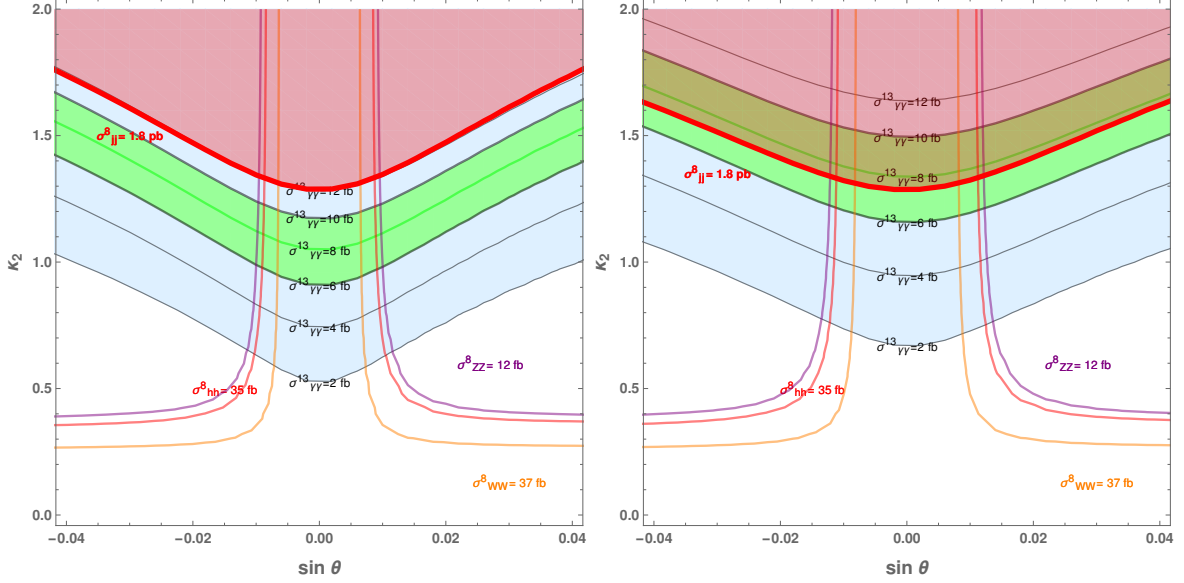


Figure 10. Scan over sine of Higgs-singlet mixing angle θ and κ_2 for octet masses of 600 GeV, $\lambda_S = 0.07$ corresponding to $v_S \simeq 1000$ GeV. The contours show the 750 GeV resonance production cross-sections σ_{YY}^X at energy X TeV decaying into channel YY . On the left plot, only leading order contributions to the decays are used; on the right, all corrections up to N^3 LO available in SARAH are included.

In [48] this is quoted as $\simeq 715$. In SARAH, before any NLO corrections are applied, the running of the Standard Model gauge couplings yields $\alpha_s(750 \text{ GeV}) = 0.091$ and we use $\alpha(0) \simeq 137^{-1}$, giving a ratio of 700, in good agreement. However, when we include corrections up to N^3 LO, this ratio rises to 1150, putting the model near the boundary of exclusion due to dijet production at 8 TeV. These differences are illustrated in plots produced from SARAH/SPheno in figure 10. To produce these plots, all branching ratios/widths are calculated in SPheno, as is the production cross-section of the resonance at 8 TeV. To calculate 13 TeV cross-sections the 8 TeV cross-section was rescaled by the parton luminosity factor for gluons of 4.693.

5.2.1.3 Vector-like $SU(2)$ triplet quark model

- **Reference:** [32]
- **Model name:** SM+VL/TripletQuarks

The model introduced in [32] considers a singlet scalar S as the candidate for the 750 GeV resonance. In order to produce the singlet via gluon fusion at the LHC, the

model is further extended with the introduction of vector-like quarks, triplet under $SU(2)_L$. Moreover, the singlet is charged under a \mathbb{Z}_2 parity, although this is softly broken by the vector-like quark mass terms.

Field	Gen.	$SU(3)_C$	$SU(2)_L$	$U(1)_Y$	\mathbb{Z}_2
S	1	1	1	0	–
F_{1L}	1	3	3	$\frac{2}{3}$	–
F_{1R}	1	3	3	$\frac{2}{3}$	+
F_{2L}	1	3	3	$-\frac{1}{3}$	–
F_{2R}	1	3	3	$-\frac{1}{3}$	+

Table 9. Extra scalar/fermionic degrees of freedom shown in the top/bottom. All SM particles are even under the imposed discrete symmetry.

This model is based on the SM gauge symmetry, extended with a \mathbb{Z}_2 parity. The fermionic and scalar particle content is summarized in Table 9. The vector-like $SU(2)_L$ triplet quarks can be expressed in 2×2 matrix notation as

$$F_1 = \begin{pmatrix} U_1/\sqrt{2} & X \\ D_1 & -U_1/\sqrt{2} \end{pmatrix}, \quad F_2 = \begin{pmatrix} D_2/\sqrt{2} & U_2 \\ Y & -D_2/\sqrt{2} \end{pmatrix}. \quad (5.27)$$

Here we see that the $U_{1,2}$ and $D_{1,2}$ components have the same electric charges as the SM up- and down-type quarks, respectively. The components X and Y are exotic coloured states with electric charges $5/3$ and $-4/3$, respectively, and thus they do not mix.

The Yukawa Lagrangian of the model can be written as

$$-\mathcal{L}_Y = \mathcal{L}_Y^{\text{SM}} + Y_1 \overline{Q}_L F_{1R} \tilde{H} + Y_2 \overline{Q}_L F_{2R} H + (m_{F_1} + Y_{F_1 S} S) \overline{F}_1 F_1 + (m_{F_2} + Y_{F_2 S} S) \overline{F}_2 F_2 + \text{h.c.}, \quad (5.28)$$

whereas the scalar potential is given by

$$V = -\mu^2 |H|^2 + \lambda_H |H|^4 + m_S^2 S^2 + \frac{1}{4} \lambda_S S^4 + \frac{1}{3} \lambda_{HS} |H|^2 S^2. \quad (5.29)$$

We note that the vector-like mass terms for F_1 and F_2 softly break the \mathbb{Z}_2 parity. We assume that the SM Higgs doublet obtains a VEV while the introduced singlet does not, hence

$$H = \frac{1}{\sqrt{2}} \begin{pmatrix} 0 \\ v + \phi_H + i \sigma_H \end{pmatrix}, \quad S = \phi_S. \quad (5.30)$$

The \mathbb{Z}_2 discrete symmetry, together with $\langle S \rangle = 0$ ensured by the symmetry, implies that no mixing between the SM Higgs boson ϕ_H and the singlet S appears at tree-level.

5.2.1.4 Single scalar leptoquark model

- **Reference:** [27]
- **Model name:** Leptoquarks/ScalarLeptoquarks

The model introduced in Ref. [27] considers a singlet scalar, S , as candidate for the 750 GeV resonance. It is based on the scalar leptoquark model in Ref. [330], with the addition of a vector-like fermion multiplet χ transforming in an a priori unspecified representation of $SU(2)_L$. The simplest model, which the authors find to work, requires χ to be a $SU(2)_L$ triplet. The model is based on the gauge symmetries of the SM, augmented with either a discrete or gauge symmetry necessary for the DM sector. For the sake of simplicity we choose to realise the model using only a discrete \mathbb{Z}_2 symmetry. The particle content beyond the SM is shown in Table 10.

Field	Gen.	$SU(3)_C$	$SU(2)_L$	$U(1)_Y$	\mathbb{Z}_2
S	1	1	1	0	+
ϕ	1	3	1	$-\frac{1}{3}$	+
χ	N_χ	1	3	Y_χ	-

Table 10. Additional scalar and fermionic particles beyond the SM shown in the top and bottom respectively. Note that all SM fields are neutral under the \mathbb{Z}_2 symmetry.

The new degrees of freedom are: the scalar leptoquarks ϕ , the gauge singlet scalar S , which is assumed to be real, and finally the vector-like triplet fermions χ . The vector-like $SU(2)_L$ triplet can be expressed in 2×2 matrix notation as

$$\chi = \begin{pmatrix} \frac{\chi^0}{\sqrt{2}} & \chi^+ \\ \chi^- & -\frac{\chi^0}{\sqrt{2}} \end{pmatrix}. \quad (5.31)$$

Due to the discrete \mathbb{Z}_2 symmetry the neutral component χ^0 is stable and a suitable DM candidate. In Ref. [27] the hypercharge Y_χ and the number of generations N_χ are left as free parameters. In order to boost the ratio of decay widths $\Gamma_{S \rightarrow \gamma\gamma} / \Gamma_{S \rightarrow gg}$ they claim that the minimal choice is $N_\chi = 2$ and $Y_\chi = 0$. The model files are implemented with these values.

The Yukawa interactions of the model and the vector-like mass term can be expressed as

$$-\mathcal{L}_Y = -\mathcal{L}_Y^{\text{SM}} + \lambda^L \overline{Q^c} L \phi^* + \lambda^R \overline{u_R^c} e_R \phi^* + \frac{1}{2} M_\chi \overline{\chi} \chi + g_{S\chi} S \overline{\chi} \chi + \text{h.c.}, \quad (5.32)$$

whereas the scalar potential is given by

$$V = V_{\text{SM}} + M_\phi^2 |\phi|^2 + \frac{1}{2} M_S^2 S^2 + \frac{1}{3} \lambda_{S_3} S^3 + \frac{1}{4} \lambda_{S_4} S^4 + \frac{1}{2} \lambda_\phi |\phi|^4 \\ + g_{SH} S^2 |H|^2 + g_{H\phi} |\phi|^2 |H|^2 + g_{S\phi} S^2 |\phi|^2 + \kappa_{S\phi} S |\phi|^2 + \kappa_{SH} S |H|^2. \quad (5.33)$$

The Lagrangian in Eq. (5.32) is not generic. One could add more renormalizable operators involving the leptoquark, like $\overline{d_R^c} u_R \phi$ for instance. An operator of this kind, together with those in Eq. (5.32), would lead to rapid proton decay, thus it must be forbidden [330]. This can be achieved by imposing a discrete symmetry (for instance another \mathbb{Z}_2 under which the leptoquark and the SM quarks are odd and everything else is even). In the model file we simply omit these dangerous operators. The potential in Eq. (5.33), on the other hand, is generic. It could be simplified by introducing yet another \mathbb{Z}_2 to avoid terms with odd powers of S , and we would still have the necessary ingredients to fit the diphoton excess.

We assume the EWSB proceeds by the usual Higgs VEV in addition to the singlet VEV v_S , where the scalar singlet is expressed as

$$S = v_S + \sigma_S. \quad (5.34)$$

5.2.1.5 Two scalar leptoquark model

- **Reference:** [65]
- **Model name:** Leptoquarks/TwoScalarLeptoquarks

This model includes four additional scalars, two of which, Φ and Ω are leptoquarks. The other two are a singlet S , which is the 750 GeV resonance, and a scalar Θ which carries hypercharge. The additional quantum numbers for these new field are shown in Table 11.

The Yukawa interactions consistent with these new fields is given by

$$-\mathcal{L}_Y = \mathcal{L}_Y^{\text{SM}} + Y_\Theta L^T i \sigma_2 L \Theta + Y_\Omega Q_L^T i \sigma_2 L \Omega + Y_\Phi e_R^T d_R \Phi + \text{h.c.}, \quad (5.35)$$

Field	Gen.	$SU(3)_C$	$SU(2)_L$	$U(1)_Y$
S	1	$\mathbf{1}$	$\mathbf{1}$	0
Θ	1	$\mathbf{1}$	$\mathbf{1}$	1
Φ	1	$\bar{\mathbf{3}}$	$\mathbf{1}$	$\frac{4}{3}$
Ω	1	$\bar{\mathbf{3}}$	$\mathbf{1}$	$\frac{1}{3}$

Table 11. Additional scalar particles beyond the SM appearing in the two scalar leptoquark model.

where the generation indices have been suppressed. These indices are important so that one obtains non-zero contractions for the first term in the above Yukawa. The scalar potential of the model is given by

$$V = V_{\text{SM}} + \sum_i \mu_\phi^2 |\phi_i|^2 + \frac{1}{2} \sum_{i,j} \lambda_{ij} |\phi_i|^2 |\phi_j|^2 + \{ \lambda S \Theta \Phi^\dagger \Omega + \text{h.c.} \} , \quad (5.36)$$

where the index $i = \{S, \Theta, \Phi, \Omega\}$ runs over the introduced scalar fields. The potential has an additional $U(1)$ symmetry which can be gauged or global. In the implementation in **SARAH** we take it as global. This symmetry can be used to forbid terms such as $u_R d_R \Omega^\dagger$, which could potentially lead to proton decay.

One can generate neutrino masses at the two-loop level using a combination of the new Yukawa couplings and the VEV of the singlet. Beyond the neutral components of the Higgs doublet, the singlet also obtains a VEV of the form

$$S = v_S + \phi_S . \quad (5.37)$$

5.2.1.6 Georgi-Machacek model

- **Reference:** [70, 108]
- **Model name:** Georgi-Machacek

The model originally proposed in Ref. [277] extends the SM by one real scalar $SU(2)_L$ -triplet η with $Y = 0$ and one complex scalar $SU(2)_L$ -triplet with χ with $Y = 1$, which can be written as

$$\eta = \frac{1}{\sqrt{2}} \begin{pmatrix} \eta^0 & -\sqrt{2}(\eta^-)^* \\ -\sqrt{2}\eta^- & -\eta^0 \end{pmatrix} , \quad \chi = \frac{1}{\sqrt{2}} \begin{pmatrix} \chi^- & \sqrt{2}(\chi^0)^* \\ -\sqrt{2}\chi^{--} & -\chi^- \end{pmatrix} . \quad (5.38)$$

The CP-even components of the new scalars mix with the neutral SM Higgs. Usually, the lightest state is the 125 GeV Higgs boson, while the second mass eigenstate is

identified with the 750 GeV resonance. The most compact form to write the Lagrangian in a $SU(2)_L \times SU(2)_R$ invariant form is to express the Higgs doublet and the two scalar triplets as

$$\Phi = \begin{pmatrix} \phi^{0*} & \phi^+ \\ \phi^- & \phi^0 \end{pmatrix}, \quad \Delta = \begin{pmatrix} \chi^{0*} & \eta^+ & \chi^{++} \\ \chi^- & \eta^0 & \chi^+ \\ \chi^{--} & \eta^- & \chi^0 \end{pmatrix}. \quad (5.39)$$

In this form, the scalar potential reads

$$\begin{aligned} V(\Phi, \Delta) = & \mu_2^2 \text{Tr} \Phi^\dagger \Phi + \frac{\mu_3^2}{2} \text{Tr} \Delta^\dagger \Delta + \lambda_1 [\text{Tr} \Phi^\dagger \Phi]^2 + \lambda_2 \text{Tr} \Phi^\dagger \Phi \text{Tr} \Delta^\dagger \Delta \\ & + \lambda_3 \text{Tr} \Delta^\dagger \Delta \Delta^\dagger \Delta + \lambda_4 [\text{Tr} \Delta^\dagger \Delta]^2 - \lambda_5 \text{Tr} (\Phi^\dagger \sigma^a \Phi \sigma^b) \text{Tr} (\Delta^\dagger t^a \Delta t^b) \\ & - M_1 \text{Tr} (\Phi^\dagger \tau^a \Phi \tau^b) (U \Delta U^\dagger)_{ab} - M_2 \text{Tr} (\Delta^\dagger t^a \Delta t^b) (U \Delta U^\dagger)_{ab}, \end{aligned}$$

τ^a and t^a are the $SU(2)$ generators for the doublet and triplet representations respectively, while U is given for instance in Ref. [331]. Because of the custodial symmetry, the VEVs for the triplets are identical, and there are no tree-level contributions to electroweak precision observables. The compact form of the potential can not be implemented in SARAH, so we have translated into the form of Eq. (5.38). For example:

$$\lambda_2 \text{Tr} \Phi^\dagger \Phi \text{Tr} \Delta^\dagger \Delta \quad \rightarrow \quad 4\lambda_2^a |H|^2 \text{Tr} (\chi^\dagger \chi) + 2\lambda_2^b |H|^2 \text{Tr} (\eta^\dagger \eta). \quad (5.40)$$

This introduces more couplings, which have to be identical to preserve the custodial symmetry. A substitution rule to apply these relations is included in the model file.

The triplets receive VEV as

$$\langle \eta \rangle = \frac{1}{\sqrt{2}} \begin{pmatrix} v_\eta & 0 \\ 0 & -v_\eta \end{pmatrix}, \quad \langle \chi \rangle = \begin{pmatrix} 0 & v_\chi \\ 0 & 0 \end{pmatrix}, \quad (5.41)$$

which fulfil $v_\eta = v_\chi$ if the custodial symmetry is preserved.

5.2.2 Two-Higgs doublet models

Two-Higgs-doublet models (THDMs) are among the most common candidates to explain the diphoton excess. In this family of models, the 750 GeV resonance is typically a heavy Higgs, whose diphoton rate is enhanced with the addition of new states that contribute to its production cross-section and/or its decay width into pairs of photons. Several realisations of this idea can be found in the recent literature. Here we review a few representative examples.

THDM generalities

We first comment on some general features and conventions used in THDMs. For a complete review we refer to Ref. [332].

Couplings to fermions

We will consider three types of THDM, depending on the way the two Higgs doublets H_1 and H_2 couple to the SM fermions, as shown in this table:

	u_R	d_R	e_R
Type-I	H_2	H_2	H_2
Type-II	H_2	H_1	H_1
Type-III	both	both	both

We note that, by convention, the right-handed up-type quarks u_R always couple to H_2 , and that the MSSM can be seen as a particular example of a type-II THDM. The type-I and type-II THDMs are usually said to be models with *natural flavour conservation*. This is because, in contrast to the general type-III THDM, flavour changing neutral currents are completely absent at tree-level, thus satisfying flavour constraints more easily. This is achieved by coupling each fermion species to only one Higgs doublet, which can be enforced using a discrete symmetry. For example, the type-I THDM couplings to fermions can be obtained by imposing that $H_1 \rightarrow -H_1$ is a symmetry of the Lagrangian. In our **SARAH** implementations we will not introduce these discrete symmetries explicitly, but simply allow only for those couplings that characterise the type of THDM under consideration. We point out that **SARAH** includes also other THDM versions, such as the lepton-specific or flipped ones. These versions can be easily combined with the extensions presented here for type I–III to include additional matter in order to explain the diphoton excess. Finally, we have also not implemented explicitly all representations for the vector-like states proposed in the literature so far. For instance, Ref. [159] introduces quarks with a very large hypercharge. However, it is easy to change the considered quantum numbers by changing the model files accordingly.

Scalar potential

We assume the following scalar potential for all THDMs considered below,

$$\begin{aligned}
 V = & m_{11}^2 |H_1|^2 + m_{22}^2 |H_2|^2 + \left[m_{12}^2 H_1^\dagger H_2 + \text{h.c.} \right] \\
 & + \frac{\lambda_1}{2} |H_1|^4 + \frac{\lambda_2}{2} |H_2|^4 + \lambda_3 |H_1|^2 |H_2|^2 \\
 & + \lambda_4 \left(H_1^\dagger H_2 \right) \left(H_2^\dagger H_1 \right) + \left[\frac{\lambda_5}{2} \left(H_1^\dagger H_2 \right)^2 + \text{h.c.} \right]. \tag{5.42}
 \end{aligned}$$

In principle, the quartic terms $\lambda_6 \left(H_1^\dagger H_1 \right) \left(H_1^\dagger H_2 \right)$ and $\lambda_7 \left(H_2^\dagger H_2 \right) \left(H_1^\dagger H_2 \right)$ are also allowed by the gauge symmetry. However, in our **SARAH** implementation we neglect

these terms. This corresponds to assuming a global symmetry, which would be softly broken by the $m_{12}^2 H_1^\dagger H_2$ term.

Symmetry breaking pattern

The symmetry breaking pattern is the same in all THDM variations, namely

$$\langle H_i \rangle = \left\langle \begin{pmatrix} H_i^+ \\ H_i^0 \end{pmatrix} \right\rangle = \frac{1}{\sqrt{2}} \begin{pmatrix} 0 \\ v_i \end{pmatrix}, \quad (5.43)$$

with $i = 1, 2$ running over the two Higgs-doublets.

In the following, we describe the THDM variations implemented in SARAH related to the diphoton excess. Broadly speaking, there are two main categories: THDMs with extra vector-like fermions and THDMs with extra scalar content. In the first case we have three examples, whereas for the second scenario we have only a single example.

5.2.2.1 Minimal vector-like THDM

- **Reference:** [41]
- **Model name:**
THDM+VL/min-3
THDM+VL/min-8

Ref. [41] considers a type-III THDM extended with two new vector-like colored fermions, S and Q^V , aiming at a simultaneous explanation of the diphoton excess and of the CMS hint for the Higgs lepton flavor violating (LFV) decay $h \rightarrow \tau\mu$ [333]. The type-III THDM has already been shown in several papers to be able to accommodate this LFV signal, see e.g. [334, 335], but [41] is the first work that addresses the diphoton excess at the same time. The representations of the new vector-like fermions under SM gauge group are shown in Table 12.

Field	Gen.	$SU(3)_C$	$SU(2)_L$	$U(1)_Y$
S	1	R_c	1	Q
Q^V	1	R_c	2	$Q + \frac{1}{2}$

Table 12. Additional fermion field content for the minimal vector-like THDM.

We choose the explicit realizations $R_c = 3$, $Q = 2$ (THDM+VL/minTHDM-3) and $R_c = 8$, $Q = 2$ (THDM+VL/minTHDM-8). In both cases, the additional interaction terms beyond those in the standard THDM are

$$-\mathcal{L}_{\text{new}} = M_Q^V \overline{Q_R^V} Q_L^V + M_S \overline{S_R} S_L + \lambda_i^D \overline{S_R} \tilde{H}_i Q_L^V + \lambda_i^S \overline{Q_R^V} H_i S_L + \text{h.c.}, \quad (5.44)$$

where M_Q^V and M_S are masses for the $SU(2)_L$ -doublet and singlet vector-like fermions, respectively, and $\lambda_i^{D,S}$ (with $i = 1, 2$) are new Yukawa interactions.

5.2.2.2 THDM with exotic vector-like fermions

- **References:** [155, 213]
- **Model name:**
THDM+VL/Type-I-VL
THDM+VL/Type-II-VL

The THDMs in Refs. [155, 213] consider a less minimal framework where three generations of new vector-like fermions are added to the standard THDM scenario. Both type-I and type-II THDMs are studied. Furthermore, the vector-like leptons have exotic hypercharge values shown in Table 13.

Field	Gen.	$SU(3)_C$	$SU(2)_L$	$U(1)_Y$	\mathbb{Z}_2
Q^V	3	3	2	$\frac{1}{6}$	–
d^V	3	3	1	$-\frac{1}{3}$	–
u^V	3	3	1	$\frac{2}{3}$	–
L^V	3	1	2	$-\frac{3}{2}$	–
e^V	3	1	1	-2	–
ν^V	3	1	1	-1	–

Table 13. Additional fermion field content for the THDM with exotic vector-like fermions. All SM fields are even under the imposed \mathbb{Z}_2 discrete symmetry.

The vector-like lepton states can be decomposed (or denoted) as

$$L^V = \begin{pmatrix} \ell'^- \\ \ell^{--} \end{pmatrix}, \quad e^V \equiv (e^V)^{--}, \quad \nu^V \equiv (\nu^V)^-, \quad (5.45)$$

where we explicitly highlight the presence of doubly-charged leptons. The additional interaction terms beyond those in the standard THDMs are

$$\begin{aligned} -\mathcal{L}_{\text{new}} = & M_Q^V \overline{Q_R^V} Q_L^V + M_L^V \overline{L_R^V} L_L^V + M_d^V \overline{d_R^V} d_L^V + M_u^V \overline{u_R^V} u_L^V + M_\nu^V \overline{\nu_R^V} \nu_L^V + M_e^V \overline{e_R^V} e_L^V \\ & + Y_{dL}^V \overline{d_R^V} \tilde{H}_1 Q_L^V + Y_{dR}^V \overline{Q_R^V} H_1 d_L^V + Y_{uL}^V \overline{u_R^V} H_2 Q_L^V + Y_{uR}^V \overline{Q_R^V} \tilde{H}_2 u_L^V \\ & + Y_{eL}^V \overline{e_R^V} \tilde{H}_1 L_L^V + Y_{eR}^V \overline{L_R^V} H_1 e_L^V + Y_{\nu L}^V \overline{\nu_R^V} H_2 L_L^V + Y_{\nu R}^V \overline{L_R^V} \tilde{H}_2 \nu_L^V + \text{h.c.} \end{aligned} \quad (5.46)$$

Here M_i^V are the bare vector-like masses and Y_i^V are Yukawa couplings. For simplicity, we assume that the vector-like states do not mix with the SM fermions. This can be

enforced with a discrete \mathbb{Z}_2 symmetry under which the vector-like states are odd and the rest of the states even.

5.2.2.3 THDM with SM-like vector-like fermions

- **Reference:** [21]
- **Model name:**
 THDM+VL/Type-I-SM-like-VL
 THDM+VL/Type-II-SM-like-VL

The THDM proposed in [21] introduces vector-like copies of the SM quarks and leptons, the $SU(2)_L$ doublets Q^V and L^V , as well as the $SU(2)_L$ singlets d^V , u^V , ν^V and e^V with their respective quantum numbers shown in Table 14.

Field	Gen.	$SU(3)_C$	$SU(2)_L$	$U(1)_Y$	\mathbb{Z}_2
Q^V	1	3	2	$\frac{1}{6}$	–
d^V	1	3	1	$-\frac{1}{3}$	–
u^V	1	3	1	$\frac{2}{3}$	–
L^V	1	1	2	$-\frac{1}{2}$	–
e^V	1	1	1	–1	–
ν^V	1	1	1	0	–

Table 14. Additional fermion field content for the THDM with SM-like vector-like fermions. All SM fields are even under the imposed \mathbb{Z}_2 discrete symmetry.

In contrast to other THDMs proposed to explain the diphoton excess, where low values of $\tan \beta$ are taken in order to increase the heavy Higgs coupling to the top quark and induce a large gluon fusion cross-section, this paper considers moderate and large values of $\tan \beta$. In this case, the heavy Higgs production is mainly induced by the new vector-like colored states. Moreover, the advantage of using largish $\tan \beta$ values is that the total decay width of the heavy Higgs is suppressed, thus allowing for a smaller $\Gamma(H \rightarrow \gamma\gamma)$ to explain the excess.

The new interaction terms take the same form as those in Eq. (5.46). Furthermore, as in the previous models, we assume that the new vector-like states do not mix with the SM fermions. For this reason, we introduce a \mathbb{Z}_2 parity under which the vector-like states are odd and the rest of the states even. Finally, Ref. [21] considers two variants of this scenario in what concerns the couplings to the SM fermions: a type-I THDM and a type-II THDM.

5.2.2.4 THDM with a real scalar septuplet

- **Reference:** [134, 187]
- **Model name:** THDM/ScalarSeptuplet

Ref. [134] explores an extension of the type-III THDM with new scalar $SU(2)_L$ representations, namely an inert complex Higgs triplet and a real scalar septuplet. A more general analysis can be found in Ref. [187], where a generic real scalar $SU(2)_L$ multiplet is considered. In both papers, the 750 GeV resonance is identified with the usual heavy Higgs of the THDM, with the additional scalars being introduced to push the diphoton rate to higher values.

For the realization of this idea here we focus on the septuplet case, closely following Ref. [134]. The introduction of such large scalar multiplets has become fairly popular recently in the context of minimal DM scenarios [336], although [134] does not explore any dark matter implications. It only takes advantage of the multicharged states contained in the septuplet which, due to their couplings to the THDM doublets, lead to a large diphoton rate for the heavy Higgs H .

The type-III THDM is extended with the addition of a real scalar which transforms as a $\mathbf{7}$ under $SU(2)_L$, see Table 15.

Field	Gen.	$SU(3)_C$	$SU(2)_L$	$U(1)_Y$
T	1	$\mathbf{1}$	$\mathbf{7}$	0

Table 15. Additional fermion field content for the scalar septuplet extended THDM.

It proves convenient to use tensor notation for the septuplet. This is the usual choice, see Refs. [337, 338], and the one implemented in SARAH. The septuplet T is represented by a symmetric tensor with six indices, T^{ijklmn} , all of which can take values of either 1 or 2. The relation with the vector notation, employed for example in [134], is given by

$$T \equiv \begin{pmatrix} T^{+++} \\ T^{++} \\ T^+ \\ T^0 \\ T^- \\ T^{--} \\ T^{---} \end{pmatrix} = i \begin{pmatrix} +T^{111111} \\ +\sqrt{6} T^{111112} \\ +\sqrt{15} T^{111122} \\ -\sqrt{20} T^{111222} \\ -\sqrt{15} T^{112222} \\ +\sqrt{6} T^{122222} \\ -T^{222222} \end{pmatrix}. \quad (5.47)$$

The prefactor i and the sign for each component are introduced in order to satisfy $T^c = T$ where T^c denotes charge conjugation of the field T , and T^0 is a real scalar.

The new potential terms involving the septuplet T are

$$V_T = M_T^2 T^2 + \sum_{i=1}^2 \lambda_i^T [T^4]_i + \lambda_3^T |H_1|^2 T^2 + \lambda_4^T |H_2|^2 T^2. \quad (5.48)$$

We note that two independent gauge invariant contractions are possible in case of T^4 , which is reflected by the second term of Eq. (5.48). Finally, the authors of [134] assume a minimum of the scalar potential with $\langle T \rangle = 0$. In this case, the components of the septuplet do not mix with the scalar doublets, but only participate in the $H \rightarrow \gamma\gamma$ rate due to the interaction terms $\lambda_{3,4}^T$.

5.3 $U(1)$ extensions of the SM

In this section we consider a class of models which extend the SM by a new $U(1)_X$ gauge group. One typically introduces, beyond the SM Higgs doublet, new scalars charged under $U(1)_X$, which serve two purposes: (i) a linear combination of them results in the 750 GeV particle, and (ii) via spontaneous symmetry breaking they give mass to the new gauge boson, the Z' boson. Typically, one also introduces new fermions charged under the $U(1)_X$ symmetry that can either be singlets under the SM gauge group, hence forming a dark or hidden sector, or vector-like under the SM. An advantage of these models is that, through a suitable choice of charge assignments under $U(1)_X$, one can avoid flavour constraints present when allowing the additional quarks to decay. Finally, the presence of a massive Z' boson can lead to new collider signals, well studied in the literature, which can serve as a smoking gun for these types of models. We note that the mixing matrix for the neutral gauge bosons can be parametrised by two angles, Θ and Θ' , with Θ' highly constrained by LEP data.

We distinguish two cases in the following: models in which the SM fermions are charged under the new Abelian group, and models in which they are singlet.

5.3.1 Models with SM states uncharged under the new $U(1)$

5.3.1.1 Dark $U(1)'$ extension

- **Reference:** [166]
- **Model name:** U1Extensions/darkU1

This model is based on a gauged $U(1)_X$ extension of the SM with a dark sector that includes three generations of dark $SU(2)_L$ -singlet fermions and a DM scalar candidate.

The properties of the new particles introduced in this model are described in Table 16. We have added three right-handed neutrinos ν_R^i , neutral under $U(1)_X$, to the

original model, since N_R (their dark partners) were considered here. Φ is the scalar field responsible for the spontaneous symmetry breaking of $U(1)_X$, while X is the DM candidate. The $U(1)_X$ charges a, b are left arbitrary, with their assignment chosen such that they fulfil the anomaly cancellation conditions.

Field	Gen.	$SU(3)_C$	$SU(2)_L$	$U(1)_Y$	$U(1)_X$
Φ	1	1	1	0	$a + b$
X	1	1	1	0	a
E_L	3	1	1	-1	a
E_R	3	1	1	-1	$-b$
N_L	3	1	1	0	$-a$
N_R	3	1	1	0	b
U_L	3	3	1	$\frac{2}{3}$	$-a$
U_R	3	3	1	$\frac{2}{3}$	b
D_L	3	3	1	$-\frac{1}{3}$	a
D_R	3	3	1	$-\frac{1}{3}$	$-b$

Table 16. New fermions and scalar fields of the **darkU1** and their charge assignments under the gauge symmetry $SU(3)_C \times SU(2)_L \times U(1)_Y \times U(1)_X$. The scalar and fermion fields are shown in the top and bottom of the table respectively.

The Yukawa interactions and the scalar potential including new fields in the dark sector are described by

$$\begin{aligned}
-\mathcal{L}_Y^{\text{new}} = & Y'_E \overline{E_R} \Phi^* E_L + Y'_N \overline{N_R} \Phi N_L + Y'_U \overline{U_R} \Phi U_L + Y'_D \overline{D_R} \Phi^* D_L + Y_{XE} \overline{e_R} X^* E_L \\
& + Y_{XU} \overline{u_R} X U_L + Y_{XD} \overline{d_R} X^* D_L + Y_{XN} \overline{\nu_R} X N_L + \text{h.c.}, \tag{5.49}
\end{aligned}$$

$$\begin{aligned}
V = & \mu^2 |H|^2 + \lambda |H|^4 + \mu_\Phi^2 |\Phi|^2 + \mu_X^2 |X|^2 + \lambda_\Phi |\Phi|^4 + \lambda_X |X|^4 + \lambda_{H\Phi} |H|^2 |\Phi|^2 \\
& + \lambda_{HX} |H|^2 |X|^2 + \lambda_{X\Phi} |X|^2 |\Phi|^2, \tag{5.50}
\end{aligned}$$

where H denotes the SM Higgs doublet. For $a = b = 1$, an extra term $\Phi^\dagger X^2$ would be allowed in the potential, which breaks $U(1)_X$ down to a Z_2 subgroup after Φ develops a non-zero VEV. Likewise, for $3a = (a + b)$, there appears an extra term $\Phi^\dagger X^3$, which breaks $U(1)_X$ down to a Z_3 subgroup after Φ develops a nonzero VEV. These possibilities are not considered here.

The gauge symmetry is broken after H and Φ get non-zero VEVs, v and v_Φ respectively, while X does not receive a VEV⁹. The scalar fields after EWSB can be expressed

⁹We also checked that this condition remains valid at NLO.

as

$$H = \frac{1}{\sqrt{2}} \begin{pmatrix} 0 \\ v + \phi_H + i\sigma_H \end{pmatrix}, \quad \Phi = \frac{1}{\sqrt{2}} (v_\Phi + \phi_\Phi + i\sigma_\Phi), \quad (5.51)$$

where ϕ_i and σ_i are the CP-even and odd components respectively. The 750 GeV candidate is the mixture of the SM Higgs ϕ_H and ϕ_Φ , which leads to constraints on $\lambda_{H\Phi}$. It is produced in gluon-gluon fusion via loops of the dark quarks, and it decays into diphotons via loops comprised only of charged dark fermions, assuming that the mixing with the SM-like Higgs is negligibly small.

5.3.1.2 Hidden $U(1)$

- **Reference:** [83]
- **Model name:** U1Extensions/hiddenU1

This is a particularly simple realisation of a gauged $U(1)_X$ extension of the SM. As previously, a hidden $U(1)_X$ is added to the SM gauge group, under which all SM particles are singlets. A scalar S_1 is added for its spontaneous symmetry breaking, and a further scalar S_2 is added which is a singlet under the entire gauge symmetry of the model. Here we assume that both S_1 and S_2 can develop a VEV, in principle.

The 750 GeV candidate is considered to be predominantly composed by S_2 . To explain the diphoton signal, a vector-like quark is also included, carrying the same charge under $U(1)_X$ as the S_1 field. Hence, it couples only to S_2 due to the choice of charge assignments.

Field	Gen.	$SU(3)_C$	$SU(2)_L$	$U(1)_Y$	$U(1)_X$
S_1	1	1	1	0	a
S_2	1	1	1	0	0
X_L	1	3	1	Y_X	a
X_R	1	3	1	Y_X	a

Table 17. New fermions and scalar fields of the `hiddenU1` and their charge assignments under the gauge symmetry $SU(3)_C \times SU(2)_L \times U(1)_Y \times U(1)_X$. The scalar and fermion fields are shown in the top and bottom of the table respectively.

In Table 17 the hypercharge of the new vector-like quark Y_X is left arbitrary. The implemented case is the most favourable one in terms of the diphoton excess, $Y_X = 2/3$, which allows a mixing with the up-type quarks. We did not considered the case of

adding also a vector-like lepton to the spectrum, which would lead to even larger rates. The $U(1)_X$ charge of the vector-like quark fields a does not affect the diphoton rate, but it has to be the same as for S_1 , which is relevant for the Z' boson mass.

The scalar potential, with the usual doublet Higgs field H is given by

$$V = \mu_H^2 |H|^2 + \mu_{S_1}^2 |S_1|^2 + \mu_{S_2}^2 S_2^2 - \lambda_H |H|^4 - \lambda_{HS_1} |H|^2 |S_1|^2 - \lambda_{S_1} |S_1|^4 - \lambda_{S_2} S_2^4 - \lambda_{HS_2} |H|^2 S_2^2 - \lambda_{S_1 S_2} |S_1|^2 S_2^2 - \sigma_1 S_2^3 - \sigma_2 |H|^2 S_2 - \sigma_3 |S_1|^2 S_2. \quad (5.52)$$

This potential leads to a mixing between the three physical neutral scalars. The structure of the new scalar fields is given by

$$S_1 = \frac{1}{\sqrt{2}} (v_{S_1} + \phi_{S_1} + i\sigma_{S_1}), \quad S_2 = v_{S_2} + \phi_{S_2}, \quad (5.53)$$

where once again ϕ_i and σ_i are the CP-even and odd components respectively. As discussed in Section 2.2.2 we have allowed all scalar fields to obtain VEVs.

The Yukawa interactions and fermionic mass terms of the hidden sector read

$$-\mathcal{L}^{\text{new}} = M_X \overline{X_R} X_L + Y_{X_L} \overline{u_R} S_1^* X_L + f_X \overline{X_R} S_2 X_L + \text{h.c.} \quad (5.54)$$

The mixing of the vector-like quark X with SM quarks via the interaction with S_1 is kept small, and purely serves the purpose of letting the new quark decay.

5.3.1.3 Simple $U(1)$

- **Reference:** [62]
- **Model name:** U1Extensions/simpleU1

This $U(1)_X$ extension of the SM augments its particle content by a pair of exotic vector-like quarks, χ_1 and χ_2 , doublets under $SU(2)_L$ and with hypercharge 7/6, and by one complex scalar Σ responsible for the spontaneous breaking of $U(1)_X$. The $U(1)_X$ -breaking Higgs boson is the 750 GeV candidate. The particle content beyond the SM is summarized in Table 18.

The scalar potential of the model is given by

$$V = -\mu_H^2 |H|^2 - \mu_\Sigma^2 |\Sigma|^2 + \lambda_H |H|^2 + \lambda_{H\Sigma} |H|^2 |\Sigma|^2 + \lambda_\Sigma |\Sigma|^4, \quad (5.55)$$

while the Yukawa and fermionic mass terms read

$$\mathcal{L} = \mathcal{L}_Y^{\text{SM}} - M_1 \overline{\chi_{1R}} \chi_{1L} - M_2 \overline{\chi_{2R}} \chi_{2L} - \lambda_1 \Sigma \overline{\chi_{2R}} \chi_{1L} - \lambda_2 \Sigma^* \overline{\chi_{1R}} \chi_{2L}. \quad (5.56)$$

Field	Gen.	$SU(3)_C$	$SU(2)_L$	$U(1)_Y$	$U(1)_X$
Σ	1	1	1	0	1
χ_1	1	3	2	7/6	1
χ_2	1	3	2	7/6	2

Table 18. Particle content of the `simpleU1` beyond the SM fields. The scalar and fermion fields are shown in the top and bottom of the table respectively. The exotic χ_1 and χ_2 quarks are vector-like.

Note that the original model proposed in [62] contains an effective operator

$$\mathcal{L} \supset -\frac{1}{\Lambda} \Sigma^* H \chi_1 u^c.$$

As `SARAH` cannot handle effective operators this term is dropped from the model and subsequent constraints pertaining to stable charged particles are ignored. Expanding the new scalar field yields

$$\Sigma = \frac{1}{\sqrt{2}} (v_\Sigma + \phi_\Sigma + i\sigma_\Sigma), \quad (5.57)$$

where once again ϕ_i and σ_i are the CP-even and odd components respectively.

5.3.1.4 Scotogenic $U(1)$ Model

- **Reference:** [210]
- **Model name:** `U1Extensions/scotoU1`

The matter particle content of the Scotogenic $U(1)$ Model is summarized in Table 19, where, in addition to the fields charged under $U(1)_D$, we introduce three copies of right-handed neutrinos ν_R which are singlets under the full gauge group. Note, that the $U(1)_D$ charge of the H' field has been changed to -1 compared to Ref. [210] in order to make the Yukawa interaction terms gauge invariant. The SM fields are not charged under the new $U(1)$ gauge group. The discrete \mathbb{Z}_2 symmetry is introduced to stabilize the dark matter candidates N .

The scalar potential reads

$$V = -\mu_1^2 |H|^2 + \mu_2^2 |H'|^2 - \mu_s^2 |\Phi|^2 + \lambda_1 |H|^4 + \lambda_2 |H'|^4 + \lambda_s |\Phi|^4 \quad (5.58)$$

$$+ \lambda_h |H|^2 |\Phi|^2 + \lambda_{h'} |H'|^2 |\Phi|^2 + \lambda_3 |H|^2 |H'|^2 + \lambda_4 |H^\dagger H'|^2,$$

Field	Gen.	$SU(3)_C$	$SU(2)_L$	$U(1)_Y$	$U(1)_D$	\mathbb{Z}_2
Φ	1	1	1	0	2	+
H'	1	1	2	$\frac{1}{2}$	-1	-
ν_R	3	1	1	0	0	+
T	1	3	1	$\frac{2}{3}$	-1	-
T'	1	3	1	$\frac{2}{3}$	1	-
N	1	1	1	0	-1	-

Table 19. Matter particle content of the `scotoU1` beyond the SM fields. The scalar and fermion fields are shown in the top and bottom of the table, respectively. The fermions T, T', N are vector-like degrees of freedom (4-component spinors).

The term $\frac{\lambda_5}{2}[(H^\dagger H')^2 + \text{h.c.}]$ proposed in Ref. [210] has been omitted here, because it is not invariant under $U(1)_D$ gauge transformations.

The Yukawa interactions beyond the SM read

$$\begin{aligned} \mathcal{L} \supset & +Y_\nu \nu_R H \ell + Y_T \overline{T}_R H' q + y_N \overline{N}_R H' L + m_T (\overline{T} T + \overline{T}' T') \\ & + M_D \overline{N} N + \eta_1 \overline{T}'_R \Phi T_L + \eta_2 \overline{T}_R \Phi^* T'_L + \eta_3 \overline{N}_R^c \Phi N_L + \text{h.c.}, \end{aligned} \quad (5.59)$$

where $H = (H^+, H^0)$ is the SM Higgs field and q and ℓ the SM left-handed quark and lepton doublets.

The $U(1)_D$ symmetry is eventually broken by the VEV of the scalar field Φ which one can decompose as

$$\langle \Phi \rangle = \frac{1}{\sqrt{2}}(v_S + S + iA_S), \quad (5.60)$$

whereas the CP-even component S is considered by the authors as the candidate for the 750 GeV resonance. The spontaneous symmetry breaking leaves the \mathbb{Z}_2 parity intact, and H' will therefore not develop any VEV.

5.3.2 Models with SM states charged under the new $U(1)$

5.3.2.1 $U(1)_{B-L}$ model with unconventional $B - L$ charges

- **Reference:** [185]
- **Model name:** U1Extensions/BL-VL

This model is based on Refs. [339, 340]. It considers a gauged $U(1)_{B-L}$ extension of the SM with an unconventional $B-L$ charge assignment for the right-handed neutrinos ν_R , and further requires 3 extra Dirac neutrinos N . It was originally proposed to explain the smallness of neutrino masses if neutrinos were Dirac particles. Finally, it also contains a scalar DM candidate, stabilised by the residual \mathbb{Z}_3 symmetry from the breaking of the $B-L$ symmetry. To fit the diphoton excess, new vector-like quarks

Field	Gen.	$SU(3)_C$	$SU(2)_L$	$U(1)_Y$	$U(1)_{B-L}$
Φ	1	1	2	$\frac{1}{2}$	0
χ_2	1	1	1	0	2
χ_3	1	1	1	0	3
χ_6	1	1	1	0	-6
Q_L	3	3	2	$\frac{1}{6}$	$\frac{1}{3}$
u_R	3	3	1	$\frac{2}{3}$	$\frac{1}{3}$
d_R	3	3	1	$-\frac{1}{3}$	$\frac{1}{3}$
L_L	3	1	2	$-\frac{1}{2}$	-1
l_R	3	1	1	-1	-1
ν_R^1	1	1	1	0	5
ν_R^2	1	1	1	0	-4
ν_R^3	1	1	1	0	-4
N_L	3	1	1	0	-1
N_R	3	1	1	0	-1
X_L	1	3	1	$\frac{2}{3}$	3
X_R	1	3	1	$\frac{2}{3}$	0
Y_L	1	3	1	$-\frac{2}{3}$	-3
Y_R	1	3	1	$-\frac{2}{3}$	0

Table 20. Particle content and charge assignments of the BL-VL model. The scalar and fermion fields are shown in the top and bottom of the table respectively.

are added so that the 750 GeV scalar, a linear combination of the SM Higgs and the χ fields, can be produced in gluon-gluon fusion. The particle content and the quantum numbers for this model are summarised in Table 20. In addition to the SM particle content, the model features three right-handed neutrinos ν_R^i , three pairs of $SU(2)_L$ singlet heavy fermions $N_{L,R}^i$, and two pairs of exotic quarks $X_{L,R}$, $Y_{L,R}$ which carry color and electromagnetic charges but are singlets under $SU(2)_L$.

The scalar potential of the model reads

$$\begin{aligned}
V = & -\mu_0^2|\Phi|^2 + m_2^2|\chi_2|^2 - \mu_3^2|\chi_3|^2 - \mu_6^2|\chi_6|^2 + \frac{1}{2}\lambda_0|\Phi|^4 + \frac{1}{2}\lambda_2|\chi_2|^4 + \frac{1}{2}\lambda_3|\chi_3|^4 + \frac{1}{2}\lambda_6|\chi_6|^4 \\
& + \lambda_{02}|\chi_2|^2|\Phi|^2 + \lambda_{03}|\chi_3|^2|\Phi|^2 + \lambda_{06}|\chi_6|^2|\Phi|^2 + \lambda_{23}|\chi_2|^2|\chi_3|^2 + \lambda_{26}|\chi_2|^2|\chi_6|^2 \\
& + \lambda_{36}|\chi_3|^2|\chi_6|^2 + \left[\frac{1}{2}f_{36}(\chi_3^2\chi_6) + \frac{1}{6}\lambda'_{26}(\chi_2^3\chi_6) + \text{h.c.} \right]. \tag{5.61}
\end{aligned}$$

The residual global \mathbb{Z}_3 symmetry protects the singlet scalar χ_2 from acquiring a VEV, i.e. $\langle\chi_2\rangle = 0$. All leptons carry a charge $\omega = e^{2i\pi/3}$ under \mathbb{Z}_3 . The CP-even degree of freedom of χ_2 is the DM candidate. The Yukawa interactions of the new sector read

$$\begin{aligned}
-\mathcal{L}_Y^{\text{new}} = & Y_{NR}\overline{N_R}\widetilde{H}L_L + f_X\overline{X_R}\chi_3^*X_L + f_Y\overline{Y_R}\chi_3Y_L \\
& + f_N\overline{\nu_{R2,3}}\chi_3^*N_L + f_{N6}\overline{\nu_{R1}}\chi_6^*N_L \\
& + f_{NL}\chi_2\overline{N_L^c}N_L + f_{NR}\chi_2\overline{N_R^c}N_R + m_N\overline{N_R}N_L + \text{h.c.} \tag{5.62}
\end{aligned}$$

In the set up considered in Ref [185], the 750 GeV scalar is given by the combination $(\chi_6 - \chi_3)$, that couples to gluons and photons via loops of X and Y fermions proportional to the Yukawa couplings f_X and f_Y . The fit to the diphoton signal was studied in a simplified scenario, where special relations are imposed to the scalar parameters. As already described in section 2.2.1, these relations are not protected by symmetries, and hence lead to a large amounts of fine tuning.

5.3.2.2 Sample of $U(1)'$ models based on different charge assignments

- **Reference:** [66]
- **Model name:** U1Extensions/VLsample

The particle content of this model is shown in Table 21. Similarly to all the previous models, a complex scalar S is added to break the $U(1)_X$ symmetry. In this paper, the mixing between the scalars is kept small, hence the 750 GeV candidate is predominantly the CP-even part of the $U(1)_X$ -breaking field. New doublet and singlet vector-like quarks, charged under $U(1)_X$, are added to fit the diphoton signal strength. In this model, the SM fermions also carry X -charges, which are fixed according to the anomaly cancellation conditions. Only the Higgs doublet is not charged, while the charge of the new scalar field S is double (in absolute magnitude) that of the vector-like quarks.

There are several possibilities to assign the $U(1)_X$ charges in an anomaly-free way, with different physical interpretations [66]:

Field	Gen.	$SU(3)_C$	$SU(2)_L$	$U(1)_Y$	$U(1)_X$
H	1	1	2	$-\frac{1}{2}$	0
S	1	1	1	0	$-2b$
Q_L	3	3	2	$\frac{1}{6}$	m
u_R	3	3	1	$\frac{2}{3}$	m
d_R	3	3	1	$-\frac{1}{3}$	m
L_L	3	1	2	$-\frac{1}{2}$	k
e_R	3	1	1	-1	k
ν_R	3	1	1	0	k
X_L	1	3	2	a	b
X_R	1	3	2	a	$-b$
y_{1L}	1	3	1	$a + \frac{1}{2}$	$-b$
y_{2L}	1	3	1	$a - \frac{1}{2}$	$-b$
y_{1R}	1	3	1	$a + \frac{1}{2}$	b
y_{2R}	1	3	1	$a - \frac{1}{2}$	b

Table 21. Particle content of the VLsample. The scalar and fermion fields are shown in the top and bottom of the table respectively.

- $X \equiv B - L$: $b = 0$, $k = -1$, $m = 1/3$
- $X \equiv B + L$: $b = -1$, $k = 1$, $m = 1/3$
- $X \equiv B$: $b = -1/2$, $k = 0$, $m = 1/3$
- $X \equiv L$: $b = -1/2$, $k = 1$, $m = 0$

Note that in all interpretations a remains a free parameter.

The Yukawa interactions of the extra particle content are given by

$$\begin{aligned} \mathcal{L}_Y^{\text{new}} = & Y_V^1 \overline{y_{1R}} S^* y_{1L} + Y_V^2 \overline{y_{2R}} S^* y_{2L} + Y_V^3 \overline{X_R} S X_L \\ & + \eta_1 \overline{X_R} H y_{1L} + \eta_2 \overline{X_R} \tilde{H} y_{2L} + \eta_3 \overline{y_{2R}} H X_L + \eta_4 \overline{y_{1R}} \tilde{H} X_L + \text{h.c.} \end{aligned} \quad (5.63)$$

Finally, the scalar potential is given by

$$-V = \mu_H^2 |H|^2 + \mu_S^2 |S|^2 - \lambda_H |H|^4 - \lambda_S |S|^4 - \lambda_{HS} |S|^2 |H|^2, \quad (5.64)$$

the symmetry breaking pattern being

$$\langle H \rangle = \frac{1}{\sqrt{2}} \begin{pmatrix} v \\ 0 \end{pmatrix}, \quad \langle S \rangle = \frac{1}{\sqrt{2}} v_S, \quad (5.65)$$

while the expansion of the scalar fields in to CP-even and odd components is analogous to Eq. (5.51).

5.3.2.3 Model with flavour-nonuniversal quark $U(1)'$ charges

- **Reference:** [178]
- **Model name:** U1Extensions/nonUniversalU1

In this model the first generation of left-handed SM quarks carries a $U(1)_X$ charge while the second and third generations do not. In this way it is possible to add exotic quarks which are vector-like under the SM gauge group and achieve anomaly cancellation with less than three generations. The scalar sector then needs to be extended with a second Higgs doublet, with a different $U(1)_X$ charge compared to the first ones, in order to have Yukawa interactions for all quark families. A further complex scalar field S , which is a singlet under the SM gauge group but charged under $U(1)_X$, is also added for the spontaneous symmetry breaking of the $U(1)_X$ symmetry.

The charge assignments that cancel all anomalies are given in [341] and are summarised in Table 22.

Field	Gen.	$SU(3)_C$	$SU(2)_L$	$U(1)_Y$	$U(1)_X$
H_1	1	1	2	$-\frac{1}{2}$	$-\frac{2}{3}$
H_2	1	1	2	$-\frac{1}{2}$	$-\frac{1}{3}$
S	1	1	1	0	$-\frac{1}{3}$
Q_L^1	1	3	2	$\frac{1}{6}$	$\frac{1}{3}$
Q_L^i	2	3	2	$\frac{1}{6}$	0
u_R	3	3	1	$\frac{2}{3}$	$-\frac{1}{3}$
d_R	3	3	1	$-\frac{1}{3}$	$\frac{2}{3}$
L_L	3	1	2	$-\frac{1}{2}$	$\frac{1}{3}$
e_R	3	1	1	-1	-1
ν_R	3	1	1	0	$\frac{1}{3}$
T_L	1	3	1	$\frac{2}{3}$	$\frac{1}{3}$
T_R	1	3	1	$\frac{2}{3}$	$\frac{2}{3}$
J_L	2	3	1	$-\frac{1}{3}$	0
J_R	2	3	1	$-\frac{1}{3}$	$-\frac{1}{3}$

Table 22. Particle content of the nonUniversalU1. The scalar and fermion fields are shown in the top and bottom of the table respectively.

The Yukawa Lagrangian of the model (ignoring here flavour indices) is given by

$$\begin{aligned} \mathcal{L}_Y = & h_1^D \overline{d}_R H_1 Q_L^1 + h_1^U \overline{u}_R \tilde{H}_1 Q_L^i + h_2^D \overline{d}_R H_2 Q_L^i + h_2^U \overline{u}_R \tilde{H}_2 Q_L^1 + h_1^J \overline{J}_R H_1 Q_L^1 \\ & + h_2^J \overline{J}_R H_2 Q_L^i + h_2^T \overline{T}_R \tilde{H}_2 Q_L^1 + h_1^T \overline{T}_R \tilde{H}_1 Q_L^i + h_X^U \overline{u}_R S^* T_L + h_X^T \overline{T}_R S^* T_L \\ & + h_X^D \overline{d}_R S J_L + h_X^J \overline{J}_R S J_L + Y_e \overline{e}_R H_1 L_L + Y_\nu \overline{\nu}_R \tilde{H}_1 L_L + \text{h.c.}, \end{aligned} \quad (5.66)$$

and the scalar potential is

$$\begin{aligned} V = & \mu_{11}^2 |H_1|^2 + \mu_{22}^2 |H_2|^2 + \mu_S^2 |S|^2 + \lambda_1 |H_1|^4 + \lambda_2 |H_2|^4 + \lambda_3 |H_1|^2 |H_2|^2 - \lambda_{H_1 S} |S|^2 |H_1|^2 \\ & - \lambda_S |S|^4 + \lambda_4 (H_2^\dagger H_1)(H_1^\dagger H_2) - \lambda_{H_2 S} |S|^2 |H_2|^2 + \left\{ \kappa_{HS} H_1^\dagger H_2 S + \text{h.c.} \right\}. \end{aligned} \quad (5.67)$$

The pattern of EWSB follows

$$H_i = \frac{1}{\sqrt{2}} \begin{pmatrix} 0 \\ v_i + \phi_i + i\sigma_i \end{pmatrix}, \quad S = \frac{1}{\sqrt{2}} (v_S + \phi_S + i\sigma_S), \quad (5.68)$$

where once again ϕ_i and σ_i are the CP-even and CP-odd components respectively. In order to obtain a massive pseudo-scalar state, κ_{HS} needs to be non-zero. Hence, for keeping the $S - H_i$ mixing small while making the pseudo-scalar massive, either the condition $v_S \gg v$ must hold, or κ_{HS} must be small, in conjunction with $\frac{v_1}{v_2} \rightarrow 0$ or ∞ . ϕ_S , the CP-even component of S , is then identified with the 750 GeV candidate. The authors of Ref. [178] estimate the diphoton rate with a simple analytical approximation which is erroneous, see the comment in Section 2.1.3. Making use of the model implementation in SARAH described above and, e.g., a MC tool, one can convince oneself that this simple analytical relation seriously overestimates the diphoton rate, rendering the presented results incorrect.¹⁰

5.3.2.4 Leptophobic $U(1)$ model

- **Reference:** [167]
- **Model name:** U1Extensions/U1Leptophobic

This model is inspired by an E_6 Grand Unified Theory (GUT), but the authors only consider the low energy version where the SM gauge group is augmented by an extra gauged $U(1)_X$ symmetry. This extra $U(1)$ symmetry has zero charges for both left- and right-handed leptons making it entirely leptophobic. However it is impossible to arrange for this to happen by taking linear combinations of the $U(1)_X$ and $U(1)_\psi$

¹⁰In addition, trying to reconstruct their results using the same analytic formulae, we find that their presented result for m_T/h_X^T is too large by a factor of roughly 10, most likely due to a typo.

groups that appear from the breakdown of E_6 . Instead, the charges from this extra $U(1)$ can only be obtained by including gauge kinetic mixing, so that the introduced mixture of $U(1)_Y$ charges exactly cancel the non-zero leptonic charges. This can be done with the $U(1)_\eta$ gauge symmetry and the charges used in this model correspond exactly to those given in Table I of Ref. [342]. It is these charges rather than the charges of the $U(1)_\eta$ which are set in this model. Of course one may discard the E_6 motivation and treat it as an ad-hoc choice of $U(1)$ charges.

The model contains two Higgs doublets, a complex scalar SM singlet (Φ), charged under $U(1)_X$, plus right handed neutrinos and other new fermions, charged under both the SM and the $U(1)_X$ symmetries. The latter are odd under an imposed \mathbb{Z}_2 symmetry, so that the lightest neutral fermion is a DM candidate.

Field	Gen.	$SU(3)_C$	$SU(2)_L$	$U(1)_Y$	$U(1)_X$	\mathbb{Z}_2
H_1	1	1	2	$-\frac{1}{2}$	0	+
H_2	1	1	2	$-\frac{1}{2}$	-1	+
Φ	1	1	1	0	-1	+
Q_L	3	3	2	$\frac{1}{6}$	$-\frac{1}{3}$	+
u_R	3	3	1	$\frac{2}{3}$	$\frac{2}{3}$	+
d_R	3	3	1	$-\frac{1}{3}$	$-\frac{1}{3}$	+
L_L	3	1	2	$-\frac{1}{2}$	0	+
e_R	3	1	1	-1	0	+
ν_R	3	1	1	0	1	+
D_L	3	3	1	$-\frac{1}{3}$	$\frac{2}{3}$	-
D_R	3	3	1	$-\frac{1}{3}$	$-\frac{1}{3}$	-
\tilde{H}_L	3	1	2	$-\frac{1}{2}$	0	-
\tilde{H}_R	3	1	2	$-\frac{1}{2}$	-1	-
N_L	3	1	1	0	-1	-

Table 23. Particle content of the U1Leptophobic. The scalar and fermion fields are shown in the top and bottom of the table respectively.

The particle content is summarized in Table 23, while the scalar potential reads

$$\begin{aligned}
V_{\text{scalar}} = & \tilde{m}_1^2 |H_1|^2 + \tilde{m}_2^2 |H_2|^2 + \frac{\lambda_1}{2} |H_1|^4 + \frac{\lambda_2}{2} |H_2|^4 + \lambda_3 |H_1|^2 |H_2|^2 + \lambda_4 H_1^\dagger H_2 H_2^\dagger H_1 \\
& + \tilde{m}_\Phi^2 |\Phi|^2 + \frac{\lambda_\Phi}{2} |\Phi|^4 + \left(\mu_\Phi H_1^\dagger H_2 \Phi + \text{h.c.} \right) + \tilde{\lambda}_1 |H_1|^2 |\Phi|^2 + \tilde{\lambda}_2 |H_2|^2 |\Phi|^2, \quad (5.69)
\end{aligned}$$

and the Yukawa interactions are given by

$$\begin{aligned} \mathcal{L}_Y = & y^u \overline{u}_R H_1^\dagger Q + y^d \overline{d}_R H_2 Q + y^e \overline{e}_R H_2 L + y^n \overline{n}_R H_1^\dagger L \\ & + y^D \overline{D}_R \Phi D_L + y_{ij}^H \overline{\widetilde{H}}_R^j \Phi \widetilde{H}_L^i + y_{ij}^N \overline{N}_L^{c_i} H_1^\dagger \widetilde{H}_L^j + y_{ij}'^N \overline{\widetilde{H}}_R^i H_2 N_L^j + \text{h.c.} . \end{aligned} \quad (5.70)$$

We assume the following symmetry breaking pattern

$$H_{1/2} = \frac{1}{\sqrt{2}} \begin{pmatrix} v_{1/2} + \phi_{1/2} + i\sigma_{1/2} \\ 0 \end{pmatrix}, \quad \Phi = \frac{1}{\sqrt{2}} (v_\Phi + \phi_\Phi + i\sigma_\Phi), \quad (5.71)$$

where once again ϕ_i and σ_i are the CP-even and CP-odd components, respectively, and we define $\tan \beta \equiv \frac{v_2}{v_1}$.

The 750 GeV candidate is taken to be dominantly composed by ϕ_Φ , that is, the real CP-even degree of freedom of the Φ field after $U(1)_X$ symmetry breaking. It couples to photons and gluons via loops of the new fermions. The model cannot explain the diphoton excess with Yukawa couplings in the perturbative range, but the authors use values between 5 and 10. As stressed in Sec. 2.1.2.1, this renders the perturbative calculation, and hence the results, very questionable.

5.3.2.5 $U(1)'$ extension with a Z' mimicking a scalar resonance

- **Reference:** [60]
- **Model name:** U1Extensions/trickingLY

The idea of this model is that the extra neutral gauge boson decays into $S\gamma$, whereas the scalar S itself decays into a diphoton final state. Because of the high boost, the two photons from S appear to be a single photon in the detector.

Ref. [60] works in a model realization where the third-generation quarks are charged under $U(1)'$ whereas the first and second generations are not. While that can be viewed as a toy model to make a point, an actual realisation would either need additional Higgs representations or flavour-universal $U(1)'$ charges in order to reproduce the correct CKM matrix. Consequently, we will work with $U(1)'$ charges for all three generations of SM quarks and also have to use three generations of each additional exotic particle for anomaly cancellation.

The particle content of the model is summarized in Table 24. For anomaly cancellation, the condition $Q_1 - Q_2 = -3$ must hold. Furthermore, there are four different valid choices for the hypercharge assignments Y_i [60]:

$$(Y_1, Y_2, Y_3) = (a, a + \frac{1}{2}, a - \frac{1}{2}). \quad (5.72)$$

Field	Gen.	$SU(3)_C$	$SU(2)_L$	$U(1)_Y$	$U(1)'$
H	1	1	2	$-\frac{1}{2}$	0
S	1	1	1	0	$Q_1 - Q_2 = -3$
Q_L	3	3	2	$\frac{1}{6}$	1
u_R	3	3	1	$\frac{2}{3}$	1
d_R	3	3	1	$-\frac{1}{3}$	1
L_L	3	1	2	$-\frac{1}{2}$	0
l_R	3	1	1	-1	0
ν_R	3	1	1	0	0
X_L	3	3	2	Y_1	Q_1
X_R	3	3	2	Y_1	Q_2
R_L	3	1	1	Y_2	Q_2
R_R	3	1	1	Y_2	Q_1
ξ_L	3	1	1	Y_3	Q_2
ξ_R	3	1	1	Y_3	Q_1

Table 24. Fermionic and scalar particle content of the `trickingLY`. Here $X_L = (x_{1L}, x_{2L})$, $X_R = (x_{1R}, x_{2R})$ and $H = (H^0, H^-)$.

In the model implementation at hand, we choose $(Y_1, Y_2, Y_3) = (\frac{1}{2}, 1, 0)$.

The Yukawa interactions including fields beyond the SM read

$$\mathcal{L} \supset Y_v \bar{\nu}_R \tilde{H} L_L + \eta_1 \bar{X}_R S^* X_L + \eta_2 \bar{R}_R S R_L + \eta_3 \bar{\xi}_R S \xi_L. \quad (5.73)$$

The scalar potential is given by

$$V = -\mu^2 |H|^2 - \mu_S^2 |S|^2 + \lambda_H |H|^4 + \lambda_S |S|^4 + \lambda_{HS} |S|^2 |H|^2, \quad (5.74)$$

where the $U(1)'$ symmetry is broken spontaneously as soon as S receives a VEV according to $\langle S \rangle = v_S / \sqrt{2}$.

Unfortunately, the most interesting vertex for this model, $Z' - S - \gamma$, only arises at the loop level. This would require a handling via an effective operator which is currently not supported in the automatized tools advertised. Hence, it is not possible to recast the results of Ref. [60] based on this model implementation only.

Note that, in principle, the decay $Z' \rightarrow ZS$ is already possible at tree level due to $Z - Z'$ mixing and dominates over the decay into $S\gamma$. Therefore, in order to achieve the desired effect, the mixed gauge interaction term $F^{\mu\nu} F'_{\mu\nu}$ must be forbidden while allowing for $S F^{\mu\nu} F'_{\mu\nu}$ which is hard to justify in general.

5.4 Non-abelian gauge-group extensions of the SM

5.4.1 Left-right symmetric models

Left-right (LR) symmetric models can potentially provide an interesting explanation of the diphoton excess through the use of an extended scalar sector that is necessary to spontaneously break the enlarged gauge group $\mathcal{G}_{L-R} \equiv SU(3)_C \times SU(2)_L \times SU(2)_R \times U(1)_{B-L}$ to the SM gauge group. However, due to the large number of fields, these models are often difficult to analyse even at tree-level. Therefore as a starting point we provide model files for four different left-right models that have been proposed in the literature to explain the diphoton excess. These four models are based on the above mentioned gauge group \mathcal{G}_{L-R} with, in two cases, further Abelian gauged or global symmetries.

5.4.1.1 Left-right symmetric model without bi-doublets

- **Reference:** [42, 92, 93] (see also Ref. [343])
- **Model name:** LRmodels/LR-VL

In Ref. [42] the authors explored the possibility of explaining the observed diphoton excess in the context of the minimal left-right symmetric model. They show that it is not possible and that an alternative model is necessary. Therefore they give up on standard Yukawa couplings, for which bi-doublets are necessary, and consider separate $SU(2)_L$ - and $SU(2)_R$ -Higgs-doublets. In order to be able to introduce Yukawa interactions, new vectorlike $SU(2)_i$ -singlet fermions are introduced. After integrating out the vectorlike fermions, the SM fermion masses are generated through a universal seesaw mechanism [344, 345].

The particle content for the model is shown in Table 25. Note that the authors consider the second-lightest CP-even Higgs, which should be predominantly singlet-like, as the particle responsible for the observed resonance. The scalar potential given the particle content and consistent with the symmetries $(SU(3)_C \times SU(2)_L \times SU(2)_R \times U(1)_{B-L})$ is

$$V = M_S^2 S^2 + (\mu_L^2 - \mu_{SL} S) |H_L|^2 + (\mu_R^2 + \mu_{SR} S) |H_R|^2 - \lambda_S S^4 - \lambda_L |H_L|^4 - \lambda_R |H_R|^4 - \lambda_{LR} |H_L|^2 |H_R|^2 - \lambda_{SL} S^2 |H_L|^2 - \lambda_{SR} S^2 |H_R|^2. \quad (5.75)$$

Field	Generations	$SU(3)_C$	$SU(2)_L$	$SU(2)_R$	$U(1)_{B-L}$
H_L	1	1	2	1	$-\frac{1}{2}$
H_R	1	1	1	2	$-\frac{1}{2}$
S	1	1	1	1	0
$q_L = (u_{L,i}, d_{L,i})^T$	3	3	2	1	$\frac{1}{6}$
$q_R = (u_{R,i}, d_{R,i})^T$	3	3	1	2	$\frac{1}{6}$
$l_L = (\nu_{L,i}, e_{L,i})^T$	3	1	2	1	$-\frac{1}{2}$
$l_R = (\nu_{R,i}, e_{R,i})^T$	3	1	1	2	$-\frac{1}{2}$
U_L	3	3	1	1	$\frac{2}{3}$
U_R	3	3	1	1	$\frac{2}{3}$
D_L	3	3	1	1	$-\frac{1}{3}$
D_R	3	3	1	1	$-\frac{1}{3}$
$E_{L/R}$	3	1	1	1	-1
$N_{L/R}$	3	1	1	1	0

Table 25. Matter content and charge assignments for the LR-VL model. The scalar/fermionic fields are shown in the top/bottom of the table respectively. The generation index i runs over $i = 1, 2, 3$.

The Yukawa interactions can be written as¹¹

$$\begin{aligned}
\mathcal{L}_Y = & Y_U (\bar{q}_L H_L U_R + \bar{q}_R H_R U_L) + Y_D (\bar{q}_L \tilde{H}_L D_R + \bar{q}_R \tilde{H}_R D_L) + Y_E (\bar{l}_L \tilde{H}_L E_R + \bar{l}_R \tilde{H}_R E_L) \\
& + Y_N (\bar{l}_L H_L N_R + \bar{l}_R H_R N_L) + \frac{1}{2} m_{NM} (\bar{N}_R^c N_R + \bar{N}_L^c N_L) + m_{ND} \bar{N}_L N_R \\
& + (m_U + \lambda_U S) \bar{U}_L U_R + (m_D + \lambda_D S) \bar{D}_L D_R + (m_E + \lambda_E S) \bar{E}_L E_R + \text{h.c.}, \quad (5.76)
\end{aligned}$$

where N_L^c is the charge conjugate of N_L . Note that we have included both Majorana and Dirac mass terms for the fermionic singlet $N_{L/R}$. We assume the following symmetry breaking VEVs

$$\langle H_L \rangle = \frac{1}{\sqrt{2}} \begin{pmatrix} v_L \\ 0 \end{pmatrix}, \quad \langle H_R \rangle = \frac{1}{\sqrt{2}} \begin{pmatrix} v_R \\ 0 \end{pmatrix}, \quad \langle S \rangle = v_S. \quad (5.77)$$

5.4.1.2 Left-right symmetric model with $U(1)_L \times U(1)_R$

¹¹Note that our Yukawa interactions differ from the literature: in Ref. [42], they are defined as, e.g., $\bar{q}_L H_L^\dagger U_L$ which contracts to zero because of the implicit left/right projection operators. Moreover, in Refs. [42, 92] the ‘conjugate’ assignments of the $H_{L/R}$ need to be exchanged in order to obtain a gauge-invariant Lagrangian.

- **Reference:** [51]
- **Model name:** LRmodels/LRLR

This model is based on the gauge group $SU(3)_C \times SU(2)_L \times SU(2)_R \times U(1)_L \times U(1)_R$. The inclusion of extra vectorlike $SU(2)$ -singlet fermions allows for the generation of the SM fermion masses via a see-saw mechanism. Additionally, a parity symmetry is imposed to ensure a vanishing $\bar{\theta}$ parameter at tree-level in the QCD Lagrangian [346], in order to solve the strong CP-problem without introducing an axion.

The particle content of this model and charge assignments under the gauge symmetries are shown in Table 26. The proposed candidate for the 750 GeV resonance is taken to be one of the CP-even scalars associated with the $SU(2)$ -singlet Higgs scalars σ_D , σ_U and σ_E that are responsible for the breaking $U(1)_L \times U(1)_R \rightarrow U(1)_{B-L}$. The decays of this state into digluon and diphoton final states are assumed to proceed via loops involving the $SU(2)$ -singlet fermions.

The Yukawa interactions consistent with the imposed parity are given by

$$\begin{aligned}
-\mathcal{L} = & y_U (\bar{q}_L \phi_L U_L^c + \bar{q}_R \phi_R U_R^c) + f_U \sigma_U^* \bar{U}_L U_R + y_D \left(\bar{q}_L \tilde{\phi}_L D_L^c + \bar{q}_R \tilde{\phi}_R D_R^c \right) + f_D \sigma_D^* \bar{D}_L D_R \\
& + y_E \left(\bar{l}_L \tilde{\phi}_L E_L^c + \bar{l}_R \tilde{\phi}_R E_R^c \right) + f_E \sigma_E^* \bar{E}_L E_R + Y_L (\bar{l}_L^c i\tau_2 \Delta_L l_L + \bar{l}_R^c i\tau_2 \Delta_R l_R) + \text{h.c.}
\end{aligned} \tag{5.78}$$

The parity symmetry is taken to be softly broken, so that the part of the scalar potential considered in Ref. [51] is given by

$$\begin{aligned}
V = & \lambda (\sigma_E^* \sigma_D^3 + \text{h.c.}) + \xi (\sigma_U \sigma_D^2 + \text{h.c.}) \\
& + \eta (\sigma_E \sigma_D^* \sigma_U + \text{h.c.}) + \mu_{\phi_L}^2 \phi_L^\dagger \phi_L + \mu_{\phi_R}^2 \phi_R^\dagger \phi_R \\
& + \mu_{\Delta_L}^2 \text{Tr} (\Delta_L^\dagger \Delta_L) + \mu_{\Delta_R}^2 \text{Tr} (\Delta_R^\dagger \Delta_R) \\
& + \rho_L (\phi_L^T i\tau_2 \Delta_L \phi_L + \text{h.c.}) + \rho_R (\phi_R^T i\tau_2 \Delta_R \phi_R + \text{h.c.}).
\end{aligned} \tag{5.79}$$

The couplings and masses λ , ξ , η , $\mu_{\phi_L}^2$, $\mu_{\phi_R}^2$, $\mu_{\Delta_L}^2$, $\mu_{\Delta_R}^2$, ρ_L and ρ_R are taken to be real, with $\mu_{\phi_L}^2 \neq \mu_{\phi_R}^2$, $\mu_{\Delta_L}^2 \neq \mu_{\Delta_R}^2$ and $\rho_L \neq \rho_R$. Note that Eq. (5.78) and Eq. (5.79) differ from Eq. (6) and Eq. (7) in Ref. [51], which as given are not gauge invariant. One may also include a large number of additional terms that are allowed by the gauge

Field	$SU(3)_c$	$SU(2)_L$	$SU(2)_R$	$U(1)_L$	$U(1)_R$
σ_U	1	1	1	$\frac{2}{3}$	$-\frac{2}{3}$
σ_D	1	1	1	$-\frac{1}{3}$	$\frac{1}{3}$
σ_E	1	1	1	-1	1
ϕ_L	1	2	1	$-\frac{1}{2}$	0
ϕ_R	1	1	2	0	$-\frac{1}{2}$
Δ_L	1	3	1	1	0
Δ_R	1	1	3	0	1
$q_{L,i} = (u_{L,i}, d_{L,i})^T$	3	2	1	$\frac{1}{6}$	0
$q_{R,i} = (u_{R,i}, d_{R,i})^T$	3	1	2	0	$\frac{1}{6}$
$l_{L,i} = (\nu_{L,i}, e_{L,i})^T$	1	2	1	$-\frac{1}{2}$	0
$l_{R,i} = (\nu_{R,i}, e_{R,i})^T$	1	1	2	0	$-\frac{1}{2}$
$U_{L,i}$	3	1	1	$-\frac{2}{3}$	0
$U_{R,i}$	3	1	1	0	$-\frac{2}{3}$
$D_{L,i}$	3	1	1	$\frac{1}{3}$	0
$D_{R,i}$	3	1	1	0	$\frac{1}{3}$
E_L	1	1	1	1	0
E_R	1	1	1	0	1

Table 26. The $SU(3)_c \times SU(2)_L \times SU(2)_R \times U(1)_L \times U(1)_R$ charge assignments for the scalar/fermions in the LRLR shown in the top/bottom of the table. The generation index i runs over $i = 1, 2, 3$.

symmetries, given by

$$\begin{aligned}
V' = & \kappa (\sigma_D \sigma_E \sigma_U^2 + \text{h.c.}) + \mu_D^2 |\sigma_D|^2 + \lambda_{DD} |\sigma_D|^4 + \mu_U^2 |\sigma_U|^2 + \lambda_{UU} |\sigma_U|^4 + \mu_E^2 |\sigma_E|^2 \\
& + \lambda_{EE} |\sigma_E|^4 + \lambda_{DU} |\sigma_D|^2 |\sigma_U|^2 + \lambda_{DE} |\sigma_D|^2 |\sigma_E|^2 + \lambda_{UE} |\sigma_U|^2 |\sigma_E|^2 + \lambda_{LL} |\phi_L|^4 \\
& + \lambda_{RR} |\phi_R|^4 + \lambda_{LR} |\phi_L|^2 |\phi_R|^2 + \rho_{R_1} \text{Tr}(\Delta_R^\dagger \Delta_R) \text{Tr}(\Delta_R^\dagger \Delta_R) + \rho_{R_2} \text{Tr}(\bar{\Delta}_R \Delta_R) \text{Tr}(\Delta_R^\dagger \Delta_R^\dagger) \\
& + \rho_{L_1} \text{Tr}(\Delta_L^\dagger \Delta_L) \text{Tr}(\Delta_L^\dagger \Delta_L) + \rho_{L_2} \text{Tr}(\Delta_L \Delta_L) \text{Tr}(\Delta_L^\dagger \Delta_L^\dagger) + \rho_3 \text{Tr}(\Delta_L^\dagger \Delta_L) \text{Tr}(\Delta_R^\dagger \Delta_R) \\
& + \eta_{LL} |\phi_L|^2 \text{Tr}(\Delta_L^\dagger \Delta_L) + \eta_{RL} |\phi_R|^2 \text{Tr}(\Delta_L^\dagger \Delta_L) + \eta_{LR} |\phi_L|^2 \text{Tr}(\Delta_R^\dagger \Delta_R) + \eta_{RR} |\phi_R|^2 \text{Tr}(\Delta_R^\dagger \Delta_R) \\
& + e_{RR_1} \phi_R^\dagger \Delta_R^\dagger \Delta_R \phi_R - e_{RR_2} \phi_R^\dagger \Delta_R \Delta_R^\dagger \phi_R + e_{LL_1} \phi_L^\dagger \Delta_L^\dagger \Delta_L \phi_L - e_{LL_2} \phi_L^\dagger \Delta_L \Delta_L^\dagger \phi_L \\
& + \sum_{f=U,D,E} |\sigma_f|^2 \left[\lambda_{fL} |\phi_L|^2 + \lambda_{fR} |\phi_R|^2 + \tilde{\lambda}_{fL} \text{Tr}(\Delta_L^\dagger \Delta_L) + \lambda_{fR} \text{Tr}(\Delta_R^\dagger \Delta_R) \right].
\end{aligned} \tag{5.80}$$

The full scalar potential that we consider is then $V + V'$.

The $SU(2)$ -singlet Higgs scalars are assumed to acquire VEVs of the form

$$\langle \sigma_D \rangle = \frac{v_D}{\sqrt{2}}, \quad \langle \sigma_U \rangle = \frac{v_U}{\sqrt{2}}, \quad \langle \sigma_E \rangle = \frac{v_E}{\sqrt{2}}. \quad (5.81)$$

resulting in the breaking $U(1)_L \times U(1)_R \rightarrow U(1)_{B-L}$. The $SU(2)$ -doublet Higgs scalars,

$$\phi_{L,R} = \begin{pmatrix} \phi_{L,R}^0 \\ \phi_{L,R}^- \end{pmatrix}, \quad (5.82)$$

are taken to develop VEVs of the form

$$\langle \phi_{L,R} \rangle = \frac{1}{\sqrt{2}} \begin{pmatrix} v_{L,R} \\ 0 \end{pmatrix}. \quad (5.83)$$

The non-zero VEV of ϕ_R^0 leads to the breakdown of $SU(2)_L \times SU(2)_R \times U(1)_{B-L}$ to $SU(2)_L \times U(1)_Y$, which is subsequently broken by the VEV of ϕ_L^0 . As a result, the triplet scalars

$$\Delta_{L,R} = \begin{pmatrix} \frac{\delta_{L,R}^+}{\sqrt{2}} & \delta_{L,R}^{++} \\ \delta_{L,R}^0 & -\frac{\delta_{L,R}^+}{\sqrt{2}} \end{pmatrix} \quad (5.84)$$

also acquire VEVs of the form

$$\langle \Delta_{L,R} \rangle = \frac{1}{\sqrt{2}} \begin{pmatrix} 0 & 0 \\ u_{L,R} & 0 \end{pmatrix}. \quad (5.85)$$

5.4.1.3 Left-right symmetric model with fermionic and scalar triplets

- **Reference:** [33]
- **Model name:** LRmodels/tripletLR

In this model the diphoton signal is produced through a cascade decay, namely, $pp \rightarrow Z' \rightarrow XY \rightarrow XX(\delta^0 \rightarrow \gamma\gamma)$ where X and Y are unspecified soft states and δ_0 is the neutral component of the $SU(2)_R$ scalar triplet. However, in order to sufficiently boost the rate three $SU(2)_R$ triplet fermion fields are added to the model, T_1 , T_2 and T_3 . The model is based on a $SU(3)_C \times SU(2)_L \times SU(2)_R \times U(1)_{B-L}$ gauge group which is broken to the SM gauge group through the VEV of the triplet field Δ_R whereby EWSB proceeds through the bi doublet Φ VEVs. The entire particle content of the model is illustrated in Table 27.

Field	Generations	$SU(3)_C$	$SU(2)_L$	$SU(2)_R$	$U(1)_{B-L}$
Φ	1	1	2	2	0
Δ_R	1	1	1	3	1
$Q_L = (u_{L,i}, d_{L,i})^T$	3	3	2	1	$\frac{1}{6}$
$Q_R = (u_{R,i}, d_{R,i})^T$	3	3	1	2	$\frac{1}{6}$
$L_L = (\nu_{L,i}, e_{L,i})^T$	3	1	2	1	$-\frac{1}{2}$
$L_R = (\nu_{R,i}, e_{R,i})^T$	3	1	1	2	$-\frac{1}{2}$
T_1	1	1	1	3	0
T_2	1	1	1	3	1
T_3	1	1	1	3	-1

Table 27. Matter content and charge assignments for the tripletLR model. The scalar/fermionic fields are shown in the top/bottom of the table respectively. The generation index i runs over $i = 1, 2, 3$.

The scalar fields of the model can be expressed as

$$\Phi = \begin{pmatrix} \phi_1^0 & \phi_2^+ \\ \phi_1^- & \phi_2^0 \end{pmatrix}, \quad \text{and} \quad \Delta_R = \begin{pmatrix} \frac{\delta_R}{\sqrt{2}} & \delta_R^{++} \\ \delta_R^0 & -\frac{\delta_R^+}{\sqrt{2}} \end{pmatrix}, \quad (5.86)$$

leading to a scalar potential of the form

$$\begin{aligned} V = & \mu_1^2 \text{Tr}(\Phi^\dagger \Phi) + \mu_2^2 \left[\text{Tr}(\tilde{\Phi} \Phi^\dagger) + \text{Tr}(\tilde{\Phi}^\dagger \Phi) \right] + \mu_3^2 \text{Tr}(\Delta_R \Delta_R^\dagger) + \lambda_1 \left[\text{Tr}(\Phi^\dagger \Phi) \right]^2 \\ & + \lambda_2 \left\{ \left[\text{Tr}(\tilde{\Phi} \Phi^\dagger) \right]^2 + \left[\text{Tr}(\tilde{\Phi}^\dagger \Phi) \right]^2 \right\} + \lambda_3 \text{Tr}(\tilde{\Phi} \Phi^\dagger) \text{Tr}(\tilde{\Phi}^\dagger \Phi) \\ & + \lambda_4 \text{Tr}(\Phi^\dagger \Phi) \left[\text{Tr}(\tilde{\Phi} \Phi^\dagger) + \text{Tr}(\tilde{\Phi}^\dagger \Phi) \right] + \rho_1 \left[\text{Tr}(\Delta_R \Delta_R^\dagger) \right]^2 + \rho_2 \text{Tr}(\Delta_R \Delta_R) \text{Tr}(\Delta_R^\dagger \Delta_R^\dagger) \\ & + \alpha_1 \text{Tr}(\Phi^\dagger \Phi) \text{Tr}(\Delta_R \Delta_R^\dagger) + \left\{ \alpha_2 e^{i\delta} \text{Tr}(\tilde{\Phi}^\dagger \Phi) \text{Tr}(\Delta_R \Delta_R^\dagger) + \text{h.c.} \right\} + \alpha_3 \text{Tr}(\Phi \Phi^\dagger \Delta_R \Delta_R^\dagger), \end{aligned} \quad (5.87)$$

where $\tilde{\Phi} \equiv -\sigma_2 \Phi^* \sigma_2$. The Yukawa interactions of the model are given by

$$\begin{aligned} \mathcal{L}_Y = & Y_1^\alpha \bar{\Psi}_L \Phi \Psi_R + Y_2^\alpha \bar{\Psi}_L \tilde{\Phi} \Psi_R + Y_{DR} L_R^T \mathcal{C}(i\sigma_2) \Delta_R L_R \\ & + \frac{1}{2} m_1 \text{Tr}(T_1 T_1) + m_{23} \text{Tr}(T_2 T_3) + \lambda_{T_{13}} \text{Tr}(T_1 T_3 \Delta_R) + \lambda_{T_{12}} \text{Tr}(T_1 T_2 \Delta_R^\dagger), \end{aligned} \quad (5.88)$$

where α runs over the quarks and leptons $\alpha = Q, L$ and $\Psi_{L,R} = (\psi_{L,R}^u, \psi_{L,R}^d)$ with $\psi^u = u, \nu$ and $\psi^d = d, \ell$. \mathcal{C} is the charge conjugation operator. The VEVs of the scalar

Field	Gen.	$SU(3)_C$	$SU(2)_L$	$SU(2)_R$	$U(1)_{B-L}$	$U(1)_S$	Lep.
Φ	1	1	2	2	0	$\frac{1}{2}$	0
Δ_L	1	1	3	1	1	-2	0
Δ_R	1	1	1	3	1	-1	0
H_L	1	1	2	1	$\frac{1}{2}$	0	0
H_R	1	1	1	2	$\frac{1}{2}$	$-\frac{1}{2}$	0
$Q_L = (u_{L,i}, d_{L,i})^T$	3	3	2	1	$\frac{1}{6}$	0	(0, 0)
$Q_R = (u_{R,i}, d_{R,i})^T$	3	3	1	2	$\frac{1}{6}$	$\frac{1}{2}$	(0, 1)
$L_L = (\nu_{L,i}, e_{L,i})^T$	3	1	2	1	$-\frac{1}{2}$	1	(1, 1)
$L_R = (\nu_{R,i}, e_{R,i})^T$	3	1	1	2	$-\frac{1}{2}$	$\frac{1}{2}$	(0, 1)
d_R	3	1	1	1	$-\frac{1}{3}$	0	0
x_L	3	1	1	1	$-\frac{1}{3}$	1	1

Table 28. Matter content and charge assignments for the **darkLR** model. The scalar/fermionic fields are shown in the top/bottom of the table respectively. The generation index, denoted Gen. in the table, i runs over $i = 1, 2, 3$. Additionally the model includes a lepton number symmetry where the quantum numbers are denoted with Lep. above.

fields in the model take the form

$$\langle \Phi \rangle = \frac{1}{\sqrt{2}} \begin{pmatrix} \kappa_1 & 0 \\ 0 & \kappa_2 \end{pmatrix} \quad \text{and} \quad \langle \Delta_R \rangle = \frac{1}{\sqrt{2}} \begin{pmatrix} 0 & 0 \\ v_R & 0 \end{pmatrix}. \quad (5.89)$$

5.4.1.4 Dark left-right symmetric model

- **Reference:** [95]
- **Model name:** LRmodels/darkLR

The main idea of this model is to add an additional symmetry in order to stabilize the DM candidate, namely right-handed neutrinos, so that they cannot decay via a W' channel. This additional symmetry takes the form of a global Abelian symmetry labelled as $U(1)_S$. The spontaneous breaking of $SU(2)_R \times U(1)_S$ is such that the combination $\tilde{L} = S - T_{3R}$, where T_{3R} is the third component of the right-handed isospin, remains unbroken. Here \tilde{L} is interpreted as a generalised lepton number.

The full particle content of the model is shown in Table 28. Note that the scalar sector of the model is enlarged to include both left- and right-handed triplets and doublets as well as the usual bi-doublet. These scalar fields can be expressed as

$$\Phi = \begin{pmatrix} \phi_1^0 & \phi_2^+ \\ \phi_1^- & \phi_2^0 \end{pmatrix}, \quad \Phi_{L,R} = \begin{pmatrix} H_{L,R}^+ \\ \phi_{L,R}^0 \end{pmatrix}, \quad \Delta_{L,R} = \begin{pmatrix} \frac{\delta_{L,R}}{\sqrt{2}} & \delta_{L,R}^{++} \\ \delta_{L,R}^0 & -\frac{\delta_{L,R}^+}{\sqrt{2}} \end{pmatrix}. \quad (5.90)$$

Subsequently, the proposed candidate for the diphoton excess is ϕ_R^0 , the neutral component of the $SU(2)_R$ doublet. Running in the loop will be W' -bosons, as well as δ_R^+ and δ_R^{++} Higgses. However, these particles are insufficient to boost the rate to diphotons, therefore additional quarks x_L and d_R are introduced.

The scalar potential of the model is

$$\begin{aligned} V = & \mu_1^2 \text{Tr}(\Phi^\dagger \Phi) + \mu_{TR}^2 \text{Tr}(\Delta_R \Delta_R^\dagger) + \mu_{TL}^2 \text{Tr}(\Delta_L \Delta_L^\dagger) \\ & + \mu_{DL}^2 H_L^\dagger H_L + \mu_{DR}^2 H_R^\dagger H_R + \lambda_1 [\text{Tr}(\Phi^\dagger \Phi)]^2 + \lambda_3 \text{Tr}(\tilde{\Phi} \Phi^\dagger) \text{Tr}(\tilde{\Phi}^\dagger \Phi) \\ & + \rho_1 \left\{ [\text{Tr}(\Delta_L \Delta_L^\dagger)]^2 + [\text{Tr}(\Delta_R \Delta_R^\dagger)]^2 \right\} + \beta_2 [\text{Tr}(\tilde{\Phi} \Delta_R \Phi^\dagger \Delta_L^\dagger) + \text{Tr}(\tilde{\Phi}^\dagger \Delta_L \Phi \Delta_R^\dagger)] \\ & + \rho_2 \left\{ \text{Tr}(\Delta_L \Delta_L) \text{Tr}(\Delta_L^\dagger \Delta_L^\dagger) + \text{Tr}(\Delta_R \Delta_R) \text{Tr}(\Delta_R^\dagger \Delta_R^\dagger) \right\} + \rho_3 \text{Tr}(\Delta_L \Delta_L^\dagger) \text{Tr}(\Delta_R \Delta_R^\dagger) \\ & + \alpha_1 \text{Tr}(\Phi^\dagger \Phi) [\text{Tr}(\Delta_L \Delta_L^\dagger) + \text{Tr}(\Delta_R \Delta_R^\dagger)] + \alpha_3 [\text{Tr}(\Phi \Phi^\dagger \Delta_L \Delta_L^\dagger) + \text{Tr}(\Phi \Phi^\dagger \Delta_R \Delta_R^\dagger)] \\ & + \eta_{LL} H_L^\dagger H_L \Delta_L \Delta_L^\dagger + \eta_{RL} H_R^\dagger H_R \Delta_L \Delta_L^\dagger + \eta_{LR} H_L^\dagger H_L \Delta_R \Delta_R^\dagger + \eta_{RR_1} H_R^\dagger H_R \Delta_R \Delta_R^\dagger \\ & + \eta_{RR_2} H_R^\dagger \Delta_R^\dagger \Delta_R H_R + \eta_{RR_3} H_R^\dagger \Delta_R \Delta_R^\dagger H_R + \lambda_L |H_L|^4 + \lambda_R |H_R|^4 + \lambda_{LR} |H_L|^2 |H_R|^2 \\ & + \beta_L |H_L|^2 \Phi^\dagger \Phi + \beta_R |H_R|^2 \Phi^\dagger \Phi \\ & + \left\{ \alpha_4 H_L^\dagger \Phi \Delta_R H_R^\dagger + \xi_R \tilde{H}_R^\dagger \Delta_R^\dagger H_R + \xi_{LR} H_R \Phi H_L^\dagger + \text{h.c.} \right\}, \end{aligned} \quad (5.91)$$

where $\tilde{\Phi} \equiv -\sigma_2 \Phi^* \sigma_2$. Note that there are a number of extra terms present in this potential compared to [95], which are allowed under the symmetries of the model. Finally the Yukawa interactions are given by

$$\begin{aligned} -\mathcal{L}_Y = & Y_{L_1} \bar{L}_L \Phi L_R + Y_{Q_1} \bar{Q}_L \tilde{\Phi} Q_R + Y_{Q_2} \bar{Q}_L H_L d_R + Y_{Q_3} \bar{x}_L \tilde{H}_R Q_R \\ & + \frac{1}{2} Y_{DL} L_L^T \mathcal{C}(i\sigma_2) \Delta_L L_L + \frac{1}{2} Y_{DR} L_R^T \mathcal{C}(i\sigma_2) \Delta_R L_R + \text{h.c.}, \end{aligned} \quad (5.92)$$

where \mathcal{C} is the charge conjugation operator. The structure of the VEVs of the model are

$$\langle \Phi \rangle = \frac{1}{\sqrt{2}} \begin{pmatrix} \kappa_1 & 0 \\ 0 & \kappa_2 \end{pmatrix}, \quad \langle \Phi_{L,R} \rangle = \frac{1}{\sqrt{2}} \begin{pmatrix} 0 \\ v_{L,R}^D \end{pmatrix}, \quad \langle \Delta_{L,R} \rangle = \frac{1}{\sqrt{2}} \begin{pmatrix} 0 & 0 \\ v_{L,R}^T & 0 \end{pmatrix}. \quad (5.93)$$

5.4.2 331 models

Models based on the $SU(3)_c \times SU(3)_L \times U(1)_X$ gauge symmetry [347–353], 331 for short, constitute an extension of the SM that could explain the number of generations of

matter fields. This is possible as anomaly cancellation forces the number of generations to be equal to the number of quark colours.

Regarding the diphoton excess, 331 models automatically include all the required ingredients to explain the hint. First, the usual $SU(2)_L$ Higgs doublet must be promoted to a $SU(2)_L$ triplet, the new component being a singlet under the standard $SU(3)_c \times SU(2)_L \times U(1)_Y$ symmetry. Similarly, the group structure requires the introduction of new coloured fermions to complete the $SU(3)_L$ quark multiplets, these exotic quarks being $SU(3)_c \times SU(2)_L \times U(1)_Y$ vector-like singlets after the breaking of $SU(3)_c \times SU(3)_L \times U(1)_X$. Therefore, $SU(3)_c \times SU(3)_L \times U(1)_X$ models naturally embed the simple *singlet + vector-like fermions* framework proposed to explain the diphoton excess.

There are several variants of $SU(3)_c \times SU(3)_L \times U(1)_X$ models. These are characterized by their β parameter¹², which defines the electric charge operator as¹³

$$Q = T_3 + \beta T_8 + \mathcal{X}. \quad (5.94)$$

First, in Sec. 5.4.2.1 we consider the model in Ref. [44]. This 331 variant has $\beta = 1/\sqrt{3}$, which fixes the electric charges of all the states contained in the $SU(2)_L$ triplets and anti-triplets to the usual $0, \pm 1$ values. In Sec. 5.4.2.2 we consider a 331 model with $\beta = -\sqrt{3}$, a value leading to exotic electric charges. This 331 variant has been discussed in the context of the diphoton excess in [53, 146, 355]. Although the mechanism to explain the diphoton excess is exactly the same as in [44], the presence of the exotic states leads to slightly different numerical results.

On the $SU(3)$ generators in SARAH

The most common choice for the $SU(3)$ generators is $T_a = \frac{\lambda_a}{2}$, with λ_a ($a = 1, \dots, 8$) the Gell-Mann matrices. However, this is just one of the possible representations. In fact, SARAH uses a different set of matrices, $T_a^{\text{SARAH}} = \frac{\Lambda_a}{2}$, following the conventions of Susyno [292]. The relation between the non-diagonal matrices in the two bases is

$$\lambda_1 = \Lambda_1, \quad (5.95a)$$

$$\lambda_2 = \Lambda_4, \quad (5.95b)$$

$$\lambda_4 = -\Lambda_6, \quad (5.95c)$$

$$\lambda_5 = -\Lambda_3, \quad (5.95d)$$

$$\lambda_6 = \Lambda_2, \quad (5.95e)$$

$$\lambda_7 = \Lambda_5. \quad (5.95f)$$

¹²See [354] for a complete discussion of 331 models with generic β .

¹³Eq. (5.94) assumes that the $SU(3)$ generators are $T_a = \frac{\lambda_a}{2}$, with λ_a ($a = 1, \dots, 8$) the Gell-Mann matrices. However, this is not the convention used in SARAH, see below.

Concerning the diagonal matrices, the usual $\lambda_{3,8}$ Gell-Mann matrices,

$$\lambda_3 = \begin{pmatrix} 1 & 0 & 0 \\ 0 & -1 & 0 \\ 0 & 0 & 0 \end{pmatrix}, \quad \lambda_8 = \frac{1}{\sqrt{3}} \begin{pmatrix} 1 & 0 & 0 \\ 0 & 1 & 0 \\ 0 & 0 & -2 \end{pmatrix}, \quad (5.96)$$

are replaced by $\Lambda_{7,8}$,

$$\Lambda_7 = \frac{1}{\sqrt{3}} \begin{pmatrix} 2 & 0 & 0 \\ 0 & -1 & 0 \\ 0 & 0 & -1 \end{pmatrix}, \quad \Lambda_8 = \begin{pmatrix} 0 & 0 & 0 \\ 0 & 1 & 0 \\ 0 & 0 & -1 \end{pmatrix}. \quad (5.97)$$

The electric charge operator can be written, using the conventions in **SARAH**, as

$$Q^{\text{SARAH}} = -T_8 - \beta T_7 + \mathcal{X}. \quad (5.98)$$

This in turn implies that the charge assignments in the $SU(3)$ multiplets must be adapted as well. For example, one can easily check that the electric charges of the first and third components of a $SU(3)$ triplet t are exchanged when going from the usual Gell-Mann representation to the basis choice employed in **SARAH**,

$$t = \begin{pmatrix} t_1 \\ t_2 \\ t_3 \end{pmatrix} \longrightarrow t^{\text{SARAH}} = \begin{pmatrix} t_3 \\ t_2 \\ t_1 \end{pmatrix}. \quad (5.99)$$

In the following we will use the standard conventions based on the Gell-Mann matrices in order to keep the discussion as close to the original works as possible. However, we emphasize that the implementation of the 331 models in **SARAH** requires this dictionary between the bases. It should also be noted that in the current implementation in **SARAH** of the 331 models described below, vertices involving four vector bosons in the generated model files for **CalcHep** cannot yet be handled correctly. In order to generate model files that will work with **CalcHep**, one must therefore exclude these vertices from being written out by **SARAH**, as described in Appendix [A.12](#).

5.4.2.1 331 model without exotic charges

- **Reference:** [\[44\]](#)
- **Model name:** 331/v1

The model is based on the $SU(3)_c \times SU(3)_L \times U(1)_\mathcal{X}$ gauge symmetry, extended with a global $U(1)_\mathcal{L}$ and an auxiliary \mathbb{Z}_2 symmetry to forbid some undesired couplings.

Field	Gen.	$SU(3)_C$	$SU(2)_L$	$U(1)_X$	$U(1)_\mathcal{L}$	\mathbb{Z}_2
Φ_1	1	$\mathbf{1}$	$\bar{\mathbf{3}}$	$\frac{2}{3}$	$\frac{2}{3}$	+
Φ_2	1	$\mathbf{1}$	$\bar{\mathbf{3}}$	$-\frac{1}{3}$	$-\frac{4}{3}$	+
Φ_3	1	$\mathbf{1}$	$\bar{\mathbf{3}}$	$-\frac{1}{3}$	$\frac{2}{3}$	-
Φ_X	1	$\mathbf{1}$	$\bar{\mathbf{3}}$	$-\frac{1}{3}$	$-\frac{4}{3}$	+
ψ_L	3	$\mathbf{1}$	$\bar{\mathbf{3}}$	$-\frac{1}{3}$	$-\frac{1}{3}$	+
e_R	3	$\mathbf{1}$	$\mathbf{1}$	-1	-1	+
s	3	$\mathbf{1}$	$\mathbf{1}$	0	1	+
$Q_L^{1,2}$	2	$\mathbf{3}$	$\mathbf{3}$	0	$-\frac{2}{3}$	+
Q_L^3	1	$\mathbf{3}$	$\bar{\mathbf{3}}$	$\frac{1}{3}$	$\frac{2}{3}$	-
u_R	3	$\mathbf{3}$	$\mathbf{1}$	$\frac{2}{3}$	0	+
T_R	1	$\mathbf{3}$	$\mathbf{1}$	$\frac{2}{3}$	0	-
d_R	3	$\mathbf{3}$	$\mathbf{1}$	$-\frac{1}{3}$	0	-
D_R, S_R	2	$\mathbf{3}$	$\mathbf{1}$	$-\frac{1}{3}$	0	+

Table 29. Fermionic and scalar particle content of the 331-v1 model. The scalar and fermion fields are shown in the top and bottom of the table respectively.

The fermionic and scalar particle content of the model is summarized in Table 29. In addition, due to the extended group structure, the model contains 17 gauge bosons: the usual 8 gluons; 8 W_i bosons associated to $SU(3)_L$ and the B boson associated to $U(1)_X$.

The fermionic $SU(3)_L$ triplets of the model can be decomposed as

$$\psi_L = \begin{pmatrix} \ell^- \\ -\nu \\ N^c \end{pmatrix}_L^{e,\mu,\tau}, \quad Q_L^1 = \begin{pmatrix} u \\ d \\ D \end{pmatrix}_L, \quad Q_L^2 = \begin{pmatrix} c \\ s \\ S \end{pmatrix}_L, \quad Q_L^3 = \begin{pmatrix} b \\ -t \\ T \end{pmatrix}_L. \quad (5.100)$$

The notation used for the extra quarks that constitute the third components of the $SU(3)_L$ triplets $Q_L^{1,2,3}$ is motivated by the fact that their electric charges are $-1/3$ and $2/3$ for D/S and T , respectively. The scalar multiplets can be written as

$$\Phi_1 = \begin{pmatrix} \phi_1 \\ -\phi_1^- \\ S_1^- \end{pmatrix}, \quad \Phi_2 = \begin{pmatrix} \phi_2^+ \\ -\phi_2 \\ S_2 \end{pmatrix}, \quad \Phi_3 = \begin{pmatrix} \phi_3^+ \\ -\phi_3 \\ S_3 \end{pmatrix}, \quad \Phi_X = \begin{pmatrix} \phi_X^+ \\ -\phi_X \\ X \end{pmatrix}. \quad (5.101)$$

While ϕ_1^- , $\phi_{2,3}^+$ and S_1^- are electrically charged scalars, the components $\phi_{1,2,3,X}$, $S_{2,3}$ and X are neutral.

The Yukawa Lagrangian of the model can be split as

$$\mathcal{L}_Y = \mathcal{L}_Y^q + \mathcal{L}_Y^\ell, \quad (5.102)$$

where

$$\begin{aligned} \mathcal{L}_Y^q = & \bar{Q}_L^{1,2} y^u u_R \Phi_1^* + \bar{Q}_L^3 \tilde{y}^d d_R \Phi_1 + \bar{Q}_L^{1,2} \tilde{y}^d \hat{d}_R \Phi_2^* + \bar{Q}_L^3 \bar{y}^u T_R \Phi_2 + \bar{Q}_L^3 \tilde{y}^u u_R \Phi_3 + \bar{Q}_L^{1,2} y^d d_R \Phi_3^* \\ & + \bar{Q}_L^{1,2} \tilde{y}_X^d \hat{d}_R \Phi_X + \bar{Q}_L^3 \bar{y}_X^u T_R \Phi_X + \text{h.c.}, \end{aligned} \quad (5.103)$$

and

$$\mathcal{L}_Y^\ell = y^\ell \bar{\psi}_L e_R \Phi_1 + y^a \bar{\psi}_L^c \psi_L \Phi_1 + y^s \bar{\psi}_L s \Phi_2 + \frac{m_s}{2} \bar{s}^c s + \text{h.c.}. \quad (5.104)$$

We defined $\hat{d}_R \equiv (D_R, S_R)$. We note that Eq. (5.104) leads to an inverse seesaw mechanism for neutrino masses [356, 357]. Here, y^a is anti-symmetric while m_s is symmetric, whereas the rest of Yukawa couplings are generic matrices, including those in Eq. (5.103). An additional term $y_X^s \bar{\psi}_L s \Phi_X$ could be added to Eq. (5.104), but given that $\langle \Phi_X \rangle = 0$, it does not contribute to neutrino masses and we will drop it for simplicity. Finally, the scalar potential is given by

$$\begin{aligned} V = & \sum_i \mu_i^2 |\Phi_i|^2 + \lambda_i |\Phi_i|^4 + \sum_{i \neq j} \lambda_{ij} |\Phi_i|^2 |\Phi_j|^2 \\ & + f (\Phi_1 \Phi_2 \Phi_3 + \text{h.c.}) + \frac{\kappa}{2} [(\Phi_2^\dagger \Phi_X)^2 + \text{h.c.}], \end{aligned} \quad (5.105)$$

where $i = 1, 2, 3, X$. The \mathbb{Z}_2 -soft-breaking term, $f \Phi_1 \Phi_2 \Phi_3$, is required to break unwanted accidental symmetries in the scalar potential.

We will assume the following symmetry breaking pattern

$$\langle \Phi_1 \rangle = \frac{1}{\sqrt{2}} \begin{pmatrix} k_1 \\ 0 \\ 0 \end{pmatrix}, \quad \langle \Phi_2 \rangle = \frac{1}{\sqrt{2}} \begin{pmatrix} 0 \\ 0 \\ n \end{pmatrix}, \quad \langle \Phi_3 \rangle = \frac{1}{\sqrt{2}} \begin{pmatrix} 0 \\ k_3 \\ 0 \end{pmatrix}, \quad \langle \Phi_X \rangle = \begin{pmatrix} 0 \\ 0 \\ 0 \end{pmatrix}. \quad (5.106)$$

5.4.2.2 331 model with exotic charges

- **Reference:** [53] (see also [146, 355] for similar constructions)
- **Model name:** 331/v2

Now, we will consider a 331 variant with $\beta = -\sqrt{3}$, as discussed in the context of the diphoton excess in [53]. The fermionic and scalar particle content of the model is

Field	Gen.	$SU(3)_C$	$SU(2)_L$	$U(1)_\chi$
ρ	1	1	3	1
η	1	1	3	0
χ	1	1	3	-1
ψ_L	3	1	$\bar{\mathbf{3}}$	-1
e_R	3	1	1	-1
E_R	3	3	3	-2
$Q_L^{1,2}$	2	3	3	$\frac{2}{3}$
Q_L^3	1	3	$\bar{\mathbf{3}}$	$-\frac{1}{3}$
u_R	3	3	1	$\frac{2}{3}$
T_R	1	3	1	$-\frac{4}{3}$
d_R	3	3	1	$-\frac{1}{3}$
D_R, S_R	2	3	1	$\frac{5}{3}$

Table 30. Fermionic and scalar particle content of the 331-v2 model. The scalar and fermion fields are shown in the top and bottom of the table respectively.

summarized in Table 30. In addition, the model contains 17 gauge bosons: the usual 8 gluons; 8 W_i bosons associated to $SU(3)_L$ and the B boson associated to $U(1)_\chi$.

The fermionic $SU(3)_L$ triplet representations of the model can be decomposed as

$$\psi_L = \begin{pmatrix} \ell^- \\ -\nu \\ E^{--} \end{pmatrix}_L^{e,\mu,\tau}, \quad Q_L^1 = \begin{pmatrix} u \\ d \\ D \end{pmatrix}_L, \quad Q_L^2 = \begin{pmatrix} c \\ s \\ S \end{pmatrix}_L, \quad Q_L^3 = \begin{pmatrix} b \\ -t \\ T \end{pmatrix}_L. \quad (5.107)$$

Due to the choice $\beta = -\sqrt{3}$, the electric charges for the extra quarks that constitute the third components of the $SU(3)_L$ triplets $Q_L^{1,2,3}$ are $5/3$, $5/3$ and $-4/3$, respectively. The scalar triplets can be written as

$$\rho = \begin{pmatrix} \rho^+ \\ \rho^0 \\ \rho^{++} \end{pmatrix}, \quad \eta = \begin{pmatrix} \eta^0 \\ \eta_1^- \\ \eta_2^+ \end{pmatrix}, \quad \chi = \begin{pmatrix} \chi^- \\ \chi^{--} \\ \chi^0 \end{pmatrix}. \quad (5.108)$$

Therefore, the particle spectrum of the model contains the exotic quarks in Eq. (5.107), as well as the doubly-charged fermion E^{--} and the scalars ρ^{++} and χ^{--} .

The Yukawa Lagrangian of the model can be split as

$$\mathcal{L}_Y = \mathcal{L}_Y^q + \mathcal{L}_Y^\ell, \quad (5.109)$$

where

$$\begin{aligned}
\mathcal{L}_Y^q &= y^d \overline{Q_L^{1,2}} \rho d_R + \tilde{y}^d \overline{Q_L^3} \eta^* d_R \\
&+ y^u \overline{Q_L^{1,2}} \eta u_R + \tilde{y}^u \overline{Q_L^3} \rho^* u_R \\
&+ y^J \overline{Q_L^{1,2}} \chi \hat{d}_R + \tilde{y}^J \overline{Q_L^3} \chi^* T_R + \text{h.c.} ,
\end{aligned} \tag{5.110}$$

where we have defined $\hat{d}_R \equiv (D_R, S_R)$, and

$$\mathcal{L}_Y^\ell = y^\ell \overline{\psi_L} \eta^* e_R + y^E \overline{\psi_L} \chi^* E_R + \text{h.c.} . \tag{5.111}$$

We note that the exotic fermions E , D , S and T only couple to the χ scalar triplet, and thus only via its vacuum expectation value (VEV) they will acquire masses. Finally, the scalar potential is given by

$$\begin{aligned}
V &= \mu_1^2 |\rho|^2 + \lambda_1 |\rho|^4 + \mu_2^2 |\eta|^2 + \lambda_2 |\eta|^4 + \mu_3^2 |\chi|^2 + \lambda_3 |\chi|^4 + \lambda_{12} |\rho|^2 |\eta|^2 + \lambda_{13} |\eta|^2 |\chi|^2 \\
&+ \lambda_{23} |\eta|^2 |\chi|^2 + \tilde{\lambda}_{12} (\rho^\dagger \eta) (\eta^\dagger \rho) + \tilde{\lambda}_{13} (\rho^\dagger \chi) (\chi^\dagger \rho) + \tilde{\lambda}_{23} (\eta^\dagger \chi) (\chi^\dagger \eta) \\
&+ \sqrt{2} f (\epsilon_{ijk} \rho^i \eta^j \chi^k + \text{h.c.}) .
\end{aligned} \tag{5.112}$$

We will assume the following symmetry breaking pattern

$$\langle \rho \rangle = \frac{1}{\sqrt{2}} \begin{pmatrix} 0 \\ v_1 \\ 0 \end{pmatrix} , \quad \langle \eta \rangle = \frac{1}{\sqrt{2}} \begin{pmatrix} v_2 \\ 0 \\ 0 \end{pmatrix} , \quad \langle \chi \rangle = \frac{1}{\sqrt{2}} \begin{pmatrix} 0 \\ 0 \\ v_3 \end{pmatrix} . \tag{5.113}$$

In this case, the non-zero VEV of χ is responsible for the breaking $SU(3)_L \times U(1)_X \rightarrow SU(2)_L \times U(1)_Y$. The requirement that this occurs at a scale much above the EW scale then imposes a hierarchy amongst the VEVs, namely that $v_3 \gg v_1, v_2$. Consequently, one of the CP-even scalar states is predominantly from the χ triplet and decouples from the SM. This scalar is then identified as the candidate for the 750 GeV resonance in this model. The decays of this state into two photons proceed via loops involving the heavy fermions, as well as those involving the charged scalars and additional charged vector bosons.

5.4.3 Other models

Gauged THD model

- **Reference:** [150]
- **Model name:** GTHDM

Field	Gen.	$SU(3)_C$	$SU(2)_L$	$U(1)_Y$	$SU(2)_H$	$U(1)_X$
$H = \begin{pmatrix} H_2^c & H_1^+ \\ H_2^0 & H_1^0 \end{pmatrix}$	1	1	2	$\frac{1}{2}$	2	1
$\Delta_H = \begin{pmatrix} \delta^0/\sqrt{2} & (\delta^-)^* \\ \delta^- & -\delta^0/\sqrt{2} \end{pmatrix}$	1	1	1	0	3	0
$\Phi = (\phi^c \phi^0)^T$	1	1	1	0	2	-1
$q = (u_L d_L)^T$	3	3	2	$\frac{1}{6}$	1	0
$l = (\nu_L e_L)^T$	3	1	2	$-\frac{1}{2}$	1	0
$d = (d_R^H d_R)^T$	3	$\bar{\mathbf{3}}$	1	$\frac{1}{3}$	2	1
$u = (u_R u_R^H)^T$	3	$\bar{\mathbf{3}}$	1	$-\frac{2}{3}$	2	-1
$\nu = (\nu_R \nu_R^H)^T$	3	1	1	0	2	-1
$e = (e_R^H e_R)^R$	3	1	1	1	2	1
χ_d	3	3	1	$-\frac{1}{3}$	1	0
χ_u	3	3	1	$\frac{2}{3}$	1	0
χ_ν	3	1	1	0	1	0
χ_e	3	1	1	-1	1	0

Table 31. Scalar and fermion fields in the GTHDM

The GTHDM model [358] comes with an additional gauged $SU(2)_H$ symmetry and a $U(1)_X$ symmetry, which is either global or gauged as well. Since the minimal, gauged version suffers from the fact that two massless vector bosons are present, $U(1)_X$ is treated as global symmetry. The scalar and fermion fields are listed in Table 31.

The Lagrangian of the GTHDM contains the SM Lagrangian, extended by the new terms

$$\begin{aligned}
\mathcal{L} = & (Y_d q d H^* - Y'_d \chi_d d \Phi + Y_e l e H^* - Y'_e \chi_e e \Phi \\
& + Y_u q u H - Y'_u \chi_u u \Phi^* + Y_\nu l \nu H - Y'_\nu \chi_\nu \nu \Phi^* + \text{h.c.}) \\
& + \mu_\Delta^2 |\Delta_H|^2 - \mu_H^2 |H|^2 - \mu_\Phi^2 |\Phi|^2 - M_H H^* \Delta_H H + M_\Phi \Phi^* \Delta_H \Phi - \lambda_D \text{Tr}(\Delta_H^\dagger \Delta_H)^2 \\
& - \lambda_{H\Delta} |H|^2 \text{Tr}(\Delta_H^\dagger \Delta_H) - \lambda_H |H|^4 - \lambda_{H\Phi} |H|^2 |\Phi|^2 - \lambda_{\Phi\Delta} |\Phi|^2 \text{Tr}(\Delta_H^\dagger \Delta_H) - \lambda_\Phi |\Phi|^4.
\end{aligned} \tag{5.114}$$

The breaking of $SU(2)_L \times U(1)_Y \times SU(2)_H \rightarrow U(1)_{em}$ is triggered by

$$\langle \Phi \rangle = \frac{1}{\sqrt{2}} \begin{pmatrix} 0 \\ v_\phi \end{pmatrix}, \quad \langle H \rangle = \frac{1}{\sqrt{2}} \begin{pmatrix} 0 & 0 \\ 0 & v \end{pmatrix}, \quad \langle \Delta_H \rangle = \frac{1}{2} \begin{pmatrix} v_T & 0 \\ 0 & -v_T \end{pmatrix}. \tag{5.115}$$

After EWSB, there are three neutral gauge bosons which mix giving rise to the γ, Z, Z' mass eigenstates and two charged ones (W, W') which do not mix. The neutral com-

ponent of the SM-singlet Φ , ϕ^0 , is considered to be the candidate for the 750 GeV resonance while its VEV gives mass to the exotic fermions that are needed to run in the loops. As ϕ^0 will typically mix with the $SU(2)_L$ doublet Higgs, this mixing needs to be suppressed by a specific parameter choice in order to avoid the tight bounds from the dijet, ZZ or dilepton channels.

5.5 Supersymmetric models

There are several ideas to explain the diphoton excess within a supersymmetric framework. Some of them make use of SUSY models which already exist in the literature, and for which also SARAH model files exist: the MSSM with trilinear R -parity violation [6, 100], the simplest models with Dirac gauginos [55], or the model with gauged $U(1)_L \times U(1)_B$ [111]. We will not make any further comment on these models, but concentrate in the following on the models which are newly implemented.

5.5.1 NMSSM extensions with vector-like multiplets

- **Reference:** [105, 128, 207, 208]
- **Model name:** NMSSM+VL

The scalar component of the gauge-singlet superfield \hat{S} of the Next to Minimal Supersymmetric Standard Model (NMSSM) can explain the 750 GeV resonance, if one adds vector-like $SU(5)$ multiplets to enhance the diphoton rate. The new multiplets are added in pairs of $(\mathbf{5}, \bar{\mathbf{5}})$ and/or $(\mathbf{10}, \bar{\mathbf{10}})$ in order to preserve gauge coupling unification. Typically one also imposes a \mathbb{Z}_2 symmetry to forbid mixing of the new vector-like particles with the MSSM particles. The authors of Ref. [208] mention the possibility to interpret the resonance as two nearly degenerate singlet-like bosons, roughly the scalar and pseudoscalar components of the singlet \hat{S} . There are some differences in the singlet and Higgs superpotential interactions included in the different papers:

- in Ref. [207] the authors assume $\lambda \hat{S} \hat{H}_u \hat{H}_d$ and $\kappa/3 \hat{S}^3$ to be present, but $\mu \hat{H}_u \hat{H}_d$ to be absent;
- in Ref. [105] $\mu \hat{H}_u H_d$, $\lambda \hat{S} \hat{H}_u \hat{H}_d$ and $M_S/2 \hat{S}^2$ are present;
- in Ref. [128] only $M_S/2 \hat{S}^2$ is present. This does not cause a mixing between the singlet and Higgs doublet at the tree level, but such a mixing is unavoidable at the loop level.

The SARAH implementations use the most general version of the superpotential: all possible interactions are present. The different limits according to the proposals of Refs. [105, 128, 207] can be obtained by setting the corresponding parameters to zero in numerical studies. In what follows we describe the models with the vector-like multiplets in different representations of $SU(5)$.

5.5.1.1 NMSSM with vectorlike top

- **Model name:** NMSSM+VL/VLtop
- **Reference:** [208]

This model is an extension of the NMSSM by a vector-like top. There is a global \mathbb{Z}_2 R -parity and a \mathbb{Z}_3 symmetry, under which all particles transform as $X \rightarrow \exp(i\frac{2\pi}{3}) X$. In this way, only terms with three superfields are allowed in the superpotential. The particle content is given in Table 32. Since this model does not introduce complete multiplets (**5** or **10**) of $SU(5)$, gauge coupling unification is not achieved. The super-

Field	Gen.	$SU(3)_C$	$SU(2)_L$	$U(1)_Y$	\mathbb{Z}_2	\mathbb{Z}_3
\hat{S}	1	1	1	0	+	$\exp(i\frac{2\pi}{3})$
\hat{T}	1	$\bar{\mathbf{3}}$	1	$-\frac{2}{3}$	-	$\exp(i\frac{2\pi}{3})$
\hat{T}'	1	3	1	$\frac{2}{3}$	-	$\exp(i\frac{2\pi}{3})$

Table 32. Superfield content beyond the MSSM superfields, including a singlet and a vector-like top.

potential is given by

$$\begin{aligned}
W = & -Y_d \hat{d} \hat{q} \hat{H}_d - Y_e \hat{e} \hat{l} \hat{H}_d + Y_u \hat{u} \hat{q} \hat{H}_u \\
& + \frac{1}{3} \kappa \hat{S}^3 + \lambda \hat{S} \hat{H}_u \hat{H}_d + Y_t \hat{T} \hat{Q} \hat{H}_u + \lambda_T \hat{T} \hat{T}' \hat{S} + \lambda_U \hat{U} \hat{T}' \hat{S}
\end{aligned} \tag{5.116}$$

Beyond the neutral scalar components of the two Higgs doublets, after EWSB the complex singlet gets a VEV and can be decomposed as

$$S = \frac{1}{\sqrt{2}} (v_S + \phi_S + i \sigma_S). \tag{5.117}$$

The fermionic components of \hat{T}, \hat{T}' mix with the up-type quarks, while the scalar components mix with the up-like squarks.

5.5.1.2 Pairs of 5 of $SU(5)$

Field	Gen.	$SU(3)_C$	$SU(2)_L$	$U(1)_Y$
\hat{S}	1	1	1	0
\hat{D}	1	$\bar{\mathbf{3}}$	1	$\frac{1}{3}$
\hat{D}'	1	3	1	$-\frac{1}{3}$
\hat{L}	1	1	2	$-\frac{1}{2}$
\hat{L}'	1	1	2	$\frac{1}{2}$

Table 33. Superfield content in the case of a pair of **5**'s of $SU(5)$.

- **Model name:** NMSSM+VL/5plets

The superfields beyond the MSSM are shown in Table 33. In the current implementation we only have one copy of (**5**, $\bar{\mathbf{5}}$) fields, but having at least three copies of them should give a better fit to the diphoton resonance. According to [105] the fit is even better with four copies, however in that case one might hit a Landau pole.

The superpotential is given by

$$\begin{aligned}
W = & -Y_d \hat{d} \hat{q} \hat{H}_d - Y_e \hat{e} \hat{l} \hat{H}_d + Y_u \hat{u} \hat{q} \hat{H}_u + \mu \hat{H}_u \hat{H}_d \\
& + \frac{1}{3} \kappa \hat{S}^3 + \lambda \hat{S} \hat{H}_u \hat{H}_d + M_S \hat{S}^2 + t_S \hat{S} \\
& + \lambda_D \hat{S} \hat{D} \hat{D}' + \lambda_L \hat{S} \hat{L} \hat{L}' + M_L \hat{L} \hat{L}' + M_D \hat{D} \hat{D}'. \tag{5.118}
\end{aligned}$$

Beyond the neutral scalar components of the two Higgs doublets, also the singlet gets a VEV after EWSB and can be decomposed as in Eq. (5.117).

5.5.1.3 Pairs of 10 of $SU(5)$

- **Model name:** NMSSM+VL/10plets

The superfields beyond the MSSM are shown in Table 34. The superpotential is given by

$$\begin{aligned}
W = & -Y_d \hat{d} \hat{q} \hat{H}_d - Y_e \hat{e} \hat{l} \hat{H}_d + Y_u \hat{u} \hat{q} \hat{H}_u + \mu \hat{H}_u \hat{H}_d \\
& + \frac{1}{3} \kappa \hat{S}^3 + \lambda \hat{S} \hat{H}_u \hat{H}_d + M_S \hat{S}^2 + t_S \hat{S} \\
& + Y_{10} \hat{Q} \hat{U} \hat{H}_u + Y'_{10} \hat{Q}' \hat{U}' \hat{H}_d + \lambda_Q \hat{S} \hat{Q} \hat{Q}' + \lambda_U \hat{S} \hat{U} \hat{U}' + \lambda_E \hat{S} \hat{E} \hat{E}' \\
& + M_U \hat{U} \hat{U}' + M_Q \hat{Q} \hat{Q}' + M_E \hat{E} \hat{E}'. \tag{5.119}
\end{aligned}$$

The symmetry breaking pattern is the same as for the model with 5-plets.

5.5.1.4 Pairs of 5 and 10 of $SU(5)$

Field	Gen.	$SU(3)_C$	$SU(2)_L$	$U(1)_Y$
\hat{S}	1	1	1	0
\hat{U}	1	$\bar{\mathbf{3}}$	1	$-\frac{2}{3}$
\hat{U}'	1	3	1	$\frac{2}{3}$
\hat{Q}	1	3	2	$\frac{1}{6}$
\hat{Q}'	1	$\bar{\mathbf{3}}$	2	$-\frac{1}{6}$
\hat{E}	1	1	1	1
\hat{E}'	1	1	1	-1

Table 34. Superfield content in the case of a pair of **10**'s of $SU(5)$.

- **Model name:** NMSSM+VL/5+10plets

This model combines the previous two setups, adding pairs of vectorlike **5** and **10** representations of $SU(5)$. The superfields beyond the MSSM are shown in Table 35. The superpotential is given by

Field	Gen.	$SU(3)_C$	$SU(2)_L$	$U(1)_Y$
\hat{S}	1	1	1	0
\hat{D}	1	$\bar{\mathbf{3}}$	1	$\frac{1}{3}$
\hat{D}'	1	3	1	$-\frac{1}{3}$
\hat{L}	1	1	2	$-\frac{1}{2}$
\hat{L}'	1	1	2	$\frac{1}{2}$
\hat{U}	1	$\bar{\mathbf{3}}$	1	$-\frac{2}{3}$
\hat{U}'	1	3	1	$\frac{2}{3}$
\hat{Q}	1	3	2	$\frac{1}{6}$
\hat{Q}'	1	$\bar{\mathbf{3}}$	2	$-\frac{1}{6}$
\hat{E}	1	1	1	1
\hat{E}'	1	1	1	-1

Table 35. Superfield content in the case of a pair of **5**'s and **10**'s of $SU(5)$.

$$\begin{aligned}
W = & -Y_d \hat{d} \hat{q} \hat{H}_d - Y_e \hat{e} \hat{l} \hat{H}_d + Y_u \hat{u} \hat{q} \hat{H}_u + \mu \hat{H}_u \hat{H}_d \\
& + \frac{1}{3} \kappa \hat{S}^3 + \lambda \hat{S} \hat{H}_u \hat{H}_d + M_S \hat{S}^2 + t_S \hat{S} \\
& + Y'_D \hat{D} \hat{Q} \hat{H}_d + Y'_E \hat{E} \hat{L} \hat{H}_d + Y'_U \hat{U} \hat{Q} \hat{H}_u + Y''_D \hat{D}' \hat{Q}' \hat{H}_u + Y''_E \hat{E}' \hat{L}' \hat{H}_u + Y''_U \hat{U}' \hat{Q}' \hat{H}_d \\
& + \lambda_D \hat{S} \hat{D} \hat{D}' + \lambda_L \hat{S} \hat{L} \hat{L}' + \lambda_Q \hat{S} \hat{Q} \hat{Q}' + \lambda_E \hat{S} \hat{E} \hat{E}' + \lambda_U \hat{S} \hat{U} \hat{U}' \\
& + M_L \hat{L} \hat{L}' + M_D \hat{D} \hat{D}' + M_Q \hat{Q} \hat{Q}' + M_E \hat{E} \hat{E}' + M_U \hat{U} \hat{U}' .
\end{aligned} \tag{5.120}$$

The symmetry breaking pattern is the same as for the model with 5-plets.

5.5.1.5 Pairs of 5 of $SU(5)$ and R -parity violation

- **Model name:** NMSSM+VL/5plets+RpV

One can relax the assumption of the \mathbb{Z}_2 symmetry that forbids mixing between vector-like fields and MSSM fields, in which case terms like $\kappa_5 \hat{S} \hat{L} \hat{H}_u$ are added to model [105]. Furthermore, this also breaks R -parity.

The superfields beyond the MSSM are shown in Table 33 and the superpotential is given by

$$\begin{aligned}
W = & -Y_d \hat{d} \hat{q} \hat{H}_d - Y_e \hat{e} \hat{l} \hat{H}_d + Y_u \hat{u} \hat{q} \hat{H}_u + \mu \hat{H}_u \hat{H}_d \\
& + \frac{1}{3} \kappa \hat{S}^3 + \lambda \hat{S} \hat{H}_u \hat{H}_d + M_S \hat{S}^2 + t_S \hat{S} \\
& + \kappa_5 \hat{S} \hat{L} \hat{H}_u + \kappa'_5 \hat{S} \hat{L}' \hat{H}_d + \lambda_D \hat{S} \hat{D} \hat{D}' + \lambda_L \hat{S} \hat{L} \hat{L}' + M_L \hat{L} \hat{L}' + M_D \hat{D} \hat{D}' .
\end{aligned} \tag{5.121}$$

The inclusion of R -parity violating terms triggers VEVs for the neutral components of \tilde{L} and \tilde{L}' ,

$$\langle \tilde{L} \rangle = \frac{1}{\sqrt{2}} \begin{pmatrix} 0 \\ v_L \end{pmatrix}, \quad \langle \tilde{L}' \rangle = \frac{1}{\sqrt{2}} \begin{pmatrix} 0 \\ v_{L'} \end{pmatrix}, \tag{5.122}$$

and causes mixing between the vector-like states and the Higgs components.

5.5.2 Broken MRSSM

- **Reference:** [58]
- **Model name:** brokenMRSSM

In the minimal R -supersymmetric model (MRSSM) the scalar R_u (see Table 36) is proposed as an explanation to the 750 GeV resonance. In order to explain the diphoton excess, it is necessary to add explicitly an R -symmetry breaking term to the Lagrangian

$$L_{\#} = T_u H_u \tilde{Q} \tilde{u}, \tag{5.123}$$

where T_u is a dimensionful trilinear coupling. This source of R -symmetry breaking has several consequences, not discussed in Ref. [58], which however are taken into account in the model implementation:

1. The term in Eq. (5.123) will introduce Majorana gaugino masses via RGE effects
2. The Majorana gaugino masses will also generate all other trilinear and bilinear soft-terms
3. This causes R -symmetry breaking terms $R_i H_i$ $i = d, u$ which will trigger VEVs for the R -fields
4. The neutralinos and gluinos are no longer Dirac particles, but mix to Majorana fermions
5. There is a mixing between fields of different R -charges.

The superfields beyond the MSSM are listed in Table 36. The superpotential, assumed

Field	Gen.	$SU(3)_C$	$SU(2)_L$	$U(1)_Y$
\hat{S}	1	1	1	0
\hat{T}	1	1	3	0
\hat{O}	1	8	1	0
\hat{R}_d	1	1	2	$+\frac{1}{2}$
\hat{R}_u	1	1	2	$-\frac{1}{2}$

Table 36. Superfields of the broken MRSSM beyond the MSSM particle content.

to conserve R -symmetry, is given by

$$\begin{aligned}
W = & -Y_d \hat{d} \hat{q} \hat{H}_d - Y_e \hat{e} \hat{l} \hat{H}_d + Y_u \hat{u} \hat{q} \hat{H}_u + \mu_D \hat{R}_d \hat{H}_d \\
& + \mu_U \hat{R}_u \hat{H}_u + \hat{S} (\lambda_d \hat{R}_d \hat{H}_d + \lambda_u \hat{R}_u \hat{H}_u) \\
& + \lambda_d^T \hat{R}_d \hat{T} \hat{H}_d + \lambda_u^T \hat{R}_u \hat{T} \hat{H}_u .
\end{aligned} \tag{5.124}$$

As explained above, because the R -symmetry is broken in the soft sector of the model, all possible tri- and bilinear soft-breaking terms corresponding to the superpotential terms will be generated.

The following VEVs appear after EWSB, beyond those of the neutral scalar components of the two Higgs doublets

$$\langle R_d \rangle = \frac{1}{\sqrt{2}} \begin{pmatrix} 0 \\ v_{R_d} \end{pmatrix}, \quad \langle R_u \rangle = \frac{1}{\sqrt{2}} \begin{pmatrix} 0 \\ v_{R_u} \end{pmatrix}, \quad \langle S \rangle = \frac{v_S}{\sqrt{2}}, \quad \langle T \rangle = \frac{1}{2} \begin{pmatrix} v_T & 0 \\ 0 & -v_T \end{pmatrix}. \tag{5.125}$$

The authors favor to have large stop mixing for a not too large R -symmetry breaking term T_u by considering the limit $v_d \sim v_u$ and $m_{\tilde{t}_L} \sim m_{\tilde{t}_R}$. However, in this limit the mass of the SM-like Higgs is tiny and often tachyonic: in the MSSM, the Higgs tree-level mass vanishes for $\tan\beta \rightarrow 1$, and this model has additional negative contributions to the mass from the new D -terms present in models with Dirac gauginos. It is also questionable if the case with very large T_u is a viable scenario because these values are highly restricted by charge and colour breaking minima [359, 360], which demands careful checks. This is similar to the vacuum stability issues discussed in Section 2.

5.5.3 $U(1)'$ -extended MSSM

- **Reference:** [154, 328]
- **Model name:** MSSM+U1prime-VL

Field	Gen.	$SU(3)_C$	$SU(2)_L$	$U(1)_Y$	$U(1)'$
\hat{Q}	3	3	2	$\frac{1}{6}$	$\frac{1}{2}$
\hat{d}^c	3	$\bar{\mathbf{3}}$	1	$\frac{1}{3}$	$\frac{1}{2}$
\hat{u}^c	3	$\bar{\mathbf{3}}$	1	$-\frac{2}{3}$	$\frac{1}{2}$
\hat{L}	3	1	2	$-\frac{1}{2}$	$\frac{1}{2}$
\hat{e}^c	3	1	1	1	$\frac{1}{2}$
$\hat{\nu}^c$	3	1	1	0	$\frac{1}{2}$
\hat{H}_d	1	1	2	$-\frac{1}{2}$	-1
\hat{H}_u	1	1	2	$\frac{1}{2}$	-1

Table 37. Quantum numbers of the MSSM fields under the full gauge group in the MSSM+U1prime-VL.

In this model all MSSM fields carry a non-zero $U(1)'$ -charge so that anomaly cancellation requires additional superfields (see Table 37), which are also responsible for the spontaneous $U(1)'$ breaking. Furthermore, colour-charged and colour-uncharged matter superfields which are vector-like with respect to the MSSM gauge group are introduced. A combination of scalar singlets S and S_i is supposed to give the 750 GeV resonance.

The complete superfield content with all gauge quantum numbers is given in Tables 37 and 38. In addition to the usual matter parity, we impose a \mathbb{Z}_2 symmetry under which all exotic matter superfields are odd and all other superfields are even in order to reduce the number of superpotential terms and hence reduce the complexity of the model.

Field	Gen.	$SU(3)_C$	$SU(2)_L$	$U(1)_Y$	$U(1)'$
\hat{T}	2	3	1	$\frac{2}{3}$	-1
\hat{T}^c	2	$\bar{\mathbf{3}}$	1	$-\frac{2}{3}$	-1
\hat{T}_3	1	3	1	$-\frac{1}{3}$	-1
\hat{T}_3^c	1	$\bar{\mathbf{3}}$	1	$\frac{1}{3}$	-1
\hat{D}	2	1	2	$\frac{1}{2}$	-1
\hat{D}^c	2	1	2	$-\frac{1}{2}$	-1
\hat{X}	1	1	1	1	2
\hat{X}^c	1	1	1	-1	2
\hat{N}	1	1	1	0	2
\hat{N}^c	1	1	1	0	2
S	1	1	1	0	2
S^c	1	1	1	0	-2
S_1	1	1	1	0	-4
S_1^c	1	1	1	0	4
S_2	1	1	1	0	-2

Table 38. Extra superfield content of the MSSM+U1prime-VL and their quantum numbers under the full gauge group.

The superpotential is given by

$$\begin{aligned}
W = & -Y_d \hat{d}^c \hat{Q} \hat{H}_d - Y_e \hat{e}^c \hat{L} \hat{H}_d + Y_u \hat{u}^c \hat{Q} \hat{H}_u + Y_\nu \hat{\nu}^c \hat{L} \hat{H}_u + \lambda \hat{S} \hat{H}_u \hat{H}_d \\
& + \lambda_N \hat{S}_1 \hat{N} \hat{N}^c + \lambda_D \hat{S} \hat{D} \hat{D}^c + \lambda_X \hat{S}_1 \hat{X} \hat{X}^c + \lambda_T \hat{S} \hat{T}^c \hat{T} + \lambda_{T3} \hat{S} \hat{T}_3^c \hat{T}_3 \\
& + \mu_S \hat{S} \hat{S}^c + \mu_{1S} \hat{S}_1 \hat{S}_1^c + \mu_{2S} \hat{S} \hat{S}_2 + \kappa_1 \hat{S} \hat{S} \hat{S}_1 + \kappa_2 \hat{S}^c \hat{S}_2 \hat{S}_1^c.
\end{aligned} \tag{5.126}$$

In addition to the neutral components of the two Higgs doublets, the MSSM singlets get VEVs according to

$$\langle S_i^{(c)} \rangle = \frac{v_{S_i}^{(c)}}{\sqrt{2}}. \tag{5.127}$$

5.5.4 E_6 -inspired SUSY models with extra $U(1)$ model

- **Reference:** [64]
- **Model name:** SUSYmodels/E6SSMalt

E_6 -inspired SUSY models predict extra SM-gauge singlets and extra exotic fermions, so they immediately have the ingredients that many authors have tried to use to fit the

diphoton excess. These models are often motivated as a solution to the μ -problem of the MSSM, because the extra $U(1)$ gauge symmetry forbids the μ -term, while when one of the singlet fields develops a VEV at the TeV scale this breaks the extra $U(1)$ giving rise to a massive Z' vector boson and at the same time generates an effective μ term through the singlet interaction with the up- and down-type Higgs fields, $\lambda \hat{S} \hat{H}_u \hat{H}_d$. The matter content of the model at low energies fills three generations of complete **27**-plet representations of E_6 , which ensures that anomalies automatically cancel.

A number of models of this nature have been proposed as explanations of the diphoton excess [64, 164, 361]. The example we implement here [64] is a variant of the E_6 SSM [362, 363]. In this version two singlet states develop VEVs and the idea is that the 750 GeV excess is explained by one of these singlet states with a loop-induced decay through the exotic states.

In E_6 models the extra $U(1)$ which extends the SM gauge group is given as a linear combination of $U(1)_\psi$ and $U(1)_\chi$ which appear from the breakdown of the E_6 symmetry as $E_6 \rightarrow SO(10) \times U(1)_\psi$ followed by $SO(10)$ into $SU(5)$, $SO(10) \rightarrow SU(5) \times U(1)_\chi$. In the E_6 SSM and the variant implemented here the specific combination is,

$$U(1)_N = \frac{1}{4}U(1)_\chi + \frac{\sqrt{15}}{4}U(1)_\psi. \quad (5.128)$$

To allow one-step gauge coupling unification however some incomplete multiplets must be included in the low energy matter content. So in addition to the matter filling complete **27** representations of E_6 there are also two $SU(2)$ multiplets \hat{H}' and $\overline{\hat{H}'}$, which are the only components from additional **27'** and $\overline{\mathbf{27}'}$ that survive to low energies. All gauge anomalies cancel between these two states, so they do not introduce any gauge anomalies. Furthermore, the low energy matter content of the model beyond the MSSM one includes three generations of exotic diquarks¹⁴, $\hat{D}_i, \overline{\hat{D}}_i$, three generations of SM singlet superfields \hat{S}_i and extra Higgs-like states $H_{1,2}^u$ and $H_{1,2}^d$ that do not get VEVs.

The full set of superfields are given in Table 39 along with their representations under $SU(3)$ and $SU(2)$ and the charges of the two $U(1)$ gauge groups and the discrete symmetries, which we will now discuss.

The \mathbb{Z}_2^L symmetry plays a role similar to R-parity in the MSSM, being imposed to avoid rapid proton decay in the model. However with this imposed there are still terms in the superpotential that can lead to dangerous flavour changing neutral currents (FCNCs). To forbid these, an approximate \mathbb{Z}_2^H symmetry is imposed. In the original

¹⁴In the original E_6 SSM these states could be either diquark or leptoquark in nature, depending on the choice of a discrete symmetry, but in the model considered here the allowed superpotential terms for the decay of these exotic quarks imply they are diquark.

Field	Gen	$SU(3)_C$	$SU(2)_L$	$U(1)_Y$	$U(1)_N$	\mathbb{Z}_2^H	\mathbb{Z}_2^L
\hat{Q}_i	3	3	2	$\frac{1}{6}$	1	-	+
\hat{u}_i^c	3	$\bar{\mathbf{3}}$	1	$-\frac{2}{3}$	1	-	+
\hat{d}_i^c	3	$\bar{\mathbf{3}}$	1	$\frac{1}{3}$	2	-	+
\hat{L}_i	3	1	2	$-\frac{1}{2}$	2	-	-
\hat{e}_i^c	3	1	1	1	1	-	-
\hat{N}_i^c	3	1	1	0	0	-	-
\hat{S}_i	2	1	1	0	5	+	+
\hat{S}_1	1	1	1	0	5	-	+
\hat{H}_u	1	1	2	$\frac{1}{2}$	-2	+	+
\hat{H}_d	1	1	2	$-\frac{1}{2}$	-3	+	+
\hat{H}_α^u	2	1	2	$\frac{1}{2}$	-2	-	+
\hat{H}_α^d	2	1	2	$-\frac{1}{2}$	-3	-	+
\hat{D}_i	3	3	1	$-\frac{1}{3}$	-2	-	+
\hat{D}	3	$\bar{\mathbf{3}}$	1	$\frac{1}{3}$	-3	-	+
\hat{L}_4	1	1	2	$-\frac{1}{2}$	2	-	+
\hat{L}_4	1	1	$\bar{\mathbf{2}}$	$\frac{1}{2}$	-2	-	+

Table 39. The representations of the chiral superfields under the $SU(3)_C$ and $SU(2)_L$ gauge groups, and their $U(1)_Y$ and $U(1)_N$ charges without the E_6 normalisation. The GUT normalisations are $\sqrt{\frac{5}{3}}$ for $U(1)_Y$ and $\sqrt{40}$ for $U(1)_N$. The transformation properties under the discrete symmetries \mathbb{Z}_2^H , \mathbb{Z}_2^L are also shown, where ‘+’ indicates the superfield is even under the symmetry and ‘-’ indicates that it is odd under the symmetry.

E_6 SSM model only \hat{S}_3 , \hat{H}_d and \hat{H}_u were even under the \mathbb{Z}_2^H symmetry, however in this variant S_2 is also even under this approximate symmetry.

The full superpotential before imposing any discrete symmetries is given by

$$W_{E6} = W_0 + W_1 + W_2, \quad (5.129)$$

where

$$W_0 = \lambda_{ijk} \hat{S}_i \hat{H}_j^d \hat{H}_k^u + \kappa_{ijk} \hat{S}_i \hat{D}_j \hat{D}_k + h_{ijk}^N \hat{N}_i^c \hat{H}_j^u \hat{L}_k + h_{ijk}^U \hat{u}_i^c \hat{H}_j^u \hat{Q}_k + h_{ijk}^D \hat{d}_i^c \hat{H}_j^d \hat{Q}_k + h_{ijk}^E \hat{e}_i^c \hat{H}_j^d \hat{L}_k, \quad (5.130)$$

$$W_1 = g_{ijk}^Q \hat{D}_i \hat{Q}_j \hat{Q}_k + g_{ijk}^a \hat{D}_i \hat{d}_j^c \hat{u}_k^c, \quad (5.131)$$

$$W_2 = g_{ijk}^N \hat{N}_i^c \hat{D}_j \hat{d}_k^c + g_{ijk}^E \hat{e}_i^c \hat{D}_j \hat{u}_k^c + g_{ijk}^D \hat{Q}_i \hat{L}_j \hat{D}_k. \quad (5.132)$$

However, with the discrete symmetries imposed and integrating out the heavy right-handed neutrinos, the superpotential in this specific variant reduces to¹⁵,

$$\begin{aligned}
W_{E_6SSM \text{ variant}} = & W_{MSSM}^{(\mu=0)} + \sum_{\alpha=2}^3 \sum_{i=1}^3 \hat{S}^\alpha (\lambda_{\alpha i} \hat{H}_u^i \hat{H}_d^i + \kappa_{\alpha i} \hat{D}^i \hat{\bar{D}}^i) \\
& + \mu' \hat{H} \hat{\bar{H}}' + h_{4j}^E (\hat{H}_d \hat{H}') \hat{e}_j^c
\end{aligned} \tag{5.133}$$

One should remember that the \mathbb{Z}_2^H can only be an approximate symmetry as otherwise the exotic quarks could not decay. In this variant the exotic quarks decay through the \mathbb{Z}_2^H violating interactions of W_1 .

In the paper it is assumed that the singlet mixing can be negligible and the numerical calculation was performed under this assumption, neglecting any mixing between the singlet state which decays to $\gamma\gamma$ via the exotic states and the other CP-even Higgs states from the standard $SU(2)$ doublets. However it is clear that there must be some mixing from the D-terms, and therefore if that is included one important check would be to test whether other decays are sufficiently suppressed. Moreover, the parameters needed to simultaneously get a 125 GeV SM-like Higgs state and a 750 GeV singlet-dominated state are not given. In this respect we note that the singlet VEVs appear both in the diagonal entries of the mass matrix and in the off-diagonal entries that mix the singlet states with the doublet states.

We finally note that other similar E_6 models have also been proposed in the context of the diphoton excess. These include a model by two authors from the original paper [164], a model with a different $U(1)$ group at low energies [364], and a model that is still E_6 -inspired, but where no extra $U(1)$ survives down to low energies [160].

6 Study of a natural SUSY explanation for the diphoton excess

We show in this section how one can use the described setup to perform easily a detailed study of a new model that aims at explaining the diphoton anomaly.

6.1 The model

We are now going to study a SUSY model which enhances the tree-level Higgs mass due to non-decoupling D -terms. The model is based on that proposed in Ref. [365] as a natural SUSY model which allows for light stops compatible with the measured Higgs boson mass, extended by three generations of pairs of vector-like quarks and

¹⁵In the paper proposing this variant to explain the excess [64], the terms involving the surviving Higgs states on the second line are omitted from the superpotential.

leptons. We want to achieve a tree-level enhancement of the SM-like Higgs mass and an explanation of the diphoton excess via the loop-induced decay of a CP-odd scalar. In addition, we will also check whether one can get a broad diphoton resonance in this model. The matter field content is shown in Table 40 and the considered superpotential

SF	Spin 0	Spin $\frac{1}{2}$	Generations	$U(1)_Y$	$SU(2)_L$	$SU(3)_C$	$U(1)_X$
\hat{q}	\tilde{q}	q	3	$\frac{1}{6}$	2	3	0
\hat{l}	\tilde{l}	l	3	$-\frac{1}{2}$	2	1	0
\hat{d}	\tilde{d}_R^*	d_R^*	3	$\frac{1}{3}$	1	$\bar{\mathbf{3}}$	$\frac{1}{2}$
\hat{u}	\tilde{u}_R^*	u_R^*	3	$-\frac{2}{3}$	1	$\bar{\mathbf{3}}$	$-\frac{1}{2}$
\hat{e}	\tilde{e}_R^*	e_R^*	3	1	1	1	$\frac{1}{2}$
$\hat{\nu}$	$\tilde{\nu}_R^*$	ν_R^*	3	0	1	1	$-\frac{1}{2}$
\hat{U}	\tilde{U}^*	U^*	3	$-\frac{2}{3}$	1	$\bar{\mathbf{3}}$	$-\frac{1}{2}$
\hat{U}	\tilde{U}	\bar{U}	3	$\frac{2}{3}$	1	3	$\frac{1}{2}$
\hat{E}	\tilde{E}^*	E^*	3	1	1	1	$\frac{1}{2}$
\hat{E}	\tilde{E}	\bar{E}	3	-1	1	1	$-\frac{1}{2}$
\hat{H}_d	H_d	\tilde{H}_d	1	$-\frac{1}{2}$	2	1	$-\frac{1}{2}$
\hat{H}_u	H_u	\tilde{H}_u	1	$\frac{1}{2}$	2	1	$\frac{1}{2}$
$\hat{\eta}$	η	$\tilde{\eta}$	1	0	1	1	-1
$\hat{\bar{\eta}}$	$\bar{\eta}$	$\tilde{\bar{\eta}}$	1	0	1	1	1
\hat{S}	S	\tilde{S}	1	0	1	1	0

Table 40. Scalars and fermions in the $U(1)_X$ -extended MSSM

reads:

$$\begin{aligned}
W = & -Y_d \hat{d} \hat{q} \hat{H}_d - Y_e \hat{e} \hat{l} \hat{H}_d + Y_u \hat{u} \hat{q} \hat{H}_u + Y_\nu \hat{\nu} \hat{l} \hat{H}_u + Y_x \hat{\nu} \hat{\eta} \hat{\nu} + (\mu + \lambda \hat{S}) \hat{H}_u \hat{H}_d \\
& + \hat{S}(\xi + \lambda_X \hat{\eta} \hat{\eta}) + M_S \hat{S} \hat{S} + \frac{1}{3} \kappa \hat{S} \hat{S} \hat{S} + \tilde{M}_E \hat{e} \hat{E} + \tilde{M}_U \hat{u} \hat{U} \\
& + \hat{S}(\lambda_e \hat{E} \hat{E} + \lambda_u \hat{U} \hat{U}) + M_e \hat{E} \hat{E} + M_u \hat{U} \hat{U} + Y'_e \hat{E} \hat{l} \hat{H}_d + Y'_u \hat{U} \hat{q} \hat{H}_u. \quad (6.1)
\end{aligned}$$

We will not make the simplifying assumption that mixings between the MSSM states and the new vector-like fields can be neglected. Of course, such mixing could have been forbidden by choosing different $U(1)_X$ charges for the new particles. However, in such case there would be a conserved \mathbb{Z}_2 symmetry associated to the vector-like states (under which all vector-like superfields are odd and the rest are even) that would make the lightest of them absolutely stable. This would be a problem unless that state is neutral and colourless, and thus this scenario can only be viable if we also consider

additional singlet vector-like states, such as vector-like partners for the right-handed neutrinos, and make them lighter than the other vector-like states. Thus, this setup would predict two stable particles to make the dark matter. Such a scenario could also be studied with the tools presented here. However, we decided not to consider this option in the following.

The other main ingredients of the model are the general soft-SUSY breaking terms, which read

$$\begin{aligned}
-\mathcal{L} = & (T_d \tilde{d} \tilde{q} H_d + (T_e \tilde{e} + T'_e \tilde{E}) \tilde{l} H_d + (T_u \tilde{u} + T'_u \tilde{U}) \tilde{q} H_u + T_\nu \tilde{\nu} \tilde{l} H_u + T_x \tilde{\nu} \tilde{\eta} \tilde{\nu} + (B_\mu + T_\lambda S) H_u H_d \\
& + S(t_\xi + T_X \eta \bar{\eta}) + B_S S S + \frac{1}{3} T_\kappa S S S + S(T_E \tilde{E} \tilde{E} + T_U \tilde{U} \tilde{U}) \\
& + B_E \tilde{E} \tilde{E} + B_U \tilde{U} \tilde{U} + \tilde{B}_E \tilde{e} \tilde{E} + \tilde{B}_U \tilde{u} \tilde{U} + \text{h.c.}) \\
& + \tilde{q}^\dagger m_q^2 \tilde{q} + \tilde{u}^\dagger m_u^2 \tilde{u} + \tilde{d}^\dagger m_d^2 \tilde{d} + \tilde{e}^\dagger m_e^2 \tilde{e} + \tilde{l}^\dagger m_l^2 \tilde{l} + \tilde{U}^\dagger m_U^2 \tilde{U} + \tilde{U}^\dagger m_U^2 \tilde{U} + \tilde{E}^\dagger m_E^2 \tilde{E} + \tilde{E}^\dagger m_E^2 \tilde{E} + \\
& + (\tilde{U}^\dagger m_{U_u}^2 \tilde{u} + \tilde{E}^\dagger m_{E_e}^2 \tilde{E} + \text{h.c.}) + m_{H_d}^2 |H_d|^2 + m_{H_u}^2 |H_u|^2 + m_{H_s}^2 |S|^2 + m_\eta^2 |\eta|^2 + m_{\bar{\eta}}^2 |\bar{\eta}|^2 \\
& + (M_1 \lambda_B \lambda_B + M_2 \lambda_W \lambda_W + M_3 \lambda_g \lambda_g + M_X \lambda_X \lambda_X + M_{1X} \lambda_B \lambda_X + \text{h.c.}) \quad (6.2)
\end{aligned}$$

Note that we have included the gaugino mass term M_{1X} arising from gauge kinetic mixing. All the terms shown in Eq. (6.2) are automatically added by SARAH based on the information provided by the user about the particle content and the superpotential. Several scalar fields acquire VEVs. We decompose them as

$$H_d^0 = \frac{1}{\sqrt{2}} (\phi_d + v_d + i\sigma_d) , \quad H_u^0 = \frac{1}{\sqrt{2}} (\phi_u + v_u + i\sigma_u) , \quad (6.3)$$

$$\eta = \frac{1}{\sqrt{2}} (\phi_\eta + v_\eta + i\sigma_\eta) , \quad \bar{\eta} = \frac{1}{\sqrt{2}} (\phi_{\bar{\eta}} + v_{\bar{\eta}} + i\sigma_{\bar{\eta}}) , \quad (6.4)$$

$$S = \frac{1}{\sqrt{2}} (\phi_s + v_s + i\sigma_s) . \quad (6.5)$$

We define $\tan \beta = \frac{v_u}{v_d}$, $v = \sqrt{v_d^2 + v_u^2}$ as well as $\tan \beta_x = \frac{v_\eta}{v_{\bar{\eta}}}$, $x = \sqrt{v_\eta^2 + v_{\bar{\eta}}^2}$. In addition, the sneutrinos are decomposed with respect to their CP eigenstates,

$$\tilde{\nu}_{L,i} \rightarrow \frac{1}{\sqrt{2}} (\phi_{L,i} + i\sigma_{L,i}) , \quad \tilde{\nu}_{R,i} \rightarrow \frac{1}{\sqrt{2}} (\phi_{R,i} + i\sigma_{R,i}) , \quad (6.6)$$

which in general have different masses due to the Majorana mass-term $Y_X \langle \bar{\eta} \rangle$ in the superpotential. Since H_d^0 and H_u^0 carry charges under both $U(1)$ gauge groups, there will be non-zero Z - Z' mixing even in the limit of vanishing gauge kinetic mixing. The

list of particle mixings, which go beyond the usual MSSM mixings reads

$$(B, W_3, B') \longrightarrow (\gamma, Z, Z'), \quad (6.7)$$

$$(\phi_d, \phi_u, \phi_\eta, \phi_{\bar{\eta}}, \phi_s) \longrightarrow h_i, \quad i = 1 \dots 5, \quad (6.8)$$

$$(\sigma_d, \sigma_u, \sigma_\eta, \sigma_{\bar{\eta}}, \sigma_s) \longrightarrow A_i^0, \quad i = 1 \dots 5, \quad (6.9)$$

$$(\phi_{L,i}, \phi_{R,i}) \longrightarrow \tilde{\nu}_j^R, \quad i = 1 \dots 3, j = 1 \dots 6, \quad (6.10)$$

$$(\sigma_{L,i}, \sigma_{R,i}) \longrightarrow \tilde{\nu}_j^I, \quad i = 1 \dots 3, j = 1 \dots 6, \quad (6.11)$$

$$(\tilde{B}, \tilde{W}_3, \tilde{H}_d^0, \tilde{H}_u^0, \tilde{X}, \tilde{\eta}, \tilde{\bar{\eta}}, \tilde{S}) \longrightarrow \tilde{\chi}_i^0, \quad i = 1 \dots 8, \quad (6.12)$$

$$(e_{L,i}, \bar{E}_i^*) / (e_{R,i}, E_i) \longrightarrow e_j, \quad i = 1 \dots 3, j = 1 \dots 6, \quad (6.13)$$

$$(u_{L,i}, \bar{U}_i^*) / (u_{R,i}, U_i) \longrightarrow u_i, \quad i = 1 \dots 3, j = 1 \dots 6, \quad (6.14)$$

$$(\tilde{e}_{L,i}, \tilde{e}_{R,i}, \tilde{E}_i, \tilde{\bar{E}}_i) \longrightarrow \tilde{e}_j, \quad i = 1 \dots 3, j = 1 \dots 12, \quad (6.15)$$

$$(\tilde{u}_{L,i}, \tilde{u}_{R,i}, \tilde{U}_i, \tilde{\bar{U}}_i) \longrightarrow \tilde{u}_j, \quad i = 1 \dots 3, j = 1 \dots 12, \quad (6.16)$$

The model files which implement this model in SARAH are discussed in Appendix B.2. In addition, we provide all files to reproduce the computations that follow at

http://sarah.hepforge.org/U1xMSSM_example.tar.gz

6.2 Analytical results with Mathematica

Before we perform a numerically precise study of the model, we show how already with just SARAH and Mathematica one can gain a lot of information about a new model.

6.2.1 Consistency Checks

The model is initialised after loading it in SARAH via

```
<<SARAH.m;
Start["U1xMSSM"];
```

SARAH automatically performs some basic consistency checks for the model. For instance, it checks whether the model is free from gauge anomalies:

```
Checking for anomalies:
{(hypercharge)^3, (left)^3, (color)^3, (extra)^3,
 (hypercharge)x(gravity)^2,
 (extra)x(gravity)^2,
 (left)^2 x hypercharge,
 (color)^2 x hypercharge,
 (extra)^2 x hypercharge,
 (hypercharge)^2 x extra,
```

```
| (left)^2 x extra,
| (color)^2 x extra,
| Witten Anomalyleft}
```

One can see that `SARAH` tests all different combinations of gauge anomalies and, given that no warning is printed on the screen, confirms that all of them cancel. Similarly, it also checks that all terms in the superpotential are in agreement with all global and local symmetries. More detailed checks can be carried out by running `CheckModel[]` when the initialisation is finished.

After a few seconds, a message is printed telling that the model is loaded.

```
| All Done. U1xMSSM is ready!
```

6.2.2 Gauge sector

Before we discuss the matter sector or the scalar potential, we have a brief look at the gauge bosons. We make use of the mass matrices calculated by `SARAH` during the initialisation of the model. We find a handy expression for the mass matrix of the neutral gauge bosons in the limit of vanishing gauge kinetic mixing ($g_{X1} = g_{1X} = 0$) via

```
| matV = Simplify[MassMatrix[VZp] /. {gX1 -> 0, g1X -> 0}]
| //.{vd^2 + vu^2 -> v^2, x1^2 + x2^2 -> x^2}
```

which reads

$$\begin{pmatrix} \frac{g_1^2 v^2}{4} & -\frac{1}{4} g_1 g_2 v^2 & \frac{1}{4} g_1 g_X v^2 \\ -\frac{1}{4} g_1 g_2 v^2 & \frac{g_2^2 v^2}{4} & -\frac{1}{4} g_2 g_X v^2 \\ \frac{1}{4} g_1 g_X v^2 & -\frac{1}{4} g_2 g_X v^2 & \frac{1}{4} g_X^2 (v^2 + 4x^2) \end{pmatrix}. \quad (6.17)$$

Note, that `MassMatrix[VP]` and `MassMatrix[VZ]` would have given the same result. We can check the eigenvalues of this matrix to first order in $\frac{v^2}{x^2}$ using the `Series` command of `Mathematica`

```
| Simplify[Normal[Series[Eigenvalues[matV]
| /. v -> r x, {r, 0, 2}]] /. r -> v/x, {x > 0, gX > 0}]
```

and find

$$\{0, \frac{1}{4}(g_1^2 + g_2^2)v^2, \frac{1}{4}g_X^2(4x^2 + v^2)\} \quad (6.18)$$

As expected, the first two eigenvalues are just the ones of the SM gauge bosons, while the mass of the new gauge boson is given by

$$M_{Z'} = \frac{1}{2} g_X \sqrt{4x^2 + v^2}. \quad (6.19)$$

We will use this relation in the following to replace x by $M_{Z'}$ in all equations.

6.2.3 Scalar Sector

Solving the tadpole equations We turn now to the scalar sector of the model. First, we make a list with a few simplifying assumptions which we are going to use in the following

```
assumptions = {
  conj[x_] -> x, Rxi[___] -> 0,
  gX1 -> 0, g1X -> 0,
  x1 -> X/Sqrt[2], x2 -> X/Sqrt[2],
      X -> Sqrt[4 MZp^2 - gX^2 v^2]/(2 gX),
  vd -> v Cos[ArcTan[TB]], vu -> v Sin[ArcTan[TB]],
  T[kappa] -> 0, kappa -> 0,
      T[lambdaH] -> 0, lambdaH -> 0, L[lw] -> 0};
```

Here we assume all parameters to be real, remove any complex conjugation (`conj`) and use the Landau gauge (`Rxi[___]->0`), then we turn off again gauge kinetic mixing and take the VEVs of η and $\bar{\eta}$ to be equal. In the fourth line, we parametrise v_d and v_u as usual in terms of v and $\tan\beta$. Finally, we set the parameters κ , T_κ , λ , T_λ and L_ξ to zero. We can now solve the tadpole equations, stored by **SARAH** in `TadpoleEquations[Eigenstates]`, with respect to the parameters $m_{H_d}^2$, $m_{H_u}^2$, m_η^2 , m_ξ^2 and ξ using the aforementioned assumptions:

```
sol = Simplify[
  Solve[(TadpoleEquations[EWSB] /. assumptions) == 0,
    {mHd2, mHu2, mC12, lw, mS2}][[1]]
];
```

We have saved the solution in the variable `sol` for further usage.

Obtaining a 750 GeV pseudo-scalar We use the solution and our assumptions to get simpler expressions for the mass matrix of the CP-even (called **hh**) and CP-odd (called **Ah**) scalars:

```
mH = FullSimplify[MassMatrix[hh] /. sol /. assumptions]
mA = FullSimplify[MassMatrix[Ah] /. sol /. assumptions]
```

These matrices can be expressed as

$$m_H^2 \simeq \begin{pmatrix} m_H^{2,\text{MSSM}} & m_H^{2,\text{mix}} \\ (m_H^{2,\text{mix}})^T & m_H^{2,X} \end{pmatrix}, \quad m_A^2 \simeq \begin{pmatrix} m_A^{2,\text{MSSM}} & 0 \\ 0 & m_A^{2,X} \end{pmatrix} \quad (6.20)$$

with

$$m_H^{2,\text{MSSM}} \simeq \begin{pmatrix} t_\beta B(\mu) + \frac{v^2(g_1^2 + g_2^2 + g_X^2)}{4(t_\beta^2 + 1)} & -B(\mu) - \frac{t_\beta v^2(g_1^2 + g_2^2 + g_X^2)}{4(t_\beta^2 + 1)} \\ -B(\mu) - \frac{t_\beta v^2(g_1^2 + g_2^2 + g_X^2)}{4(t_\beta^2 + 1)} & \frac{B(\mu)}{t_\beta} + \frac{t_\beta^2 v^2(g_1^2 + g_2^2 + g_X^2)}{4(t_\beta^2 + 1)} \end{pmatrix}, \quad (6.21)$$

$$m_H^{2,\text{mix}} \simeq \begin{pmatrix} \frac{1}{4} g_X v \sqrt{\frac{4M_{Z'}^2 - g_X^2 v^2}{2t_\beta^2 + 2}} & -\frac{1}{4} g_X v \sqrt{\frac{4M_{Z'}^2 - g_X^2 v^2}{2t_\beta^2 + 2}} & 0 \\ -\frac{1}{4} g_X t_\beta v \sqrt{\frac{4M_{Z'}^2 - g_X^2 v^2}{2t_\beta^2 + 2}} & \frac{1}{4} g_X t_\beta v \sqrt{\frac{4M_{Z'}^2 - g_X^2 v^2}{2t_\beta^2 + 2}} & 0 \end{pmatrix}, \quad (6.22)$$

$$m_A^{2,\text{MSSM}} \simeq \begin{pmatrix} t_\beta B(\mu) & B(\mu) \\ B(\mu) & \frac{B(\mu)}{t_\beta} \end{pmatrix}. \quad (6.23)$$

We omit here the analytical expressions for $m_A^{2,X}$ and $m_H^{2,X}$ because of their length and since they are not needed for the following brief discussion. The mass matrix for the CP-odd states is block-diagonal since the MSSM part is unchanged, while we have mixing in the CP-even sector among all five components.¹⁶ The additional D -Terms can be found in the MSSM block, $m_H^{2,\text{MSSM}}$. This also explains our choice of a pseudo-scalar as the resonance behind the diphoton excess: the tree-level mixing between the scalar singlet and the doublets would cause tree-level decays of a 750 GeV scalar into all kinds of SM particles. In particular, those into WW and ZZ are constrained and could easily spoil our setup as an explanation of the excess in this model. Of course, we have to check whether it is possible to obtain a pseudo-scalar of the correct mass, and get the corresponding scalar sufficiently heavy so as to escape detection. For that purpose, we calculate the eigenvalues of the lower 3×3 block of the pseudo-scalar mass matrix, and fix B_S by demanding to have a pseudo-scalar of the correct mass:

```
| Eigenvalues[Take[mA, {3, 5}, {3, 5}]];
| sol750 = Solve[%[[2]] == M750^2, B[MS]][[1]];
```

We now make an arbitrary choice for the numerical values of the remaining parameters, except m_η^2 and $M_{Z'}$,

```
| num = {g1 -> 0.36, g2 -> 0.65, v -> 246,
| B[\[Mu]] -> 10^6, \[Mu] -> 1000,
| TB -> 20, gX -> 0.5, MS -> -100, xS -> 500,
| T[lambdaC] -> -200, lambdaC -> -0.2, M750 -> 750}
```

and calculate all CP-even and CP-odd mass eigenvalues for specific values of m_η^2 and $M_{Z'}$:

¹⁶The mixing between the MSSM scalars and S is vanishing here only because of our simplifying assumption $\lambda = 0$ but is non-zero in general.

```

Sqrt /@ Eigenvalues[
  MassMatrix[Ah] //. assumptions //. sol /. sol750 ↔
  //. assumptions /.
  num /. mC22 -> 10^6 /. MZp -> 3000 ]
Sqrt /@ Eigenvalues[
  MassMatrix[hh] //. assumptions //. sol /. sol750 //. ↔
  assumptions /.
  num /. mC22 -> 10^6 /. MZp -> 3000 ]

```

The results are

```

{4477.72, 1792.7, 750., 6.60725*10^-6, 0.}
{4477.74, 3319.15, 2797.53, 822.054, 94.6205}

```

Thus, as expected, we have two massless (up to numerical errors) states in the CP-odd sector, which are the neutral Goldstone bosons to be eaten by the Z and Z' gauge bosons, accompanied by a particle with a mass of 750 GeV. In the scalar sector we find the lightest state with a mass very close to M_Z and another scalar below 1 TeV. However, checking the composition of the 750 and 825 GeV particles via

```

Eigensystem[MassMatrix[hh] //. assumptions //. sol /. ↔
  sol750 //. assumptions /.
  num /. mC22 -> 10^6 /. MZp -> 3000 ][[2, -2]]
{0., 0., -0.704932, -0.704932, -0.0783774}
Eigensystem[MassMatrix[Ah] //. assumptions //. sol /. ↔
  sol750 //. assumptions /.
  num /. mC22 -> 10^6 /. MZp -> 3000 ][[2, -3]]
{0., 0., -0.299786, -0.299786, 0.90568}

```

we see that the CP-odd state is, as expected, mainly a singlet while the CP-even one is mainly a X -Higgs (composed by ϕ_η and $\phi_{\bar{\eta}}$). That looks already very promising.

Higgs mass enhancement via non-decoupling D -terms Now, we want to confirm that one gets non-decoupling D -terms in this model which cause an enhancement of the tree-level mass of the SM-like scalar. For this purpose, we define a simple function which calculates the lightest CP-even mass for input values of $m_{\bar{\eta}}$ and $M_{Z'}$,

```

TreeMH[msoft_, mzp_] :=
  Sqrt[Eigenvalues[mH /. sol750 /. num
  /. mC22 -> msoft^2 /. MZp -> mzp ]][[-1]]];

```

and create a contour plot using this function. The result is depicted in Fig. 11, where one sees that for $m_{\bar{\eta}} \gg M_{Z'}$ it is indeed possible to find a tree-level mass well above 100 GeV, while for $m_{\bar{\eta}} \ll M_{Z'}$ the tree-level mass approaches $M_{Z'}$.

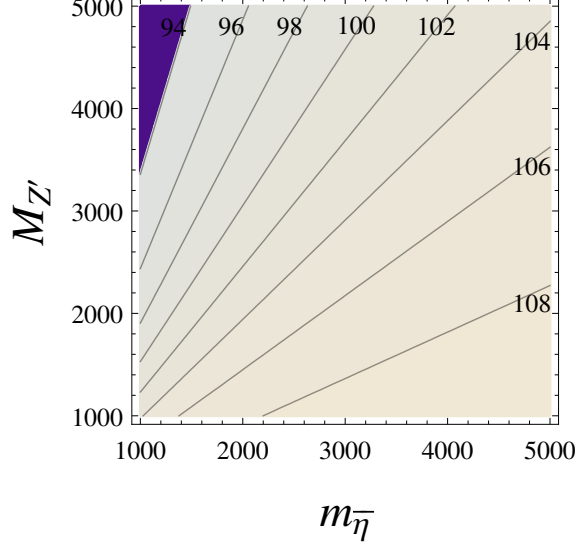


Figure 11. Contours of the mass of the lightest CP-even scalar in the model as a function of $M_{Z'}$ and $m_{\bar{\eta}}$.

Is there a second light scalar? One can now start to play also with the values we have chosen for `num` to see how the eigenvalues of both matrices change. One finds, for instance, that it is also possible to get a second, relatively light scalar in the model. With the values

$$\left| \begin{array}{l} \text{num} = \{ \dots, \text{lambdaC} \rightarrow -0.3, \text{MS} \rightarrow -100, \text{xS} \rightarrow 3500, \\ \text{TL} \rightarrow -225, \text{MZp} \rightarrow 2500, \text{mC22} \rightarrow 100 \} \end{array} \right.$$

we find a tree-level mass of 38 GeV for the lightest CP-even scalar, which is mainly a mixture of η and $\bar{\eta}$. It will be interesting to see if this scenario is still in agreement with all experimental constraints and how important the loop corrections are.

How to obtain a broad width? So far, we have not considered the total decay width of the 750 GeV scalar. The experimental data shows a slight preference for a rather large width of about 40 GeV, which is not easy to accommodate in weakly coupled models, typically requiring a large branching ratio into invisible states. Therefore, it would be interesting to see if this can be realised in this model. There are three possibilities for invisible decays: (i) neutralinos, (ii) (heavy) neutrinos, (iii) sneutrinos.

We are going to consider the third option here. For this purpose, we have to check two ingredients: can the mass of the sneutrinos be sufficiently light and how can the coupling to the 750 GeV scalar be maximised? To get a feeling for that, we first consider the mass matrix of the CP-even and CP-odd sneutrinos. We assume that flavour and left-right mixing effects are negligible. In that case, it is sufficient to take a look only at the (4,4) entry of the mass matrices:

$$\left| \begin{array}{l} \text{MassMatrix}[\text{SvIm}][[4, 4]] \\ \text{MassMatrix}[\text{SvRe}][[4, 4]] \end{array} \right|$$

After some simplifications, we get the following expressions from SARAH:

$$M_{\tilde{\nu}^I, \tilde{\nu}^R}^2 = \frac{1}{8} \frac{g_X^2 v^2}{(1+t_\beta^2)} - \frac{1}{8} \frac{g_X^2 t_\beta^2 v^2}{(1+t_\beta^2)} + m_{\nu,11}^2 + \frac{Y_{x,11}^2}{4g_X^2} (4M_{Z'}^2 - g_X^2 v^2) \pm \left(\frac{v_S Y_{x,11}}{2\sqrt{2}g_X} \lambda_C \sqrt{4M_{Z'}^2 - g_X^2 v^2} + \frac{1}{2g_X} \sqrt{4M_{Z'}^2 - g_X^2 v^2} T_{x,11} \right). \quad (6.24)$$

We see that the terms in the second line, $\propto T_x M_{Z'}$ and $\propto v_S \lambda_C Y_x$, induce a mass splitting between the CP-even and CP-odd states. Thus, in order to have the decay $A \rightarrow \tilde{\nu}^I \tilde{\nu}^R$ kinematically allowed, these terms must be individually small or cancel each other. In addition, one has to compensate the large terms $\sim M_{Z'}$ in order to get sufficiently light sneutrinos. This could be done by assuming a negative $m_\nu^2 = -\frac{1}{4g_X^2} (4M_{Z'}^2 - g_X^2 v^2) Y_{x,11}^2$. Of course, we must check whether this leads to spontaneous R -parity breaking via sneutrino VEVs, and for this purpose one can use `Vevacious`, see below.

We can now check the vertex $A \tilde{\nu}^I \tilde{\nu}^R$ using the same assumptions:

$$\left| \text{Vertex}[\{\text{Ah}, \text{SvIm}, \text{SvRe}\}][[2, 1]] \right|$$

and we obtain after some simplification

$$\frac{1}{2} \frac{1}{\sqrt{2}g_X} \lambda_C \sqrt{4M_{Z'}^2 - g_X^2 v^2} Y_{x,11} Z_{35}^A + \lambda_C v_S Y_{x,11} Z_{33}^A - \sqrt{2} Z_{34}^A T_{x,11}. \quad (6.25)$$

If the pseudo-scalar is a pure singlet, only the term $\propto Z_{35}^A$ contributes. This term is independent of v_S and T_x , i.e. we can reduce the mass splitting between the CP-even and CP-odd sneutrinos by adjusting these parameters without having a negative impact on the coupling strength to the 750 GeV scalar.

6.2.4 Vector-like sector

Before we finish the analytical discussion of the masses, we briefly discuss the extended matter sector. The mass matrices responsible for the mixing between the SM fermions and the vector-like fermions can be obtained from SARAH by calling


```
| MassMatrix[Fe]
| MassMatrix[Fu]
```

which return

$$m_e = \begin{pmatrix} \frac{v_d Y_e}{\sqrt{2}} & -\frac{v_d Y'_e}{\sqrt{2}} \\ 0 & \frac{\lambda_e v_S}{\sqrt{2}} + M_e \end{pmatrix}, \quad m_u = \begin{pmatrix} \frac{v_u Y_u}{\sqrt{2}} & \frac{v_u Y'_u}{\sqrt{2}} \\ 0 & \frac{\lambda_u v_S}{\sqrt{2}} + M_u \end{pmatrix}. \quad (6.26)$$

Thus, for large λ_i ($i = u, e$) and v_S , there are two important sources for the mass of the vector-like states. The full sfermion matrices containing the new scalars are too lengthy to be shown here. We only check the new mass matrix for one generation of the vector-like selectrons which are the 7th and 10th gauge eigenstates. We can pick the values via

```
| ({{M[[7, 7]], M[[7, 10]]}, {M[[7, 10]], M[[10, 10]]}} /.
| M -> (MassMatrix[Se]))
```

and obtain by setting all parameters to be diagonal

$$\begin{pmatrix} \frac{\tilde{D} + 4(t_\beta^2 + 1)(\lambda_e^2 v_S^2 + 2\sqrt{2}\lambda_e M_e v_S + 2m_E^2 + 2M_e^2)}{8(t_\beta^2 + 1)} & B_E + \lambda_e \left(\frac{\lambda_X M_{Z'}^2}{4g_X^2} - \frac{\lambda_X v^2}{16} + \xi + \sqrt{2}M_S v_S \right) \\ B_E + \lambda_e \left(\frac{\lambda_X M_{Z'}^2}{4g_X^2} - \frac{\lambda_X v^2}{16} + \xi + \sqrt{2}M_S v_S \right) & \frac{4(t_\beta^2 + 1)(\lambda_e^2 v_S^2 + 2\sqrt{2}\lambda_e M_e v_S + 2m_E^2 + 2M_e^2) - \tilde{D}}{8(t_\beta^2 + 1)} \end{pmatrix} \quad (6.27)$$

where we have defined $\tilde{D} = (t_\beta^2 - 1)v^2(2g_1^2 + g_X^2)$. There is a potentially dangerous term $\lambda_e \xi$ which rapidly increases for increasing λ_e . To keep all scalar masses positive, it is necessary to choose a rather large B_E as well. Therefore, we are going to choose always

$$B_E = -\lambda_e(\xi + \sqrt{2}M_S v_S), \quad B_U = -\lambda_u(\xi + \sqrt{2}M_S v_S) \quad (6.28)$$

in our numerical study to circumvent tachyonic scalars.

6.2.5 RGEs and gauge kinetic mixing

We have so far made the simplifying assumption that gauge kinetic mixing vanishes. However, if the two Abelian gauge groups are not orthogonal, kinetic mixing would be generated via RGE running even if it vanishes at some energy scale. Thus, one of the first checks on the RGEs of the model we can make is whether the two $U(1)$ gauge groups are orthogonal. For this purpose, we first calculate the one-loop RGEs with SARAH via

```
| CalcRGEs[TwoLoop->False];
```

We have chosen one-loop RGEs only to save time. Without the `TwoLoop->False` flag, the full two-loop RGEs would have been calculated automatically. We can now check the entries in `BetaGauge` and find

$$\begin{aligned}
16\pi^2\beta_{g_Y} &= 15g_Y^3 + 15g_Y g_{YX}^2 + 16\sqrt{\frac{3}{5}}g_Y g_{YX} g_X + 32\sqrt{\frac{3}{5}}g_Y^2 g_{XY} \\
&\quad + 16\sqrt{\frac{3}{5}}g_{YX}^2 g_{XY} + 15g_{YX} g_X g_{XY} + 15g_Y g_{XY}^2,
\end{aligned} \tag{6.29}$$

$$\begin{aligned}
16\pi^2\beta_{g_X} &= 15g_{YX}^2 g_X + 15g_X^3 + 16\sqrt{\frac{3}{5}}g_Y g_X g_{XY} + 15g_X g_{XY}^2 \\
&\quad + g_{YX} \left(32\sqrt{\frac{3}{5}}g_X^2 + 15g_Y g_{XY} + 16\sqrt{\frac{3}{5}}g_{XY}^2 \right),
\end{aligned} \tag{6.30}$$

$$\begin{aligned}
16\pi^2\beta_{g_{XY}} &= 15g_{YX}^3 + 32\sqrt{\frac{3}{5}}g_{YX}^2 g_X + 15g_{YX} g_X^2 + g_Y^2 \left(15g_{YX} + 16\sqrt{\frac{3}{5}}g_X \right) \\
&\quad + g_Y \left(16\sqrt{\frac{3}{5}}g_{YX} g_{XY} + 15g_X g_{XY} \right),
\end{aligned} \tag{6.31}$$

$$\begin{aligned}
16\pi^2\beta_{g_{YX}} &= 15g_{YX}^3 + 32\sqrt{\frac{3}{5}}g_{YX}^2 g_X + 15g_{YX} g_X^2 + g_Y^2 \left(15g_{YX} + 16\sqrt{\frac{3}{5}}g_X \right) \\
&\quad + g_Y \left(16\sqrt{\frac{3}{5}}g_{YX} g_{XY} + 15g_X g_{XY} \right).
\end{aligned} \tag{6.32}$$

The standard normalisation factor $\sqrt{5/3}$ for the hypercharge has been included. One can see that the β -functions for g_{YX} and g_{XY} are non-zero even in the limit $g_{XY}, g_{YX} \rightarrow 0$, i.e. these couplings will be induced radiatively. Thus, in general one has not only two couplings g_1 and g_X in this model, but a gauge coupling matrix G defined as

$$G = \begin{pmatrix} g_{YY} & g_{XY} \\ g_{YX} & g_{XX} \end{pmatrix}. \tag{6.33}$$

In the limit of vanishing kinetic mixing, $g_{YX} = g_{XZ} = 0$, the relations $g_{YY} = g_1$ and $g_{XX} = g_X$ hold. Even if gauge kinetic mixing is present, one has the freedom to perform a change in basis to bring G into a particular form. The most commonly considered cases are the symmetric basis with $g_{XY} = g_{YX}$ and the triangle basis with $g_{YX} = 0$. The triangle basis has the advantage that the new scalars do not contribute to the electroweak VEV, and the entire impact of gauge kinetic mixing is encoded in one new

coupling \tilde{g} . The relation between g_{ij} ($i, j = X, Y$) and g_1, g_X, \tilde{g} are [366]

$$g_1 = \frac{g_{YY}g_{XX} - g_{XY}g_{YX}}{\sqrt{g_{XX}^2 + g_{XY}^2}}, \quad (6.34)$$

$$g_X = \sqrt{g_{XX}^2 + g_{XY}^2}, \quad (6.35)$$

$$\tilde{g} = \frac{g_{YX}g_{XX} + g_{YY}g_{XY}}{\sqrt{g_{XX}^2 + g_{XY}^2}}. \quad (6.36)$$

It is interesting to see how large \tilde{g} is naturally. With ‘naturally’ we mean under the assumption that the off-diagonal g_{YX} and g_{XY} couplings vanish at some high scale Λ and are generated by RGE running down to the SUSY scale. Thus, in this setup, the size of gauge kinetic mixing is a function of Λ and g_X at this scale. We can write a simple `Mathematica` function to get a feeling for the off-diagonal gauge couplings:

```
<< "Output/U1yMSSM/RGEs/RunRGEs.m";
RunningGKM[scale_, gXIN_] := Block[{}],
  logS = scale;
  runUp = RunRGEs[{g1 -> 0.45}, 3, logS, TwoLoop -> <=>
    False][[1]];
  runDown = RunRGEs[{g1 -> (g1[logS] /. runUp), gX -> <=>
    gXIN}, logS, 3, TwoLoop -> False][[1]];
  g1run = Sqrt[3/5] g1[3] /. runDown;
  gXrun = gX[3] /. runDown;
  g1Xrun = Sqrt[3/5] g1X[3] /. runDown;
  gX1run = gX1[3] /. runDown;
  g1out = (g1run*gXrun - g1Xrun gX1run)/Sqrt[gXrun^2 <=>
    + gX1run^2];
  gXout = Sqrt[gXrun^2 + gX1run^2];
  g1Xout = (g1Xrun gXrun + g1run gX1run)/Sqrt[gXrun^2 <=>
    + gX1run^2];
  Return[{g1out, gXout, g1Xout}];
];
```

In the first line, we load the file written by SARAH which provides the RGEs in a form which `Mathematica` can solve. This file also contains the function `RunRGEs` that can be used to solve the RGEs numerically. As boundary condition, we used $g_1 = 0.45$ at the scale 1 TeV. After the running we rotate the couplings to the basis where g_{XY} vanishes. We can make a contour plot via

```
ContourPlot[RunningGKM[lambda, gx][[3]],
  {lambda, 4, 17}, {gx, 0, 1}, ContourLabels -> True]
```

and get the result shown in Fig. 12. Thus, we find that at the SUSY scale the gauge

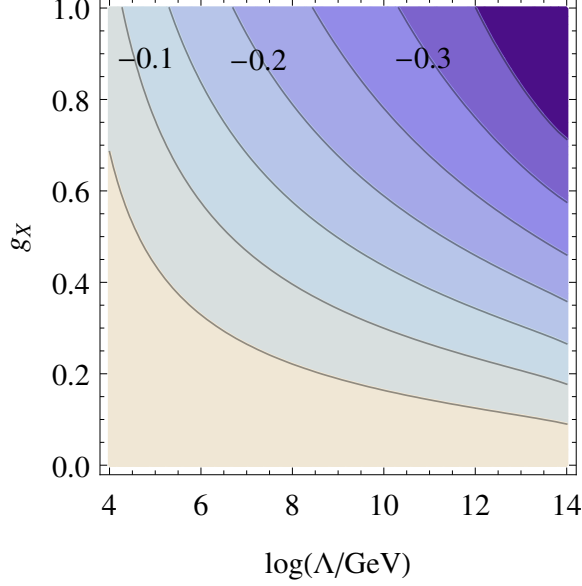


Figure 12. Gauge kinetic mixing \tilde{g} at the SUSY scale as a function of the high energy scale Λ , where it is assumed to vanish, and of the coupling $g_X(\Lambda)$.

mixing coupling \tilde{g} is negative and not much smaller than an ordinary gauge coupling unless Λ is assumed to be very small.

6.2.6 Boundary conditions and free parameters

For the subsequent numerical analysis we are going to assume some simplified boundary conditions applied at the SUSY scale:

$$m_q^2 = m_d^2 = m_u^2 = m_l^2 = m_e^2 = m_E^2 = m_{\tilde{E}}^2 = m_U^2 = m_{\tilde{U}}^2 \equiv \mathbf{1}m_{SUSY}^2 \quad (6.37)$$

$$\lambda_e = \mathbf{1}\lambda_E, \quad \lambda_u \equiv \mathbf{1}\lambda_U \quad (6.38)$$

$$M_e = \mathbf{1}M_E, \quad M_u \equiv \mathbf{1}M_U \quad (6.39)$$

$$T_i = A_0 Y_i \quad (i = \{u, e, d\}), \quad T'_i = A_0 Y'_i \quad (i = \{u, e\}), \quad T_i = A_0 \lambda_i \quad (i = \{U, E\}) \quad (6.40)$$

$$T_\lambda = A_\lambda \lambda, \quad T_X = A_X \lambda_X \quad (6.41)$$

$$M_1 = M_2 = \frac{1}{2}M_3 = M_X \equiv M_\lambda \quad (6.42)$$

In addition, we can set $Y_\nu = 0$ since this parameter is highly constrained to be small by the small neutrino masses. In addition, we set the mixing parameters m_{eE}^2 , m_{uU}^2 , \tilde{M}_E , \tilde{M}_U , \tilde{B}_E , \tilde{B}_U , M_{1X} to zero and also assume vanishing λ , κ , and T_κ . However, we stress that this is just done to keep the following discussion short and simple. All

effects of these parameters can be included without any additional efforts. Thus, the free parameters mainly considered in the following are

$$\begin{aligned}
& m_{SUSY}, M_\lambda, \mu, B_\mu, A_0, \tan \beta, \\
& g_X, g_{1X}, M_{Z'}, m_{\bar{\eta}}, \tan \beta_X, \lambda_X, A_X, Y_x, \\
& M_S, B_S, v_s, A_\lambda, \\
& \lambda_E, \lambda_U, M_E, M_U, Y'_u, Y'_e.
\end{aligned}$$

The tadpole equations are solved for $m_{H_d}^2$, $m_{H_u}^2$, m_η^2 , m_S^2 and ξ , while B_E and B_U are fixed via Eq. (6.28).

6.3 Analysis of the important loop corrections to the Higgs mass

We now turn to the numerical analysis of this model. In the first step, we have written a `SPheno.m` file for the boundary conditions, see Section 6.2.6, and generated the `SPheno` code with the `SARAH` command

```
| MakeSPheno [] ;
```

We copy the generated Fortran code to a new sub-directory of `SPheno-3.3.8` and compile it via

```
$ cd $PATH/SPheno-3.3.8
$ mkdir U1xMSSM
$ cp $PATH/SARAH/Output/U1xMSSM/EWSB/SPheno/* U1xMSSM/
$ make Model=U1xMSSM
```

We now have an executable `SPhenoU1xMSSM` which expects the input parameters from a file called `LesHouches.in.U1xMSSM`. The `SPheno` code provides many important calculations which would be very time-consuming to be performed ‘by hand’ for this model, but could be expected to be relevant. A central point is the calculation of the pole mass spectrum at the full one-loop (and partially two-loop) level. In particular, the loop corrections from the vector-like states are known to be very important. However, the focus in the literature has usually been only on the impact on the SM-like Higgs. We can automatically go beyond that and consider the corrections to the 750 GeV state as well. Moreover, `SPheno` calculates all additional two-loop corrections in the gaugeless limit including all new matter interactions. Thus, we can check the impact of the vector-like states even at two-loop level. These effects have not been studied in any of the SUSY models proposed so far to explain the diphoton excess. Of course, `SPheno` also makes a very precise prediction for the diphoton and digluon decay rate of all neutral scalars as described in Section 4.4, and it checks for any potential decay

mode. Thus, it is impossible to miss any important decay as sometimes has happened in the literature when discussing the diphoton excess. Finally, there are also other important constraints for this model like those from flavour observables or Higgs coupling measurements. As will be shown in the next sections, all of this can be checked automatically with `SPheno` and tools interacting with it.

If not mentioned otherwise, we make the following choice for the input parameters

$$\begin{aligned}
m_{SUSY} &= 1.5 \text{ TeV}, M_\lambda = 1 \text{ TeV}, \\
\tan \beta &= 20, \tan \beta_x = 1, g_X = 0.5, M_{Z'} = 3 \text{ TeV}, m_{\bar{\eta}} = 2 \text{ TeV}, \\
\mu &= 1 \text{ TeV}, B_\mu = (1 \text{ TeV})^2, v_S = 0.5 \text{ TeV}, M_S = -0.1 \text{ TeV}, B_S = 3.895 \text{ TeV}^2, \\
\lambda_X &= -0.2, A_X = 1 \text{ TeV}, \lambda_E = \lambda_U = 1, M_E = 0.4 \text{ TeV}, M_U = 1 \text{ TeV}.
\end{aligned}$$

6.3.1 New loop corrections to the SM-like Higgs

In this model we have two new important loop corrections to the SM-like Higgs: (i) the corrections from vector-like states, proportional to Y'_u and Y'_e , and (ii) the new corrections from the extended gauge sector. The corrections from vector-like (s)tops up to two-loop have been discussed in detail in Ref. [279] using the `SARAH/SPheno` framework. There are several important effects which are often neglected in studies of vector-like states which only make use of the one-loop effective potential: the momentum effects at one-loop, the two-loop corrections, and the shift of the top-Yukawa coupling. In general, the user does not need to worry about these details because `SARAH/SPheno` take care of them automatically. However, it might be interesting to have an intuitive feeling about the size of the different effects. Since it demands some ‘hacking’ of the code to disentangle the calculation in that way, we are not making this analysis here, but we briefly summarise the main results of Ref. [279] in Fig. 13. We see that all these effects can alter the Higgs mass by several GeV. Thus, an estimated uncertainty of about 2–3 GeV when using only the one-loop effective potential approximation is usually over optimistic.

Furthermore, in models with non-decoupling D -terms the new loop corrections are usually neglected in the literature. Therefore, we are going to check whether this is a good approximation or not. For this purpose we show the SM-like Higgs pole mass at tree and one-loop level as a function of g_X for two different values of $M_{Z'}$. Since `SPheno` performs the two-loop corrections in the gaugeless limit, additional corrections from the extended gauge sector are not included at two-loop, and we concentrate on the one-loop effects here. For this purpose, we use the different flags in the `Les Houches` input file from `SPheno` to turn the corrections at the different loop levels on or off:

```

1 | Block SPhenoInput      # SPheno specific input

```

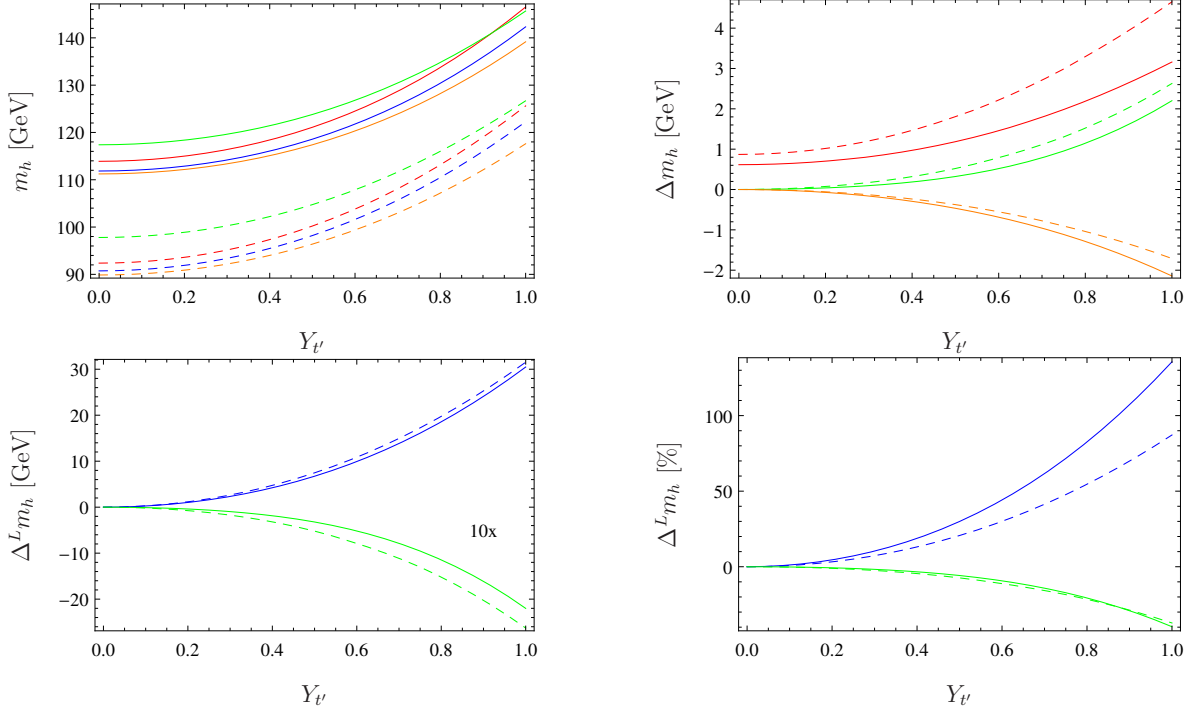


Figure 13. Top left: light Higgs mass as a function of $Y_{t'}$ (which corresponds to $Y'_{u,33}$ in this model) with all other entries of Y'_u vanishing. The red line corresponds to the effective potential calculation at one-loop, orange is the one-loop corrections with external momenta but neglecting the new threshold correction stemming from vector-like states, blue is the full one-loop calculation including the momentum dependence and all thresholds, and green includes the dominant two-loop corrections together with the full one-loop correction. Top right: impact of the threshold corrections (red), the momentum dependence at one-loop (orange) and the two-loop corrections (green), given as the difference $\Delta m_h = m_h - m_h(1L, p^2 \neq 0, \text{all thresholds})$. Bottom left: absolute size of the one- (blue) and two-loop (green) corrections stemming from the vector-like states. For better readability we re-scaled the two-loop corrections by a factor of 10. Bottom right: relative importance of the one- (blue) and two-loop (green) corrections normalised to the size of the purely MSSM-like corrections. The solid lines are for $\tan \beta = 10$ and the dashed ones are for $\tan \beta = 2$. Here, a mass of 1 TeV for the vector-like quarks was assumed. These plots are taken from Ref. [279].

2	...		
3	7	A	# Skip 2-loop Higgs corrections
4	55	B	# Calculate loop corrected masses

Here, A and B are either 1 or 0. With flag 55 the entire loop-corrections to all masses can be turned on (1) or off (0), while flag 7 only skips (1) or includes (0) the two-loop

corrections in the Higgs sector. The results are shown in Fig. 14. All scans have been performed using the `Mathematica` package `SSP` [367] for which `SARAH` already writes a template input when generating the `SPheno` code (`SSP_Template.m.U1xMSSM`) for a given model. We see that the tree-level mass rises quickly with increasing g_X . However,

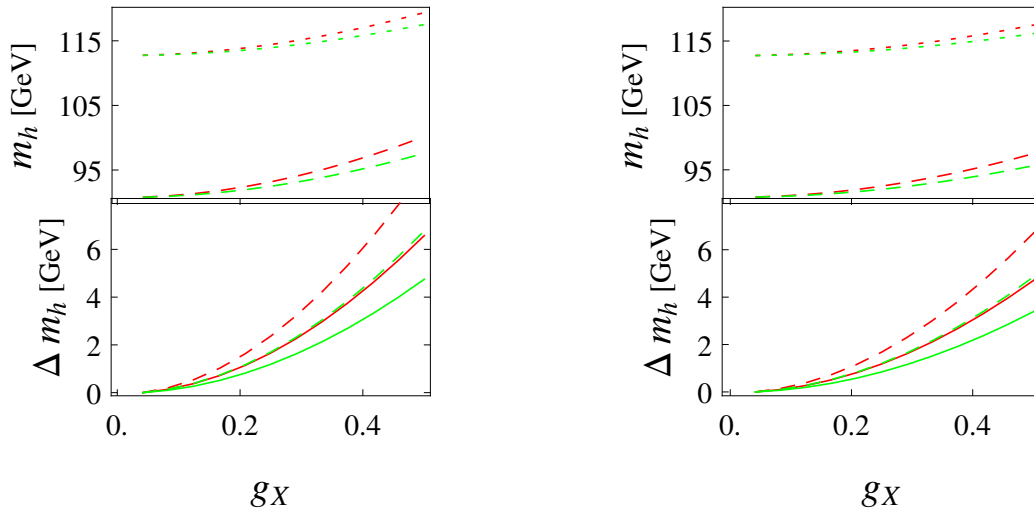


Figure 14. Mass of the SM-like Higgs as a function of g_X at tree-level (dashed) and one-loop (full line). The red lines are without gauge-kinetic mixing, for the green ones we set $g_{1X} = \frac{1}{5}g_X$. $M_{Z'}$ on the left is 3 TeV and 4 TeV on the right. On the bottom we show the difference $\Delta m_h \equiv m_h(g_X) - m_h(g_X = 0)$ at tree-level (dashed) and including loop corrections (full) for the case with gauge kinetic mixing (green) and without (red).

for both $M_{Z'}$ values this shift is compensated to some extent when one-loop corrections are included. Thus, the inclusion of non-decoupling D -terms only at tree-level would overestimate the positive effect on the SM-like Higgs mass by 20–30%. In addition, we also see that off-diagonal gauge couplings of a realistic size as consequence of gauge kinetic mixing reduce the positive effect from the non-decoupled D -terms on the Higgs mass by a few GeV.

6.3.2 Loop corrections to the 750 GeV scalar

There are also important loop corrections to all other scalars in the model if large Yukawa-like couplings are present. We discuss this briefly for the 750 GeV pseudo-scalar: in Fig. 15, the mass at tree, one- and two-loop level for varying $\lambda_V \equiv \lambda_e = \lambda_u$ for two different values of m_{SUSY} , 1.5 and 2.5 TeV, is given. For $m_{SUSY} = 1.5$ TeV there is only a moderate difference between tree-level, one- and two-loop for $\lambda_V \rightarrow 0$, but for λ_V of $O(1)$ the one-loop corrections cause a shift by 100 GeV and more, which

is compensated to some extent by the two-loop corrections. For larger m_{SUSY} we see already a large positive shift for small λ_V , which quickly increases and reaches 300–400 GeV for $\lambda_V \sim 0.8$. For even larger values of λ_V , the difference between tree-level and the loop corrected mass becomes smaller. Still, the overall shift is more than 100 GeV, and this would be highly overestimated by only including one-loop corrections. As we will see in the next section, one needs $\lambda_V \sim O(1)$ to explain the diphoton signal. For this value, a naive tree-level analysis gives a mass for the lightest CP-odd state which is far off the correct value. Thus, one has to be much more careful with the choice for B_S .

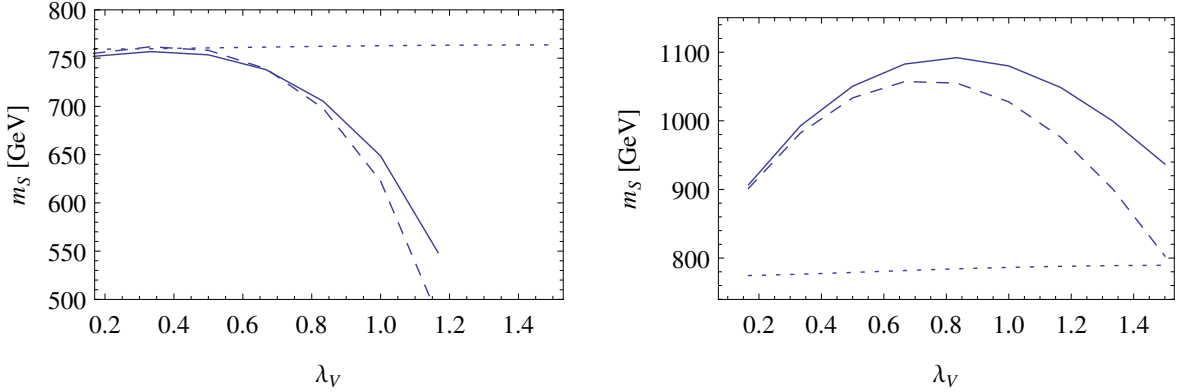


Figure 15. Mass of the CP-odd scalar with a tree-level mass of 750 GeV (dotted), at one-loop (dashed) and two-loop (full) for a variation of $\lambda_V \equiv \lambda_e = \lambda_u$. On the left we set $m_{SUSY} = 1.5$ TeV, on the right $m_{SUSY} = 2.5$ TeV.

6.4 Diphoton and digluon rate

We now discuss the diphoton and digluon decay rate of the pseudo-scalar, and its dependence on the new Yukawa-like couplings. As we have just seen, large couplings induce a non-negligible mass shift. Therefore, it is necessary to adjust B_S carefully to get the correct mass, 750 GeV, after including all loop corrections. This can be done by SSP, which can adjust B_S for each point to obtain the correct mass within 5 GeV uncertainty. The results for the calculated diphoton and digluon rate at LO and with the higher order corrections discussed in Section 4.2.2 are shown in Fig. 16. In order to see the size of the higher order corrections, one can use the flag 521 in SPheno to turn them on and off

```

1 | Block SPhenoInput      # SPheno specific input
2 | ...

```

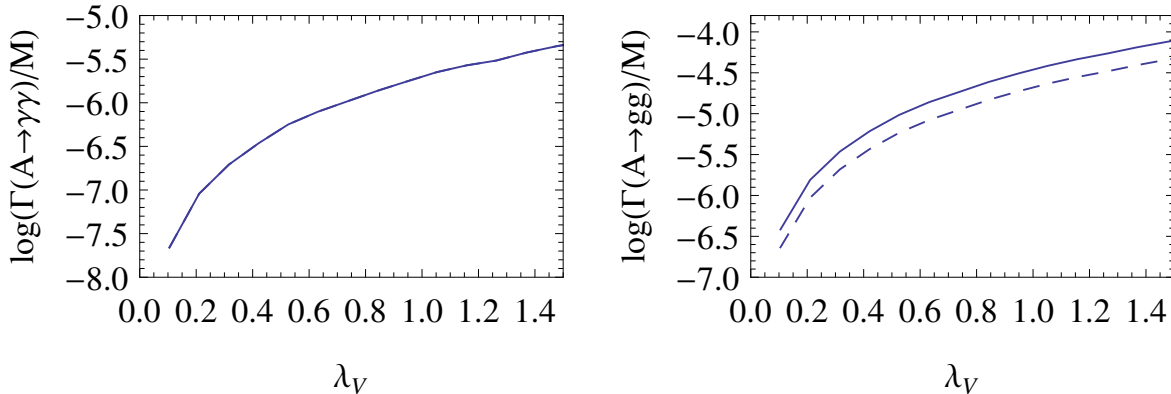


Figure 16. Partial widths into two photons (left) and two gluons (right) of the lightest pseudo-scalar, normalised to the mass M_S . B_S was adjusted to keep the mass constant within (750 ± 5) GeV. The solid lines were drawn including higher order QCD corrections to loop induced decays, the dashed ones at leading order only.

One finds the expected behaviour: the partial widths rise quadratically with the coupling. For about $\lambda_V \simeq 1.0$ one has $\Gamma(S \rightarrow \gamma\gamma)/M_S \sim 10^{-6}$, which is necessary to explain the observed excess. In Fig. 16 we also show a comparison between a purely LO calculation and the one including the higher order QCD corrections described in Section 4.2.2. There is no change for the decay into two photons, because its NLO corrections for a pseudo-scalar are non vanishing only for $m_A > 2M_F$. Instead, the digluon width is enhanced by a factor of 2 when including NLO and NNLO QCD corrections. This also changes the ratio of the digluon-to-diphoton width from about 10 (LO only) to 20 (including higher orders).

6.5 Constraints on choice of parameters

6.5.1 Singlet-doublet mixing

So far, we made some strong assumptions about some parameters in this model. In particular, we set the coupling between the singlet and the two Higgs doublets $\lambda = 0$. This raises the question how sensitive the results are to this choice. For this purpose, we can test what happens if we slightly deviate from it. The branching ratios of the CP-odd scalar of 750 GeV mass, which is nearly a pure singlet, as a function of λ are shown in Fig. 17. For comparison we also show the branching ratios for the CP-even scalar with a mass around 800 GeV. This particle is mainly a mixture of η and $\bar{\eta}$ with a small

singlet component. For both particles we depict the branching ratios when calculating only tree-level masses and when including loop-corrections. At the tree level we find

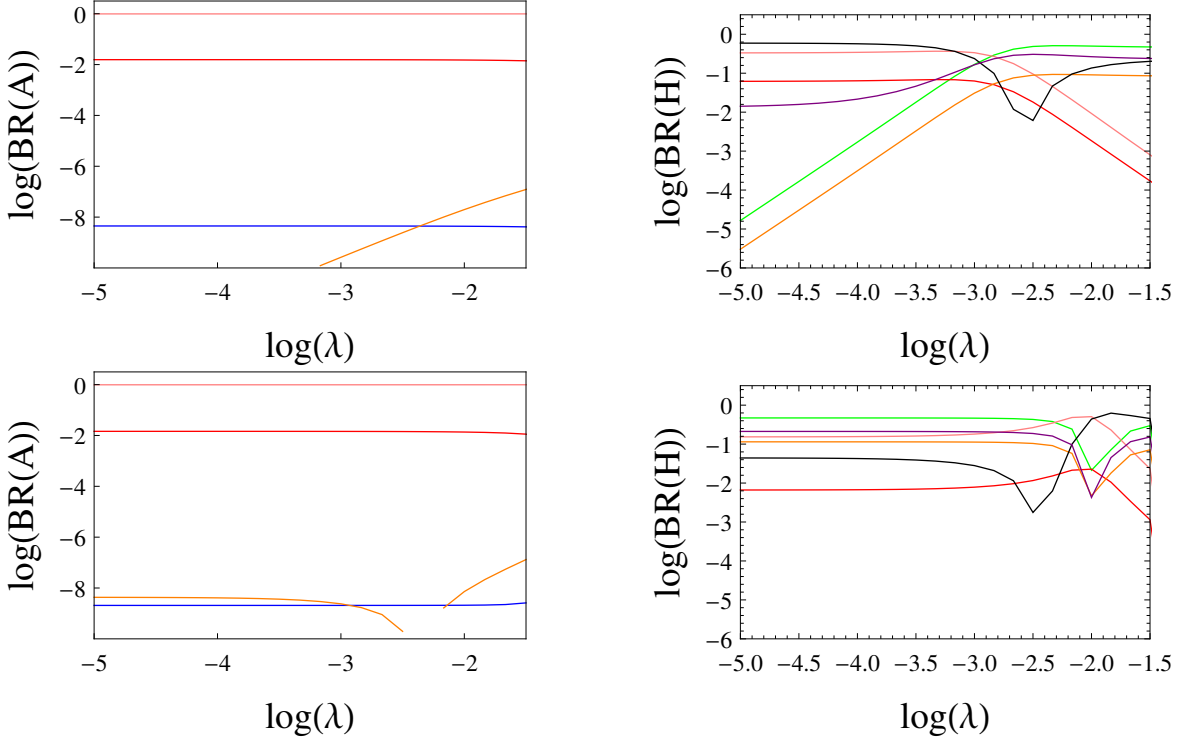


Figure 17. Branching ratios of the 750 GeV CP-odd particle (left), and a CP-even scalar (right) close in mass as function of λ . In the first row the tree-level rotation matrices are used, while in the second row the rotation matrices including loop corrections are used. Here, we set $A_\lambda = 1$ TeV. The colour code is as follows: $\gamma\gamma$ (pink), gg (red), hZ (blue), $t\bar{t}$ (orange), hh (black), ZZ (purple), W^+W^- (green).

that the impact of λ on the branching ratios of A is very small. This does not change much when including the loop corrections to the pseudo-scalar rotation matrix. On the other hand, for vanishing λ we already have a large branching ratio of the CP-even scalar into hh even at tree level. Moreover, the decay modes into two massive vector bosons or $t\bar{t}$ at tree level increase very quickly with λ and for $\lambda > 0.01$ they already dominate. At one-loop level, the large dependence on λ is no longer visible, because for very small λ the branching ratios into massive SM vector bosons and fermions are already large. This can be seen in Fig. 18 where we compare the doublet fraction of the two states at tree level and one loop. In general, the behaviour shows that a CP-odd scalar might be a much less fine-tuned candidate for the observed excess.

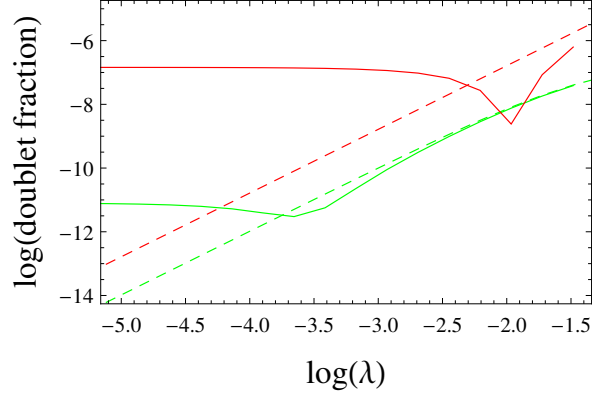


Figure 18. Doublet fraction of the 750 GeV pseudo-scalar (green) and the 800 GeV scalar (red) at tree-level (dashed lines) and including loop corrections (full lines), as function of λ .

6.5.2 Constraints from Higgs coupling measurements

We have seen in the `Mathematica` session that it is possible to obtain two light scalars at tree-level. One question is: is this also possible when including all loop contributions? In order to address this question we change some input parameters to

$$m_{SUSY} = 1.75 \text{ TeV}, \tan \beta = 20, m_{\tilde{\eta}} = 1 \text{ TeV}, M_{Z'} = 2.5 \text{ TeV}, \\ v_S = 3.5 \text{ TeV}, B_S = 45000 \text{ GeV}^2, \lambda_X = -0.3, A_X = 750 \text{ GeV}.$$

The pole masses and the doublet fraction of two lightest CP even states as a function of $\tan \beta_X$ is shown in Fig. 19. We find the very strong dependence on $\tan \beta_X$, known in many $U(1)$ extensions [366, 368, 369]. One difference here is that, due to the mixing with the singlet, the light state in the extended sector does not become massless for $\tan \beta_X = 1$, but for small deviations from it. We see in Fig. 19 that the SM-like Higgs gets a positive mass shift after the level crossing, while the mass of the lightest state drops very quickly. Of course, it is important to know if such light Higgs-like particles are compatible with all limits from Higgs searches at LEP, Tevatron and the LHC. For this purpose, we can make use of `HiggsBounds`, which checks whether the decay rates of a scalar into SM states are compatible with the observations at all experiments performed so far. If any of these rates is above 1 (normalised to the SM expectation), such a parameter point would be ruled out. Similarly, we can use `HiggsSignals` to obtain a χ^2 estimator for each parameter point, based on how well the measured Higgs properties are reproduced. In order to use `HiggsBounds` and `HiggsSignals`, we set the flag

```

1 Block SPhenoInput      # SPheno specific input
2 ...

```

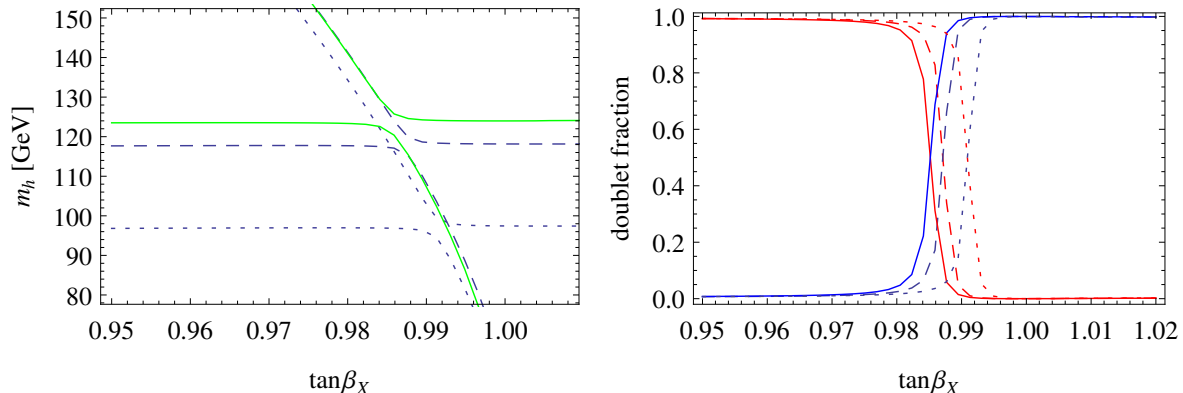


Figure 19. Left: the masses of the two lightest CP-even eigenstates as a function of $\tan \beta_X$ at tree-level (dotted), one-loop (dashed) and two-loop (full green line). Right: the corresponding doublet fraction of the lightest (blue) and second lightest (red) scalar at tree-level (dotted), one-loop (dashed) and two-loop (full) levels.

3

76 1

Write HiggsBounds file

in the input file for `SPheno`. In this way, `SPheno` writes out all files which are necessary to run `HiggsBounds` and `HiggsSignals` via the effective couplings input mode (`effC`). However, there is one caveat: `SPheno` does not automatically write the file `MHall_uncertainties` which gives an estimate for the theoretical uncertainty in the mass prediction of all scalars. The reason is that `SPheno` cannot do such an estimate automatically. However, if this file is missing, `HiggsBounds` and `HiggsSignals` would assume that the uncertainty is zero. Therefore, we add this file by hand and assume a 3 GeV uncertainty for all masses. We can now use this setup to make a scan in the $(\tan \beta_X, \lambda)$ plane, for instance by using the `SSP` option to automatically call `HiggsBounds` and `HiggsSignals` during a parameter scan. The results are shown in Fig. 20. One can see that both, the discovery potential and the χ^2 value, are very sensitive on small changes in these two parameters. The reason is mainly the large dependence of the masses of the two lightest scalars and their mixing. One sees that the best χ^2 value is found close to the $\tan \beta_X$ range where the SM-like particle is the second lightest CP-even state, and the lightest one is about 80 GeV. In addition, for a very small stripe close to $\lambda = 0$ also points with very light scalars with masses below 40 GeV pass all constraints, but for slightly larger values of λ the mixing already becomes too large and the points are excluded by $e^+e^- \rightarrow (h_1)Z \rightarrow (b\bar{b})Z$ from LEP searches.

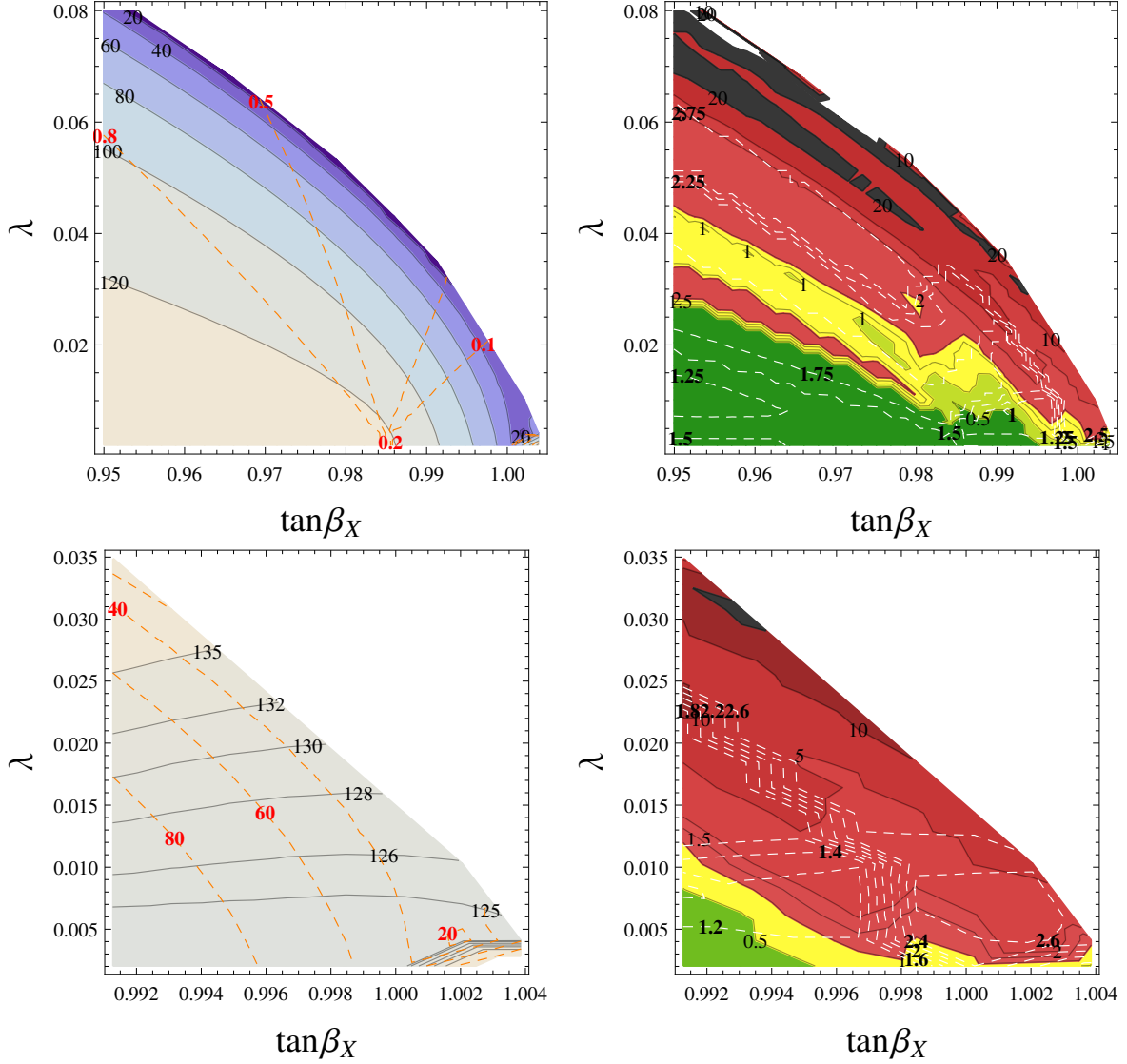


Figure 20. **First row:** On the left, we show the mass of the lightest CP-even scalar in the $(\tan\beta_X, \lambda)$ plane. On top of this, we give the contour lines for constant values of the doublet fraction of the lightest scalar (orange lines with red labels). On the right, we show the results from HiggsBounds and HiggsSignals (white contour lines with bold labels for constant χ^2 divided by the number of considered Higgs observables: 81) in the same plane. The red shaded regions are excluded by Higgs searches. **Second row:** Zoom into the region with $\tan\beta_X$ close to 1. On the left, the mass of the two lightest CP-even scalars are shown. The plot on the right provides the same information as the one in the first row.

6.5.3 Large decay width and constraints from vacuum stability

We have already considered the possibility to enhance the total decay width of the CP-odd scalar via decays in pairs of right-sneutrinos. In our tree-level analysis with **SARAH** we found that one can reduce the mass splitting between the two mass eigenstates by demanding

$$T_x = -\frac{1}{\sqrt{2}}\lambda_X v_S Y_x. \quad (6.43)$$

In addition, as already discussed above, one has to use a negative soft-mass for the sneutrinos,

$$m_\nu^2 = -\frac{Y_x^2}{4g_X^2} (4M_{Z'}^2 - g_X^2 v^2), \quad (6.44)$$

to get the states light enough. This immediately raises two questions: (i) how large can the total width be for large values of Y_x ? (ii) Is the electroweak vacuum stable or not? First of all, we notice that a negative m_ν^2 does not necessarily imply spontaneous R -parity violation, as shown in Ref. [370], in contrast to some claims in this direction in the previous literature. However, the danger of disastrous vacuum decays increases, of course, with decreasing m_ν^2 . Therefore, we use **Vevacious** to check the stability of the potential. For this purpose, we have written a second **SARAH** model file where we include the possibility of VEVs for the right sneutrinos. We also added in this new implementation those mixings among states which were forbidden by R -parity conservation. This is actually necessary because **Vevacious** calculates the one-loop corrections to the effective potential and the full mass matrices are required. The **Vevacious** model file is generated via

```
| MakeVevacious [] ;
```

We can now run a point with **SPheno**. If we turn on

```
1 Block SPhenoInput      # SPheno specific input
2   ...
3 530 1                  # Write Blocks for Vevacious
```

we can pass the **SPheno** spectrum file in a second step to **Vevacious**, which finds all minima of the potential with the additional VEV. If the global minimum is not the local one found by **SPheno** with correct EWSB, **Vevacious** uses **CosmoTransitions** [327] to get the life-time of ‘our’ vacuum. If our survival probability is found to be below 10%, we label the points as short-lived. Metastable points with a longer life-time

are called long-lived. We choose the following set of input parameters¹⁷

$$m_{SUSY} = 2.5 \text{ TeV}, \tan \beta = 10, \tan \beta_x = 1, g_X = 0.5, M_{Z'} = 2.5 \text{ TeV}, m_{\tilde{\eta}} = 1 \text{ TeV}, \\ v_S = 0.5 \text{ TeV}, B_S = 755000 \text{ GeV}^2, \lambda_X = -0.4, A_X = 0.4 \text{ TeV}.$$

The final result is summarised in Fig. 21.¹⁸ To maximise the effect on the total width, we take all sneutrinos to be degenerate and with the same coupling to the 750 GeV scalar.

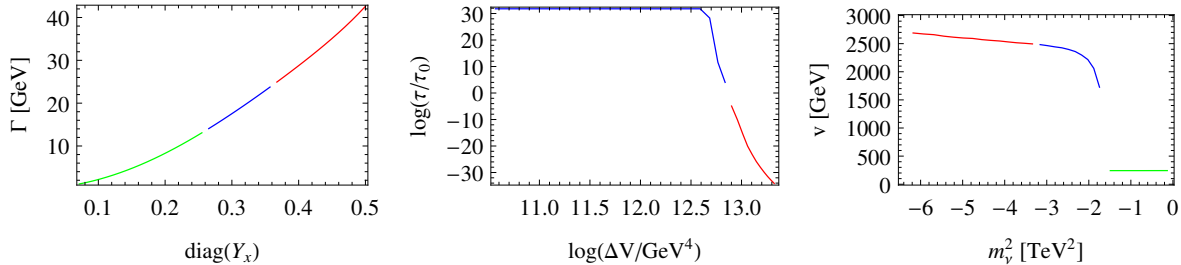


Figure 21. Left: Total width of the 750 GeV particle as function of the diagonal entries in Y_x . The stability of the vacuum has been checked with `Vevacious`: the green region is absolutely stable, in the blue region the vacuum is unstable but long-lived, while in the red region the EW vacuum would decay too fast. Middle: the life-time τ in ages of the universe, τ_0 , as a function of the potential difference between the electroweak minimum and the global one. Note that the largest value `Vevacious` returns is 10^{30} . Right: the value of the electroweak VEV v at the global minimum of the potential as function of the diagonal entries of m_ν^2 .

We see that we can get a large total width of the pseudo-scalar for large diagonal entries in Y_x . Up to values of Y_x of 0.25, which corresponds to a total width of 15 GeV, the vacuum is absolutely stable. One can even reach $Y_x \sim 0.36$ ($\Gamma \sim 30$ GeV) before the life-time of the correct vacuum becomes too short. The dependence of the tunnelling time on the value of m_ν^2 is shown in the middle of Fig. 21. One might wonder how dangerous this vacuum decay is, since spontaneous R -parity violation is not a problem *per se*. However, we show also in the right plot in Fig. 21 that the electroweak VEV v changes dramatically in the global minimum. Therefore, these points are clearly ruled out.

¹⁷This choice might be a bit unlucky but shows the dangers of the two-loop effective potential calculation: in the gauge-less limit, one of the pseudo-scalars has a tree-level mass close to 0. This causes divergencies (‘Goldstone catastrophe’) [371, 372] and makes it necessary to turn off the 2L corrections in `SPheno` via the flag 7 set to 1.

¹⁸For this example we had to turn off the thermal corrections to the tunnelling by inserting `vcs.ShouldTunnelThermally = False` in `Vevacious.py` because `CosmoTransitions` failed otherwise to calculate the tunnelling time in the six-dimensional potential.

Even if we cannot reach a width of 45 GeV with the chosen point, we see that the principle idea to enhance the width is working very well. Thus, with a bit more tuning of the parameters, one might even be able to accommodate this value. However, this is beyond the scope of this example. We emphasise that, since the large coupling responsible for the large width is a dimensionful parameter, it will not generate a Landau pole. Thus, the large width hypothesis does not necessarily point to a strongly coupled sector close to the observed resonance.

6.5.4 Dark matter relic density

We have seen in the last section that light sneutrinos are a good possibility in this model to enhance the width of the 750 GeV particle. Of course, it would be interesting to see if they can also be a dark matter candidate. For this purpose, we can implement the model in `MicrOmegas` to calculate the relic density and to check current limits from direct and indirect detection experiments. In order to implement the model in `MicrOmegas`, it is sufficient to generate the model files for `CalcHep` with `SARAH` via

```
| MakeCHep []
```

and copy the generated files into the `work/models` directory of a new `MicrOmegas` project. `SARAH` also writes main files which can be used to run `MicrOmegas`. For instance, the file `CalcOmega.cpp` calculates the dark matter relic density and writes the result as well as all important annihilation channels to an external file. This information can then be stored when running a parameter scan. The parameters are easily exchanged between `MicrOmegas` and a `SARAH`-based spectrum generator by copying the spectrum file into the main directory of the current `MicrOmegas` project directory.¹⁹ However, it is important to remember that `MicrOmegas` cannot handle complex parameters. Therefore, one has to make sure, even in the case without CP violation, that all rotation matrices of Majorana fermions are real. This can be done by using the following flag for `SPheno`:

```
1 Block SPhenoInput      # SPheno specific input
2   ...
3 50 0                   # Majorana phases: use only positive ↪
   masses
```

The results from a small scan²⁰ are shown in Fig. 22. Here, we have used again the condition of Eq. (6.44) as well as very small deviations from it. One can see that the

¹⁹If the spectrum file is not called `SPheno.spc.$MODEL`, one can change the file-name by editing the fourth line in `func1.mdl` written by `SARAH`

²⁰The relic density calculation for this model can be very time-consuming, especially for the sneutrinos where a large number of co-annihilation channels have to be calculated: the first parameter point

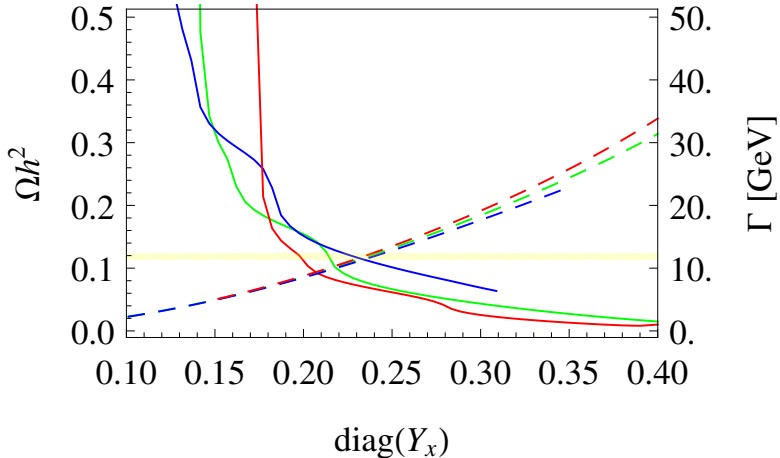


Figure 22. Dark matter relic density Ωh^2 (solid lines) of the lightest sneutrino and total width of the 750 GeV scalar (dashed lines) as function of Y_x . For the green line the relation Eq. (6.44) was used, while the red and blue lines deviate from this relation by $\pm 0.4\%$. The yellow shaded region is the 3σ band of Planck + WP + hihgL + BAO [373].

impact of this small variation on the total width is marginal, but the relic density is clearly affected. Thus, with some tuning of the parameters one can expect that it is possible to explain the dark matter relic density and the total width by light right-handed sneutrinos. However, also finding such a point is again beyond the scope of the example here.

Moreover, there are plenty of other dark matter candidates which mainly correspond to the gauge eigenstates \tilde{S} , \tilde{X} , $\tilde{\eta}$, $\tilde{\bar{\eta}}$ beyond the ones from the MSSM. The properties of all of them could be checked with `MicrOmegas` as well. A detailed discussion of neutralino and sneutrino dark matter in $U(1)$ extensions of the MSSM and different mechanism to obtain the correct abundance was given for instance in Ref. [374].

6.5.5 Flavour constraints

As mentioned above, we decided to include in this model mixing terms between the extra vector-like fermions and the MSSM particles in order to let the new states decay. In this way, we have a safe solution to circumvent any potential cosmological problem. If one assumes the new coupling matrices to have a generic form, i.e. large entries of $O(1)$, including off-diagonal ones as well, they can trigger flavour violation effects. For

might take several hours, all following points should take no longer than seconds, if no new channels are needed.

instance, let us assume that Y'_e has the following form

$$Y'_e = \begin{pmatrix} X & \alpha & \gamma \\ \alpha & X & \beta \\ \gamma & \beta & X \end{pmatrix}, \quad (6.45)$$

with degenerate diagonal entries X , and flavour violating entries α, β, γ . We can now check how strong the constraints on α, β, γ would be for given X . For this purpose, we use the results from `SPheno` for $\text{Br}(\mu \rightarrow 3e)$, $\text{Br}(\tau \rightarrow 3\mu)$, $\text{Br}(\tau \rightarrow 3e)$, and μ - e conversion in Ti and Au, and compare the results with the current experimental limits, see Fig. 23. We find, for instance for $X = 0.1$, that α must be smaller than $\sim 10^{-9}$,

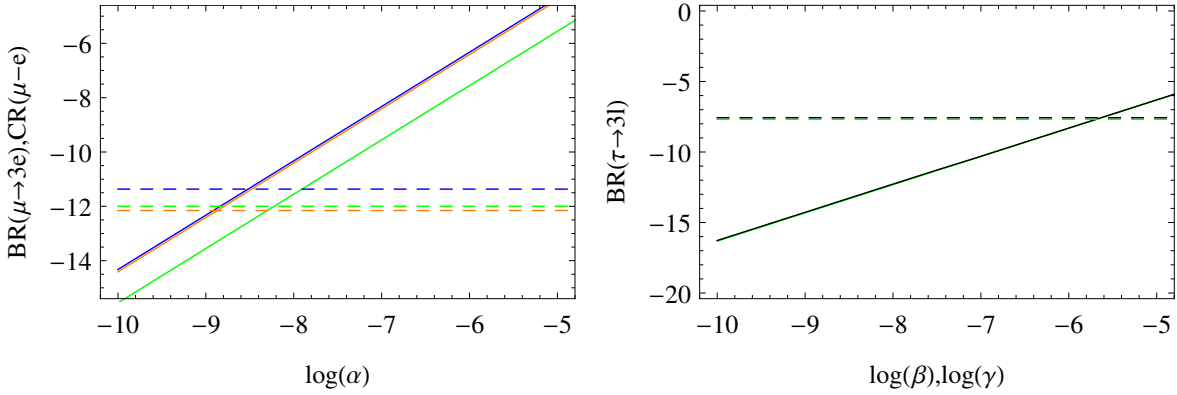


Figure 23. Left: $\text{Br}(\mu \rightarrow 3e)$ (green), and μ - e conversion in Ti (blue) or Au (orange). Right: $\text{Br}(\tau \rightarrow 3\mu)$ (green), $\text{Br}(\tau \rightarrow 3e)$ (black). The dashed lines are the current experimental limits [375–378]. Here, we used $X = 0.1$.

while the limits on β, γ , obtained from τ decays, can still be as large as $O(10^{-6})$.

If other vector-like states mixing with the left-handed quarks or the right-handed down-like quarks would be present – as would be the case for instance when assuming 5 or 10-plets of $SU(5)$ – there would also be stringent constraints on their couplings: they would cause tree-level contributions to ΔM_{B_s} . Since these observables are also calculated by `SPheno`, one can easily check the limits on models featuring those states.

6.6 Z' mass limits

So far, we have picked a Z' mass of at least 2.5 TeV. Of course, we have to check that this is consistent with current exclusion limits. Recent exclusion limits for $pp \rightarrow Z' \rightarrow e^+e^-$ have been released by ATLAS using 13 TeV data and 3.2 fb^{-1} [379]. To compare the prediction for our model with these numbers, we can use the UFO model files generated by SARAH via

```
| MakeUFO [] ;
```

and add them to MadGraph. For this purpose, we copy the SARAH generated files to a subdirectory `models/U1xMSSM` of the MadGraph installation. Afterwards, we generate all necessary files to calculate the cross section for the process under consideration by running in MadGraph

```
import model U1xMSSM -modelname
generate p p > Zp > e1 e1bar
output pp_Zp_ee
```

Note the option `-modelname` when loading the model. This ensures that MadGraph is using the names for the particles as defined in our model implementation. Using the default names of MadGraph causes naming conflicts because of the extended Higgs sector. One can give the spectrum files written by SPheno as input (`param_card.dat`) for MadGraph. One just has to make sure that the blocks written for `HiggsBounds` and `HiggsSignals` are turned off because the SLHA parser of MadGraph is not able to handle them. This can be done by setting the following flag in the Les Houches input file:

```
1 Block SPhenoInput      # SPheno specific input
2   ...
3 520 0                  # Write effective Higgs couplings
4                        # (HiggsBounds blocks)
```

In principle, one could also change the mass directly in the `param_card` without re-running SPheno for each point. However, the advantage of SPheno is that it calculates the width of the Z' gauge boson including SUSY and non-SUSY states. This usually has some impact on the obtained limits [369, 380, 381]. We can now scan over $M_{Z'}$ for fixed values of g_X and compare the predicted cross section with the exclusion limits. In addition, we can also check the impact of gauge-kinetic mixing: as we have seen, these couplings are negative and can be sizeable. Therefore, we compare the results without gauge kinetic mixing and when setting $g_{1X} = -\frac{1}{5}g_X$ at the SUSY scale. The results are summarised in Fig. 24. We see that for $g_X = 0.5$ the limit is about 2.8 TeV without gauge-kinetic mixing. Including kinetic mixing, it gets reduced by about 200 GeV. Thus, one sees that kinetic mixing is not necessarily a small effect. This contradicts some claims that sometimes appear in the literature, where it is often argued that kinetic mixing can be ignored. In particular, we emphasise that this is very relevant when discussing a GUT theory with RGE running over many orders of magnitude in energy scale.

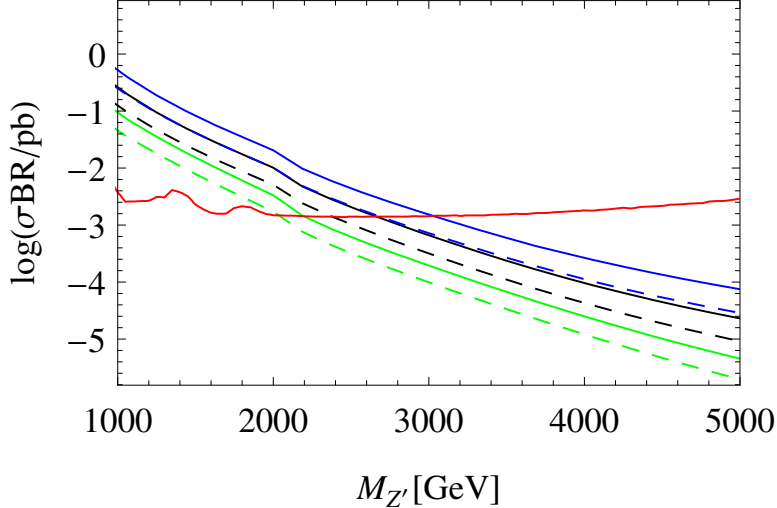


Figure 24. Limit on $M_{Z'}$ for three different values of g_X : 0.3 (green), 0.5 (black), 0.7 (blue). For the dashed line, we assumed in addition $g_{1X} = -\frac{1}{5}g_X$, while for the full lines gauge kinetic mixing has been neglected. The red line shows the exclusion limit from ATLAS [379].

7 Summary

We have given an overview on weakly-coupled renormalisable models proposed to explain the excess observed by ATLAS and CMS around 750 GeV in the diphoton channel. We have pointed out that many of the papers quickly written after the announcement of the excess are based on assumptions and simplifications which are often unjustified and can lead to wrong conclusions. A very common mistake is the lack of inclusion of higher order corrections to the digluon and diphoton decay rates, which results in underestimating the ratio typically by a factor of 2. Several authors assume that the new 750 GeV scalar does not mix with the SM Higgs, which is often not justified. Including such a mixing can give large constraints. These and other problems can be easily avoided by using **SARAH** and related tools which were created with the purpose of facilitating precision studies of high energy physics models. In particular, the link between **SARAH** and the spectrum generators **FlexibleSUSY** and **SPheno** is a powerful approach to obtain the mass spectrum and all the rotation matrices for any given model *without neglecting flavour mixing, complex phases or 1st and 2nd generation Yukawa couplings*. Optionally, one can also include all the important radiative corrections up to two loops. In addition, we have improved the functionality of **FlexibleSUSY** and **SPheno** to calculate the diphoton and digluon decay widths of neutral scalars, including the higher order QCD corrections up to $N^3\text{LO}$. One can now pass on this information directly to Monte-Carlo tools, like **CalcHep** and **MadGraph**, by using the appropriate

model files generated with **SARAH**.

In order to study as many models in as much detail as possible, we have created a database of **SARAH** model files for many of the ideas proposed so far in the literature. The database is also meant to provide many examples in the context of the diphoton excess with which the novel user can try out to familiarise with **SARAH**, in order to build up the level of expertise needed to implement their own models in the future.

Finally, we have introduced an attractive SUSY model which combines the idea of non-decoupling D -terms with the explanation of the diphoton excess. We have used this as a new example to show how to use **SARAH** to first understand the model analytically at leading order. As a second step, we have performed a numerical analysis of the important loop corrections to the different masses, checked limits from Higgs searches, neutral gauge bosons searches, and from lepton flavour violation. We have demonstrated that this model could explain a large width of the 750 GeV scalar, but in this context limits from spontaneous R -parity violation become important. These limits can be checked by using the interface to **Vevacious**.

Acknowledgements

We thank Martin Winkler for beta-testing and valuable impact. Mark Goodsell acknowledges support from Agence Nationale de Recherche grant ANR-15-CE31-0002 “HiggsAutomator,” and would like to thank Pietro Slavich and Luc Darmé for interesting discussions. Avelino Vicente acknowledges financial support by the Spanish grants FPA2014-58183-P, Multidark CSD2009-00064 and SEV-2014-0398 (MINECO), FPA2011-22975 and PROMETEOII/2014/084 (Generalitat Valenciana) and is grateful to Wei-Chih Huang for discussions about the GTHDM model. Manuel E. Krauss is supported by the BMBF grant 00160287 and thanks Cesar Bonilla for useful discussions on left-right models. Lorenzo Basso acknowledges support by the OCEVU Labex (ANR-11-LABX- 0060) and the A*MIDEX project (ANR-11-IDEX-0001-02), funded by the “Investissements d’Avenir” French government program managed by the ANR. Florian Staub thanks Alfredo Urbano for discussions about the Georgi-Machacek model and for testing the model file.

A How to use SARAH and related tools

We briefly summarise here the important commands and steps to use many powerful features of **SARAH**. For pedagogical introductions see [219, 382].

A.1 How do I install SARAH?

The installation of SARAH is very simple: the package can be downloaded from

<http://sarah.hepforge.org>

After copying the tar file to the directory \$PATH, it can be extracted

```
$ cp [Download-Directory]/SARAH-X.Y.Z.tar.gz $PATH/  
$ cd $PATH  
$ tar -xf SARAH-X.Y.Z.tar.gz  
$ ln -s SARAH-X.Y.Z SARAH
```

X.Y.Z must be replaced by the version which was downloaded. In the last line a symbolic link SARAH to the directory SARAH-X.Y.Z is created. There is no compilation necessary, SARAH can directly be used with any Mathematica version between 7 and 10.

A.2 How do I load a model in SARAH?

To load an existing model (called \$MODEL in the following) run in Mathematica

```
<<[$PATH]/SARAH/SARAH.m;  
Start["$MODEL"];
```

After some time, depending on the complexity of the model,

```
| All Done. $MODEL is ready!
```

should appear and no error messages or warnings should show up during the evaluation.

A.3 How do I get analytical expressions for masses, vertices and tadpoles?

- **Mass matrices** : The mass matrix for a particle (**Particle**) is returned by

```
MassMatrix[Particle]
```

- **Tadpole equations** : The tadpole equation corresponding to a scalar (**Scalar**) is printed by using

```
TadpoleEquation[Scalar]
```

- **Vertices** : To calculate the vertices for a list of external states (**Particles**) use

```
Vertex[{Particles},Options];
```

The options define the considered eigenstates (`Eigenstates -> EWSB/GaugeES`) as well as the treatment of dependences among parameters (`UseDependences -> False/True`).

All vertices for a set of eigenstates are calculated at once by

```
MakeVertexList[$EIGENSTATES, Options];
```

Here, first the eigenstates (`$EIGENSTATES: GaugeES, EWSB`) are defined and as an option it can be defined whether only specific generic classes should be considered (e.g. `GenericClasses -> FFS`).

A.4 How do I get the renormalisation group equations for a model?

The calculation of the RGEs at the one- and two-loop level can be performed after the initialization of a model via

```
CalcRGEs[Options];
```

The results are saved in three-dimensional arrays: the first entry is the name of the considered parameter, the second entry is the one-loop β -function ($\times 16\pi^2$) and the third one is the two-loop β -function ($\times (16\pi^2)^2$). For non-SUSY models, the RGEs of the different parameters are saved in

- `Gij`: Anomalous dimensions of all fermions and scalars
- `BetaGauge`: Beta functions of all gauge couplings
- `BetaLijkl`: Beta functions of all quartic scalar couplings
- `BetaYijk`: Beta functions of all interactions between two fermions and one scalar
- `BetaTijk`: Beta functions of all cubic scalar interactions
- `BetaMuij`: Beta functions of all bilinear fermion terms
- `BetaBij`: Beta functions of all bilinear scalar terms
- `BetaVEV`: Beta functions of all VEVs

The output for SUSY models is saved in the following arrays:

- `Gij`: Anomalous dimensions of all chiral superfields
- `BetaWijkl`: Quartic superpotential parameters

- `BetaYijk`: Trilinear superpotential parameters
- `BetaMuij`: Bilinear superpotential parameters
- `BetaLi`: Linear superpotential parameters
- `BetaQijkl`: Quartic soft-breaking parameters
- `BetaTijk`: Trilinear soft-breaking parameters
- `BetaBij`: Bilinear soft-breaking parameters
- `BetaSLi`: Linear soft-breaking parameters
- `Betam2ij`: Scalar squared masses
- `BetaMi`: Majorana Gaugino masses
- `BetaGauge`: Gauge couplings
- `BetaVEV`: VEVs
- `BetaDGi`: Dirac gaugino mass terms
- `BetaFIi` Fayet-Iliopoulos terms

A.5 How can I run the RGEs in Mathematica?

SARAH writes a file to run the RGEs numerically within Mathematica. One can load this file in any Mathematica session and use the provided function `RunRGEs` to solve the RGEs numerically. For instance,

```
<< [$PATH]/SARAH/Output/$MODEL/RGEs/RunRGEs.m;
sol = RunRGEs[{g1 -> 0.46, g2 -> 0.63, g3 -> 1.05}, 3, 17][[1]];
Plot[{g1[x], g2[x], g3[x]} /. sol, {x, 3, 17}, Frame -> True, Axes -> False];
```

First, the file is loaded and then the RGEs are evaluated from 10^3 to 10^{17} GeV. The initial conditions at 1 TeV are $g_1 = 0.46$, $g_2 = 0.63$, $g_3 = 1.05$. The interpolation functions were saved in the variable `sol` which can then be used for plotting.

A.6 How do I get analytical expressions for the one-loop corrections?

Loop corrections are calculated via
`CalcLoopCorrections[$EIGENSTATES];`

As argument only the considered eigenstates (e.g. `$EIGENSTATES=EWSB`) have to be defined. The results are saved in the variables `Tadpoles1LoopSums[$EIGENSTATES]` and `SelfEnergy1LoopSum[$EIGENSTATES]` as sums of all contributions, or as list of the different contributions in `Tadpoles1LoopList[$EIGENSTATES]` and `SelfEnergy1LoopList[$EIGENSTATES]`.

A.7 How do I get a spectrum generator based on SPheno for a new model?

To obtain the SPheno output (after SARAH has been loaded in Mathematica and the model initialised), type the command

```
| MakeSPheno [] ;
```

When executing `MakeSPheno`, SARAH first calculates all the information it needs, i.e. it is not necessary to run the calculation of vertices or RGEs before. When SARAH is done, the source code for SPheno is stored in `$PATH/SARAH/Output/$MODEL/EWSB/SPheno/`.

The compilation of this code is done as follows: enter the directory of the SPheno installation, create a new sub-directory (named `$MODEL`) and copy the code into this directory.

```
$ cd $PATH/SPHENO  
$ mkdir $MODEL  
$ cp $PATH/SARAH/Output/$MODEL/EWSB/SPheno/* $MODEL/
```

Afterwards, the code is compiled via

```
$ make Model=$MODEL
```

and a new executable `SPheno$MODEL` is available in the `bin` subfolder.

An input file, by default called `LesHouches.in.$MODEL`, is needed to run `SPheno$MODEL`. SARAH writes a template for that file which has been copied to the `$MODEL` subdirectory of SPheno together with the Fortran code. You can move it to the root directory of SPheno

```
$ cp $MODEL/LesHouches.in.$MODEL .
```

By doing this we can work now from the SPheno main directory and we do not have to give the file as argument when running SPheno. Thus, SPheno can be called via

```
$ ./bin/SPheno$MODEL
```

Alternatively, one can keep the Les Houches file in the \$MODEL and work with it via

```
$ ./bin/SPheno$MODEL $MODEL/LesHouches.in.$MODEL
```

Note: If no default values are given in the model file, the corresponding parameters are set to zero in the template input file. The user should enter a set of suitable values before running SPheno.

A.8 How to I get a spectrum generator with FlexibleSUSY?

Download FlexibleSUSY (at least version 1.4.0) from

<https://flexiblesusy.hepforge.org>

and unpack it:

```
$ wget \
    https://www.hepforge.org/archive/flexiblesusy/
    FlexibleSUSY-1.4.0.tar.gz
$ tar -xf FlexibleSUSY-1.4.0.tar.gz
$ cd FlexibleSUSY-1.4.0/
```

The FlexibleSUSY model file FlexibleSUSY.m.in for the model under consideration should be put into a sub-directory of the model_files/ directory with the name of the model:

```
$ mkdir model_files/$MODEL/
$ cp FlexibleSUSY.m.in model_files/$MODEL/
```

Afterwards, the spectrum generator for the model can be generated as²¹

```
$ ./createmodel --name=$MODEL
$ ./configure --with-models=$MODEL
$ make
```

To run the spectrum generator, an SLHA input file has to be provided. The full path to the SLHA input file must be specified using the --slha-input-file= argument, for example:

²¹FlexibleSUSY assumes that SARAH can be loaded from within Mathematica using the Needs["SARAH'"] command. Please refer to the installation instructions within the README file in the FlexibleSUSY/ directory for installation instructions.

```
$ ./models/$MODEL/run_$MODEL.x \  
  --slha-input-file=LesHouches.in.$MODEL  
  --slha-output-file=LesHouches.out.$MODEL
```

Please run `./models/$MODEL/run_$MODEL.x --help` for more options or refer to the README file.

A.9 How can I check points with HiggsBounds and HiggsSignals?

In the same directory in which the SPheno spectrum file is located, all other input files for HiggsBounds and HiggsSignals are saved by SPheno. The (relative) path to this directory has to be given as the last argument to HiggsBounds when executing it. Thus, working from the directory `$PATH`, HiggsBounds is started via:

```
$ ./HiggsBounds/HiggsBounds LandH effC #neutral \  
  #charged SPHENO/
```

From other directories, one can use absolute paths:

```
$ $PATH/HiggsBounds/HiggsBounds LandH effC #neutral \  
  #charged $PATH/SPHENO/
```

`#neutral` and `#charged` are the number of (physical) neutral and charged Higgs bosons in the model.

HiggsSignals is the complement to HiggsBounds and checks how well a point reproduces the Higgs mass and rate measurements. The syntax is very similar to HiggsBounds:

```
$ ./HiggsSignals/HiggsSignals latestresults peak 2 \  
  effC #neutral #charged SPHENO/
```

A.10 How do I implement a model in MadGraph and link it to SPheno/FlexibleSUSY?

A new model in MadGraph can be implemented via the UFO format which is also supported by other tools like Herwig++ or Sherpa. The command to generate the UFO files is

```
| MakeUFO []
```

All files written by SARA have to be copied to a new sub-directory in MadGraph's model directory:

```
cd $PATH/MADGRAPH/  
mkdir models/$MODEL  
cp $PATH/SARA/Output/$MODEL/EWSB/UFO/* models/$MODEL
```

The model can be loaded in MadGraph via

```
import model $MODEL -modelname
```

The option `-modelname` is used to keep the names of the particles as given in the model files. This prevents conflicts with internal MadGraph conventions.

The spectrum files written by SPheno and FlexibleSUSY can be given as a parameter card to MadGraph (`param_card.dat`). One must only make sure that the HiggsBounds blocks are not included²², because MadGraph cannot parse them and would consider the file to be corrupted.

A.11 How do I implement a model in WHIZARD/O’Mega and link it to SPheno?

The model files for WHIZARD/O’Mega are obtained by

```
| MakeWHIZARD []
```

After the interface has completed, the generated files are stored in the directory `$PATH/SARAH/Output/$MODEL/EWSB/WHIZARD_Omega/`

In order to use the model with WHIZARD and O’Mega, the generated code must be compiled and installed. In most cases this is done by

```
$ cd $PATH/SARAH/Output/$MODEL/EWSB/WHIZARD_Omega
$ ./configure --prefix=$PATH/WHIZARD/ \
  WO_CONFIG=$PATH/WHIZARD/bin/
$ make
$ make install
```

If WHIZARD has not been installed globally in the home directory of the current user, WHIZARD will not be able to find the binaries. Thus, the `WO_CONFIG` environment variable is used to point explicitly to the binaries. By default, the `configure` script would install the compiled model into `.whizard` in the home directory of the user. If the user wants to have several WHIZARD installations or install WHIZARD locally, it might be better to provide a model just for one installation. For these cases the installation path has been defined via the `--prefix` option of the `configure` script. More information on the available options is shown with the command

```
./configure --help
```

To link WHIZARD and SPheno, all SPheno modules created by SARAH write the information about the parameters and masses into an additional file. This file is written in the WHIZARD specific format and can be directly read by WHIZARD. One just has to make

²²The output of these blocks is suppressed via flag 520 in SPheno.

sure that the corresponding flag is turned on in the Les Houches input for `SPheno` to get this output:

LesHouches.in.\$MODEL

```
Block SPhenoInput    # SPheno specific input
...
75 1                  # Write WHIZARD files
```

The parameter file can then be included in the Sindarin input file for `WHIZARD` via

Example.sin

```
model = $model_sarah
...
include("$PATH/SPHENO/WHIZARD.par.$MODEL")
```

A.12 How do I implement a model in `CalcHep`/`MicrOmegas` and link it to `SPheno`?

Model files for `CalcHep` can be obtained by running

```
MakeCHep[Options];
```

The options provided may be used to configure exactly what is to be included in the generated model files. For example, one might prevent vertices involving four vector bosons from being included in the model files by specifying `Exclude -> {VVVV}`. When `SARAH` is finished with `MakeCHep`, the `CalcHep` model files are located in the directory `$PATH/SARAH/Output/$MODEL/EWSB/CHep/`

To implement the new model in `CalcHep`, it is sufficient to use the internal “import model” routine from the GUI menu, and give the above absolute path.

The model files for `CalcHep` are also suitable for `MicrOmegas`, since the latter uses `CalcHep` to obtain the cross section and all necessary decay widths to evaluate the dark matter abundance. To implement the model in `MicrOmegas`, a new project has to be created and the files have to be copied in the working directory of this project:

```
$ cd $PATH/MICROMEGAS
$ ./newProject MODEL
$ cd $MODEL
$ cp $PATH/SARAH/Output/$MODEL/EWSB/CHep/* \
  work/models
```

c++ files written by SARAH to run `MicrOmegas` for the given model were copied together with all model files into the working directory of the current project. You can move them to the main project directory and compile them

```
$ mv work/models/CalcOmega_with_DDetection.cpp .
$ make main=CalcOmega_with_DDetection.cpp
```

A new binary `CalcOmega_with_DDetection` is now available.

The only missing piece are the input parameters. Providing the numerical parameters is simple because `CalcHep/MicrOmegas` can read the SLHA files written by `SPheno` or `FlexibleSUSY`²³. However, the user must make sure that no complex rotation matrices show up in the spectrum file: in the case of Majorana matrices and no CP violation, there are two equivalent outputs: (i) all Majorana masses are positive, but some entries of the corresponding rotation matrices are complex; (ii) all mixing matrices are real, but some masses are negative. `CalcHep` can only handle the second case with real matrices. Hence, one has to use the flag

LesHouches.in.\$MODEL

```
Block SPhenoInput      # SPheno specific input
...
50 0                   # Majorana phases: use only positive ↔
      masses
```

to get the spectrum according to that convention. Afterwards, the spectrum file must be moved to the same directory as the `CalcHep` numerical session (typically the folder `results`) for `CalcHep`, or where `CalcOmega_with_DDetection` is located for `MicrOmegas`, and start the calculation.

For `CalcHep`

```
$ cp $PATH/SPHENO/SPheno.spc.$MODEL \
    /$CALCHEP/results/
$ ./n_calchep
```

For `MicrOmegas`

```
$ cp $PATH/SPHENO/SPheno.spc.$MODEL \
    /$MICRMEGAS/$MODEL
$ ./CalcOmega_with_DDetection
```

²³It might be just necessary to adjust the name of the spectrum file at the beginning of `func1.mdl`.

A.13 How do I implement a new model in Vevacious?

The model files for Vevacious are generated by SARAH via

```
| MakeVevacious [] ;
```

As soon as the model file is created, it is convenient to copy them to the model directory of the local Vevacious installation. In addition, one can also generate a new subdirectory which contains the SPheno spectrum files for the \$MODEL used as input for Vevacious, as well as the output written by Vevacious

```
$ cd $PATH/VEVACIOUS
$ mkdir $MODEL/
$ cp $PATH/SARAH/Output/$MODEL/Vevacious/$MODEL.vin \
  models/
$ cp $PATH/SPHENO/SPheno.spc.$MODEL $MODEL/
```

These steps are optional. The user can provide other locations of the model and spectrum files within the initialisation file used by Vevacious. Independent of the location of the files, one has to write this initialisation file for a new study. The easiest way is to start with the file included in the Vevacious package in the subdirectory bin and edit it

```
$ cd $PATH/VEVACIOUS/bin
$ cp VevaciousInitialization.xml \
  VevaciousInitialization_ $MODEL.xml
```

A.14 How do I get the model files for FeynArts/FormCalc?

Run

```
MakeFeynArts []
```

and copy the files to

```
/home/user/.Mathematica/Applications/FeynArts/Models/
```

The model can then be chosen as option for the InsertFields command of FeynArts.

A.15 How do I get all expression in L^AT_EX format?

Use

```
| MakeTeX [] ;
```

When SARAH is done with the output, the .tex file are stored in

The main file which can be compiled with `pdflatex` is `\$MODEL_EWSB.tex`. SARAH usually also generates Feynman diagrams using the \LaTeX package `feynmf` [383]. In order to compile all Feynman diagrams and the pdf file at once, a shell script `MakePDF.sh` is generated by SARAH.

B What is necessary to implement a model in SARAH?

All information about the model is saved in three different files: `\$MODEL.m`, `parameters.m` and `particles.m` must be located in the subdirectory `\$MODEL` in the `Models` directory of SARAH. Only the first file, `MODEL.m`, is absolutely necessary and contains all physical information about the model: the symmetries, particle content, (super)potential and mixings. In `parameters.m` properties of all parameters can be defined, e.g. \LaTeX name, Les Houches block and number, relations among parameters, real/complex, etc. In `particles.m` additional information about particles are set: mass, width, electric charge, PDG, \LaTeX name, output name, and so on. The optional information in `parameters.m` and `particles.m` might be needed for the different outputs of SARAH. We give here two examples to show that also more complicated SUSY and non-SUSY models can be defined in SARAH in a rather short form. Detailed information about the meaning and syntax are given in Refs. [219]

B.1 Definition of a non-SUSY model

As an example how to define a non-SUSY model in SARAH we picked the model with two scalar leptoquarks discussed in Sec. 5.2.1.5. The different pieces of the model file are:

Gauge Sector

```
1 Gauge [[1]]={B,    U[1], hypercharge, g1,False};
2 Gauge [[2]]={WB,  SU[2], left,          g2,True};
3 Gauge [[3]]={G,   SU[3], color,         g3,False};
```

Matter Content

```
1 FermionFields [[1]] = {q, 3, {uL, dL},    1/6, 2, 3};
2 FermionFields [[2]] = {l, 3, {vL, eL},    -1/2, 2, 1};
3 FermionFields [[3]] = {d, 3, conj[dR],    1/3, 1, -3};
4 FermionFields [[4]] = {u, 3, conj[uR],    -2/3, 1, -3};
5 FermionFields [[5]] = {e, 3, conj[eR],    1, 1, 1};
6
```

```

7 ScalarFields[[1]] = {H, 1, {Hp, H0},      1/2, 2, 1};
8 ScalarFields[[2]] = {Phi, 1, PhiLQ,      -4/3, 1, 3};
9 ScalarFields[[3]] = {Omega, 1, OmegaLQ,  -1/3, 1, 3};
10 ScalarFields[[4]] = {The, 1, theta,      1, 1, 1};
11 ScalarFields[[5]] = {s, 1, sing,         0, 1, 1};

```

Potential

```

1 DEFINITION[GaugeES][LagrangianInput]= {
2     {LagHC, {AddHC->True}},
3     {LagNoHC, {AddHC->False}}};
4
5 LagNoHC = -(muH2 conj[H].H
6 + muS2 conj[s].s + muP2 conj[Phi].Phi
7 + muO2 conj[Omega].Omega + muT2 conj[The].The
8 + LambdaH/2 conj[H].H.conj[H].H
9 + LambdaS conj[s].s.conj[s].s
10 + LambdaOS conj[Omega].Omega.conj[s].s
11 + LambdaPS conj[Phi].Phi.conj[s].s
12 + LambdaTS conj[The].The.conj[s].s
13 + LambdaHS conj[H].H.conj[s].s
14 + LambdaHO conj[H].H.conj[Omega].Omega
15 + LambdaHT conj[H].H.conj[The].The
16 + LambdaHP conj[H].H.conj[Phi].Phi
17 + LambdaOP Delta[col1,col2] Delta[col3,col4] \
18     *conj[Omega].Omega.conj[Phi].Phi
19 + LambdaOT conj[Omega].Omega.conj[The].The
20 + LambdaPT conj[Phi].Phi.conj[The].The
21 + LambdaO Delta[col1,col2] Delta[col3,col4] \
22     *conj[Omega].Omega.conj[Omega].Omega
23 + LambdaT conj[The].The.conj[The].The
24 + LambdaP Delta[col1,col2] Delta[col3,col4]
25     *conj[Phi].Phi.conj[Phi].Phi);
26
27 LagHC = -(Yd conj[H].d.q + Ye conj[H].e.l + Yu H.u.q
28 + YT l.l.The
29 + YO q.l.conj[Omega]
30 + YP e.d.Phi
31 + Sqrt[2] LambdaHat s.The.Phi.conj[Omega] );

```

Rotations in gauge sector

```
1 DEFINITION[EWSB][GaugeSector] =
2 {
3   {{VB, VWB[3]}, {VP, VZ}, ZZ},
4   {{VWB[1], VWB[2]}, {VWp, conj[VWp]}, ZW}
5 };
```

VEVs

```
1 DEFINITION[EWSB][VEVs]= {
2 {H0, {v, 1/Sqrt[2]}, {sigmaH, I/Sqrt[2]}, {phiH, 1/Sqrt[2]}},
3 {sing, {vS, 1/Sqrt[2]}, {sigmaS, I/Sqrt[2]}, {phiS, 1/Sqrt[2]}}
4 };
```

Rotations in matter sector

```
1 DEFINITION[EWSB][MatterSector]=
2   {{{phiH, phiS}, {hh, ZH}},
3   {{sigmaH, sigmaS}, {Ah, ZA}},
4   {{{dL}, {conj[dR]}}, {{DL, Vd}, {DR, Ud}}},
5   {{{uL}, {conj[uR]}}, {{UL, Vu}, {UR, Uu}}},
6   {{{eL}, {conj[eR]}}, {{EL, Ve}, {ER, Ue}}}};
```

Dirac spinors

```
1 DEFINITION[EWSB][DiracSpinors]={
2   Fd ->{ DL, conj[DR]},
3   Fe ->{ EL, conj[ER]},
4   Fu ->{ UL, conj[UR]},
5   Fv ->{ vL, 0}
6 };
```

B.2 Definition of a SUSY model

As an example how to define a SUSY model in SARAH we show the model file for the model discussed in Section 6.

Global symmetries

```
1 Global[[1]] = {Z[2], MParity};
2 MpM = {-1, -1, 1};
```

```
3 MpP = {1,1,-1};
```

Gauge symmetries

```
1 Gauge[[1]]={B, U[1], hypercharge, g1, False, MpM};
2 Gauge[[2]]={WB, SU[2], left, g2, True, MpM};
3 Gauge[[3]]={G, SU[3], color, g3, False, MpM};
4 Gauge[[4]]={BX, U[1], extra, gX, False, MpM};
```

Chiral superfields

```
1 SuperFields[[1]] = {q, 3, {uL, dL}, 1/6, 2, 3, 0, MpM};
2 SuperFields[[2]] = {l, 3, {vL, eL}, -1/2, 2, 1, 0, MpM};
3 SuperFields[[3]] = {Hd,1, {Hd0, Hdm}, -1/2, 2, 1, -1/2, ↔
  MpP};
4 SuperFields[[4]] = {Hu,1, {Hup, Hu0}, 1/2, 2, 1, 1/2, ↔
  MpP};
5
6 SuperFields[[5]] = {d, 3, conj[dR], 1/3, 1, -3, 1/2, ↔
  MpM};
7 SuperFields[[6]] = {u, 3, conj[uR], -2/3, 1, -3, -1/2, ↔
  MpM};
8 SuperFields[[7]] = {e, 3, conj[eR], 1, 1, 1, 1/2, MpM};
9 SuperFields[[8]] = {vR,3, conj[vR], 0, 1, 1, -1/2, MpM};
10
11 SuperFields[[9]] = {C1, 1, C10, 0, 1, 1, -1, MpP};
12 SuperFields[[10]] = {C2, 1, C20, 0, 1, 1, 1, MpP};
13 SuperFields[[11]] = {S, 1, sing, 0, 1, 1, 0, MpP};
14
15
16 SuperFields[[12]] = {UX, 3, conj[uRx], -2/3, 1, -3, -1/2, ↔
  MpM};
17 SuperFields[[13]] = {UXp,3,uRxp, 2/3, 1, 3, 1/2, ↔
  MpM};
18 SuperFields[[14]] = {EX, 3, conj[eRx], 1, 1, 1, 1/2, ↔
  MpM};
19 SuperFields[[15]] = {EXp,3,eRxp, -1, 1, 1, -1/2, ↔
  MpM};
```

Superpotential

```

1 SuperPotential = Yu u.q.Hu - Yd d.q.Hd - Ye e.l.Hd \
2 + \[Mu] Hu.Hd + lambdaH S.Hu.Hd + Yv vR.l.Hu \
3 + lambdaC S.C1.C2 + lw S + Yn vR.C2.vR
4 + MS S.S + kappa/3 S.S.S + MtE e.EXp + MtU u.UXp \
5 + lambdaE S.EX.EXp + MVE EX.EXp + lambdaU S.UX.UXp \
6 + MVU UX.UXp + Yep EX.l.Hd + Yup UX.q.Hu;

```

Rotations in gauge sector

```

1 DEFINITION[EWSB][GaugeSector] =
2 {
3   {{VB, VWB[3], VBX}, {VP, VZ, VZp}, ZZ},
4   {{VWB[1], VWB[2]}, {VWm, conj[VWm]}, ZW},
5   {{fWB[1], fWB[2], fWB[3]}, {fWm, fWp, fW0}, ZfW}
6 };

```

VEVs

```

1 DEFINITION[EWSB][VEVs]= {
2   {SHd0, {vd, 1/Sqrt[2]}, {sigmad, I/Sqrt[2]}, {phid, 1/Sqrt[2]}},
3   {SHu0, {vu, 1/Sqrt[2]}, {sigmau, I/Sqrt[2]}, {phiu, 1/Sqrt[2]}},
4   {SC10, {x1, 1/Sqrt[2]}, {sigma1, I/Sqrt[2]}, {phi1, 1/Sqrt[2]}},
5   {SC20, {x2, 1/Sqrt[2]}, {sigma2, I/Sqrt[2]}, {phi2, 1/Sqrt[2]}},
6   {Ssing, {xS, 1/Sqrt[2]}, {sigmaS, I/Sqrt[2]}, {phiS, 1/Sqrt[2]}},
7   {SvL, {0, 0}, {sigmaL, I/Sqrt[2]}, {phiL, 1/Sqrt[2]}},
8   {SvR, {0, 0}, {sigmaR, I/Sqrt[2]}, {phiR, 1/Sqrt[2]}}
9 };

```

Rotations in matter sector

```

1 DEFINITION[EWSB][MatterSector]=
2 { {{SdL, SdR}, {Sd, ZD}},
3   {{SuL, SuR, SuRx, SuRxp}, {Su, ZU}},
4   {{SeL, SeR, SeRx, SeRxp}, {Se, ZE}},
5   {{sigmaL, sigmaR}, {SvIm, ZVI}},
6   {{phiL, phiR}, {SvRe, ZVR}},
7   {{phid, phiu, phi1, phi2, phiS}, {hh, ZH}},

```

```

8   {{sigmad, sigmau, sigma1, sigma2, sigmaS}, {Ah, ZA}},
9   {{SHdm, conj[SHup]}, {Hpm, ZP}},
10  {{fB, fW0, FHd0, FHu0, fBX, FC10, FC20, Fsing}, {L0, ZN}},
11  {{{fWm, FHdm}, {fWp, FHup}}, {{Lm, UM}, {Lp, UP}}},
12  {{FvL, conj[FvR]}, {Fvm, UV}},
13  {{{FeL, FeRxp}, {conj[FeR], conj[FeRx]}}, {{FEL, ZEL}, {FER, ZER}}},
14  {{{FdL}, {conj[FdR]}}, {{FDL, ZDL}, {FDR, ZDR}}},
15  {{{FuL, FuRxp}, {conj[FuR], conj[FuRx]}}, {{FUL, ZUL}, {FUR, ZUR}}}
16  };

```

Phases

```

1  DEFINITION[EWSB][Phases]=
2  {   {fG, PhaseGlu}
3      };

```

Dirac Spinors

```

1  DEFINITION[EWSB][DiracSpinors]={
2  Fd ->{  FDL, conj[FDR]},
3  Fe ->{  FEL, conj[FER]},
4  Fu ->{  FUL, conj[FUR]},
5  Fv ->{  Fvm, conj[Fvm]},
6  Chi ->{ L0, conj[L0]},
7  Cha ->{ Lm, conj[Lp]},
8  Glu ->{ fG, conj[fG]}
9  };

```

C How can I define the features of a SPheno or FlexibleSUSY version?

Before we can use FlexibleSUSY or SPheno for a model, it is necessary to provide an additional input file which defines the basic setup. In general, there are two different kinds of input versions the user can create which need a different amount of input:

- **High-scale version:** In a high-scale version of SPheno or FlexibleSUSY a RGE running between the electroweak scale, an intermediate renormalisation scale and a high (or GUT) scale is supported. The user can define appropriate boundary

conditions at each of these three scales. Furthermore, threshold effects by including additional scales where heavy particles are integrated out can optionally be included. Finally, the user can specify a condition which defines the high-energy scale. The most common choice is the unification scale of gauge couplings, but other choices such as Yukawa unification are possible. In addition, these high-scale versions also include the possibility to define the entire input at the intermediate renormalisation scale and skip the RGE running to the GUT scale. The high-scale version is usually the appropriate option for SUSY models, models with heavy mass spectra, or models which should be studied at very high scales.

- **Low-scale version:** In a low-scale version usually no RGE running is included. The FlexibleSUSY or SPheno low-scale versions expect all free parameters to be given at the low-energy or the renormalisation scale. This version is usually used for non-SUSY models or models with light mass spectra, which should not be studied at very high scales.

The corresponding files are called SPheno.m or FlexibleSUSY.m and we give here two examples for them.

C.1 FlexibleSUSY.m for a high-scale version

Model information

```

1 FSMoDelName = "@CLASSNAME@";
2 FSDefaultSARAHModel = MSSM;
3 FSEigenstates = SARAH'EWSB;

```

Input parameters

```

1 MINPAR = {
2     {1, m0},
3     {2, m12},
4     {3, TanBeta},
5     {4, Sign[\[Mu]]},
6     {5, Azero}
7 };

```

Parameters fixed by the electroweak symmetry breaking conditions

```

1 EWSBOutputParameters = {\[Mu], B\[Mu]};

```

Definition of the renormalisation scale, at which the pole masses should be calculated

```

1 SUSYScaleFirstGuess = Sqrt[m0^2 + 4 m12^2];
2 SUSYScale = Sqrt[Product[M[Su[i]]^(Abs[ZU[i,3]]^2 + ↵
    Abs[ZU[i,6]]^2), {i,6}]];

```

Condition defining the GUT scale

```

1 HighScaleFirstGuess = 2.0 10^16;
2 HighScale = g1 == g2;

```

Condition defining the Standard Model matching scale

```

1 LowScaleFirstGuess = LowEnergyConstant[MZ];
2 LowScale = LowEnergyConstant[MZ];

```

Boundary conditions

```

1 HighScaleInput = {
2   {T[Ye], Azero*Ye},
3   {T[Yd], Azero*Yd},
4   {T[Yu], Azero*Yu},
5   {mq2, UNITMATRIX[3] m0^2},
6   {m12, UNITMATRIX[3] m0^2},
7   {md2, UNITMATRIX[3] m0^2},
8   {mu2, UNITMATRIX[3] m0^2},
9   {me2, UNITMATRIX[3] m0^2},
10  {mHd2, m0^2},
11  {mHu2, m0^2},
12  {MassB, m12},
13  {MassWB, m12},
14  {MassG, m12}
15 };
16
17 SUSYScaleInput = {
18   (* solve EWSB conditions for \[Mu] and B\[Mu]
19   at this scale *)
20   FSSolveEWSBFor[EWSBOutputParameters]
21 };
22
23 LowScaleInput = {
24   {vd, 2 MZDRbar Cos[ArcTan[TanBeta]] /

```



```

25     Sqrt[GUTNormalization[g1]^2 g1^2 + g2^2}},
26     {vu, 2 MZDRbar Sin[ArcTan[TanBeta]] /
27     Sqrt[GUTNormalization[g1]^2 g1^2 + g2^2}},
28     {Yu, Automatic},
29     {Yd, Automatic},
30     {Ye, Automatic}
31 };

```

Initial parameter guess

```

1  InitialGuessAtLowScale = {
2     {vd, LowEnergyConstant[vev] Cos[ArcTan[TanBeta]]},
3     {vu, LowEnergyConstant[vev] Sin[ArcTan[TanBeta]]},
4     {Yu, Automatic},
5     {Yd, Automatic},
6     {Ye, Automatic}
7  };
8
9  InitialGuessAtHighScale = {
10     {\[Mu]    , 1.0},
11     {B\[Mu]] , 0.0}
12 };

```

MSSM-specific options

```

1  (* use 2L Higgs self-energy contributions *)
2  UseHiggs2LoopMSSM = True;
3  EffectiveMu = \[Mu];
4
5  (* use 3L MSSM RGEs *)
6  UseMSSM3LoopRGEs = True;

```

Definition of additional SLHA output blocks

```

1  (* add FlexibleSUSYOutput block containing the scales *)
2  ExtraSLHAOutputBlocks = {
3     {FlexibleSUSYOutput,
4         {{0, Hold[HighScale]},
5          {1, Hold[SUSYScale]},
6          {2, Hold[LowScale] }}}
7  };

```

C.2 FlexibleSUSY.m for a low-scale version

Model information

```
1 FSModelName = "@CLASSNAME@";  
2 FSDefaultSARAHModel = SMgaugegroup/TwoScalarLeptoquarks;  
3 FSEigenstates = SARAH'EWSB';  
4 FSRGELoopOrder = 0; (* do not generate RGEs *)
```

Flag to choose a low-scale FlexibleSUSY variant without high-scale boundary condition

```
1 OnlyLowEnergyFlexibleSUSY = True;
```

Input parameters

```
1 MINPAR = {  
2     {1, mhIN},  
3     {2, msIN},  
4     {3, LambdaTinput},  
5     {4, LambdaPinput},  
6     {5, Lambda0input},  
7     {6, LambdaHSinput},  
8     {7, LambdaHTinput},  
9     {8, LambdaHPinput},  
10    {9, LambdaH0input},  
11    {10, LambdaSTinput},  
12    {11, LambdaSPinput},  
13    {12, LambdaS0input},  
14    {13, LambdaTPinput},  
15    {14, LambdaT0input},  
16    {15, LambdaP0input},  
17    {16, LambdaHATinput},  
18    {21, mTinput},  
19    {22, mPinput},  
20    {23, m0input},  
21    {25, vSinput}  
22 };
```

Parameters fixed by the electroweak symmetry breaking conditions

```
1 EWSBOutputParameters = {muH2, muS2};
```

Definition of the renormalisation scale, at which the pole masses should be calculated

```

1 SUSYScaleFirstGuess = LowScaleFirstGuess;
2 SUSYScale = LowScale;

```

Condition defining the Standard Model matching scale

```

1 LowScaleFirstGuess = LowEnergyConstant [MZ];
2 LowScale = LowEnergyConstant [MZ];

```

Boundary conditions

```

1 SUSYScaleInput = {};
2
3 LowScaleInput = {
4   {vS, vSinput},
5   {LambdaT, LambdaTinput},
6   {LambdaP, LambdaPinput},
7   {Lambda0, Lambda0input},
8   {LambdaHS, LambdaHSinput},
9   {LambdaH, (mhIN^2*v^2 + msIN^2*v^2 -
10              Sqrt[mhIN^4*v^4 - 2*mhIN^2*msIN^2*v^4 +
11                  msIN^4*v^4 - 4*LambdaHS^2*v^6*vS^2]
12              )/(2*v^4)},
13  {LambdaS, (mhIN^2 + msIN^2 +
14            Sqrt[v^4*(mhIN^4 - 2*mhIN^2*msIN^2 + msIN^4
15                - 4*LambdaHS^2*v^2*vS^2)]/v^2)/(4*vS^2)},
16  {LambdaHT, LambdaHTinput},
17  {LambdaHP, LambdaHPinput},
18  {LambdaHO, LambdaHOinput},
19  {LambdaTS, LambdaSTinput},
20  {LambdaPS, LambdaSPinput},
21  {LambdaOS, LambdaSOinput},
22  {LambdaPT, LambdaTPinput},
23  {LambdaOT, LambdaTOinput},
24  {LambdaOP, LambdaPOinput},
25  {LambdaHat, LambdaHATinput},
26  {muT2, (2*mTinput^2 - LambdaHT*v^2 - ↔
          LambdaTS*vS^2)/2},

```

```

27 {muP2, (2*mPinput^2 - LambdaHP*v^2 - ↔
      LambdaPS*vS^2)/2},
28 {muO2, (2*mOinput^2 - LambdaHO*v^2 - ↔
      LambdaOS*vS^2)/2},
29 {YT, LHInput[YT]},
30 {YO, LHInput[YO]},
31 {YP, LHInput[YP]},
32 {v, 2 MZDRbar /
      Sqrt[GUTNormalization[g1]^2 g1^2 + g2^2]},
33 {Ye, Automatic},
34 {Yd, Automatic},
35 {Yu, Automatic}
36 };
37

```

Initial parameter guess

```

1 InitialGuessAtLowScale = {
2   {vS, vSinput},
3   {LambdaT, LambdaTinput},
4   {LambdaP, LambdaPinput},
5   {LambdaO, LambdaOinput},
6   {LambdaHS, LambdaHSinput},
7   {LambdaH, (mhIN^2*v^2 + msIN^2*v^2 -
8             Sqrt[mhIN^4*v^4 - 2*mhIN^2*msIN^2*v^4 +
9             msIN^4*v^4 - 4*LambdaHS^2*v^6*vS^2]
10            )/(2*v^4)},
11  {LambdaS, (mhIN^2 + msIN^2 +
12            Sqrt[v^4*(mhIN^4 - 2*mhIN^2*msIN^2 + msIN^4
13            - 4*LambdaHS^2*v^2*vS^2)]/v^2)/(4*vS^2)},
14  {LambdaHT, LambdaHTinput},
15  {LambdaHP, LambdaHPinput},
16  {LambdaHO, LambdaHOinput},
17  {LambdaTS, LambdaSTinput},
18  {LambdaPS, LambdaSPinput},
19  {LambdaOS, LambdaSOinput},
20  {LambdaPT, LambdaTPinput},
21  {LambdaOT, LambdaTOinput},
22  {LambdaOP, LambdaPOinput},
23  {LambdaHat, LambdaHATinput},

```

```

24     {YT, LHInput[YT]},
25     {Y0, LHInput[Y0]},
26     {YP, LHInput[YP]},
27     {v , LowEnergyConstant[vev]},
28     {Yu, Automatic},
29     {Yd, Automatic},
30     {Ye, Automatic}
31 };

```

C.3 SPheno.m for a high-scale version

Expected Input parameters

```

1  MINPAR={{1, m0},
2         {2, m12},
3         {3, TanBeta},
4         {4, SignumMu},
5         {5, Azero}};
6
7  RealParameters = {TanBeta, m0};

```

Parameters obtained from tadpole equations

```

1  ParametersToSolveTadpoles = {\[Mu], B\[Mu]};

```

Definition of Renormalisation scale

```

1  RenormalizationScaleFirstGuess = m0^2 + 4 m12^2;
2  RenormalizationScale = Sqrt[(mq2[3, 3]
3  + (vu^2*conj[Yu[3, 3]]*Yu[3, 3])/2)*(mu2[3, 3]
4  + (vu^2*conj[Yu[3, 3]]*Yu[3, 3])/2)
5  -((vd*\[Mu]*conj[Yu[3, 3]] - vu*conj[T[Yu][3, 3]])
6  *(vd*conj\[Mu]*Yu[3, 3] - vu*T[Yu][3, 3]))/2];

```

Condition for GUT scale

```

1  ConditionGUTscale = g1 == g2;

```

Boundary conditions

```

1  BoundaryHighScale={
2  {T[Ye], Azero*Ye},
3  {T[Yd], Azero*Yd},

```

```

4 {T[Yu], Azero*Yu},
5 {mq2, DIAGONAL m0^2},
6 {m12, DIAGONAL m0^2},
7 {md2, DIAGONAL m0^2},
8 {mu2, DIAGONAL m0^2},
9 {me2, DIAGONAL m0^2},
10 {mHd2, m0^2},
11 {mHu2, m0^2},
12 {MassB, m12},
13 {MassWB, m12},
14 {MassG, m12}
15 };
16 BoundarySUSYSscale={};
17 BoundaryEWSBSscale={};

```

List of particles for which the decays shall be calculated by SPheno

```

1 ListDecayParticles = Automatic;
2 ListDecayParticles3B = Automatic;

```

C.4 SPheno.m for a low-scale version

Flag to choose a low-scale SPheno version

```

1 OnlyLowEnergySPheno = True;

```

Expected Input parameters

```

1 MINPAR={
2 {1, mhIN},
3 {2, msIN},
4 {3, LambdaTinput},
5 {4, LambdaPinput},
6 {5, LambdaOinput},
7 {6, LambdaHSinput},
8 {7, LambdaHTinput},
9 {8, LambdaHPinput},
10 {9, LambdaHOinput},
11 {10, LambdaSTinput},
12 {11, LambdaSPinput},
13 {12, LambdaSOinput},

```

```

14 {13, LambdaTPinput},
15 {14, LambdaT0input},
16 {15, LambdaP0input},
17 {16, LambdaHATinput},
18
19 {21, mTinput},
20 {22, mPinput},
21 {23, m0input},
22
23 {25, vSinput}
24 };

```

Parameters obtained from tadpole equations

```

1 ParametersToSolveTadpoles = {muH2, muS2};

```

Boundary conditions

```

1 BoundaryLowScaleInput={
2 {v, vSM},
3 {Ye, YeSM},
4 {Yd, YdSM},
5 {Yu, YuSM},
6 {g1, g1SM},
7 {g2, g2SM},
8 {g3, g3SM},
9 {vS, vSinput},
10 {LambdaT, LambdaTinput},
11 {LambdaP, LambdaPinput},
12 {Lambda0, Lambda0input},
13 {LambdaHS, LambdaHSinput},
14 {LambdaH, (mhIN^2*v^2 + msIN^2*v^2 -
15 Sqrt[mhIN^4*v^4 - 2*mhIN^2*msIN^2*v^4 + msIN^4*v^4
16 - 4*LambdaHS^2*v^6*vS^2])/(2*v^4)},
17 {LambdaS, (mhIN^2 + msIN^2 +
18 Sqrt[v^4*(mhIN^4 - 2*mhIN^2*msIN^2 + msIN^4
19 - 4*LambdaHS^2*v^2*vS^2)]/v^2)/(4*vS^2)},
20 {LambdaHT, LambdaHTinput},
21 {LambdaHP, LambdaHPinput},
22 {LambdaHO, LambdaHOinput},

```

```

23 {LambdaTS ,           LambdaSTinput},
24 {LambdaPS ,           LambdaSPinput},
25 {LambdaOS ,           LambdaSOinput},
26 {LambdaPT ,           LambdaTPinput},
27 {LambdaOT ,           LambdaTOinput},
28 {LambdaOP ,           LambdaPOinput},
29 {LambdaHat ,          LambdaHATinput},
30
31 {muT2 , (2*mTinput^2 - LambdaHT*v^2 - LambdaTS*vS^2)/2},
32 {muP2 , (2*mPinput^2 - LambdaHP*v^2 - LambdaPS*vS^2)/2},
33 {muO2 , (2*mOinput^2 - LambdaHO*v^2 - LambdaOS*vS^2)/2},
34
35
36 {YT , LHInput[YT]},
37 {YO , LHInput[YO]},
38 {YP , LHInput[YP]}
39 };

```

List of particles for which the decays shall be calculated by SPheno

```

1 ListDecayParticles = {Fu,Fe,Fd,hh,Ah,PhiLQ,theta,OmegaLQ};
2 ListDecayParticles3B = ↔
   {{Fu,"Fu.f90"},{Fe,"Fe.f90"},{Fd,"Fd.f90"}};

```

References

- [1] **ATLAS** Collaboration, A. collaboration, *Search for resonances decaying to photon pairs in 3.2 fb^{-1} of pp collisions at $\sqrt{s} = 13 \text{ TeV}$ with the ATLAS detector*, .
- [2] **CMS** Collaboration, C. Collaboration, *Search for new physics in high mass diphoton events in proton-proton collisions at 13TeV* , .
- [3] S. Abel and V. V. Khoze, *Photo-production of a 750 GeV di-photon resonance mediated by Kaluza-Klein leptons in the loop*, [arXiv:1601.07167](#).
- [4] P. Agrawal, J. Fan, B. Heidenreich, M. Reece, and M. Strassler, *Experimental Considerations Motivated by the Diphoton Excess at the LHC*, [arXiv:1512.05775](#).
- [5] A. Ahmed, B. M. Dillon, B. Grzadkowski, J. F. Gunion, and Y. Jiang, *Higgs-radion interpretation of 750 GeV di-photon excess at the LHC*, [arXiv:1512.05771](#).
- [6] B. C. Allanach, P. S. B. Dev, S. A. Renner, and K. Sakurai, *Di-photon Excess Explained by a Resonant Sneutrino in R-parity Violating Supersymmetry*, [arXiv:1512.07645](#).

- [7] S. Alexander and L. Smolin, *Enhanced color gauge invariance and a new di-photon state at the LHC*, [arXiv:1601.03091](#).
- [8] W. Altmannshofer, J. Galloway, S. Gori, A. L. Kagan, A. Martin, and J. Zupan, *On the 750 GeV di-photon excess*, [arXiv:1512.07616](#).
- [9] D. Aloni, K. Blum, A. Dery, A. Efrati, and Y. Nir, *On a possible large width 750 GeV diphoton resonance at ATLAS and CMS*, [arXiv:1512.05778](#).
- [10] A. Alves, A. G. Dias, and K. Sinha, *The 750 GeV S-cion: Where else should we look for it?*, [arXiv:1512.06091](#).
- [11] H. An, C. Cheung, and Y. Zhang, *Broad Diphotons from Narrow States*, [arXiv:1512.08378](#).
- [12] L. A. Anchordoqui, I. Antoniadis, H. Goldberg, X. Huang, D. Lust, and T. R. Taylor, *750 GeV diphotons from closed string states*, [arXiv:1512.08502](#).
- [13] O. Antipin, M. Mojaza, and F. Sannino, *A natural Coleman-Weinberg theory explains the diphoton excess*, [arXiv:1512.06708](#).
- [14] L. Aparicio, A. Azatov, E. Hardy, and A. Romanino, *Diphotons from Diaxions*, [arXiv:1602.00949](#).
- [15] C. Arbelaez, A. E. C. Hernandez, S. Kovalenko, and I. Schmidt, *Linking radiative seesaw-type mechanism of fermion masses and non-trivial quark mixing with the 750 GeV diphoton excess*, [arXiv:1602.03607](#).
- [16] Y. Mambrini, G. Arcadi, and A. Djouadi, *The LHC diphoton resonance and dark matter*, [arXiv:1512.04913](#).
- [17] M. T. Arun and D. Choudhury, *Bulk gauge and matter fields in nested warping: II. Symmetry Breaking and phenomenological consequences*, [arXiv:1601.02321](#).
- [18] M. T. Arun and P. Saha, *Gravitons in multiply warped scenarios - at 750 GeV and beyond*, [arXiv:1512.06335](#).
- [19] U. Aydemir and T. Mandal, *Interpretation of the 750 GeV diphoton excess with colored scalars in $\mathbf{SO}(10)$ grand unification*, [arXiv:1601.06761](#).
- [20] M. Backovic, A. Mariotti, and D. Redigolo, *Di-photon excess illuminates Dark Matter*, [arXiv:1512.04917](#).
- [21] M. Badziak, *Interpreting the 750 GeV diphoton excess in minimal extensions of Two-Higgs-Doublet models*, [arXiv:1512.07497](#).
- [22] K. J. Bae, M. Endo, K. Hamaguchi, and T. Moroi, *Diphoton Excess and Running Couplings*, [arXiv:1602.03653](#).
- [23] Y. Bai, J. Berger, and R. Lu, *A 750 GeV Dark Pion: Cousin of a Dark G-parity-odd WIMP*, [arXiv:1512.05779](#).

- [24] D. Bardhan, D. Bhatia, A. Chakraborty, U. Maitra, S. Raychaudhuri, and T. Samui, *Radion Candidate for the LHC Diphoton Resonance*, [arXiv:1512.06674](#).
- [25] D. Barducci, A. Goudelis, S. Kulkarni, and D. Sengupta, *One jet to rule them all: monojet constraints and invisible decays of a 750 GeV diphoton resonance*, [arXiv:1512.06842](#).
- [26] N. D. Barrie, A. Kobakhidze, M. Talia, and L. Wu, *750 GeV Composite Axion as the LHC Diphoton Resonance*, [arXiv:1602.00475](#).
- [27] M. Bauer and M. Neubert, *Flavor Anomalies, the Diphoton Excess and a Dark Matter Candidate*, [arXiv:1512.06828](#).
- [28] D. Becirevic, E. Bertuzzo, O. Sumensari, and R. Z. Funchal, *Can the new resonance at LHC be a CP-Odd Higgs boson?*, [arXiv:1512.05623](#).
- [29] B. Bellazzini, R. Franceschini, F. Sala, and J. Serra, *Goldstones in Diphotons*, [arXiv:1512.05330](#).
- [30] A. Belyaev, G. Cacciapaglia, H. Cai, T. Flacke, A. Parolini, and H. Serôdio, *Singlets in Composite Higgs Models in light of the LHC di-photon searches*, [arXiv:1512.07242](#).
- [31] I. Ben-Dayan and R. Brustein, *Hypercharge Axion and the Diphoton 750 GeV Resonance*, [arXiv:1601.07564](#).
- [32] R. Benbrik, C.-H. Chen, and T. Nomura, *Higgs singlet as a diphoton resonance in a vector-like quark model*, [arXiv:1512.06028](#).
- [33] A. Berlin, *The Diphoton and Diboson Excesses in a Left-Right Symmetric Theory of Dark Matter*, [arXiv:1601.01381](#).
- [34] J. Bernon and C. Smith, *Could the width of the diphoton anomaly signal a three-body decay ?*, [arXiv:1512.06113](#).
- [35] L. Berthier, J. M. Cline, W. Shepherd, and M. Trott, *Effective interpretations of a diphoton excess*, [arXiv:1512.06799](#).
- [36] E. Bertuzzo, P. A. N. Machado, and M. Taoso, *Di-Photon excess in the 2HDM: hastening towards the instability and the non-perturbative regime*, [arXiv:1601.07508](#).
- [37] S. Bhattacharya, S. Patra, N. Sahoo, and N. Sahu, *750 GeV Di-photon excess at CERN LHC from a dark sector assisted scalar decay*, [arXiv:1601.01569](#).
- [38] X.-J. Bi, R. Ding, Y. Fan, L. Huang, C. Li, T. Li, S. Raza, X.-C. Wang, and B. Zhu, *A Promising Interpretation of Diphoton Resonance at 750 GeV*, [arXiv:1512.08497](#).
- [39] X.-J. Bi, Q.-F. Xiang, P.-F. Yin, and Z.-H. Yu, *The 750 GeV diphoton excess at the LHC and dark matter constraints*, [arXiv:1512.06787](#).
- [40] L. Bian, N. Chen, D. Liu, and J. Shu, *A hidden confining world on the 750 GeV diphoton excess*, [arXiv:1512.05759](#).

- [41] N. Bizot, S. Davidson, M. Frigerio, and J. L. Kneur, *Two Higgs doublets to explain the excesses $pp \rightarrow \gamma\gamma(750 \text{ GeV})$ and $h \rightarrow \tau^\pm\mu^\mp$* , [arXiv:1512.08508](#).
- [42] A. Dasgupta, M. Mitra, and D. Borah, *Minimal Left-Right Symmetry Confronted with the 750 GeV Di-photon Excess at LHC*, [arXiv:1512.09202](#).
- [43] D. Borah, S. Patra, and S. Sahoo, *Subdominant Left-Right Scalar Dark Matter as Origin of the 750 GeV Di-photon Excess at LHC*, [arXiv:1601.01828](#).
- [44] S. M. Boucenna, S. Morisi, and A. Vicente, *The LHC diphoton resonance from gauge symmetry*, [arXiv:1512.06878](#).
- [45] M. R. Buckley, *Wide or Narrow? The Phenomenology of 750 GeV Diphotons*, [arXiv:1601.04751](#).
- [46] D. Buttazzo, A. Greljo, and D. Marzocca, *Knocking on New Physics' door with a Scalar Resonance*, [arXiv:1512.04929](#).
- [47] C. Cai, Z.-H. Yu, and H.-H. Zhang, *The 750 GeV diphoton resonance as a singlet scalar in an extra dimensional model*, [arXiv:1512.08440](#).
- [48] J. Cao, C. Han, L. Shang, W. Su, J. M. Yang, and Y. Zhang, *Interpreting the 750 GeV diphoton excess by the singlet extension of the Manohar-Wise Model*, [arXiv:1512.06728](#).
- [49] J. Cao, L. Shang, W. Su, Y. Zhang, and J. Zhu, *Interpreting the 750 GeV diphoton excess in the Minimal Dilaton Model*, [arXiv:1601.02570](#).
- [50] J. Cao, F. Wang, and Y. Zhang, *Interpreting The 750 GeV Diphton Excess Within TopFlavor Seesaw Model*, [arXiv:1512.08392](#).
- [51] Q.-H. Cao, S.-L. Chen, and P.-H. Gu, *Strong CP Problem, Neutrino Masses and the 750 GeV Diphoton Resonance*, [arXiv:1512.07541](#).
- [52] Q.-H. Cao, Y.-Q. Gong, X. Wang, B. Yan, and L. L. Yang, *One Bump or Two Peaks? The 750 GeV Diphoton Excess and Dark Matter with a Complex Mediator*, [arXiv:1601.06374](#).
- [53] Q.-H. Cao, Y. Liu, K.-P. Xie, B. Yan, and D.-M. Zhang, *The Diphoton Excess, Low Energy Theorem and the 331 Model*, [arXiv:1512.08441](#).
- [54] Q.-H. Cao, Y. Liu, K.-P. Xie, B. Yan, and D.-M. Zhang, *A Boost Test of Anomalous Diphoton Resonance at the LHC*, [arXiv:1512.05542](#).
- [55] L. M. Carpenter, R. Colburn, and J. Goodman, *Supersoft SUSY Models and the 750 GeV Diphoton Excess, Beyond Effective Operators*, [arXiv:1512.06107](#).
- [56] J. A. Casas, J. R. Espinosa, and J. M. Moreno, *The 750 GeV Diphoton Excess as a First Light on Supersymmetry Breaking*, [arXiv:1512.07895](#).

- [57] J. Chakraborty, A. Choudhury, P. Ghosh, S. Mondal, and T. Srivastava, *Di-photon resonance around 750 GeV: shedding light on the theory underneath*, [arXiv:1512.05767](#).
- [58] S. Chakraborty, A. Chakraborty, and S. Raychaudhuri, *Diphoton resonance at 750 GeV in the broken MRSSM*, [arXiv:1512.07527](#).
- [59] I. Chakraborty and A. Kundu, *Diphoton excess at 750 GeV: Singlet scalars confront naturalness*, [arXiv:1512.06508](#).
- [60] M. Chala, M. Duerr, F. Kahlhoefer, and K. Schmidt-Hoberg, *Tricking Landau-Yang: How to obtain the diphoton excess from a vector resonance*, [arXiv:1512.06833](#).
- [61] J. Chang, K. Cheung, and C.-T. Lu, *Interpreting the 750 GeV Di-photon Resonance using photon-jets in Hidden-Valley-like models*, [arXiv:1512.06671](#).
- [62] S. Chang, *A Simple U(1) Gauge Theory Explanation of the Diphoton Excess*, [arXiv:1512.06426](#).
- [63] W. Chao, *The Diphoton Excess Inspired Electroweak Baryogenesis*, [arXiv:1601.04678](#).
- [64] W. Chao, *The Diphoton Excess from an Exceptional Supersymmetric Standard Model*, [arXiv:1601.00633](#).
- [65] W. Chao, *Neutrino Catalyzed Diphoton Excess*, [arXiv:1512.08484](#).
- [66] W. Chao, *Symmetries Behind the 750 GeV Diphoton Excess*, [arXiv:1512.06297](#).
- [67] W. Chao, R. Huo, and J.-H. Yu, *The Minimal Scalar-Stealth Top Interpretation of the Diphoton Excess*, [arXiv:1512.05738](#).
- [68] K. Cheung, P. Ko, J. S. Lee, J. Park, and P.-Y. Tseng, *A Higgcision study on the 750 GeV Di-photon Resonance and 125 GeV SM Higgs boson with the Higgs-Singlet Mixing*, [arXiv:1512.07853](#).
- [69] C.-W. Chiang, M. Ibe, and T. T. Yanagida, *Revisiting Scalar Quark Hidden Sector in Light of 750-GeV Diphoton Resonance*, [arXiv:1512.08895](#).
- [70] C.-W. Chiang and A.-L. Kuo, *Can the 750-GeV diphoton resonance be the singlet Higgs boson of custodial Higgs triplet model?*, [arXiv:1601.06394](#).
- [71] W. S. Cho, D. Kim, K. Kong, S. H. Lim, K. T. Matchev, J.-C. Park, and M. Park, *The 750 GeV Diphoton Excess May Not Imply a 750 GeV Resonance*, [arXiv:1512.06824](#).
- [72] D. Chway, R. Dermíšek, T. H. Jung, and H. D. Kim, *Glue to light signal of a new particle*, [arXiv:1512.08221](#).
- [73] J. M. Cline and Z. Liu, *LHC diphotons from electroweakly pair-produced composite pseudoscalars*, [arXiv:1512.06827](#).

- [74] P. Cox, A. D. Medina, T. S. Ray, and A. Spray, *Diphoton Excess at 750 GeV from a Radion in the Bulk-Higgs Scenario*, [arXiv:1512.05618](#).
- [75] N. Craig, P. Draper, C. Kilic, and S. Thomas, *How the $\gamma\gamma$ Resonance Stole Christmas*, [arXiv:1512.07733](#).
- [76] C. Csaki, J. Hubisz, S. Lombardo, and J. Terning, *Gluon vs. Photon Production of a 750 GeV Diphoton Resonance*, [arXiv:1601.00638](#).
- [77] C. Csaki, J. Hubisz, and J. Terning, *The Minimal Model of a Diphoton Resonance: Production without Gluon Couplings*, [arXiv:1512.05776](#).
- [78] D. Curtin and C. B. Verhaaren, *Quirky Explanations for the Diphoton Excess*, [arXiv:1512.05753](#).
- [79] M. Cvetič, J. Halverson, and P. Langacker, *String Consistency, Heavy Exotics, and the 750 GeV Diphoton Excess at the LHC*, [arXiv:1512.07622](#).
- [80] F. D’Eramo, J. de Vries, and P. Panci, *A 750 GeV Portal: LHC Phenomenology and Dark Matter Candidates*, [arXiv:1601.01571](#).
- [81] U. Danielsson, R. Enberg, G. Ingelman, and T. Mandal, *The force awakens - the 750 GeV diphoton excess at the LHC from a varying electromagnetic coupling*, [arXiv:1601.00624](#).
- [82] L. V. Laperashvili, H. B. Nielsen, and C. R. Das, *New results at LHC confirming the vacuum stability and Multiple Point Principle*, [arXiv:1601.03231](#).
- [83] K. Das and S. K. Rai, *The 750 GeV Diphoton excess in a U(1) hidden symmetry model*, [arXiv:1512.07789](#).
- [84] J. H. Davis, M. Fairbairn, J. Heal, and P. Tunney, *The Significance of the 750 GeV Fluctuation in the ATLAS Run 2 Diphoton Data*, [arXiv:1601.03153](#).
- [85] H. Davoudiasl and C. Zhang, *A 750 GeV Messenger of Dark Conformal Symmetry Breaking*, [arXiv:1512.07672](#).
- [86] J. S. Kim, J. Reuter, K. Rolbiecki, and R. R. de Austri, *A resonance without resonance: scrutinizing the diphoton excess at 750 GeV*, [arXiv:1512.06083](#).
- [87] J. S. Kim, K. Rolbiecki, and R. R. de Austri, *Model-independent combination of diphoton constraints at 750 GeV*, [arXiv:1512.06797](#).
- [88] B. Dasgupta, J. Kopp, and P. Schwaller, *Photons, Photon Jets and Dark Photons at 750 GeV and Beyond*, [arXiv:1602.04692](#).
- [89] J. de Blas, J. Santiago, and R. Vega-Morales, *New vector bosons and the diphoton excess*, [arXiv:1512.07229](#).
- [90] C. Delaunay and Y. Soreq, *Probing New Physics with Isotope Shift Spectroscopy*, [arXiv:1602.04838](#).

- [91] S. V. Demidov and D. S. Gorbunov, *On sgoldstino interpretation of the diphoton excess*, [arXiv:1512.05723](#).
- [92] F. F. Deppisch, C. Hati, S. Patra, P. Pritimita, and U. Sarkar, *Implications of the diphoton excess on Left-Right models and gauge unification*, [arXiv:1601.00952](#).
- [93] P. S. B. Dev, R. N. Mohapatra, and Y. Zhang, *Quark Seesaw Vectorlike Fermions and Diphoton Excess*, [arXiv:1512.08507](#).
- [94] P. S. B. Dev and D. Teresi, *Asymmetric Dark Matter in the Sun and the Diphoton Excess at the LHC*, [arXiv:1512.07243](#).
- [95] U. K. Dey, S. Mohanty, and G. Tomar, *750 GeV resonance in the Dark Left-Right Model*, [arXiv:1512.07212](#).
- [96] M. Dhuria and G. Goswami, *Perturbativity, vacuum stability and inflation in the light of 750 GeV diphoton excess*, [arXiv:1512.06782](#).
- [97] S. Di Chiara, L. Marzola, and M. Raidal, *First interpretation of the 750 GeV di-photon resonance at the LHC*, [arXiv:1512.04939](#).
- [98] R. Ding, Y. Fan, L. Huang, C. Li, T. Li, S. Raza, and B. Zhu, *Systematic Study of Diphoton Resonance at 750 GeV from Sgoldstino*, [arXiv:1602.00977](#).
- [99] R. Ding, Z.-L. Han, Y. Liao, and X.-D. Ma, *Interpretation of 750 GeV Diphoton Excess at LHC in Singlet Extension of Color-octet Neutrino Mass Model*, [arXiv:1601.02714](#).
- [100] R. Ding, L. Huang, T. Li, and B. Zhu, *Interpreting 750 GeV Diphoton Excess with R-parity Violation Supersymmetry*, [arXiv:1512.06560](#).
- [101] A. Djouadi, J. Ellis, R. Godbole, and J. Quevillon, *Future Collider Signatures of the Possible 750 GeV State*, [arXiv:1601.03696](#).
- [102] I. Dorsner, S. Fajfer, and N. Kosnik, *Is symmetry breaking of SU(5) theory responsible for the diphoton excess?*, [arXiv:1601.03267](#).
- [103] P. Draper and D. McKeen, *Diphotons, New Vacuum Angles, and Strong CP*, [arXiv:1602.03604](#).
- [104] B. Dutta, Y. Gao, T. Ghosh, I. Gogoladze, and T. Li, *Interpretation of the diphoton excess at CMS and ATLAS*, [arXiv:1512.05439](#).
- [105] B. Dutta, Y. Gao, T. Ghosh, I. Gogoladze, T. Li, Q. Shafi, and J. W. Walker, *Diphoton Excess in Consistent Supersymmetric SU(5) Models with Vector-like Particles*, [arXiv:1601.00866](#).
- [106] J. Ellis, S. A. R. Ellis, J. Quevillon, V. Sanz, and T. You, *On the Interpretation of a Possible ~ 750 GeV Particle Decaying into $\gamma\gamma$* , [arXiv:1512.05327](#).

- [107] U. Ellwanger and C. Hugonie, *A 750 GeV Diphoton Signal from a Very Light Pseudoscalar in the NMSSM*, [arXiv:1602.03344](#).
- [108] M. Fabbrichesi and A. Urbano, *The breaking of the $SU(2)_L \times U(1)_Y$ symmetry: The 750 GeV resonance at the LHC and perturbative unitarity*, [arXiv:1601.02447](#).
- [109] A. Falkowski, O. Slone, and T. Volansky, *Phenomenology of a 750 GeV Singlet*, [arXiv:1512.05777](#).
- [110] A. E. Faraggi and J. Rizos, *The 750 GeV diphoton LHC excess and Extra Z's in Heterotic-String Derived Models*, [arXiv:1601.03604](#).
- [111] T.-F. Feng, X.-Q. Li, H.-B. Zhang, and S.-M. Zhao, *The LHC 750 GeV diphoton excess in supersymmetry with gauged baryon and lepton numbers*, [arXiv:1512.06696](#).
- [112] S. Fichtel, G. von Gersdorff, and C. Royon, *Scattering Light by Light at 750 GeV at the LHC*, [arXiv:1512.05751](#).
- [113] S. Fichtel, G. von Gersdorff, and C. Royon, *Measuring the diphoton coupling of a 750 GeV resonance*, [arXiv:1601.01712](#).
- [114] R. Franceschini, G. F. Giudice, J. F. Kamenik, M. McCullough, A. Pomarol, R. Rattazzi, M. Redi, F. Riva, A. Strumia, and R. Torre, *What is the gamma gamma resonance at 750 GeV?*, [arXiv:1512.04933](#).
- [115] D. B. Franzosi and M. T. Frandsen, *Symmetries and composite dynamics for the 750 GeV diphoton excess*, [arXiv:1601.05357](#).
- [116] E. Gabrielli, K. Kannike, B. Mele, M. Raidal, C. Spethmann, and H. Veermäe, *A SUSY Inspired Simplified Model for the 750 GeV Diphoton Excess*, [arXiv:1512.05961](#).
- [117] J. Gao, H. Zhang, and H. X. Zhu, *Diphoton excess at 750 GeV: gluon-gluon fusion or quark-antiquark annihilation?*, [arXiv:1512.08478](#).
- [118] S.-F. Ge, H.-J. He, J. Ren, and Z.-Z. Xianyu, *Realizing Dark Matter and Higgs Inflation in Light of LHC Diphoton Excess*, [arXiv:1602.01801](#).
- [119] C.-Q. Geng and D. Huang, *Note on Spin-2 Particle Interpretation of the 750 GeV Diphoton Excess*, [arXiv:1601.07385](#).
- [120] K. Ghorbani and H. Ghorbani, *The 750 GeV Diphoton Excess from a Pseudoscalar in Fermionic Dark Matter Scenario*, [arXiv:1601.00602](#).
- [121] A. Ghoshal, *On Electroweak Phase Transition and Di-photon Excess with a 750 GeV Scalar Resonance*, [arXiv:1601.04291](#).
- [122] S. B. Giddings and H. Zhang, *Kaluza-Klein graviton phenomenology for warped compactifications, and the 750 GeV diphoton excess*, [arXiv:1602.02793](#).
- [123] S. I. Godunov, A. N. Rozanov, M. I. Vysotsky, and E. V. Zhemchugov, *New Physics at 1 TeV?*, [arXiv:1602.02380](#).

- [124] F. Goertz, J. F. Kamenik, A. Katz, and M. Nardecchia, *Indirect Constraints on the Scalar Di-Photon Resonance at the LHC*, [arXiv:1512.08500](#).
- [125] C. Gross, O. Lebedev, and J. M. No, *Drell-Yan Constraints on New Electroweak States and the Di-photon Anomaly*, [arXiv:1602.03877](#).
- [126] J. Gu and Z. Liu, *Running after Diphoton*, [arXiv:1512.07624](#).
- [127] R. S. Gupta, S. Jaeger, Y. Kats, G. Perez, and E. Stamou, *Interpreting a 750 GeV Diphoton Resonance*, [arXiv:1512.05332](#).
- [128] L. J. Hall, K. Harigaya, and Y. Nomura, *750 GeV Diphotons: Implications for Supersymmetric Unification*, [arXiv:1512.07904](#).
- [129] Y. Hamada, T. Noumi, S. Sun, and G. Shiu, *An $O(750)$ GeV Resonance and Inflation*, [arXiv:1512.08984](#).
- [130] Y. Hamada, H. Kawai, K. Kawana, and K. Tsumura, *Models of LHC Diphoton Excesses Valid up to the Planck scale*, [arXiv:1602.04170](#).
- [131] C. Han, H. M. Lee, M. Park, and V. Sanz, *The diphoton resonance as a gravity mediator of dark matter*, [arXiv:1512.06376](#).
- [132] H. Han, S. Wang, and S. Zheng, *Dark Matter Theories in the Light of Diphoton Excess*, [arXiv:1512.07992](#).
- [133] H. Han, S. Wang, and S. Zheng, *Scalar Explanation of Diphoton Excess at LHC*, [arXiv:1512.06562](#).
- [134] X.-F. Han and L. Wang, *Implication of the 750 GeV diphoton resonance on two-Higgs-doublet model and its extensions with Higgs field*, [arXiv:1512.06587](#).
- [135] X.-F. Han, L. Wang, L. Wu, J. M. Yang, and M. Zhang, *Explaining 750 GeV diphoton excess from top/bottom partner cascade decay in two-Higgs-doublet model extension*, [arXiv:1601.00534](#).
- [136] X.-F. Han, L. Wang, and J. M. Yang, *An extension of two-Higgs-doublet model and the excesses of 750 GeV diphoton, muon $g-2$ and $h \rightarrow \mu\tau$* , [arXiv:1601.04954](#).
- [137] C. Han, T. T. Yanagida, and N. Yokozaki, *Implications of the 750 GeV Diphoton Excess in Gaugino Mediation*, [arXiv:1602.04204](#).
- [138] K. Harigaya and Y. Nomura, *A Composite Model for the 750 GeV Diphoton Excess*, [arXiv:1602.01092](#).
- [139] K. Harigaya and Y. Nomura, *Composite Models for the 750 GeV Diphoton Excess*, [arXiv:1512.04850](#).
- [140] L. A. Harland-Lang, V. A. Khoze, and M. G. Ryskin, *The production of a diphoton resonance via photon-photon fusion*, [arXiv:1601.07187](#).

- [141] L. A. Harland-Lang, V. A. Khoze, and M. G. Ryskin, *The photon PDF in events with rapidity gaps*, [arXiv:1601.03772](#).
- [142] C. Hati, *Explaining the diphoton excess in Alternative Left-Right Symmetric Model*, [arXiv:1601.02457](#).
- [143] J. J. Heckman, *750 GeV Diphotons from a D3-brane*, [arXiv:1512.06773](#).
- [144] A. Hektor and L. Marzola, *Di-photon excess at LHC and the gamma ray excess at the Galactic Centre*, [arXiv:1602.00004](#).
- [145] A. E. C. Hernández, *The 750 GeV diphoton resonance can cause the SM fermion mass and mixing pattern*, [arXiv:1512.09092](#).
- [146] A. E. C. Hernández and I. Nisandzic, *LHC diphoton 750 GeV resonance as an indication of $SU(3)_c \times SU(3)_L \times U(1)_X$ gauge symmetry*, [arXiv:1512.07165](#).
- [147] A. E. C. Hernández, I. d. M. Varzielas, and E. Schumacher, *The 750 GeV diphoton resonance in the light of a 2HDM with S_3 flavour symmetry*, [arXiv:1601.00661](#).
- [148] T. Higaki, K. S. Jeong, N. Kitajima, and F. Takahashi, *The QCD Axion from Aligned Axions and Diphoton Excess*, [arXiv:1512.05295](#).
- [149] F. P. Huang, C. S. Li, Z. L. Liu, and Y. Wang, *750 GeV Diphoton Excess from Cascade Decay*, [arXiv:1512.06732](#).
- [150] W.-C. Huang, Y.-L. S. Tsai, and T.-C. Yuan, *Gauged Two Higgs Doublet Model confronts the LHC 750 GeV di-photon anomaly*, [arXiv:1512.07268](#).
- [151] X.-J. Huang, W.-H. Zhang, and Y.-F. Zhou, *A 750 GeV dark matter messenger at the Galactic Center*, [arXiv:1512.08992](#).
- [152] L. E. Ibanez and V. Martin-Lozano, *A Megaxion at 750 GeV as a First Hint of Low Scale String Theory*, [arXiv:1512.08777](#).
- [153] H. Ito, T. Moroi, and Y. Takaesu, *Studying 750 GeV Di-photon Resonance at Photon-Photon Collider*, [arXiv:1601.01144](#).
- [154] Y. Jiang, Y.-Y. Li, and T. Liu, *750 GeV Resonance in the Gauged $U(1)'$ -Extended MSSM*, [arXiv:1512.09127](#).
- [155] S. Jung, J. Song, and Y. W. Yoon, *How Resonance-Continuum Interference Changes 750 GeV Diphoton Excess: Signal Enhancement and Peak Shift*, [arXiv:1601.00006](#).
- [156] S. Kanemura, N. Machida, S. Odori, and T. Shindou, *Diphoton excess at 750 GeV in an extended scalar sector*, [arXiv:1512.09053](#).
- [157] S. Kanemura, K. Nishiwaki, H. Okada, Y. Orikasa, S. C. Park, and R. Watanabe, *LHC 750 GeV Diphoton excess in a radiative seesaw model*, [arXiv:1512.09048](#).
- [158] K. Kaneta, S. Kang, and H.-S. Lee, *Diphoton excess at the LHC Run 2 and its implications for a new heavy gauge boson*, [arXiv:1512.09129](#).

- [159] S. K. Kang and J. Song, *Top-phobic heavy Higgs boson as the 750 GeV diphoton resonance*, [arXiv:1512.08963](#).
- [160] A. Karozas, S. F. King, G. K. Leontaris, and A. K. Meadowcroft, *Diphoton excess from E_6 in F-theory GUTs*, [arXiv:1601.00640](#).
- [161] B. J. Kavanagh, *Re-examining the significance of the 750 GeV diphoton excess at ATLAS*, [arXiv:1601.07330](#).
- [162] J. Kawamura and Y. Omura, *Diphoton excess at 750 GeV and LHC constraints in models with vector-like particles*, [arXiv:1601.07396](#).
- [163] J. E. Kim, *Is an axizilla possible for di-photon resonance?*, [arXiv:1512.08467](#).
- [164] S. F. King and R. Nevzorov, *750 GeV Diphoton Resonance from Singlets in an Exceptional Supersymmetric Standard Model*, [arXiv:1601.07242](#).
- [165] S. Knapen, T. Melia, M. Papucci, and K. Zurek, *Rays of light from the LHC*, [arXiv:1512.04928](#).
- [166] P. Ko and T. Nomura, *Dark sector shining through 750 GeV dark Higgs boson at the LHC*, [arXiv:1601.02490](#).
- [167] P. Ko, Y. Omura, and C. Yu, *Diphoton Excess at 750 GeV in leptophobic $U(1)'$ model inspired by E_6 GUT*, [arXiv:1601.00586](#).
- [168] A. Kobakhidze, F. Wang, L. Wu, J. M. Yang, and M. Zhang, *LHC 750 GeV diphoton resonance explained as a heavy scalar in top-seesaw model*, [arXiv:1512.05585](#).
- [169] K. Kulkarni, *Extension of ν MSM model and possible explanations of recent astronomical and collider observations*, [arXiv:1512.06836](#).
- [170] G. Li, Y.-n. Mao, Y.-L. Tang, C. Zhang, Y. Zhou, and S.-h. Zhu, *A Loop-philic Pseudoscalar*, [arXiv:1512.08255](#).
- [171] T. Li, J. A. Maxin, V. E. Mayes, and D. V. Nanopoulos, *A Flippon Related Singlet at the LHC II*, [arXiv:1602.01377](#).
- [172] W. Liao and H.-q. Zheng, *Scalar resonance at 750 GeV as composite of heavy vector-like fermions*, [arXiv:1512.06741](#).
- [173] J. Liu, X.-P. Wang, and W. Xue, *LHC diphoton excess from colorful resonances*, [arXiv:1512.07885](#).
- [174] I. Low and J. Lykken, *Implications of Gauge Invariance on a Heavy Diphoton Resonance*, [arXiv:1512.09089](#).
- [175] M. Low, A. Tesi, and L.-T. Wang, *A pseudoscalar decaying to photon pairs in the early LHC run 2 data*, [arXiv:1512.05328](#).
- [176] M.-x. Luo, K. Wang, T. Xu, L. Zhang, and G. Zhu, *Squarkonium/Diquarkonium and the Di-photon Excess*, [arXiv:1512.06670](#).

- [177] A. D. Martin and M. G. Ryskin, *Advantages of exclusive $\gamma\gamma$ production to probe high mass systems*, [arXiv:1601.07774](#).
- [178] R. Martinez, F. Ochoa, and C. F. Sierra, *Diphoton decay for a 750 GeV scalar boson in an $U(1)'$ model*, [arXiv:1512.05617](#).
- [179] A. Martini, K. Mawatari, and D. Sengupta, *Diphoton excess in phenomenological spin-2 resonance scenarios*, [arXiv:1601.05729](#).
- [180] L. Marzola, A. Racioppi, M. Raidal, F. R. Urban, and H. Veermäe, *Non-minimal CW inflation, electroweak symmetry breaking and the 750 GeV anomaly*, [arXiv:1512.09136](#).
- [181] S. Matsuzaki and K. Yamawaki, *750 GeV Diphoton Signal from One-Family Walking Technipion*, [arXiv:1512.05564](#).
- [182] A. Salvio and A. Mazumdar, *Higgs Stability and the 750 GeV Diphoton Excess*, [arXiv:1512.08184](#).
- [183] S. D. McDermott, P. Meade, and H. Ramani, *Singlet Scalar Resonances and the Diphoton Excess*, [arXiv:1512.05326](#).
- [184] E. Megias, O. Pujolas, and M. Quiros, *On dilatons and the LHC diphoton excess*, [arXiv:1512.06106](#).
- [185] T. Modak, S. Sadhukhan, and R. Srivastava, *750 GeV Diphoton excess from Gauged $B - L$ Symmetry*, [arXiv:1601.00836](#).
- [186] E. Molinaro, F. Sannino, and N. Vignaroli, *Minimal Composite Dynamics versus Axion Origin of the Diphoton excess*, [arXiv:1512.05334](#).
- [187] S. Moretti and K. Yagyu, *The 750 GeV diphoton excess and its explanation in 2-Higgs Doublet Models with a real inert scalar multiplet*, [arXiv:1512.07462](#).
- [188] C. W. Murphy, *Vector Leptoquarks and the 750 GeV Diphoton Resonance at the LHC*, [arXiv:1512.06976](#).
- [189] Y. Nakai, R. Sato, and K. Tobioka, *Footprints of New Strong Dynamics via Anomaly*, [arXiv:1512.04924](#).
- [190] J. M. No, V. Sanz, and J. Setford, *See-Saw Composite Higgses at the LHC: Linking Naturalness to the 750 GeV Di-Photon Resonance*, [arXiv:1512.05700](#).
- [191] T. Nomura and H. Okada, *Generalized Zee-Babu model with 750 GeV Diphoton Resonance*, [arXiv:1601.07339](#).
- [192] T. Nomura and H. Okada, *Four-loop Radiative Seesaw Model with 750 GeV Diphoton Resonance*, [arXiv:1601.04516](#).
- [193] T. Nomura and H. Okada, *Four-loop Neutrino Model Inspired by Diphoton Excess at 750 GeV*, [arXiv:1601.00386](#).

- [194] H. Okada and K. Yagyu, *Renormalizable Model for Neutrino Mass, Dark Matter, Muon $g - 2$ and 750 GeV Diphoton Excess*, [arXiv:1601.05038](#).
- [195] E. Palti, *Vector-Like Exotics in F-Theory and 750 GeV Diphotons*, [arXiv:1601.00285](#).
- [196] D. Palle, *On the possible new 750 GeV heavy boson resonance at the LHC*, [arXiv:1601.00618](#).
- [197] J.-C. Park and S. C. Park, *Indirect signature of dark matter with the diphoton resonance at 750 GeV*, [arXiv:1512.08117](#).
- [198] K. M. Patel and P. Sharma, *Interpreting 750 GeV diphoton excess in SU(5) grand unified theory*, [arXiv:1512.07468](#).
- [199] G. M. Pelaggi, A. Strumia, and E. Vigiani, *Trinification can explain the di-photon and di-boson LHC anomalies*, [arXiv:1512.07225](#).
- [200] C. Petersson and R. Torre, *The 750 GeV diphoton excess from the goldstino superpartner*, [arXiv:1512.05333](#).
- [201] A. Pilaftsis, *Diphoton Signatures from Heavy Axion Decays at LHC*, [arXiv:1512.04931](#).
- [202] C. T. Potter, *Pseudoscalar Gluonia to Diphotons at the LHC*, [arXiv:1601.00240](#).
- [203] I. Sahin, *Semi-elastic cross section for a scalar resonance of mass 750 GeV*, [arXiv:1601.01676](#).
- [204] A. Salvio, F. Staub, A. Strumia, and A. Urbano, *On the maximal diphoton width*, [arXiv:1602.01460](#).
- [205] M. Son and A. Urbano, *A new scalar resonance at 750 GeV: Towards a proof of concept in favor of strongly interacting theories*, [arXiv:1512.08307](#).
- [206] D. Stolarski and R. Vega-Morales, *The Virtual Diphoton Excess*, [arXiv:1601.02004](#).
- [207] Y.-L. Tang and S.-h. Zhu, *NMSSM extended with vector-like particles and the diphoton excess on the LHC*, [arXiv:1512.08323](#).
- [208] F. Wang, W. Wang, L. Wu, J. M. Yang, and M. Zhang, *Interpreting 750 GeV Diphoton Resonance in the NMSSM with Vector-like Particles*, [arXiv:1512.08434](#).
- [209] F. Wang, L. Wu, J. M. Yang, and M. Zhang, *750 GeV Diphoton Resonance, 125 GeV Higgs and Muon $g-2$ Anomaly in Deflected Anomaly Mediation SUSY Breaking Scenario*, [arXiv:1512.06715](#).
- [210] J.-H. Yu, *Hidden Gauged U(1) Model: Unifying Scotogenic Neutrino and Flavor Dark Matter*, [arXiv:1601.02609](#).
- [211] H. Zhang, *The 750GeV diphoton excess: who introduces it?*, [arXiv:1601.01355](#).

- [212] J. Zhang and S. Zhou, *Electroweak Vacuum Stability and Diphoton Excess at 750 GeV*, [arXiv:1512.07889](#).
- [213] A. Angelescu, A. Djouadi, and G. Moreau, *Scenarii for interpretations of the LHC diphoton excess: two Higgs doublets and vector-like quarks and leptons*, [arXiv:1512.04921](#).
- [214] F. Staub, *SARAH*, [arXiv:0806.0538](#).
- [215] F. Staub, *From Superpotential to Model Files for FeynArts and CalcHep/CompHep*, *Comput. Phys. Commun.* **181** (2010) 1077–1086, [[arXiv:0909.2863](#)].
- [216] F. Staub, *Automatic Calculation of supersymmetric Renormalization Group Equations and Self Energies*, *Comput. Phys. Commun.* **182** (2011) 808–833, [[arXiv:1002.0840](#)].
- [217] F. Staub, *SARAH 3.2: Dirac Gauginos, UFO output, and more*, *Comput. Phys. Commun.* **184** (2013) 1792–1809, [[arXiv:1207.0906](#)].
- [218] F. Staub, *SARAH 4 : A tool for (not only SUSY) model builders*, *Comput. Phys. Commun.* **185** (2014) 1773–1790, [[arXiv:1309.7223](#)].
- [219] F. Staub, *Exploring new models in all detail with SARAH*, *Adv. High Energy Phys.* **2015** (2015) 840780, [[arXiv:1503.04200](#)].
- [220] W. Porod, *SPheno, a program for calculating supersymmetric spectra, SUSY particle decays and SUSY particle production at e^+e^- colliders*, *Comput. Phys. Commun.* **153** (2003) 275–315, [[hep-ph/0301101](#)].
- [221] W. Porod and F. Staub, *SPheno 3.1: Extensions including flavour, CP-phases and models beyond the MSSM*, *Comput. Phys. Commun.* **183** (2012) 2458–2469, [[arXiv:1104.1573](#)].
- [222] P. Athron, J.-h. Park, D. Stöckinger, and A. Voigt, *FlexibleSUSY - A spectrum generator generator for supersymmetric models*, *Comput. Phys. Commun.* **190** (2015) 139–172, [[arXiv:1406.2319](#)].
- [223] F. Staub, P. Athron, U. Ellwanger, R. Grober, M. Muhlleitner, P. Slavich, and A. Voigt, *Higgs mass predictions of public NMSSM spectrum generators*, [arXiv:1507.05093](#).
- [224] G. Degrandi, P. Slavich, and F. Zwirner, *On the neutral Higgs boson masses in the MSSM for arbitrary stop mixing*, *Nucl. Phys.* **B611** (2001) 403–422, [[hep-ph/0105096](#)].
- [225] A. Brignole, G. Degrandi, P. Slavich, and F. Zwirner, *On the $O(\alpha(t)^{**2})$ two loop corrections to the neutral Higgs boson masses in the MSSM*, *Nucl. Phys.* **B631** (2002) 195–218, [[hep-ph/0112177](#)].

- [226] A. Dedes and P. Slavich, *Two loop corrections to radiative electroweak symmetry breaking in the MSSM*, *Nucl. Phys.* **B657** (2003) 333–354, [[hep-ph/0212132](#)].
- [227] A. Brignole, G. Degrossi, P. Slavich, and F. Zwirner, *On the two loop sbottom corrections to the neutral Higgs boson masses in the MSSM*, *Nucl. Phys.* **B643** (2002) 79–92, [[hep-ph/0206101](#)].
- [228] A. Dedes, G. Degrossi, and P. Slavich, *On the two loop Yukawa corrections to the MSSM Higgs boson masses at large tan beta*, *Nucl. Phys.* **B672** (2003) 144–162, [[hep-ph/0305127](#)].
- [229] G. Degrossi and P. Slavich, *On the radiative corrections to the neutral Higgs boson masses in the NMSSM*, *Nucl. Phys.* **B825** (2010) 119–150, [[arXiv:0907.4682](#)].
- [230] M. D. Goodsell, K. Nickel, and F. Staub, *Two-Loop Higgs mass calculations in supersymmetric models beyond the MSSM with SARAH and SPheno*, *Eur. Phys. J.* **C75** (2015), no. 1 32, [[arXiv:1411.0675](#)].
- [231] M. Goodsell, K. Nickel, and F. Staub, *Generic two-loop Higgs mass calculation from a diagrammatic approach*, *Eur. Phys. J.* **C75** (2015), no. 6 290, [[arXiv:1503.03098](#)].
- [232] A. Pukhov, *CalcHEP 2.3: MSSM, structure functions, event generation, batchs, and generation of matrix elements for other packages*, [hep-ph/0412191](#).
- [233] E. E. Boos, M. N. Dubinin, V. A. Ilyin, A. E. Pukhov, and V. I. Savrin, *CompHEP: Specialized package for automatic calculations of elementary particle decays and collisions*, 1994. [hep-ph/9503280](#).
- [234] J. Alwall, M. Herquet, F. Maltoni, O. Mattelaer, and T. Stelzer, *MadGraph 5 : Going Beyond*, *JHEP* **06** (2011) 128, [[arXiv:1106.0522](#)].
- [235] J. Alwall, R. Frederix, S. Frixione, V. Hirschi, F. Maltoni, O. Mattelaer, H. S. Shao, T. Stelzer, P. Torrielli, and M. Zaro, *The automated computation of tree-level and next-to-leading order differential cross sections, and their matching to parton shower simulations*, *JHEP* **07** (2014) 079, [[arXiv:1405.0301](#)].
- [236] G. Belanger, F. Boudjema, and A. Pukhov, *micrOMEGAs : a code for the calculation of Dark Matter properties in generic models of particle interaction*, in *The Dark Secrets of the Terascale*, pp. 739–790, 2013. [arXiv:1402.0787](#).
- [237] P. Bechtle, O. Brein, S. Heinemeyer, G. Weiglein, and K. E. Williams, *HiggsBounds: Confronting Arbitrary Higgs Sectors with Exclusion Bounds from LEP and the Tevatron*, *Comput. Phys. Commun.* **181** (2010) 138–167, [[arXiv:0811.4169](#)].
- [238] P. Bechtle, O. Brein, S. Heinemeyer, G. Weiglein, and K. E. Williams, *HiggsBounds 2.0.0: Confronting Neutral and Charged Higgs Sector Predictions with Exclusion Bounds from LEP and the Tevatron*, *Comput. Phys. Commun.* **182** (2011) 2605–2631, [[arXiv:1102.1898](#)].

- [239] P. Bechtle, S. Heinemeyer, O. Stål, T. Stefaniak, and G. Weiglein, *HiggsSignals: Confronting arbitrary Higgs sectors with measurements at the Tevatron and the LHC*, *Eur. Phys. J.* **C74** (2014), no. 2 2711, [[arXiv:1305.1933](#)].
- [240] J. E. Camargo-Molina, B. O’Leary, W. Porod, and F. Staub, *Vevacious: A Tool For Finding The Global Minima Of One-Loop Effective Potentials With Many Scalars*, *Eur. Phys. J.* **C73** (2013), no. 10 2588, [[arXiv:1307.1477](#)].
- [241] M. Bahr et al., *Herwig++ Physics and Manual*, *Eur. Phys. J.* **C58** (2008) 639–707, [[arXiv:0803.0883](#)].
- [242] J. Bellm et al., *Herwig 7.0 / Herwig++ 3.0 Release Note*, [[arXiv:1512.01178](#)].
- [243] T. Sjostrand, S. Mrenna, and P. Z. Skands, *PYTHIA 6.4 Physics and Manual*, *JHEP* **05** (2006) 026, [[hep-ph/0603175](#)].
- [244] T. Sjöstrand, S. Ask, J. R. Christiansen, R. Corke, N. Desai, P. Ilten, S. Mrenna, S. Prestel, C. O. Rasmussen, and P. Z. Skands, *An Introduction to PYTHIA 8.2*, *Comput. Phys. Commun.* **191** (2015) 159–177, [[arXiv:1410.3012](#)].
- [245] T. Gleisberg, S. Hoeche, F. Krauss, M. Schonherr, S. Schumann, F. Siegert, and J. Winter, *Event generation with SHERPA 1.1*, *JHEP* **02** (2009) 007, [[arXiv:0811.4622](#)].
- [246] S. Höche, F. Krauss, M. Schön herr, and F. Siegert, *W+ n-Jet predictions at the Large Hadron Collider at next-to-leading order matched with a parton shower*, *Phys. Rev. Lett.* **110** (2013), no. 5 052001, [[arXiv:1201.5882](#)].
- [247] B. C. Allanach, *SOFTSUSY: a program for calculating supersymmetric spectra*, *Comput. Phys. Commun.* **143** (2002) 305–331, [[hep-ph/0104145](#)].
- [248] B. C. Allanach, P. Athron, L. C. Tunstall, A. Voigt, and A. G. Williams, *Next-to-Minimal SOFTSUSY*, *Comput. Phys. Commun.* **185** (2014) 2322–2339, [[arXiv:1311.7659](#)].
- [249] B. C. Allanach and M. A. Bernhardt, *Including R-parity violation in the numerical computation of the spectrum of the minimal supersymmetric standard model: SOFTSUSY*, *Comput. Phys. Commun.* **181** (2010) 232–245, [[arXiv:0903.1805](#)].
- [250] B. C. Allanach, C. H. Kom, and M. Hanussek, *Computation of Neutrino Masses in R-parity Violating Supersymmetry: SOFTSUSY3.2*, *Comput. Phys. Commun.* **183** (2012) 785–793, [[arXiv:1109.3735](#)].
- [251] B. C. Allanach, A. Bednyakov, and R. Ruiz de Austri, *Higher order corrections and unification in the minimal supersymmetric standard model: SOFTSUSY3.5*, *Comput. Phys. Commun.* **189** (2015) 192–206, [[arXiv:1407.6130](#)].
- [252] B. C. Allanach, S. P. Martin, D. G. Robertson, and R. R. de Austri, *The Inclusion of Two-Loop SUSYQCD Corrections to Gluino and Squark Pole Masses in the Minimal*

and Next-to-Minimal Supersymmetric Standard Model: SOFTSUSY3.7, [arXiv:1601.06657](#).

- [253] A. Djouadi, J.-L. Kneur, and G. Moultaka, *SuSpect: A Fortran code for the supersymmetric and Higgs particle spectrum in the MSSM*, *Comput. Phys. Commun.* **176** (2007) 426–455, [[hep-ph/0211331](#)].
- [254] S. Heinemeyer, W. Hollik, and G. Weiglein, *FeynHiggs: A Program for the calculation of the masses of the neutral CP even Higgs bosons in the MSSM*, *Comput. Phys. Commun.* **124** (2000) 76–89, [[hep-ph/9812320](#)].
- [255] P. Drechsel, L. Galeta, S. Heinemeyer, and G. Weiglein, *Precise Predictions for the Higgs-Boson Masses in the NMSSM*, [arXiv:1601.08100](#).
- [256] U. Ellwanger and C. Hugonie, *NMSPEC: A Fortran code for the sparticle and Higgs masses in the NMSSM with GUT scale boundary conditions*, *Comput. Phys. Commun.* **177** (2007) 399–407, [[hep-ph/0612134](#)].
- [257] J. Baglio, R. Gröber, M. Mühlleitner, D. T. Nhung, H. Rzehak, M. Spira, J. Streicher, and K. Walz, *NMSSMCALC: A Program Package for the Calculation of Loop-Corrected Higgs Boson Masses and Decay Widths in the (Complex) NMSSM*, *Comput. Phys. Commun.* **185** (2014), no. 12 3372–3391, [[arXiv:1312.4788](#)].
- [258] J. P. Vega and G. Villadoro, *SusyHD: Higgs mass Determination in Supersymmetry*, *JHEP* **07** (2015) 159, [[arXiv:1504.05200](#)].
- [259] A. Djouadi, J. Kalinowski, and M. Spira, *HDECAY: A Program for Higgs boson decays in the standard model and its supersymmetric extension*, *Comput. Phys. Commun.* **108** (1998) 56–74, [[hep-ph/9704448](#)].
- [260] W. Frisch, H. Eberl, and H. Hlucha, *HFOLD - a program package for calculating two-body MSSM Higgs decays at full one-loop level*, *Comput. Phys. Commun.* **182** (2011) 2219–2226, [[arXiv:1012.5025](#)].
- [261] U. Ellwanger, J. F. Gunion, and C. Hugonie, *NMHDECAY: A Fortran code for the Higgs masses, couplings and decay widths in the NMSSM*, *JHEP* **02** (2005) 066, [[hep-ph/0406215](#)].
- [262] U. Ellwanger and C. Hugonie, *NMHDECAY 2.0: An Updated program for sparticle masses, Higgs masses, couplings and decay widths in the NMSSM*, *Comput. Phys. Commun.* **175** (2006) 290–303, [[hep-ph/0508022](#)].
- [263] M. Muhlleitner, A. Djouadi, and Y. Mambrini, *SDECAY: A Fortran code for the decays of the supersymmetric particles in the MSSM*, *Comput. Phys. Commun.* **168** (2005) 46–70, [[hep-ph/0311167](#)].
- [264] H. Hlucha, H. Eberl, and W. Frisch, *SFOLD - a program package for calculating*

- two-body sfermion decays at full one-loop level in the MSSM*, *Comput. Phys. Commun.* **183** (2012) 2307–2312, [[arXiv:1104.2151](#)].
- [265] D. Das, U. Ellwanger, and A. M. Teixeira, *NMSDECAY: A Fortran Code for Supersymmetric Particle Decays in the Next-to-Minimal Supersymmetric Standard Model*, *Comput. Phys. Commun.* **183** (2012) 774–779, [[arXiv:1106.5633](#)].
- [266] G. Degrandi, P. Gambino, and P. Slavich, *SusyBSG: A Fortran code for $BR[B \rightarrow X(s) \gamma]$ in the MSSM with Minimal Flavor Violation*, *Comput. Phys. Commun.* **179** (2008) 759–771, [[arXiv:0712.3265](#)].
- [267] F. Mahmoudi, *SuperIso v2.3: A Program for calculating flavor physics observables in Supersymmetry*, *Comput. Phys. Commun.* **180** (2009) 1579–1613, [[arXiv:0808.3144](#)].
- [268] J. Rosiek, P. Chankowski, A. Dedes, S. Jager, and P. Tanedo, *SUSY_FLAVOR: A Computational Tool for FCNC and CP-violating Processes in the MSSM*, *Comput. Phys. Commun.* **181** (2010) 2180–2205, [[arXiv:1003.4260](#)].
- [269] A. Crivellin, J. Rosiek, P. H. Chankowski, A. Dedes, S. Jaeger, and P. Tanedo, *SUSY_FLAVOR v2: A Computational tool for FCNC and CP-violating processes in the MSSM*, *Comput. Phys. Commun.* **184** (2013) 1004–1032, [[arXiv:1203.5023](#)].
- [270] J. S. Lee, M. Carena, J. Ellis, A. Pilaftsis, and C. E. M. Wagner, *CPsuperH2.3: an Updated Tool for Phenomenology in the MSSM with Explicit CP Violation*, *Comput. Phys. Commun.* **184** (2013) 1220–1233, [[arXiv:1208.2212](#)].
- [271] P. Athron, M. Bach, H. G. Fargnoli, C. Gnendiger, R. Greifenhagen, J.-h. Park, S. Paßehr, D. Stöckinger, H. Stöckinger-Kim, and A. Voigt, *GM2Calc: Precise MSSM prediction for $(g - 2)$ of the muon*, [[arXiv:1510.08071](#)].
- [272] M. Spira, A. Djouadi, D. Graudenz, and P. M. Zerwas, *Higgs boson production at the LHC*, *Nucl. Phys.* **B453** (1995) 17–82, [[hep-ph/9504378](#)].
- [273] C. Hartmann and M. Trott, *On one-loop corrections in the standard model effective field theory; the $\Gamma(h \rightarrow \gamma\gamma)$ case*, *JHEP* **07** (2015) 151, [[arXiv:1505.02646](#)].
- [274] F. Goertz, A. Katz, M. Son, and A. Urbano, *Precision Drell-Yan Measurements at the LHC and Implications for the Diphoton Excess*, [[arXiv:1602.04801](#)].
- [275] **LHC Higgs Cross Section Working Group** Collaboration, S. Dittmaier et al., *Handbook of LHC Higgs Cross Sections: 1. Inclusive Observables*, [[arXiv:1101.0593](#)].
- [276] **ATLAS** Collaboration, G. Aad et al., *Search for new phenomena in the dijet mass distribution using $p - p$ collision data at $\sqrt{s} = 8$ TeV with the ATLAS detector*, *Phys. Rev.* **D91** (2015), no. 5 052007, [[arXiv:1407.1376](#)].
- [277] H. Georgi and M. Machacek, *Doubly Charged Higgs Bosons*, *Nucl. Phys.* **B262** (1985) 463.

- [278] P. Kant, R. V. Harlander, L. Mihaila, and M. Steinhauser, *Light MSSM Higgs boson mass to three-loop accuracy*, *JHEP* **08** (2010) 104, [[arXiv:1005.5709](#)].
- [279] K. Nickel and F. Staub, *Precise determination of the Higgs mass in supersymmetric models with vectorlike tops and the impact on naturalness in minimal GMSB*, *JHEP* **07** (2015) 139, [[arXiv:1505.06077](#)].
- [280] T. Hahn, *Generating Feynman diagrams and amplitudes with FeynArts 3*, *Comput. Phys. Commun.* **140** (2001) 418–431, [[hep-ph/0012260](#)].
- [281] T. Hahn, *FormCalc 6*, *PoS ACAT08* (2008) 121, [[arXiv:0901.1528](#)].
- [282] W. Kilian, T. Ohl, and J. Reuter, *WHIZARD: Simulating Multi-Particle Processes at LHC and ILC*, *Eur. Phys. J.* **C71** (2011) 1742, [[arXiv:0708.4233](#)].
- [283] M. Moretti, T. Ohl, and J. Reuter, *O’Mega: An Optimizing matrix element generator*, [hep-ph/0102195](#).
- [284] C. Degrande, C. Duhr, B. Fuks, D. Grellscheid, O. Mattelaer, and T. Reiter, *UFO - The Universal FeynRules Output*, *Comput. Phys. Commun.* **183** (2012) 1201–1214, [[arXiv:1108.2040](#)].
- [285] G. Cullen, N. Greiner, G. Heinrich, G. Luisoni, P. Mastrolia, G. Ossola, T. Reiter, and F. Tramontano, *Automated One-Loop Calculations with GoSam*, *Eur. Phys. J.* **C72** (2012) 1889, [[arXiv:1111.2034](#)].
- [286] S. Gieseke, A. Ribon, M. H. Seymour, P. Stephens, and B. Webber, *Herwig++ 1.0: An Event generator for $e^+ e^-$ annihilation*, *JHEP* **02** (2004) 005, [[hep-ph/0311208](#)].
- [287] S. Gieseke, D. Grellscheid, K. Hamilton, A. Ribon, P. Richardson, M. H. Seymour, P. Stephens, and B. R. Webber, *Herwig++ 2.0 Release Note*, [hep-ph/0609306](#).
- [288] J. Bellm et al., *Herwig++ 2.7 Release Note*, [arXiv:1310.6877](#).
- [289] T. Gleisberg, S. Hoeche, F. Krauss, A. Schalicke, S. Schumann, and J.-C. Winter, *SHERPA 1. alpha: A Proof of concept version*, *JHEP* **02** (2004) 056, [[hep-ph/0311263](#)].
- [290] S. Höche, S. Kuttimalai, S. Schumann, and F. Siegert, *Beyond Standard Model calculations with Sherpa*, *Eur. Phys. J.* **C75** (2015), no. 3 135, [[arXiv:1412.6478](#)].
- [291] W. Porod, F. Staub, and A. Vicente, *A Flavor Kit for BSM models*, *Eur. Phys. J.* **C74** (2014), no. 8 2992, [[arXiv:1405.1434](#)].
- [292] R. M. Fonseca, *Calculating the renormalisation group equations of a SUSY model with Susyno*, *Comput. Phys. Commun.* **183** (2012) 2298–2306, [[arXiv:1106.5016](#)].
- [293] B. Holdom, *Two $U(1)$ ’s and Epsilon Charge Shifts*, *Phys. Lett.* **B166** (1986) 196.
- [294] K. Benakli, *Dirac Gauginos: A User Manual*, *Fortsch. Phys.* **59** (2011) 1079–1082, [[arXiv:1106.1649](#)].

- [295] M. D. Goodsell, *Two-loop RGEs with Dirac gaugino masses*, *JHEP* **01** (2013) 066, [[arXiv:1206.6697](#)].
- [296] E. Witten, *An $SU(2)$ Anomaly*, *Phys. Lett.* **B117** (1982) 324–328.
- [297] S. P. Martin and M. T. Vaughn, *Two loop renormalization group equations for soft supersymmetry breaking couplings*, *Phys. Rev.* **D50** (1994) 2282, [[hep-ph/9311340](#)]. [Erratum: *Phys. Rev.*D78,039903(2008)].
- [298] R. M. Fonseca, M. Malinsky, W. Porod, and F. Staub, *Running soft parameters in SUSY models with multiple $U(1)$ gauge factors*, *Nucl. Phys.* **B854** (2012) 28–53, [[arXiv:1107.2670](#)].
- [299] M. Sperling, D. Stöckinger, and A. Voigt, *Renormalization of vacuum expectation values in spontaneously broken gauge theories*, *JHEP* **07** (2013) 132, [[arXiv:1305.1548](#)].
- [300] M. Sperling, D. Stöckinger, and A. Voigt, *Renormalization of vacuum expectation values in spontaneously broken gauge theories: Two-loop results*, *JHEP* **01** (2014) 068, [[arXiv:1310.7629](#)].
- [301] M. E. Machacek and M. T. Vaughn, *Two Loop Renormalization Group Equations in a General Quantum Field Theory. 1. Wave Function Renormalization*, *Nucl. Phys.* **B222** (1983) 83.
- [302] M. E. Machacek and M. T. Vaughn, *Two Loop Renormalization Group Equations in a General Quantum Field Theory. 2. Yukawa Couplings*, *Nucl. Phys.* **B236** (1984) 221.
- [303] M. E. Machacek and M. T. Vaughn, *Two Loop Renormalization Group Equations in a General Quantum Field Theory. 3. Scalar Quartic Couplings*, *Nucl. Phys.* **B249** (1985) 70.
- [304] M.-x. Luo, H.-w. Wang, and Y. Xiao, *Two loop renormalization group equations in general gauge field theories*, *Phys. Rev.* **D67** (2003) 065019, [[hep-ph/0211440](#)].
- [305] R. M. Fonseca, M. Malinský, and F. Staub, *Renormalization group equations and matching in a general quantum field theory with kinetic mixing*, *Phys. Lett.* **B726** (2013) 882–886, [[arXiv:1308.1674](#)].
- [306] D. M. Pierce, J. A. Bagger, K. T. Matchev, and R.-j. Zhang, *Precision corrections in the minimal supersymmetric standard model*, *Nucl. Phys.* **B491** (1997) 3–67, [[hep-ph/9606211](#)].
- [307] S. P. Martin, *Two loop effective potential for a general renormalizable theory and softly broken supersymmetry*, *Phys. Rev.* **D65** (2002) 116003, [[hep-ph/0111209](#)].
- [308] S. P. Martin, *Complete two loop effective potential approximation to the lightest Higgs scalar boson mass in supersymmetry*, *Phys. Rev.* **D67** (2003) 095012, [[hep-ph/0211366](#)].

- [309] M. D. Goodsell, K. Nickel, and F. Staub, *Two-loop corrections to the Higgs masses in the NMSSM*, *Phys. Rev.* **D91** (2015) 035021, [[arXiv:1411.4665](#)].
- [310] J. R. Ellis, K. Enqvist, D. V. Nanopoulos, and F. Zwirner, *Observables in Low-Energy Superstring Models*, *Mod. Phys. Lett.* **A1** (1986) 57.
- [311] R. Barbieri and G. F. Giudice, *Upper Bounds on Supersymmetric Particle Masses*, *Nucl. Phys.* **B306** (1988) 63.
- [312] G. Degrandi, S. Di Vita, J. Elias-Miro, J. R. Espinosa, G. F. Giudice, G. Isidori, and A. Strumia, *Higgs mass and vacuum stability in the Standard Model at NNLO*, *JHEP* **08** (2012) 098, [[arXiv:1205.6497](#)].
- [313] K. Benakli, L. Darmé, M. D. Goodsell, and P. Slavich, *A Fake Split Supersymmetry Model for the 126 GeV Higgs*, *JHEP* **05** (2014) 113, [[arXiv:1312.5220](#)].
- [314] A. Djouadi, *The Anatomy of electro-weak symmetry breaking. I: The Higgs boson in the standard model*, *Phys. Rept.* **457** (2008) 1–216, [[hep-ph/0503172](#)].
- [315] M. Kramer, E. Laenen, and M. Spira, *Soft gluon radiation in Higgs boson production at the LHC*, *Nucl. Phys.* **B511** (1998) 523–549, [[hep-ph/9611272](#)].
- [316] K. G. Chetyrkin, B. A. Kniehl, and M. Steinhauser, *Hadronic Higgs decay to order α_s^4* , *Phys. Rev. Lett.* **79** (1997) 353–356, [[hep-ph/9705240](#)].
- [317] K. G. Chetyrkin, J. H. Kuhn, and C. Sturm, *QCD decoupling at four loops*, *Nucl. Phys.* **B744** (2006) 121–135, [[hep-ph/0512060](#)].
- [318] Y. Schroder and M. Steinhauser, *Four-loop decoupling relations for the strong coupling*, *JHEP* **01** (2006) 051, [[hep-ph/0512058](#)].
- [319] P. A. Baikov and K. G. Chetyrkin, *Top Quark Mediated Higgs Boson Decay into Hadrons to Order α_s^5* , *Phys. Rev. Lett.* **97** (2006) 061803, [[hep-ph/0604194](#)].
- [320] **LHC Higgs Cross Section Working Group** Collaboration, J. R. Andersen et al., *Handbook of LHC Higgs Cross Sections: 3. Higgs Properties*, [arXiv:1307.1347](#).
- [321] G. Belanger, N. D. Christensen, A. Pukhov, and A. Semenov, *SLHAplus: a library for implementing extensions of the standard model*, *Comput. Phys. Commun.* **182** (2011) 763–774, [[arXiv:1008.0181](#)].
- [322] P. de Aquino, W. Link, F. Maltoni, O. Mattelaer, and T. Stelzer, *ALOHA: Automatic Libraries Of Helicity Amplitudes for Feynman Diagram Computations*, *Comput. Phys. Commun.* **183** (2012) 2254–2263, [[arXiv:1108.2041](#)].
- [323] E. Conte, B. Fuks, and G. Serret, *MadAnalysis 5, A User-Friendly Framework for Collider Phenomenology*, *Comput. Phys. Commun.* **184** (2013) 222–256, [[arXiv:1206.1599](#)].

- [324] P. Bechtle, O. Brein, S. Heinemeyer, O. Stål, T. Stefaniak, G. Weiglein, and K. E. Williams, *HiggsBounds – 4: Improved Tests of Extended Higgs Sectors against Exclusion Bounds from LEP, the Tevatron and the LHC*, *Eur. Phys. J.* **C74** (2014), no. 3 2693, [[arXiv:1311.0055](#)].
- [325] T. L. Lee, T. Y. Li, and C. H. Tsai, *HOM4PS-2.0: a software package for solving polynomial systems by the polyhedral homotopy continuation method*, *Computing* **83** (2008), no. 2 109–133.
- [326] F. James and M. Roos, *Minuit: A System for Function Minimization and Analysis of the Parameter Errors and Correlations*, *Comput. Phys. Commun.* **10** (1975) 343–367.
- [327] C. L. Wainwright, *CosmoTransitions: Computing Cosmological Phase Transition Temperatures and Bubble Profiles with Multiple Fields*, *Comput. Phys. Commun.* **183** (2012) 2006–2013, [[arXiv:1109.4189](#)].
- [328] H. An, T. Liu, and L.-T. Wang, *125 GeV Higgs Boson, Enhanced Di-photon Rate, and Gauged $U(1)_{PQ}$ -Extended MSSM*, *Phys. Rev.* **D86** (2012) 075030, [[arXiv:1207.2473](#)].
- [329] A. V. Manohar and M. B. Wise, *Flavor changing neutral currents, an extended scalar sector, and the Higgs production rate at the CERN LHC*, *Phys. Rev.* **D74** (2006) 035009, [[hep-ph/0606172](#)].
- [330] M. Bauer and M. Neubert, *One Leptoquark to Rule Them All: A Minimal Explanation for $R_{D^{(*)}}$, R_K and $(g-2)_\mu$* , [arXiv:1511.01900](#).
- [331] K. Hartling, K. Kumar, and H. E. Logan, *The decoupling limit in the Georgi-Machacek model*, *Phys. Rev.* **D90** (2014), no. 1 015007, [[arXiv:1404.2640](#)].
- [332] G. C. Branco, P. M. Ferreira, L. Lavoura, M. N. Rebelo, M. Sher, and J. P. Silva, *Theory and phenomenology of two-Higgs-doublet models*, *Phys. Rept.* **516** (2012) 1–102, [[arXiv:1106.0034](#)].
- [333] CMS Collaboration, V. Khachatryan et al., *Search for Lepton-Flavour-Violating Decays of the Higgs Boson*, *Phys. Lett.* **B749** (2015) 337–362, [[arXiv:1502.07400](#)].
- [334] D. Aristizabal Sierra and A. Vicente, *Explaining the CMS Higgs flavor violating decay excess*, *Phys. Rev.* **D90** (2014), no. 11 115004, [[arXiv:1409.7690](#)].
- [335] I. Doršner, S. Fajfer, A. Greljo, J. F. Kamenik, N. Košnik, and I. Nišandžić, *New Physics Models Facing Lepton Flavor Violating Higgs Decays at the Percent Level*, *JHEP* **06** (2015) 108, [[arXiv:1502.07784](#)].
- [336] M. Cirelli, N. Fornengo, and A. Strumia, *Minimal dark matter*, *Nucl. Phys.* **B753** (2006) 178–194, [[hep-ph/0512090](#)].
- [337] J. Hisano and K. Tsumura, *Higgs boson mixes with an $SU(2)$ septet representation*, *Phys. Rev.* **D87** (2013) 053004, [[arXiv:1301.6455](#)].

- [338] C. Alvarado, L. Lehman, and B. Ostdiek, *Surveying the Scope of the $SU(2)_L$ Scalar Septet Sector*, *JHEP* **05** (2014) 150, [[arXiv:1404.3208](#)].
- [339] E. Ma and R. Srivastava, *Dirac or inverse seesaw neutrino masses with $B - L$ gauge symmetry and S_3 flavor symmetry*, *Phys. Lett.* **B741** (2015) 217–222, [[arXiv:1411.5042](#)].
- [340] E. Ma, N. Pollard, R. Srivastava, and M. Zakeri, *Gauge $B - L$ Model with Residual Z_3 Symmetry*, *Phys. Lett.* **B750** (2015) 135–138, [[arXiv:1507.03943](#)].
- [341] R. Martinez, F. Ochoa, and J. P. Rubio, *Some phenomenological aspects of a new $U(1)'$ model*, *Phys. Rev.* **D89** (2014), no. 5 056008, [[arXiv:1303.2734](#)].
- [342] M. R. Buckley, D. Hooper, and J. L. Rosner, *A Leptophobic Z' And Dark Matter From Grand Unification*, *Phys. Lett.* **B703** (2011) 343–347, [[arXiv:1106.3583](#)].
- [343] P.-H. Gu, *A Left-Right Symmetric Model for Neutrino Masses, Baryon Asymmetry and Dark Matter*, *Phys. Rev.* **D81** (2010) 095002, [[arXiv:1001.1341](#)].
- [344] B. Brahmachari, E. Ma, and U. Sarkar, *Truly minimal left right model of quark and lepton masses*, *Phys. Rev. Lett.* **91** (2003) 011801, [[hep-ph/0301041](#)].
- [345] A. Davidson and K. C. Wali, *Universal Seesaw Mechanism?*, *Phys. Rev. Lett.* **59** (1987) 393.
- [346] K. S. Babu and R. N. Mohapatra, *A Solution to the Strong CP Problem Without an Axion*, *Phys. Rev.* **D41** (1990) 1286.
- [347] M. Singer, J. W. F. Valle, and J. Schechter, *Canonical Neutral Current Predictions From the Weak Electromagnetic Gauge Group $SU(3) \times U(1)$* , *Phys. Rev.* **D22** (1980) 738.
- [348] J. W. F. Valle and M. Singer, *Lepton Number Violation With Quasi Dirac Neutrinos*, *Phys. Rev.* **D28** (1983) 540.
- [349] F. Pisano and V. Pleitez, *An $SU(3) \times U(1)$ model for electroweak interactions*, *Phys. Rev.* **D46** (1992) 410–417, [[hep-ph/9206242](#)].
- [350] P. H. Frampton, *Chiral dilepton model and the flavor question*, *Phys. Rev. Lett.* **69** (1992) 2889–2891.
- [351] R. Foot, O. F. Hernandez, F. Pisano, and V. Pleitez, *Lepton masses in an $SU(3)-L \times U(1)-N$ gauge model*, *Phys. Rev.* **D47** (1993) 4158–4161, [[hep-ph/9207264](#)].
- [352] J. C. Montero, F. Pisano, and V. Pleitez, *Neutral currents and GIM mechanism in $SU(3)-L \times U(1)-N$ models for electroweak interactions*, *Phys. Rev.* **D47** (1993) 2918–2929, [[hep-ph/9212271](#)].
- [353] V. Pleitez and M. D. Tonasse, *Heavy charged leptons in an $SU(3)-L \times U(1)-N$ model*, *Phys. Rev.* **D48** (1993) 2353–2355, [[hep-ph/9301232](#)].

- [354] A. J. Buras, F. De Fazio, J. Girrbach, and M. V. Carlucci, *The Anatomy of Quark Flavour Observables in 331 Models in the Flavour Precision Era*, *JHEP* **02** (2013) 023, [[arXiv:1211.1237](#)].
- [355] P. V. Dong and N. T. K. Ngan, *Phenomenology of the simple 3-3-1 model with inert scalars*, [arXiv:1512.09073](#).
- [356] R. N. Mohapatra and J. W. F. Valle, *Neutrino Mass and Baryon Number Nonconservation in Superstring Models*, *Phys. Rev.* **D34** (1986) 1642.
- [357] S. M. Boucenna, J. W. F. Valle, and A. Vicente, *Predicting charged lepton flavor violation from 3-3-1 gauge symmetry*, *Phys. Rev.* **D92** (2015), no. 5 053001, [[arXiv:1502.07546](#)].
- [358] W.-C. Huang, Y.-L. S. Tsai, and T.-C. Yuan, *G2HDM : Gauged Two Higgs Doublet Model*, [arXiv:1512.00229](#).
- [359] J. E. Camargo-Molina, B. Garbrecht, B. O’Leary, W. Porod, and F. Staub, *Constraining the Natural MSSM through tunneling to color-breaking vacua at zero and non-zero temperature*, *Phys. Lett.* **B737** (2014) 156–161, [[arXiv:1405.7376](#)].
- [360] J. E. Camargo-Molina, B. O’Leary, W. Porod, and F. Staub, *Stability of the CMSSM against sfermion VEVs*, *JHEP* **12** (2013) 103, [[arXiv:1309.7212](#)].
- [361] E. Ma, *Diphoton Revelation of the Utilitarian Supersymmetric Standard Model*, [arXiv:1512.09159](#).
- [362] S. F. King, S. Moretti, and R. Nevzorov, *Theory and phenomenology of an exceptional supersymmetric standard model*, *Phys. Rev.* **D73** (2006) 035009, [[hep-ph/0510419](#)].
- [363] S. F. King, S. Moretti, and R. Nevzorov, *Exceptional supersymmetric standard model*, *Phys. Lett.* **B634** (2006) 278–284, [[hep-ph/0511256](#)].
- [364] E. Ma, *Compendium of Models from a Gauge $U(1)$ Framework*, [arXiv:1601.01400](#).
- [365] R. M. Capdevilla, A. Delgado, and A. Martin, *Light Stops in a minimal $U(1)_X$ extension of the MSSM*, *Phys. Rev.* **D92** (2015), no. 11 115020, [[arXiv:1509.02472](#)].
- [366] B. O’Leary, W. Porod, and F. Staub, *Mass spectrum of the minimal SUSY B-L model*, *JHEP* **05** (2012) 042, [[arXiv:1112.4600](#)].
- [367] F. Staub, T. Ohl, W. Porod, and C. Speckner, *A Tool Box for Implementing Supersymmetric Models*, *Comput. Phys. Commun.* **183** (2012) 2165–2206, [[arXiv:1109.5147](#)].
- [368] M. Hirsch, M. Malinsky, W. Porod, L. Reichert, and F. Staub, *Hefty MSSM-like light Higgs in extended gauge models*, *JHEP* **02** (2012) 084, [[arXiv:1110.3037](#)].
- [369] M. Hirsch, W. Porod, L. Reichert, and F. Staub, *Phenomenology of the minimal*

- supersymmetric $U(1)_{B-L} \times U(1)_R$ extension of the standard model, *Phys. Rev.* **D86** (2012) 093018, [[arXiv:1206.3516](#)].
- [370] J. E. Camargo-Molina, B. O’Leary, W. Porod, and F. Staub, *The Stability Of R-Parity In Supersymmetric Models Extended By $U(1)_{B-L}$* , *Phys. Rev.* **D88** (2013) 015033, [[arXiv:1212.4146](#)].
- [371] S. P. Martin, *Taming the Goldstone contributions to the effective potential*, *Phys. Rev.* **D90** (2014), no. 1 016013, [[arXiv:1406.2355](#)].
- [372] J. Elias-Miro, J. R. Espinosa, and T. Konstandin, *Taming Infrared Divergences in the Effective Potential*, *JHEP* **08** (2014) 034, [[arXiv:1406.2652](#)].
- [373] **Planck** Collaboration, P. A. R. Ade et al., *Planck 2013 results. XVI. Cosmological parameters*, *Astron. Astrophys.* **571** (2014) A16, [[arXiv:1303.5076](#)].
- [374] L. Basso, B. O’Leary, W. Porod, and F. Staub, *Dark matter scenarios in the minimal SUSY B-L model*, *JHEP* **09** (2012) 054, [[arXiv:1207.0507](#)].
- [375] **SINDRUM** Collaboration, U. Bellgardt et al., *Search for the Decay $\mu^+ \rightarrow e^+ e^-$* , *Nucl. Phys.* **B299** (1988) 1.
- [376] K. Hayasaka et al., *Search for Lepton Flavor Violating Tau Decays into Three Leptons with 719 Million Produced Tau+Tau- Pairs*, *Phys. Lett.* **B687** (2010) 139–143, [[arXiv:1001.3221](#)].
- [377] **SINDRUM II** Collaboration, C. Dohmen et al., *Test of lepton flavor conservation in $\mu \rightarrow e$ conversion on titanium*, *Phys. Lett.* **B317** (1993) 631–636.
- [378] **SINDRUM II** Collaboration, W. H. Bertl et al., *A Search for muon to electron conversion in muonic gold*, *Eur. Phys. J.* **C47** (2006) 337–346.
- [379] T. A. collaboration, *Search for new phenomena in the dilepton final state using proton-proton collisions at $\sqrt{s} = 13$ TeV with the ATLAS detector*, .
- [380] M. E. Krauss, B. O’Leary, W. Porod, and F. Staub, *Implications of gauge kinetic mixing on Z' and slepton production at the LHC*, *Phys. Rev.* **D86** (2012) 055017, [[arXiv:1206.3513](#)].
- [381] L. Basso, B. Fuks, M. E. Krauss, and W. Porod, *Doubly-charged Higgs and vacuum stability in left-right supersymmetry*, *JHEP* **07** (2015) 147, [[arXiv:1503.08211](#)].
- [382] A. Vicente, *Computer tools in particle physics*, [arXiv:1507.06349](#).
- [383] T. Ohl, *Drawing Feynman diagrams with Latex and Metafont*, *Comput. Phys. Commun.* **90** (1995) 340–354, [[hep-ph/9505351](#)].